Measurements and modelling of evapotranspiration to assess agricultural water productivity in basins with changing land use patterns

A case study in the São Francisco River basin, Brazil

Promotoren: Prof. dr. W.G.M. Bastiaanssen
                 Hoogleraar in waterbeheer en Remote Sensing,
Technische   Universiteit Delft

                 Prof. dr. ir. M. G. Bos
                 Hoogleraar in irrigatie waterbeheer, ITC, Enschede;

Samenstelling Promotiecommissie:

Prof. dr. ir. R.A. Feddes
Wageningen Universiteit

Prof. B.B da Silva
Federal University of Campina Grande, Brazil

Prof. dr. ir. N.C. van de Giesen
Technische Universiteit Delft

Dr. A.S.M. Gieske
ITC, Enschede

Measurements and modelling of evapotranspiration to assess agricultural water productivity in basins with changing land use patterns

A case study in the São Francisco River basin, Brazil

Antônio Heriberto de Castro Teixeira

Proefschrift
ter verkrijging van de graad van doctor
op gezag van de Rector Magnificus
van Wageningen Universiteit,
Prof. dr. M.J. Kropff
in het openbaar te verdedigen
op dinsdag 21 oktober 2008
des middags te 13.30 uur in de Aula

Table of Contents

iii

List of abbreviations

ABREVIATION	Interpretation
ANA	National Water Agency
BR	Bowen ratio
CODEVASF	São Francisco Valley Development Company
WP	Water productivity
CWP	Crop water productivity
EC	Eddy correlation
EMBRAPA	Brazilian Agricultural Research Corporation
FAO	Food Agricultural Organization
FP	Flux profile
GIS	Geographic information systems
GPP	Gross primary production
GR	Gross return
GS	Growing season
IBGE	Geographic and Statistic Brazilian Institute
ITC	International Institute for Geo-Information Science and Earth Observations
IWMI	International Water Management Institute
LAI	Leaf area index
lw	Longwave radiation
OIV	Organisation Internatinale de la Vigne et du Vin
SEBAL	Surface energy balance algorithm for land
sw	Shortwave radiation
TM	Thematic mapper

List of frequently used symbols

SYMBOL	Interpretation	Unit
AE	Available energy	W m^{-2} or MJ m^{-2} d^{-1}
AHI	Apparent harvest index	-
APAR	Absorbed photosyntetically active radiation	W m^{-2} or MJ m^{-2} d^{-1}
BIO	Biomass production	Kg ha^{-1} or t ha^{-1}
c_p	Air specific heat	J kg^{-1} K^{-1}
CR	Capillary rise	mm
CWP	Crop water productivity	L m^{-3} or kg m^{-3}
D	Vapour pressure deficit	kPa
d	Zero plane displacement height	m
DP	Deep percolation	mm
e_a	Actual vapour pressure of the air	kPa
e_s	Saturation vapour pressure of the air	kPa
E_a	Actual soil evaporation	mm time^{-1}
E_F	Evaporative fraction	-
ET_a	Instantaneous actual evapotranspiration rate	mm time^{-1}
ET_0	Reference evapotranspiration	mm time^{-1}
ET_p	Potential evapotranspiration rate	mm time^{-1}
g	Gravitational constant	m s^{-2}
G	Soil heat flux	W m^{-2} or MJ m^{-2} d^{-1}
H	Sensible heat flux	W m^{-2} or MJ m^{-2} d^{-1}
HA	Harvested area	ha
H_v	Vineyard sensible heat flux	W m^{-2} or MJ m^{-2} d^{-1}
h_v	Height of the vegetation	m
I	Irrigation	mm
K_c	Crop coefficient based on evapotranspratiomn	-
K_{cb}	Crop coefficient based on transpiration	-
K_e	Crop coefficient based on soil evaporation	-
K_s	Water stress coefficient	-
L	Obukhov length	m
LAI	Leaf are index	-

SYMBOL	Interpretation	Unit
L_v	Latent heat of vaporization	W or MJ
NDVI	Normalized difference vegetation index	-
P	Pluvial precipitation	mm
PAR	Photosyntetically active radiation	$W\ m^{-2}$ or $MJ\ m^{-2}\ d^{-1}$
P_D	Deep Percolation	mm
R_a	Extraterrestrial solar radiation	$W\ m^{-2}$ or $MJ\ m^{-2}\ d^{-1}$
r_a	Aerodynamic resistance to heat transport	$s\ m^{-1}$
r_c	Canopy resistance to water vapour	$s\ m^{-1}$
R_G	Incoming global solar radiation	$W\ m^{-2}$ or $MJ\ m^{-2}\ d^{-1}$
RH	Relative humidity	%
$R_L\downarrow$	Incoming longwave radiation	$W\ m^{-2}$ or $MJ\ m^{-2}\ d^{-1}$
$R_L\uparrow$	Outgoing longwave radiation	$W\ m^{-2}$ or $MJ\ m^{-2}\ d^{-1}$
R_n	Net radiation flux	$W\ m^{-2}$ or $MJ\ m^{-2}\ d^{-1}$
R_{n_c}	Canopy net radiation	$W\ m^{-2}$ or $MJ\ m^{-2}\ d^{-1}$
R_{n_g}	Soil net radiation	$W\ m^{-2}$ or $MJ\ m^{-2}\ d^{-1}$
R_{n_i}	Intercepted net radiation	$W\ m^{-2}$ or $MJ\ m^{-2}\ d^{-1}$
R_{nl}	Net long wave radiation	$W\ m^{-2}$ or $MJ\ m^{-2}\ d^{-1}$
R_{ns}	Net shortwave radiation	$W\ m^{-2}$ or $MJ\ m^{-2}\ d^{-1}$
R_{n_v}	Vineyard net radiation	$W\ m^{-2}$ or $MJ\ m^{-2}\ d^{-}$
R_R	Reflected global solar radiation	$W\ m^{-2}$ or $MJ\ m^{-2}\ d^{-1}$
r_s	Bulk surface resistance to water vapour	$s\ m^{-1}$
r_{st}	Stomatal resistance to water vapour	$s\ m^{-1}$
T	Air temperature	$^o C$ or K
T'	instantaneous departures from the average horizontal air temperature with respect to the mean values	$^o C$ or K
T_a	Actual transpiration	$mm\ time^{-1}$
T_g	Soil temperature	K
T_0	Surface temperature	K
T_{sat}	Satellite brightness temperature	K
u	Horizontal wind speed at a height z	$m\ s^{-1}$
u'	instantaneous departures from the average horizontal wind speed with respect to the mean values	$m\ s^{-1}$

SYMBOL	Interpretation	Unit
u_*	Friction velocity	m s^{-1}
w	Vertical wind speed at a height z	m s^{-1}
W	Water storage in the root zone	mm
w'	instantaneous departures from the average vertical wind speed with respect to the mean values	m s^{-1}
Y_a	Actual yield	L or Kg
Y_{GS}	Yield for the growing season	L or Kg
z	Height above the surface	m
z_g	Soil depth	m
z_{0m}	Roughness length for moment transfer	m
z_{0h}	Roughness length for heat and vapour transfer	m
θ	Soil moisture	cm^3 cm^{-3}
α_0	Surface albedo	-
α_p	Planetary albedo	-
β	Bowen ratio	-
γ	Psychrometric constant	kPa $^\circ$C^{-1}
r_c	Canopy resistance to water vapour	s m^{-1}
Δ	Slope of the saturation vapour pressure temperature relationship	kPa $^\circ$C^{-1}
ε	Light use efficiency	g MJ^{-1}
ε_a	Atmospheric emissivity	-
ε_0	Surface emissivity	-
λE	Latent heat flux	W m^{-2} or MJ m^{-2} d^{-1}
λE_c	Canopy latent heat flux	W m^{-2} or MJ m^{-2} d^{-1}
λE_v	Vineyard latent heat flux	
λ_g	Soil thermal conductivity	W m^{-1} K^{-1}
ρ_a	Air density	kg m^{-3}
ρ_v'	instantaneous departures from the average horizontal water vapour density with respect to the mean values	kg m^{-3}
σ	Stefan-Boltzmann constant	W m^{-2} K^{-4}
τ_{sw}	Atmospheric transmissivity	-
Ψ_h	Integrated stability of temperature	-
Ψ_m	Integrated stability of momentum	-

Abstract

Teixeira, A. H. de C. *Measurements and modelling of evapotranspiration to assess agricultural water productivity in basins with changing land use patterns: a case study in the Sao Francisco River basin, Brazil*, PhD thesis, Wageningen University, the Netherlands.

The São Francisco River basin in Brazil is marked by socio-economic disparities and environmental vulnerabilities. Water managers in the semi-arid region of the basin are faced with several challenges, such as competition among different water user groups, local over-exploitation of aquifers, climate and land use changes, non-source pollution, erosion, and sedimentation. Water policy makers have to work out strategies for integrated water management, which rely on a proper knowledge base of the physical conditions encountered in the basin. The intensification of horticulture in the semi-arid north-eastern region of Brazil replaces natural vegetation (i.e. caatinga) by irrigated fruit crops. A proper knowledge of the water balance from these different agro-ecosystems is an essential pre-requisite for sound water resources planning in the basin context.

Because of the importance of agricultural water management practices on basin hydrology, daily and seasonal actual evapotranspiration were measured in irrigated crops, along with experimental data collection over caatinga. Advanced radiation and energy balance measurements were conducted using the Bowen ratio and eddy correlation energy balance methods. Remote sensing algorithms are potentially suitable for the extrapolation of these local fluxes on a regional scale, and the opportunities of these tools were investigated.

The key crop water parameters identified from this data set included actual evapotranspiration, actual transpiration, actual soil evaporation, evaporative fractions, aerodynamic resistances, surface resistances, crop coefficients, percolation fluxes and water productivity. The energy balance measurements on the irrigated fields revealed high evaporative fractions, which pointed out that soils are very wet and that a large majority of the net available energy is converted into latent heat flux. The average crop water consumption in wine grape were found to be 478 mm per growing season, while table grapes show 373 mm per growing season. The seasonal accumulated values for mango orchards were typically 1419 mm. On average the caatinga natural ecosystem evapotranspirated only 533 mm yr^{-1}. The irrigation induced an

incremental evapotranspiration of 2.2 mm d^{-1} or 8,030 m^3 ha^{-1} yr^{-1}. The water balances revealed that systematic over-irrigation is a common practice and that a continuous deep percolation flux occurs. The detailed results allowed expressing water consumption into specific bio-physical parameters, rather than only into more generic crop coefficients that lump together several individual crop water parameters. The stomata of irrigated crops seem to respond very tightly to atmospheric vapour pressure deficit while natural vegetation responds to the rainfall regime.

The field results have been used further to calibrate and validate an existing remote sensing algorithm for the estimation of spatially distributed energy balance fluxes: the Surface Energy Balance Algorithm for Land (SEBAL). It was shown that it is required to apply the hot and cold pixel calibration for every individual image. A generic solution for the internal calibration of the sensible heat flux through the linear relationship between surface radiation temperature and vertical air temperature differences adjacent to the land surface could not be found. For daily scale, the values of the instantaneous evaporative fraction needed to be adjusted. The difference between field measurements and SEBAL was 4.4 % and 0.6% for natural vegetation and irrigated mango orchard, respectively, for annual scale.

Further to the estimate of depleted water volumes in irrigated horticulture, it was investigated whether the incremental evapotranspiration values are productive. After calibration, the SEBAL algorithm was applied to determine regional scale evapotranspiration and biomass production. The remote sensing tools shows spatial variation of crop water productivity values and detects regions and farms where water can be saved. The net water withdrawal in the Low-Middle São Francisco River basin was also estimated. The biophysical water productivity based on actual evapotranspiration appeared to be around 0.90 L m^{-3}, 2.80 kg m^{-3} and 3.4 kg m^{-3} for respectively wine grapes, table grapes, and mangos. The economic water productivities indicated that irrigated fruit crops have around 20 times more value per unit water consumed than irrigated arable crops.

The area with fruit crops in the semi-arid region of the Low-Middle São Francisco River basin are expanding mainly with vineyards and mango orchards. The crop water consumption is high due to over-irrigation together with high thermal availability. The water is, however, productively used and creates a boost for the rural economy. The drawback is that agricultural drainage can adversely affect the water quality, and this requires a lower irrigation supply in the near-future.

Knowledge of spatially variable actual evapotranspiration can help to optimize the necessary reduction in irrigation supplies.

Acknowledgements

Embrapa I give special thanks to my colleague R.A. Barbosa for his patience in taking care about the experiments as well as for collecting the field data.

Finally, I wish to express my appreciation to all the people from the chair group of Soil Physics, Ecohydrology and Groundwater Management of Wageningen University; from the Department of Water Resources of the International Institute for Geo-Information Science and Earth Observation-ITC; from the International Water Management Institute-IWMI; and from Embrapa Semi-Árido for the facilities and logistics provided.

Antônio Heriberto de Castro Teixeira
Wageningen
October 2008

1. Introduction

1.1 Basin-wide water resources

Water demand already <u>exceeds supply</u> in many parts of the world, and as world population continues to rise, many more areas are expected to experience water scarcity (Vörösmarty et al. 2000; Naiman et al. 2002; Smakhtin et al., 2004; Bos et al., 2005; Gourbesville, 2008). According to Figure 1.1 population growth will continue into the 21st century, although more slowly. The world population is projected to grow from 6 billion in 2000 to more than 9 billion by 2050, an increase of 50%. As the human population is increasing, water use is multiplying (Seckler et al., 1998).
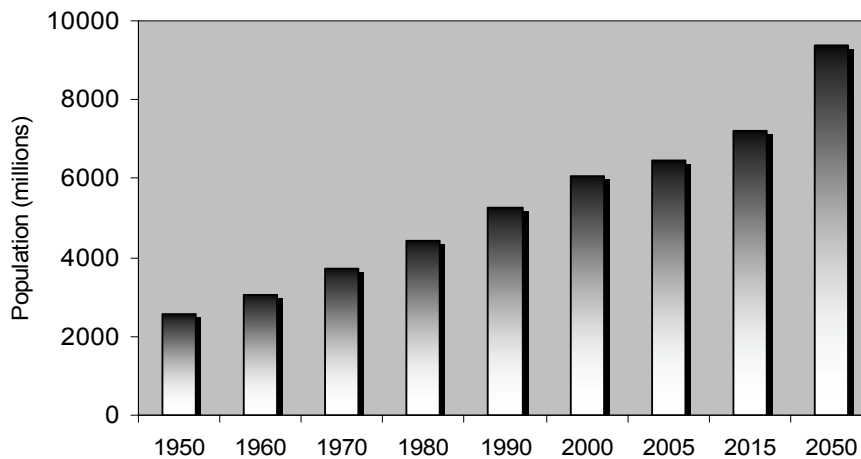
Figure 1.1. Estimates and projections of world population for 1950-2050. Source: U. S. Census Bureau, International Data Base, 2008.

The World Commission on Water (2000) estimates that water use will increase by about 50% after 30 years. An estimated 4 billion people – one half of the world's population – will live under conditions of severe water stress in 2025, particularly in Africa and in the Middle East and South Asia (Bos et al., 2005). Compounding the relative scarcity of water is the continuous deterioration of water quality in most developing countries.

The local solution of water scarcity related problems is hampered by: the lack of commitment to water and poverty, inadequate and inadequately targeted investment, insufficient human capacity, ineffective institutions, and poor governance (Molden et al., 2007b). A

global picture of environmental water scarcity per river basin is provided in Figure 1.2. The water stress indicator of this figure is defined by the ratio of (or a percentage) total withdrawals to utilizable water. If the index exceeds 1, the basin is classified as water scarce. Smaller index values indicate progressively lower water resources exploitation, and consequently, lower risk of environmental water scarcity. Red areas show basins where too much water is being withdrawn.

To achieve sustainable water resources development and secure water availability to competing user groups, future water management may take notice of the water accounting approach (Molden, 1997; Cai et al., 2002), which recognizes the various inhabitants of a basin and the water flows in terms of net water production (i.e. when rainfall exceeds evapotranspiration) or net water consumption (i.e. when evapotranspiration exceeds rainfall).
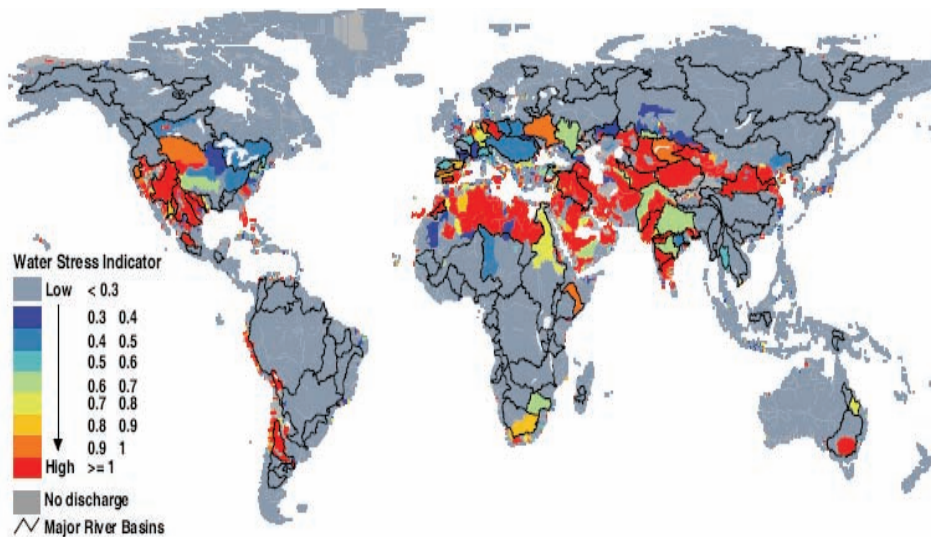
Figure 1.2. Environmental Water Scarcity Index by Basin (Source: Smakhtin et al., 2004).

Hydrologic problems downstream are related to the effect of drainage water on river flows and the timing of peaks and troughs. Low flows are a particular problem because concentrations of pollutants are considerably higher during these periods. Hydrologic basin-wide studies are important to ascertain the impact of discharges (quantity, peak drainage flows, and the time of the peak flow) from a specific project area on the flows of the basin. Drainage flows can affect the proper

ecological functioning of downstream river reaches, floodplains, wetlands, and estuaries in the same way that upstream abstractions for irrigation can affect the flow regime of a river (Gourbesville, 2008).

Disputes over shared water resources continue to raise local, national, and even international tensions (Gleick, 2000). Rising conflicts are expected as populations expand, economies grow, and the competition for limited water supplies intensifies. Basin-level dialogues among different users, including local communities, to negotiate and agree on the allocation of water resources, are required. The success of any dialogue depends on the knowledge base and the general trust in (international) data sources. Minimum data sets include information on land use, water use, and the water accounts of each land use type.

1.2   The São Francisco River basin, Brazil

Figure 1.3 shows the estimates and projections of Brazilian population for 1950-2050. The average population density in Brazil varies according to region: the north with around 3.3 inhabitants per km², the northeast 29.8, the southeast 73.8, the south 41.0 and the centre-west inhabitants per km².
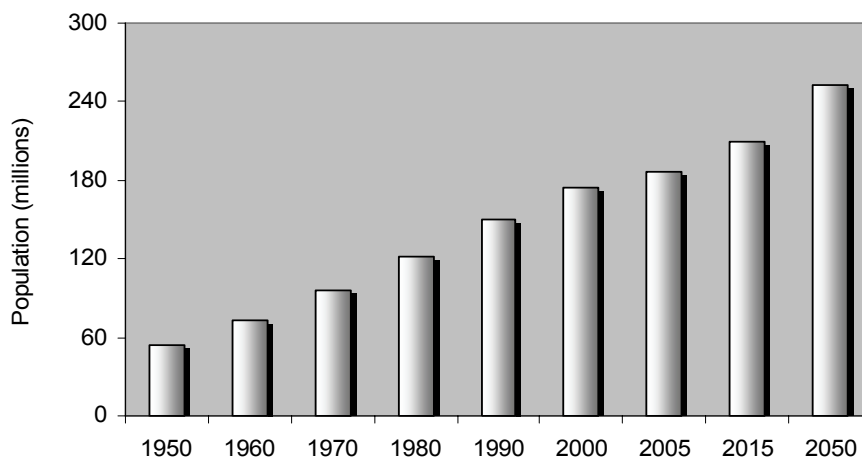
Figure 1.3. Estimates and projections of the Brazilian population for 1950-2050. Source: UN Common Database, 2005.

The Brazilian population increased from 73 million in 1960 to 174 million by 2000, more than a double that occurred over 40 years. According to Figure 1.3 population growth will continue into the 21st

3

century, being projected to grow from 174 million in 2000 to more than 250 million by 2050, an increase of 44 %.

The São Francisco River basin is a vast and complex system encompassing several Brazilian states. The basin is marked by socio-economic disparities and environmental vulnerabilities, in which wealthy areas with high population densities coexist alongside areas with severe poverty and low population densities. The socio-economic data of the state areas inside the São Francisco River basin are shown in Table 1.1. Minas Gerais presents the biggest both population (59%) and area (37%) inside the basin, followed by Bahia (19% and 48%) and Pernambuco (12% and 11%).

Table 1.1: Area, population and number of municipalities in São Francisco River basin, by State for 2007. Source: IBGE, 2007.

State	Area (km^2)	Population (total of inhabitants)	Municipalities (Number)
Minas Gerais	234,634	8,984,808	240
Goiás	3,041	133,427	3
Bahia	305,866	2,910,107	114
Pernambuco	69,607	1,864,783	69
Alagoas	14,321	1,122,678	49
Sergipe	8,046	342,248	27
Total	635,515	15,358,051	502

The total population in the basin increased 16% from 2002 to 2007. Several types of water resources use can be found together with the increase of population. For this reason the region provides an important focus for studies on how to optimize and harmonize various forms of water use to ensure adequate flows for preservation of the environment.

Because of irrigation, the cities Petrolina and Juazeiro, situated in the semi-arid region of the Pernambuco (PE) and Bahia (BA) states, respectively, inside the Low-Middle São Francisco River basin, developed considerably. The main reason for the growth of these cities is the result of the construction of the Sobradinho dam and the availability of water for irrigation. As a consequence, the region has gained population through immigration. Figure 1.4 shows the evolution of population of these cities from 2000 to 2007. There was a bigger development of Petrolina with a population being 16% more than for Juazeiro in 2007. The population in the first city grew by 23% from 2000 to 2007, while in the second city grew by 19% during the same period.
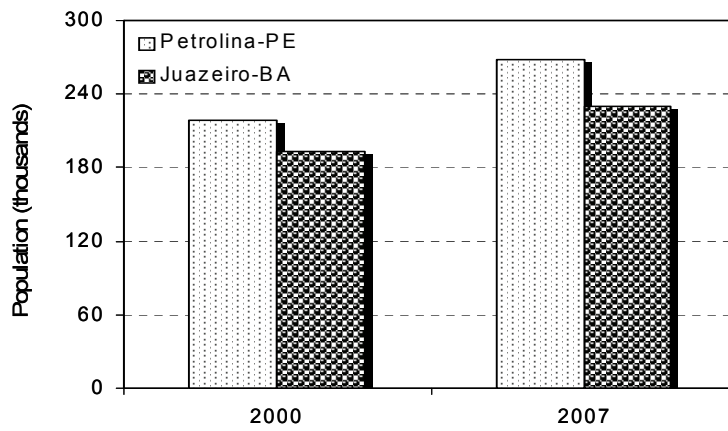
Figure 1.4. Evolution of population for Petrolina-PE and Juazeiro-BA, during the period of 2000-2007. IBGE (2007)

The São Francisco River flows through the six Brazilian states of Table 1.1 and has a basin size of 636,920 km^2. The basin is divided into four physiographic regions: The Upper, the Middle, the Low-Middle and the Lower São Francisco sub basins (Figure 1.5).
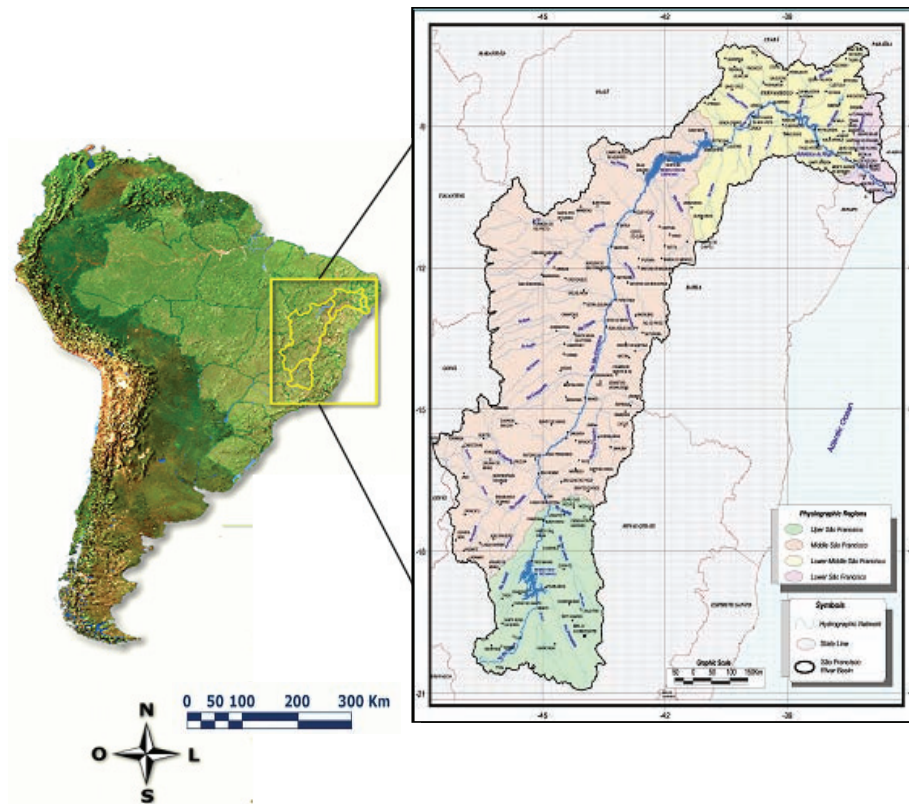
Figure 1.5. Location of the São Francisco River basin and the physiographic boundaries. Source: ANA, 2004

The physical characteristics for each physiographic region are shown in Table 1.2.

Table 1.2: Physical characteristics of the São Francisco River basin by physiographic region. Source: (ANA, 2004).

Characteristic	Upper	Middle	Low-Middle	Lower and Adjacent Coastal Zone
•Area, km^2	99,387	401,559	115,987	19,987
•Area, %	15.6%	63.1%	18.2%	3.1%
•Irrigated area , ha	44,091	170,760	93,180	34,681
•Elevation, m	1,600 to 600	1,400 to 500	800 to 200	(480 to sea level)
•Prevailing climate	Tropical humid and temperate	Tropical semi-arid and sub-humid dry	Semi-arid and arid	Sub-humid
•Mean total P, mm	1,372	1,052	693	957
•Mean annual T, °C	23	24	27	25
•Mean annual ET_0, mm	1,000	1,300	1,550	1,500
•Predominant vegetation cover	Cerrado and forest remnant	Cerrado, "caatinga" and small, high altitude forest	"Caatinga"	Semi-deciduous seasonal forest, mangrove swamps and coastal vegetation

*P, T and ET_0 are pluvial precipitation, air temperature and reference evapotranspiration, respectively.

Land use

The predominant land uses are described in Table 1.2 according to the physiographic region. The Figure 1.6 shows a land use map based on FAO data.
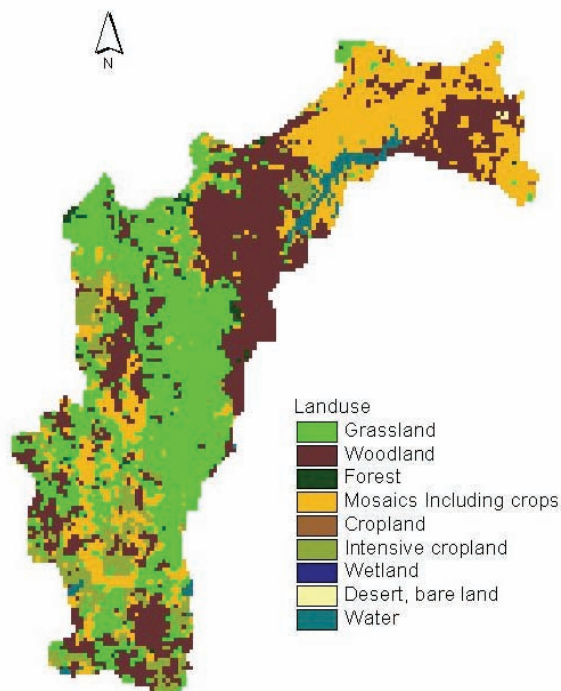
Figure 1.6. Land use map for the São Francisco River basin (Source: FAO, 2007).

It seems that the class "Woodland" could be associated with caatinga (savannah type of vegetation), while "Grassland" could be related to cerrado (extensive savanna formations crossed by gallery forest and stream valleys). The class "Mosaics including crops" could be considered as a mixed area of agricultural crops and natural vegetation. The land use class "intensive cropland" coincides with irrigated areas. While irrigated crops are well supplied with water throughout the growing seasons, the natural vegetation becomes dry and dormant outside the rainy period, being highly non-homogeneous.

Approximately 27% of the land area of the São Francisco River basin is suitable for farming yielding to a 3,000,000 ha that is potentially suitable for irrigation. According to the São Francisco Valley Development Company (Codevasf), this total could be increased to as much as 8,000,000 ha. The irrigated areas in the basin for the year of 1989 are shown in Figure 1.7.

Figure 1.7. Irrigated areas in the São Francisco River basin. Source: ANA/Codevasf, 1989.

The area with fruit crops in the semi arid region of Low-Middle São Francisco River basin are expanding mainly with vineyards and mango orchards. Figure 1.8 shows the five years evolution of harvested areas with these fruit crops in the Pernambuco and Bahia states inside the São Francisco Valley. The linear trend for both crops reveals the continuous increase in irrigated areas. In the last decades, the external market for grapes and mangos increased, although for wine this market is still developing. Brazil is now competitive in these markets and Juazeiro (Bahia State) and Petrolina (Pernambuco State) are good examples of exporting their production to the main world markets.
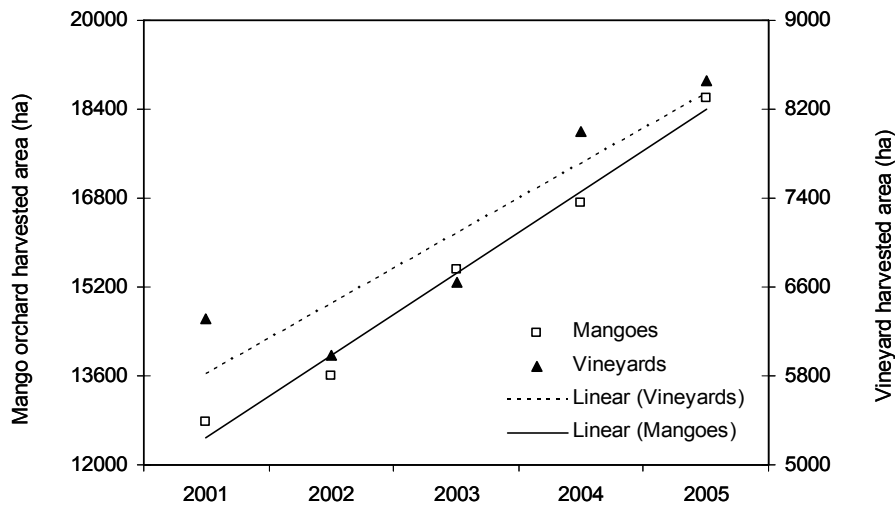
Figure 1.8. Evolution of vineyards and mangos harvested areas in the São Francisco River Valley areas located in the Pernambuco and Bahia states from 2001 to 2005. Source: IBGE, 2007.

Figure 1.8 reveals that water is wisely used and creates a boost for the rural economy, however, agricultural drainage can adversely affect the water quality; both locally and further downstream. With decreasing water quality, all water users (urban, industrial, agricultural, and ecological) will call for an appropriate and fair share of the fresh water resources.

Climate

The upstream region of the São Francisco River basin in Minas Gerais has an average annual precipitation of more than 2,000 mm. In the semi-arid and arid zones of the states of Bahia and Pernambuco, the rainfall amounts to less than 350 mm yr^{-1}. Near the mouth of the river, oceanic influence gradually increases rainfall again to about 1,300 mm yr^{-1}. Most of the precipitation falls during the summer months (December to March), while the rest of the year is dry.

More than 50% of the territory of the São Francisco River basin is located in the semi-arid region of Brazil. This region is situated in the northeastern part of the country. Disturbed currents of South, North, East and West influence the climatology of the Brazilian Northeast. Excluding the areas of high altitude, all semi arid regions in Low-Middle sub-basin present annual averaged air temperatures (T) higher than 24° C, even higher than 26° C in the depressions at 200 to 250m of altitude (Teixeira, 2001). The average maximum air temperature for this sub basin is 33° C and the average minimum is 19° C. The highest recorded air temperature is 42° C. The averaged monthly values are in the range from 17° C to 29° C (Figure 1.9).

January February March
April May June
July August September
October November December

Air temperature (°C)

17 19 21 23 25 27 29
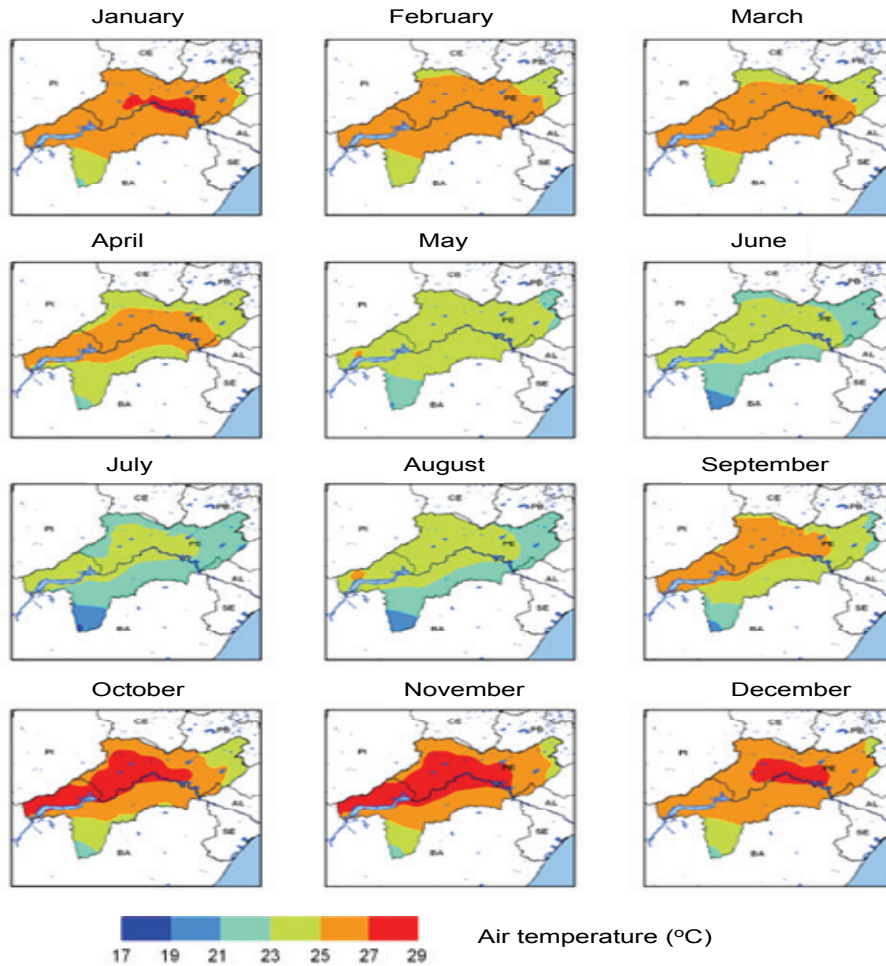
Figure 1.9. Monthly average air temperatures (T) in the Low-Middle São Francisco River basin.
*Interpolated data from 192 stations with series longer than 30 years.

Despite the relatively small thermal annual amplitude due to the proximity of the equator, the increase of T together with higher solar radiation in summer is significant, because the intensification of the evapotranspiration. The warmest months are October and November (21° C – 29° C) when the sun is near the zenith position in the region and the coldest months are June and July (19° C – 25° C) at winter solstice in the southern hemisphere.

The thermal homogeneity strongly contrasts with the spatial and temporal heterogeneity of the precipitation regime (Figure 1.10).

11
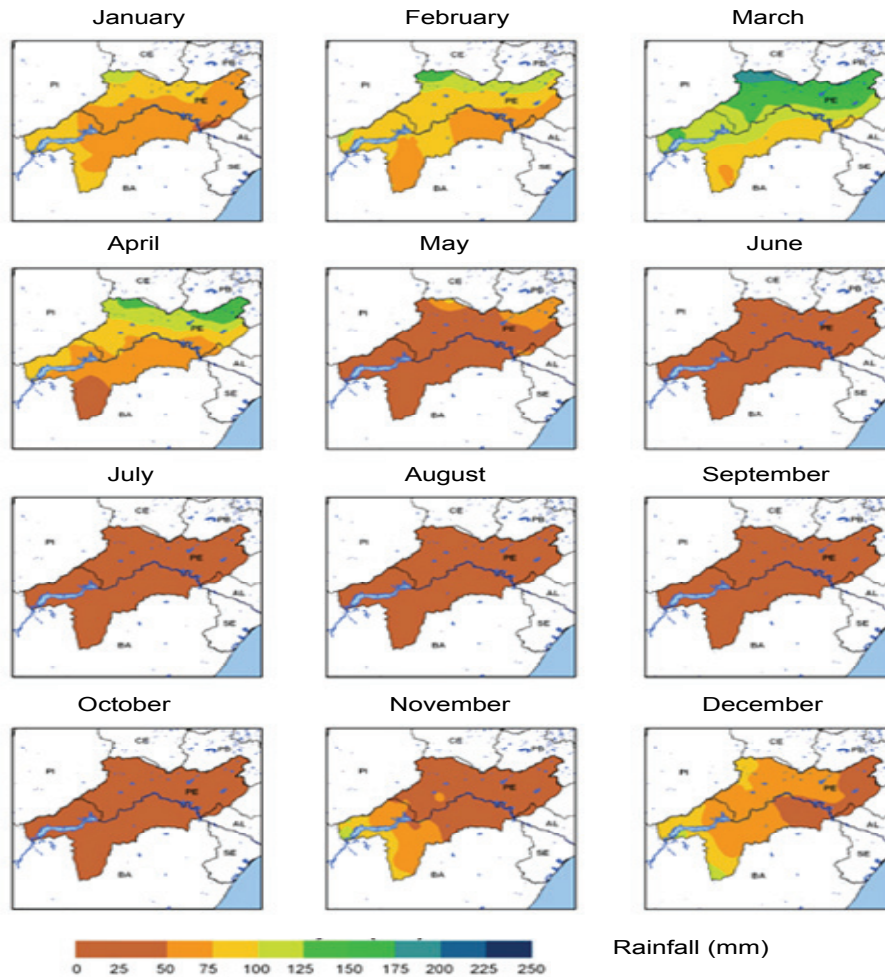
Figure 1.10. Monthly averaged precipitations (P) in the Low-Middle São Francisco River basin.
*Interpolated data from 192 stations with series longer than 30 years.

The long term annual precipitation (P) for the Low-Middle sub-basin is in average 693 mm with 70% of the rainy period concentrated during the months January - April, being March (50 mm - 230 mm) and August (0 mm - 50 mm) the wettest and the driest months, respectively. In the Petrolina-Juazeiro region, the long term rainfall is about 570 mm yr^{-1} with the rainy period from November to April (90% of the annual total), the period January to April representing 68% of the annual amount. As a result of the temporal variability of rainfall, there are water deficits in the climatic water balance along the year, with the exception

of March, when the conditions of this month are rarely dry (Teixeira, 2001).

Hydrology

Considering the São Francisco River flow in the four physiographic regions the average is 2850 m^3 s^{-1}. The river accounts for roughly two thirds of the freshwater available in the entire northeastern region of Brazil. The availability and demand for water by physiographic regions of the São Francisco River basin is shown in Table 1.3.

Table 1.3: Availability and demand for water in the São Francisco River basin: urban, rural, livestock, industry, irrigation and total. Source: ANA, 2003.

Physiographic Region	Area (Km^2)	Flow (m^3 s^{-1})	Urban (m^3 s^{-1})	Rural (m^3 s^{-1})	Livestock (m^3 s^{-1})	Industry (m^3 s^{-1})	Irrigation (m^3 s^{-1})	Total (m^3 s^{-1})
Upper	99,387	1,189	26.8	2.2	2.5	11.4	14.4	57.3
Middle	401,559	1,522	4.6	2.8	3.2	0.8	58.8	70.2
Low-Middle	115,987	111	2.8	2.3	1.4	0.4	50.5	57.4
Lower	19,987	28	1.1	1.4	0.7	0.3	14.4	17.9
Total	636,920	2,850	35.3	8.7	7.8	12.9	138.1	202.8

The Sobradinho Reservoir stores water throughout the year. The highest water demand (68%) comes from the irrigation areas followed by urban demand (Table 1.3). As a consequence of water use, the principal impacts of interactions between water resources and the environment in the São Francisco River basin are widespread pollution caused by agriculture, including discharges into intermittent water courses; uncontrolled discharges and inadequate disposal of solid wastes; and water shortages owing to the intermittent nature of tributaries.

1.3 Research objectives

This thesis is meant to investigate the accuracy of a selected energy balance model based on remote sensing together with agro-meteorological data, and to assess on how it can be used in monitoring and planning of irrigation systems at local and regional scales in the São Francisco River basin. The general objectives are:

1) Determination of model parameters associated with energy transfers from irrigated crops and natural vegetation, which can be useful in guiding the calculation of actual evapotranspiration and water productivity at field and regional scales.

2) Assessment of the overall level of confidence of using energy balance models for irrigation management of fruit trees.
3) Calibration and validation of an existing package of remote sensing-based surface energy balance equations for the conditions encountered in the Low-Middle Sao Francisco River basin aiming future regional scale studies in the entire basin.
4) Quantification of the net water withdrawals in the Low-Middle São Francisco River basin by assessing the incremental evapotranspiration between natural vegetation and irrigated crops.
5) Provision of benchmark values of biomass of natural vegetation and crop water productivity in irrigated crops in the Low-Middle São Francisco River basin.

1.4   Thesis outline

An overview of the theory concerning evapotranspiration, crop production and crop water productivity will be given in Chapter 2. The methods used to calculate actual evapotranspiration will be reviewed and the use or remote sensing to upscale these calculations for water productivity analysis will be highlighted in this chapter.

In Chapter 3, some background understanding of attainable yields, water consumption and water productivities of vineyards and mango orchards will be provided. The water situation in Brazilian fruit vineyards and mango orchards will be compared to the practices of other producing countries. This chapter will describe therefore the overall situation of these crops from the perspective of climatology, area and production statistics. Applications of field measured crop coefficients in vineyards and mango orchard together the reference evapotranspiration will allow crop water productivity analyses of these fruit crops in some municipal districts of the Brazilian states inside the Low-Middle São Francisco River basin aiming to support programs of expansion of irrigated areas alongside natural vegetation.

In Chapter 4, detailed descriptions will be made about the energy and water balances field experiments in wine grape, table grape, mango orchard and natural vegetation together with the agro-meteorological stations used for reference evapotranspiration and SEBAL calculations. Also the Landsat satellite images used for regional water productivity analyses will be described in this chapter.

In Chapter 5, crop water parameters of irrigated wine and table grapes will be investigated to support water productivity analyses in the Low-Middle São Francisco River basin, Brazil. Water parameters related to evapotranspiration for wine and table grapes growing under different trellis and irrigation systems will be studied in this chapter. Albedo, evaporative fractions, beneficial/non-beneficial water consumption, aerodynamic resistance, bulk surface resistance and canopy resistance will be derived from the field data set and compared with the international literature. The results will allow expressing water consumption from vineyards in more specific bio-physical parameters, rather than in crop coefficients that lump together other crop water parameters. Up-scaling of these data sets will be done in Chapter 8 to analyze incremental evapotranspiration due to irrigation and to provide benchmark values of vineyards water productivity at a regional scale.

In Chapter 6, measurements of energy and water balance for water productivity analyses in irrigated mango trees will be analysed in the Low-Middle São Francisco River basin, Brazil. Useful recommendations for a rational and strategic water management in this orchard will be described. Crop water parameters, including actual evapotranspiration, transpiration, soil evaporation, crop coefficients, evaporative fractions, aerodynamic resistances, surface resistances and percolation fluxes will be estimated. The results presented in this chapter will be important for irrigation management, water allocation, water savings and environmental sustainability of irrigated mango orchards. Also, quantifying water productivity at field scale will be useful in subsequent upscaling study what will be dealt in Chapter 8.

In Chapter 7, Analyses of energy fluxes and vegetation-atmosphere parameters in irrigated and natural ecosystems in the semi-arid region of the São Francisco River basin will be done. Improved parameterizations of radiation and energy balances will be reviewed. The diurnal and seasonal variations of these balances will be investigated. These investigations will allow a better understanding of the energy fluxes and the physical vegetation properties that affect these exchange processes. Analytical relationships will be derived which will be useful to predict spatial variation of evaporation resistances in a river basin context and these parameters are important in crop water productivity analyses from field to regional scale.

In Chapter 8, the SEBAL input parameters will be calibrated and validated with field data and regional actual evapotranspiration, biomass production and crop water productivity will be assessed for the Low-Middle São Francisco River basin. It will be demonstrated that satellite measurements, combined with agro-meteorological data, are useful to determine evaporative depletion and biomass production for irrigated land and natural vegetation. The net water withdrawals will be also quantified by assessing the incremental evapotranspiration between natural vegetation and irrigated crops and the crop water productivity will be quantified for three representative producer farms of wine grapes, table grapes and mangos in the semi-arid conditions of the São Francisco River basin.

Finally, in Chapter 9, the results of this study will be summarized with conclusions and recommendations to improve the evaluation of different irrigation schemes in terms of crop water productivity and their impact on water resources, by the intensification of agriculture in the semi-arid region of Brazil.

2. Background on crop water consumption and productivity

2.1 Evapotranspiration

General

The physical process whereby water flows from evaporating surfaces into the atmosphere is referred to as actual evapotranspiration (ET_a). This water flux occurs via canopies through stomata as actual transpiration (T_a) and directly from the soil surface as actual evaporation (E_a). Stomata are small openings on the plant leaf through which gases and water vapour pass (Figure 2.1). The vaporization occurs within the leaf, in the intercellular spaces, and the vapour exchange with the atmosphere is controlled by the stomatal aperture. The stomatal aperture can be open and closed, depending on the pressure of the guard cell. Nearly all soil water taken up by roots is lost by T_a and a negligible fraction is used within the plant. Not only the type of crop, but also the crop development, environment, cultural management and irrigation system should be considered when assessing T_a.
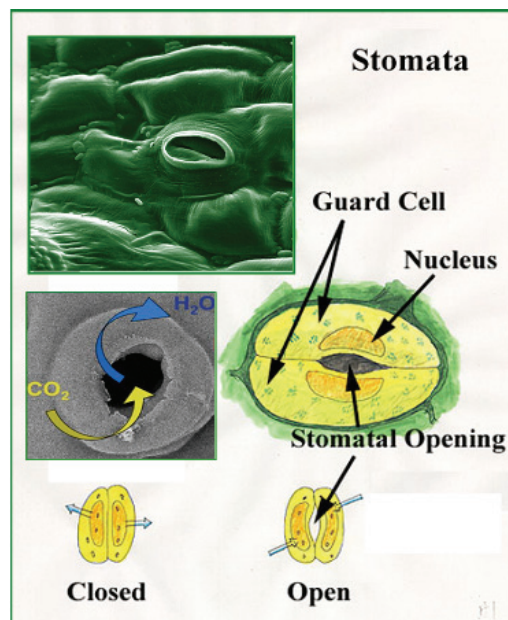
Figure 2.1. Schematic representations of stomata (Sources: Wikipedia/www.puc.edu/ksjtracker.mit.edu).

Distinctions are made between reference crop evapotranspiration (ET_0), potential evapotranspiration (ET_p) and actual evapotranspiration (ET_a). ET_0 is the evapotranspiration rate from a reference surface, not short of water, which can be a hypothetical grass surface with specific characteristics. ET_p may be referred as the water flux from crops that are grown in large fields under optimum soil moisture, excellent management and environmental conditions, and achieve full production under the given climatic conditions. ET_a involves all conditions of the vegetated surface. Due to sub-optimal crop management and environmental constraints that affect crop growth and limit evapotranspiration, ET_a is generally smaller than ET_p (Allen et al., 1998).

The capability to predict levels of ET_a is a valuable asset for water resource managers, as it describes the water consumption from vegetation. Water consumption is paramount information for irrigation supply planning, water rights regulation, and river basin hydrologic studies. Agro-meteorological parameters, crop characteristics, management and environmental aspects are factors affecting ET_a. Other factors to be considered are ground cover, plant density, plant architecture, microclimate and soil moisture. Cultivation practices and the type of irrigation system can alter the microclimate, affecting the crop characteristics and the wetting of the soil and canopy. The effect of soil moisture on water fluxes is primarily conditioned by the magnitude of the water deficit and the type of soil. On the other hand, too much water will result in water logging which might damage the root and limit root water uptake by inhibiting respiration. Accurate estimations of ET_a reduce uncertainties in water balances and facilitate the allocation of water resources in river basins.

The evapotranspiration process is an energy consuming process, referred to as the latent heat flux (λE). ET_a can be derived from the latent heat of vaporization (λ), density of water and λE. As a first approximation, an ET_a of 1 mm d^{-1} is equivalent to λE of 28 W m^{-2}. ET_a is therefore the chain between the water and energy balances. All energy fluxes should be considered when deriving the energy balance equation, which for a given surface can be written as:

$$R_n - \lambda E - H - G = 0 \qquad (2.1)$$

where R_n is the net radiation, H is the sensible heat flux and G is the soil heat flux. All terms in Equation 2.1 can be expressed in W m^{-2} or MJ m^{-2} d^{-1}, being either positive or negative. Positive R_n means energy flux to

the surface and positive G, λE and H indicate fluxes of energy from the surface. The Equation 2.1 states that the R_n is redistributed over H, λE and G, considering only vertical fluxes and ignoring the net rate at which energy is being transferred horizontally, by advection; however this term can be significant near the edges of crops or natural vegetation (Garrat, 1992). Therefore it is accurate only when applied to large, extensive surfaces. Other energy terms, such as heat stored or released in the canopies, or the energy used in metabolic activities, are not considered. These last terms account only for a small fraction of the daily net radiation ($R_{n_{24}}$) and can be neglected in hydrological studies. In the rest of this thesis, this simplified version of the energy balance will be considered.

In field conditions R_n can be measured from pyrgeometers and pyranometers or from net radiometers above the vegetated surface. The H and λE can be determined directly by available energy, the gradients of temperature and humidity and the aerodynamic transfer coefficient (Shuttleworth, 1991). Generally, in field experiments G is measured with flux plates buried at the soil surface or together thermocouples at different soil depths.

The energy available to warm up soil induces a temperature gradient between the land surface and the sub-surface (ΔT_g) during daylight hours. Because of this gradient, a heat flux into the soil is established which can be computed as:

$$G = \lambda_g \frac{\Delta T_g}{\Delta z_g}$$

(2.2)

where λ_g is the soil thermal conductivity (W m^{-1} K^{-1}), T_g is the soil temperature (K) and z_g is the soil depth (m). Given a certain amount of energy at the soil surface, G depends predominantly on thermal soil properties, which are a function of soil composition and soil moisture content (Ten Berge, 1990).

Atmosphere also warms up when R_n is positive. Heating of the atmosphere occurs from the land surface, thus the surface temperature (T_0) during daylight hours exceeds the air temperature (T). H is the rate of heat loss to the air by convection and conduction, due to a temperature difference, being expressed by the following equation for heat transport (Monteith, 1973):

$$H = \frac{\rho_a c_p \Delta T}{r_a}$$ (2.3)

where ρ_a is air density (kg m^{-3}), c_p is air specific heat at constant pressure (J kg^{-1} K^{-1}), ΔT (K) is the temperature difference between two heights, and r_a is the aerodynamic resistance to heat transport in the boundary above the land surface (s m^{-1}) applicable to the same two heights.

λE can be determined as:

$$\lambda E = \frac{\rho_a c_p}{\gamma} \left[\frac{e_s(T_0) - e_a}{r_a + r_s} \right]$$ (2.4)

where γ is the psychrometric constant (kPa °C^{-1}), e_a is the actual water vapour pressure of the air at the reference height (z) above the surface (kPa), r_s is the surface resistance from the vegetation, $e_s(T_0)$ is the saturated water vapour pressure (kPa) at the surface temperature T_0.

Penman (1948) combined the transfer equation for H (Equation 2.3) and λE (Equation 2.4) into the surface energy balance, and developed by doing so his world wide accepted combination equation for open water evaporation. Monteith (1965) continued the work of Penman, and modified it into a version that can be applied to the vegetated surfaces by inserting a canopy resistance. The Penman-Monteith combination equation can be used for directly determining λE. This method requires routine weather data and the two evaporation related resistances r_a and r_s:

$$\lambda E = \frac{\Delta(R_n - G) + \rho_a c_p \dfrac{(e_s - e_a)}{r_a}}{\Delta + \gamma(1 + \dfrac{r_s}{r_a})}$$ (2.5)

where (e_s - e_a) represents the vapour pressure deficit of the air (kPa) and Δ is the slope of the saturation vapour pressure temperature relationship (kPa °C^{-1}).

The difficulty of using Equation 2.5, especially at regional scale, is the estimation of r_a and r_s (Menenti and Choudhury, 1993; Jia, 2004). Differences in crop height and leaf area index (LAI) determine crop roughness and thereby r_a. Crop rooting characteristics, root water uptake

and LAI describe the value of canopy resistance (r_c). With the availability of the evaporation resistances, ET_a can be derived from agro-meteorological data by means of Equation 2.5 The absence of values on r_a and r_s, makes the Penman-Monteith equation difficult to implement in operational hydrology and water management studies. This shortcoming has been solved in the irrigation community by introducing the concept of crop reference ET and a crop coefficient.

Resistance approach

The transfer of heat and water vapour from the evaporating surface into the air above the canopy is determined by r_a, which can be estimated using flux profile relationships (FP) or eddy correlation measurements (EC). The atmospheric surface-layer similarity theory is applied in both situations to estimate the roughness elements related to mechanically generated turbulence. The universal functions suggested by Businger et al. (1971) and the integrated stability functions of temperature (Ψ_h) and momentum (Ψ_m) can be applied. For unstable situations the following stability functions are used:

$$\psi_h\left(\frac{z-d}{L}\right) = 2\ln\left(\frac{1+x^2}{2}\right), \text{ with } x = \left(1-16\frac{z-d}{L}\right)^{\frac{1}{4}} \qquad (2.6)$$

$$\psi_m\left(\frac{z-d}{L}\right) = 2\ln\left(\frac{1+x}{2}\right) + \ln\left(\frac{1+x^2}{2}\right) - 2\arctan(x) + \frac{\pi}{2} \qquad (2.7)$$

For stable situations, the equation below is applied:

$$\psi_h\left(\frac{z-d}{L}\right) = \psi_m\left(\frac{z-d}{L}\right) = -5\frac{z-d}{L} \qquad (2.8)$$

where z is the height above the surface, d is the zero plane displacement height and L is the Obukhov length. This last stability parameter can be obtained applying the following equation:

$$L = -\frac{\rho_a\, c_p\, u_*^3\, T}{k\, g\, H} \qquad (2.9)$$

21

Where u_* is the friction velocity (m s^{-1}), k is the von Karman's constant (0.41) and g is the gravitational constant (9.81 m s^{-2}).

The roughness length for moment transfer (z_{0m}) can be calculated by:

$$z_{0m} = \frac{z-d}{\exp\left[\dfrac{k\ u}{u_*} + \psi_m\left(\dfrac{z-d}{L}\right)\right]} \qquad (2.10)$$

where u is the horizontal wind speed at one level (z) above the vegetation.

The r_a (s m^{-1}), that is a turbulence parameter expressing the momentum present between two vertical levels is then expressed as:

$$r_a = \frac{\ln\left[\dfrac{z-d}{z_{0h}}\right] - \psi_h}{ku_*} \qquad (2.11)$$

where z_{0h} is the roughness length governing transfer of heat and vapour that can be estimated as a function of z_{0m}.

The magnitude of r_s is mainly governed by environmental entities and soil moisture status (Jarvis, 1976; Stewart, 1989). Where the vegetation does not completely cover the soil, the r_s includes the effects of E_a. With field values of λE and r_a, r_s can be estimated inverting the general Penman-Monteith equation (Equation 2.5). In this thesis the influence of r_a and r_s on ET_a and the effect of soil moisture and climatic parameters on these resistances will be discussed.

Crop coefficient approach

Values of ET_a can deviate from ET_p due to the presence of pests and diseases, soil salinity, low soil fertility, water shortage or water logging. This deviation from the optimum conditions affects the productivity and quality of the harvested products. The effects of characteristics that distinguish field crops from grass are integrated into the crop coefficient (K_c). The ET_p is estimated by multiplying ET_0 by K_c. ET_0 is calculated by Equation 2.5 with resistance values for the reference surface. The upper envelope of ET_a/ET_0 values during a growing season may represent the seasonal behaviour of K_c and values of this coefficient

are often published in tables (e.g. Snyder et al, 1989; Allen et al. 1998; Consoli et al., 2006). The crop evapotranspiration under non-potential conditions can be estimated by using a water stress coefficient (K_s) and/or by adjusting K_c for all kinds of other stresses and environmental constraints on ET_p (Allen et al., 1998).

According to Allen et al. (1998), differences in soil evaporation and transpiration between field crops and the reference grass surface without water stress can be integrated into two coefficients: a basal crop coefficient (K_{cb}) and a soil evaporation coefficient (K_e), i.e., $K_c = K_{cb} + K_e$. When the interval between rains or irrigation increases, the soil moisture drops reducing E_a. After rainfall or irrigation, the effect of E_a is predominant when the crop is small and scarcely shades the ground. In these conditions, the ratio ET_a/ET_0 is determined largely by the frequency of rainfall events and irrigation. Where the soil is wet for most of the time from irrigation or rain, E_a is considerable and ET_a/ET_0 may exceed 1. For the evaluation of T_a and E_a, the crop coefficients K_{cb} (basal coefficient) can be applied using measured daily fluctuations of ET_a/ET_0 during a growing a season (Teixeira et al., 2007, 2008a). Minimum values of this last ratio can be used to fit a curve of K_{cb} for obtaining T_a values, while E_a is the difference between ET_a and T_a. Hence:

$$T_a = K_{cb}ET_0 \qquad\qquad (2.12)$$

$$E_a = ET_a - T_a \qquad\qquad (2.13)$$

Field measurements of actual evapotranspiration

Due to large rooting depths, the ET_a measurements in trees are very difficult to be made with weighing lysimeters and soil water balance. There are considerable uncertainties related to the measurements of the depth of soil affected by root water uptake, percolation, runoff and capillarity rise. According to Rana et al (2005), the use of the soil water balance to determine ET_a is not ideal, especially in the case of discontinuous crops, and in regions subjected to semi-arid climates. Separating T_a and E_a may be approached in several ways, all of them with its advantages and disadvantages. Direct measurements of T_a can be performed with the heat pulse-sap flow technique, which has been applied in vineyards (Yunusa et al., 2004) and olive groves (Testi et al., 2006). This method may give good results, but is affected by individual

tree variability. Micro-meteorological methods for ET_a measurements, as Bowen ratio (BR) and eddy correlation (EC), do not have these limitations and together estimations of ET_0, Equations 2.12 and 2.13 can be used for water fluxes separation (Teixeira et al., 2007; Teixeira et al., 2008a).

The Bowen ratio method has been applied in agricultural crops and natural vegetation (Heilman et al., 1996; Scott et al., 2003; Inman-Bamber and McGlinchey, 2003; Lee et al., 2004; Teixeira et al., 2007). Examples of eddy correlation measurements can be found in Oliver and Sene (1992), Sene (1994); Trambouze et al., 1998; Cleverly et al., 2002; Humphreys et al., 2003; Lund and Soegaard, 2003; Prueguer et al., 2004; Villalobos et al., 2004; Testi et al., 2004; Simmons et al., 2007, Teixeira et al., 2008a,b). Meijninger and De Bruin (2000) and Meijninger et al. (2002) showed examples on how λE can be measured by means of scintillometers across a path length of several kilometres. Comparisons between methods of λE measurements were carried out (Unland et al., 1996; Spano et al., 2000, Beringer and Tapper, 2000; Olejnik et al., 2001; Azevedo et al., 2003; van Dijk et al., 2004; Ortega-Farias et al., 2007; Simmons et al., 2007). The basic conclusion of these comparisons is that at daily time scales or longer the differences between methods are reduced. In relation to comparisons of eddy correlation systems with other methods, the lack of energy balance closure is the main reason for the differences at shorter time scales.

All these field methods however provide values for specific sites and fail to estimate the ET_a at a regional scale. The spatial variability is significant and the variation is caused by different amounts of precipitation, seepage, flooding, irrigation, hydraulic characteristics of soils, vegetation types (expressed as leaf area, moisture sensitivity, rooting depth) and densities. The temporal changes in ET_a can be ascribed to weather conditions and vegetation development. Directly extrapolation of energy balance data from flux towers to a surrounding landscape environment can lead to inaccurate regional estimates, because a few tower sites cannot provide a fair sample of a whole biome (Pelgrum and Bastiaanssen, 1996; Wylie et al, 2003). A similar hydrological problem occurs with rainfall. A few gauge reading will not necessary reflect a proper reference value for a region.

Remote sensing modelling of actual evapotranspiration

The difficulties to measure regional scale water balance prompted the use of remotely sensed data from satellites to evaluate ET_a from composite terrain. Remote sensing excludes the need to quantify other complex hydrological processes, being an excellent means for determining and mapping the spatial and temporal structure of the energy balance components. Another advantage is that the ET_a populations of a given land use type is feasible, making the spatial variation in irrigated crops very well described. Hydrological models can be too complex and costly because of non availability of data sets in different hydrological uniform sub-areas (Majumdar et al., 2007) and with a lack of input data, these models can yield to ill-defined results. Studies showed that the oversimplification of land surface complexity may cause eco-hydrological models to be considerably biased (Michell et al., 2005). Yet, one of the biggest impediments to global, multi-temporal ET_a monitoring is the conflicting requirement for algorithms that are biophysically realistic – albeit – simple enough for global parameterization and implementation (Cleugh et al., 2007). According to Nagler et al. (2005a), if species-specific algorithms were needed to scale tower data to larger areas, detailed, species-level vegetation maps of each river stretch would be also needed. These are difficult to construct even with high-resolution aerial photography.

Jackson et al. (1977) was one of the major pioneers in determining ET_a by remote sensing, with the use of infrared thermometry for the estimation of wheat water consumption. After this, several methods using remote sensing for regional ET_a calculations have been applied (Kustas and Norman, 1996; Roerink et al., 1997; Liu et al, 2003; Boegh et al., 2004; Van Niel and McVicar, 2004; Cleugh et al., 2007, Kimura et al., 2007; Majumdar et al., 2007; Akbari et al., 2007) and for obtaining crop coefficients (Gutman, 1999; Hunsaker et al., 2003; Hunsaker et al., 2005; Duchemin et al., 2006; Tasumi and Allen, 2007; Er-Raki et al., 2007; Wang et al., 2007; Kimura, 2007; Sobrino et al., 2007).

Liu et al. (2003) reported that adequate calculations of regional ET_a should enhance the reliability of runoff estimations for watersheds in supporting hydroelectric power generation. Allen et al. (2005) provided an overview of potential remote sensing applications in Western US states, involving net depletion of river flows, administering water rights, crop water requirements and irrigation management. Moller et al, (2007)

25

demonstrated the effectiveness of using very high resolution Visible and Thermal Infrared images in an Israeli vineyard for scheduling irrigation. Evapotranspiration maps have been used to improve regional water resource management and to help resolve water rights conflicts (Allen et al., 2007b). Naor (2006) concluded that Thermal Infrared measurements enable growers to produce maps of relative water stress in orchards, however, according to Kustas et al. (2006), the remote surface temperature and vegetation cover must be at high enough resolutions where different land surface conditions can be distinguished, being important the validation of flux distributions predicted by land surface models.

Procedures for the validation of regional energy balance models with remote sensing data have been carried out (Bastiaanssen et al., 1998b; Havstad et al., 2000; Roerink et al., 2000; Hemakumara et al., 2003; Jia et al., 2003; Brunsell and Gillies, 2003; Liu et al., 2003; Boegh et al., 2004; Pellenq and Boulet, 2004; Nagler et al., 2005a; Su et al., 2005; Leuning et al., 2005; Batra et al. 2006; Kustas et al., 2006; Cleugh et al., 2007; Nagler et all, 2007; Tasumi and Allen, 2007; Er-Raki et al., 2007). Research on the validation primarily involved comparisons with energy balance measurements from tower-based systems using eddy correlation and Bowen ratio methods. Data from flux stations can make a valuable contribution to increase the confidence in remote sensing techniques; however, it is also possible to validate the remote sensing results with regional scale water balances.

Among the satellite-based ET_a models developed during recent years is the SEBAL (Surface Energy Balance Algorithm for Land) for heterogeneous surfaces. This model involves the spatial variability of the most agro-meteorological variables and can be applied to various ecosystems (Bastiaanssen et al., 1998b, 2000, 2001, 2002, 2005, 2008a). SEBAL requires spatially distributed, visible, near-infrared and thermal infrared data together with routine weather data. The algorithm computes R_n, H and G for every pixel of a satellite image and λE is acquired as a residual in energy balance equation (Equation 2.1). This is accomplished by first computing the surface radiation balance, followed by the surface energy balance. Although SEBAL has been designed to calculate the energy partition at the regional scale with minimum ground data, according to Duchemin et al. (2006) calibration of any remote sensing algorithm can improve the accuracy of λE estimations. One of the arguments for selecting SEBAL for ET_a calculations is that crop classifications can be omitted. The identification of fruit trees from

satellite data is not straightforward (Menenti et al., 1996). Noordman et al. (2003) reported unresolved problems for multi-spectrally identifying different fruit crops in the semi-arid region of São Francisco River basin in Brazil. Bastiaanssen et al. (2008a) confirmed that it is easier to determine ET_a on the basis of thermal infrared imagery, rather than through the laboursome procedures of crop classification.

2.2 Crop production

Estimations of crop production at regional scales are becoming more important in both developing and developed countries for supporting policy planning and decision-making in agriculture. The need for crop production modelling is increasing with climate changing and the current emerging crisis in food security, due to the growing world population and the conversion of crop land into biofuels, among others. Regional estimates of crop yield are important for managing large agricultural lands (Macdonald and Hall, 1980; Hutchinson, 1991). The main ways to estimate crop production include remote sensing-based calculations, crop growth models, agro-meteorological models, and statistical sampling methods (Dadhwal and Ray, 2000; Baez-Gonzalez et al., 2002; Prasad et al., 2006). Remote sensing technology provides a suitable alternative for large scale analyses.

Agriculture is concerned with the conversion of solar energy to energy usable by people for food, fibre, and fuel. The total amount of energy captured by the plants used in photosynthesis usually amounts to only 1 or 2% of the total solar energy input. Biomass production (BIO) is associated with photosynthetically active radiation (PAR) that is part of the short wave solar radiation which is absorbed by chlorophyll for photosynthesis in the plants, regulating primary productivity, or the rate of carbon fixed by the plants. The raw materials and the end products of photosynthesis can be summarized in the following chemical equation:

$$nCO_2 + 2nH_2O + \text{light energy} \rightarrow (CH_2O)_n + nH_2O + nO_2 \quad (2.14)$$
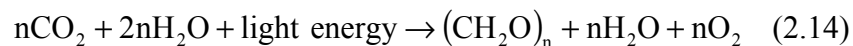
According to Equation 2.14, if we assume 6 molecules of carbon dioxide (n = 6), 12 molecules of water, and sufficient light energy will yield 1 molecule of glucose, 6 molecules of water vapour and 6 molecules of molecular oxygen. This statement does not show the true complexity of the process, for dozens of contributory biochemical processes and energy exchanges which take place during the photosynthetic process.

27

In a gross manner, respiration can be characterized as the reverse of the simplified photosynthetic equation. Of the energy released and made available by respiration, part is lost as heat and part is utilized in biosynthesis and chemical work. To a large extent the net amount of energy incorporated into organic matter represents the difference between photosynthesis and respiration. Respiration in plants has been examined in terms of two conceptual components – growth and maintenance (Loomis and Amthor, 1999), both requiring a high proportion of carbohydrates, which are part of the total production. Growth respiration is considered as the energy source for the synthesis of new phytomass. Maintenance respiration supplies energy to maintain current phytomass. Through photosynthesis plants utilize light energy to form sugars, which are then broken down by the respiration process, releasing the energy required by plant cells for growth and development. The growth of plants is a function of the efficiency with which they produce dry matter. This involves the efficiency with which they capture solar radiation and the efficiency with which they transform it into organic matter. One important factor that determines the actual photosynthetic efficiency of a leaf is the manner in which the rate of photosynthesis changes with radiation intensity. The rate of photosynthesis changes with radiation intensity only up to a certain point. At this intensity the leaf is light-saturated.

Solar radiation may pass through only a few layers of leaves in low crops but may pass through as many as 15 or 20 layers in tropical forests, where 95% of the solar radiation may be absorbed before reaching the ground. In natural vegetation stands the amount of light reaching the lower leaves is below the compensation point – that light intensity required to maintain a rate of photosynthesis equal to the rate of respiration. Low crops, with leaves in a relatively narrow zone close to the ground, seem to be more efficient producers than natural vegetation, in which leaves are spread over a wide range of heights. This is because in low crops a smaller percentage of leaves are exposed to solar radiation below the compensation point. Moreover, trees have a more extensive transportation system through which the compounds move and the movement of compounds requires much energy.

The plant's source of carbon dioxide is the atmosphere. Carbon dioxide enters the plant through the stomata in the leaves, and this is where it can be seen why transpiration represents a compromise to photosynthesis for the plant. Plants have control over whether the stomata are open or closed. They are closed at night and open in response

to the increasing light intensity that comes with the morning sun. The plant begins to photosynthesize and the stomata open in order to allow more carbon dioxide into the leaf (Figure 2.1). As light intensity increases, so does leaf temperature, and water vapour is lost from the leaf. The compromise with photosynthesis occurs when the heat stress in the environment causes such a loss of water vapour through the stomata that the movement of carbon dioxide into the leaf is reduced. The other factor involved with this process is the water vapour pressure gradient between the leaf and the atmosphere. The transpiration stress on a leaf, and the plant at any given temperature, is greater at lower air humidity. There is also a point where the transpiration stress on the plant can be so great that the stomata close and photosynthesis stops completely.

The energy captured in photosynthesis is represented in part by the total dry matter on a unit area of the earth's surface at any given time. Dry matter production or biomass production refers to organic matter on an oven-dry-weight basis. Even though a crude measure, biomass is useful for making comparisons of different crops and different land areas. An important step towards quantifying the net production (dry matter minus respiration) is the net CO_2 uptake in crop systems, termed net primary production (NPP) or biomass production (BIO). According to Field et al. (1995), in terms of gas exchange, BIO can be defined as:

$$BIO = GPP + R_{aut} \qquad\qquad (2.15)$$

where GPP (gross primary production) is the carbon fixed during the photosynthesis and R_{aut} is autotrophic respiration. BIO is the sum of GPP and R_{aut} when GPP and R_{aut} have opposite signs.

For obtaining estimates of carbon balance the light-use efficiency concept devised by Monteith (1972, 1977) and Kumar and Monteith (1981), and modified by Prince (1990) can be applied:

$$BIO = \varepsilon \, f \, PAR \qquad\qquad (2.16)$$

where ε is the light use efficiency, f is the ratio of absorbed (APAR) to incident (PAR) photosynthetically active radiation

The slope of the linear regression between BIO and cumulative PAR intercepted by a crop has been used to determine the light use efficiency – ε (e.g. Muchow et al., 1993; Muchow and Sinclair, 1994; Ceotto and Castelli, 2002; Tesfaye et al., 2006). This relationship is also

employed to develop simple crop models. Russell et al. (1989) expressed yield as a function of radiation intercepted by the crop (APAR), ε, and a harvest index (HI). Radiation interception is variable throughout a crop growing period (Sivakumar and Virmani, 1984; Watiki et al., 1993, Tesfaye et al., 2006, Teixeira et al., 2007). Comparisons of species with respect to photosynthetic processes indicate that C4 species have higher ε than C3 species (Gosse et al., 1986). Reductions in ε due to water deficits have been reported (e.g. Hughes and Keatinge, 1983; Muchow, 1985; Green et al., 1985; Singh and Sri Rama, 1989). Typical legumes c3 crops are soybeans, pigeon pea, groundnut, cowpea, lucernes, etc. Typical non-legumes c3 crops are wheat, rice, cotton, barley, sunflower, oats, rye, alfalfa, pastures, sugar beet, potato, orchards, eucalyptus, etc. Typical c4 crops are sorghum, millet, sugarcane and maize. In general, ε is stable across environments under optimal growing conditions (Sinclair and Muchow, 1999), because it is a relatively constant property of plants. Light harvesting can be adjusted to the availability of resources needed to use the absorbed light (Monteith, 1977; Bloom et al., 1985; Russell et al., 1989; Field et al., 1995).

Several more sophisticated crop models have been developed in order to optimize agricultural management, but also to investigate the effect of climatic variability and soil hydrology on crop yields. They in general employ data of plant phenology and physiology, and have been applied over different scales, from point (Eitzinger et al., 2004) to regional scales (Saarikko, 2000; Boogaard et al., 2002), resulting in laborious parameterization and calibration. Reviews about the general features and mechanisms of process-based crop models are provided by Tubiello and Ewert (2002) who focus on the effects of elevated CO_2 concentrations and by Lipiec et al. (2003) who deals with crop growth, water movement and solute transport. The farmer decision making together with spatial variations in soil, hydrology and weather conditions makes parameterisation of these models a difficult task. To avoid this problem, empirical models have been developed for global scale applications (Fischer et al., 2002; Leemans and van den Born, 1994, Gervois et al., 2004; Osborne et al., 2007, Bondeau et al., 2007). Ecological planning models have been used to assess the availability of additional land for agriculture (e.g. Kenny et al., 2000; Fischer et al., 2002), to investigate the impact of climate change on future land use (Alcamo et al., 1998) or on future economic welfare (Matsuoka et al., 2001).

Monteith and Scott (1982) analyzed crop yield accounting temperature effects on leaf area development and crop ontogeny, and solar radiation effects on BIO. This approach was also used to study the influence of temperature and solar radiation on crop yield under optimum conditions for soybean (Spaeth et al., 1987), corn (Muchow, 1990), wheat (Amir and Sinclair, 1991), and rice (Sheehy et al., 2004; Pirmoradian and Sepaskhah, 2005). Temperature influences incremental BIO at each time-step and, via accumulation of growing degree-days, the total duration of crop stages. This causes a complicated overall effect on final crop yield as higher temperatures often increase daily production, but leave less time for the plant to grow. Therefore the optimum temperature for total yield is lower than the optimum temperature for daily BIO, assuming constant temperature over the entire growth period (Stehfest et al., 2007).

Satellite remote sensing is an efficient tool for crop area and BIO estimates because it provides spatial and temporal information on the location and state of vegetation (Kumar and Monteith, 1981; Moulin et al., 1998). However, successful use of remote sensing requires that remotely measured radiance can be related to physical plant properties and that these properties can then be related to BIO or yield. BIO is directly related to yield according to the fraction of plant biomass that is harvested (harvest index, HI) and the carbon fraction of biomass by weight (~45%, Schlesinger, 1997). To estimate crop yield by satellite data, a commonly applied method is the development of empirical relationships between the Normalized Difference Vegetation Index - NDVI, and actual crop yield - Y_a (e.g. Groten, 1993; Sharma et al., 2000), being NDVI defined by:

$$NDVI = \frac{\alpha_{p(NIR)} - \alpha_{p(VIS)}}{\alpha_{p(NIR)} + \alpha_{p(VIS)}}$$

(2.17)

where $\alpha_{p(NIR)}$ and $\alpha_{p(VIS)}$ represent the planetary albedo over ranges of wavelengths in the near infrared (NIR) and visible (VIS) regions of the solar spectrum, respectively.

To obtain the coefficients of the relationship of NDVI and Y_a, excessive field measurements need to be done, which at the regional scale are difficult and expensive. Hamar et al. (1996) established a linear regression model to estimate corn and wheat yield at a regional scale based on vegetation indices computed with Landsat MSS data. Maselli

and Rembold (2001) demonstrated the potential of using multi-year NOAA-AVHRR NDVI data to estimate wheat yield in North African countries. Similar relationships were obtained for various crops in other areas (Rasmussen (1992) for millet yield, Manjunath and Potdar (2002) for wheat yield). Some papers of literature suggest that the BIO model proposed by Monteith (1972) based on incident global solar radiation (R_G) and canopy development have acceptable accuracy, and that it can be used together with satellite data (e.g. Kumar and Monteith, 1982; Daughtry et al., 1992; Gower et al., 1999, Bastiaanssen and Ali, 2003). Although the PAR/R_G fraction varies with visibility, optical depth and ozone amount, among others (Frouin and Pinker, 1995), a value of approximately 45-50% is generally used to represent the 24 h average conditions (Moran et al., 1995).

To acquire crop yield for a growing season (GS), BIO_{GS} is multiplied by the apparent harvest index (AHI) and the harvested area (HA). AHI is the ratio of harvested product to above ground biomass. This index includes the water content of the fresh harvested product and in most studies does not include roots (Lobell et al., 2003):

$$Y_{GS} = BIO_{GS} \; AHI \; HA \; (kg) \tag{2.18}$$

Although AHI is a crop – and variety – specific parameter and can be reduced by water stress, a constant value fine-tuned to the average condition on the estate will provide some first yield estimation at farm level.

2.3 Crop Water Productivity

Water productivity (WP) can be defined as the ratio of the net benefits from crop, forestry, fishery, livestock and mixed agricultural systems to the amount of water required to produce those benefits (Molden and Sakthivadivel, 1999, Kijne et al., 2003; Bos et al., 2005; Molden et al., 2007a). Considering vegetation, WP can be BIO per land (L) or per water consumed, including water that originates from rainfall, irrigation, seepage and changes in soil water storage. Agricultural production and water consumption are two closely linked processes. The crop water productivity (CWP) can be considered as the ratio of the actual yield (Y_a) to cultivated land or to the amount of water consumed. Many promised pathways for raising CWP in agriculture are available

over the continuum from fully rainfed to fully irrigated farming systems. Table 2.1 shows the different water productivity indicators.

Table 2.1: Different water productivity indicators: Water productivity and crop water productivity based per land (L), irrigation (I), actual evapotranspiration (ET_a) and actual transpiration (T_a), together with the economic values of these indices ($).

Output	Land (ha)	Irrigation (m³)	ET_a (m³)	T_a (m³)
BIO (kg)	WP_L (kg ha⁻¹)	WP_I (kg m⁻³)	WP_{ET_a} (kg m⁻³)	WP_{T_a} (kg m⁻³)
Net benefit ($)	$WP\$_L$ ($ ha⁻¹)	$WP\$_I$ ($ m⁻³)	$WP\$_{ET_a}$ ($ m⁻³)	$WP\$_{T_a}$ ($ m⁻³)
Y_a (kg)	CWP_L (kg ha⁻¹)	CWP_I (kg m⁻³)	CWP_{ET_a} (kg m⁻³)	CWP_{T_a} (kg m⁻³)
Gross return ($)	$CWP\$_L$ ($ ha⁻¹)	$CWP\$_I$ ($ m⁻³)	$CWP\$_{ET_a}$ ($ m⁻³)	$CWP\$_{T_a}$ ($ m⁻³)

Organizations responsible for irrigation management are interested in yield per unit applied irrigation water, as it is their duty to enhance yield through man-induced irrigation processes, but the drawback is that not all irrigation water is used for generating crop production. Renault et al. (2001) showed that perennial vegetation at Kirindi Oya system in Sri Lanka has water consumption around the same amount as rice and generates valuable ecosystem services. Moreover, crop production is also a consequence of rainfall. CWP is commonly expressed in yield per unit of applied water, including rainfall and irrigation (Peacock et al., 1977; Araujo et al., 1995; Srinivas et al. 1999), however, it is also important to analyze the CWP in terms ET_a and T_a, including capillary rise and soil moisture changes (e.g. Droogers and Kite, 1999). These water resources also contribute to crop production, and thus CWP cannot be related to rainfall and irrigation water supply only. The CWP for a growing season (GS) can be calculated as:

$$CWP_{(ET_a, T_a, I)} = \frac{Y_{GS}}{W_{(ET_a, T_a, I)}} \qquad (2.19)$$

where W represents water flux or applied water and the subscripts ET_a and T_a denote the water fluxes by actual evapotranspiration and actual

transpiration, respectively; the subscript I means the amount of water supplied by irrigation and Y_{GS} is the yield for the growing season. The economic water productivity is the value derived per unit of water used. Increases in economic water productivity may indicate a shift towards higher valued crops, increase in yields or a saving in water input (Bos et al, 2005). According to Droogers et al. (2000) and Bos et al. (2005), the economic indicators (Table 2.1) are the standard gross value of production over the irrigation supply ($CWP\$_I$), over actual evapotranspiration ($CWP\$_{ET_a}$) or over actual transpiration ($CWP\$_{T_a}$).

Water productivity gains are context dependent and can be assessed only by taking an integrated basin perspective. Increasing CWP is an effective means of intensifying agricultural production and reducing environmental degradation. In irrigated regions of dry areas it is common to document ratios of ET_a to irrigation plus rain greater than 60%, often depleting more water than it is renewable and leading to aquifer mining. Such areas include the Gediz Basin in Turkey (Droogers and Kite, 1999), Egypt's Nile (Keller and Keller, 1995), the Christian subdivision in Pakistan (Molden et al., 2000), the Bhakra irrigation system in India (Molden et al., 2000), the Nilo Coelho in Brazil (Bastiaanssen et al., 2001), the Tunuyuan irrigated area in Argentina (Bos, 2004), Fayoum (Bos, 2004), the Rio Grande Basin in Mexico and the United States (Booker et al., 2005) and the Liu Yuan Ku irrigation system in China (Hafeez and Khan, 2006). According to Molden et al. (2007b), the additional amount of water needed to support irrigated agriculture by incremental evapotranspiration depends on the gains in CWP.

The actual crop yield per unit of water consumed (Y_a/ET_a) can be broken down into three different processes, which each of them having a physical meaning:

$$\frac{Y_a}{ET_a} = \frac{Y_a}{BIO} \frac{BIO}{T_a} \frac{T_a}{ET_a} \qquad 2.20)$$

The terms Y_a/BIO and BIO/T_a reflect agronomical processes and aspects of plant-physiology respectively. The ratio Y_a/BIO is known as the harvest index and T_a/ET_a is the intrinsic transpiration coefficient. For a given crop variety, fertility level and climate there is a well established linear relationship BIO and T_a (Tanner and Sinclair, 1983, Steduto and Albrizio, 2005). High BIO requires high T_a because when stomata open, carbon dioxide flows into the leaves for photosynthesis and water flows

34

out (Figure 2.1). Stomata close during dry conditions limiting transpiration, photosynthesis and production. The ratio T_a/ET_a is depends to a large extent on the type of irrigation in place. While there is a fixed relation between BIO and T_a, this is not true for Y_a relative to ET_a because of differences in soil evaporation, harvest index, climate conditions, water stress, pest and diseases, nutritional and soil status, and other agronomic practices. Thus there seems to be considerable scope for raising Y_a/ET_a before reaching the upper limit. The variability in CWP being due to crop and water management practices is important because it offers hope of possible improvements if other practices are adopted (Molden et al., 2007c).

There is ample scope for higher physical crop water productivity – getting more produce per unit of water – in low-yielding rainfed areas and in poorly performing irrigation systems, where poverty and food insecurity prevail. Good agricultural practices – managing soil fertility and reducing land degradation – are important for increasing CWP. Higher physical and economic values of CWP reduce poverty in two ways. First, targeted interventions enable poor people or marginal producers to gain access to water or to use water more productively for nutrition and income generation. Second, the multiplier effects on food security, employment, and income can benefit the poor. But programs must ensure that the gains reach the poor and are not captured by wealthier or more powerful users (Molden et al., 2007b).

Benchmark values for water productivity of irrigated crops (wheat, rice, cotton, maize) are summarized by Zwart and Bastiaanssen (2004); for dryland crops by Oweis and Hachum (2006) and for rainfed crops by Rockstrom and Barron (2007). Bouman et al. (2005) conducted a special study on rice showing that several practices are applicable to increase CWP, such alternate wet and dry irrigation. Supplemental irrigation to rain is also an excellent way to increase the productivity of water. In western Syria wheat yields increased from 2 to 5 metric tonnes per hectare with the timely application of 100-200 mm of water and CWP_{ET_a} improved from 0.60 to 1.85 kg m^{-3} (Oweis and Hachum, 2003). Yields of sorghum in Burkina Faso and maize in Kenya were increased from 0.5 metric tons per ha to 1.5-2.0 metric tonnes with supplemental irrigation plus soil fertility management (Rockström et al., 2003). On the other hand CWP can also be improved with deficit irrigation (Zhang, 2003).

According to the field scale studies above it can be concluded that there is a substantial scope to conserve irrigation water supplies by a

35

range of technical and management practices as drip and micro sprinkle irrigation, more precise application practices, canal lining or delivery through pipes, reduced allocations of water to farmers, or pricing to influence demand. A complete assessment of irrigation performance requires a view beyond crops that includes other functions of irrigation and their value (Molden et al., 2007c).

Considering regional scale, remote sensing and Geographic Information System (GIS) have proved to be useful tools in identifying the range of possible values for CWP and, combined with ground data, can help to pinpoint constraints for on-farm and system management improvements.

Thiruvengadachari and Sakthivadivel (1997) performed a rice study in the Bhadra Project in Southern India and showed that the spatial and temporal information has helped analysts to evaluate the performance of the agricultural system over several years and across the irrigation scheme. The data have confirmed that changes initiated by the National Water Management Project have resulted in significant improvements as indicated by extent of irrigation and changes in agricultural productivity. In addition rice productivity and equity have been identified for follow-up action to improve performance.

Bastiaanssen et al. (1999) conducted a study to identify the spatially distributed patterns of wheat yield and ET_a in the Bakhra irrigation system of Punjab and Haryana state and detected that areas with the highest grain yield correspond to the areas having the highest ET_a. Consequently, the spatial variations in crop production per unit ET_a identified by the values of coefficient of variation (CV) were less (CV = 0.10) than spatial variations in productivity of land (CV = 0.17).

McVicar et al. (2000) applied GIS in China to assess whether changes in management practices increased regional CWP_{ET_a}. From 1984 to 1996 the values for wheat increased from 0.70 kg m^{-3} to 1.43 kg m^{-3}, while for corn the values increased from 0.90 kg m^{-3} to 1.01kg m^{-3} for the same period. Countries with high mean CWP_{ET_a} but were somewhat inconsistent from year to year were identified as those with the highest potential for water management improvement.

It can be concluded that reduction of the spatial and temporal variation in agricultural yield and ET_a are thus a crucial elements for increasing the total CWP of irrigation schemes. The combination of agro-meteorological data together with spatially distributed satellite images is technically feasible to acquire key elements of the regional water fluxes

and water productivity. The better knowledge of variation in CWP provides valuable information for achieving local water conservation practices without losing good productivity levels of irrigated crops.

3. Global review of grape and mango water productivities

An adequate benchmarking of the water management situation in Brazilian horticulture requires a good review on the world current practices and a comparison against other producing countries. This chapter will therefore describe the overall situation from the perspective of area and production statistics for vineyards and for mango orchards.

3.1 Climatology

Vineyard climatology

The cultivation of grapes (*Vitis vinifera L.*) has a long history dating back about 8,000 years. It is thought that *Vitis vinifera L.* originates from Georgia or Iran in Central Asia, appearing in Europe about 6,500 years ago in Greece being a very common fruit crop in classical Greece and Rome. The genus Vitis is part of the family *Vitaceae*, which involves 90 species. Most American grapes originate from cultivars of *Vitis vinifera*, such as:

- *Vitis labrusca*, the North American table and grape juice grapevines, sometimes used for wine. It is native to the Eastern United States and Canada.
- *Vitis riparia*, a wild vine of North America, sometimes used for winemaking and for jam. It is native to the entire Eastern U.S. and north to Quebec, New York.
- *Vitis rotundifolia*, the muscadines, used for jams and wine. It is native to the South eastern U.S. from Delaware to the Gulf of Mexico.
- *Vitis vulpine*, frost grape. It is native to the Midwest east to the coast up through New York.
- *Vitis amurensis*. Most important Asian species.

The distribution of vineyards in the world is conditioned, in particular by air temperature, solar radiation, atmospheric humidity and soil moisture that all determine the photosynthetic activity and water consumption (Costacurta and Roselli, 1980). It should be remarked that the sugar concentration increases and the acid content decreases simultaneously in the fruits with increasing air temperature (Coombe, 1987). Air temperature is also important for the evapotranspiration process. Wind speed above the vegetation acts in actual evapotranspiration (ET_a) and this process is affected by the canopy architectures. Solar radiation is the source of energy for the

photosynthesis and evapotranspiration processes. Further to leaf area, the type of trellis systems and cultural management practices will control ET_a and photosynthesis, and hence the production (Smart, 1985). The photosynthesis process in vineyards is less intense at air temperatures below 20° C due to partial closure of the stomata. The maximum activity – and thus the most favourable production – occurs between 25 and 30° C. Photosynthesis reduces again when air temperature is near 45° C and the grapes exhibit heat stress. The considered ideal range for the cultivation of grapes lies thus between 25 and 35° C. Climates with low precipitation are suitable for vineyards, because falling rain drops cause direct damage to the skin of the berries and increase the risk of diseases. Dry climates have the drawback, however, of providing insufficient soil moisture. Irrigation technologies are an important asset for controlling water deficiencies at a predefined acceptable level, i.e. an intermediate soil moisture level that varies somewhere between 0.15 to 0.25 cm^3 cm^{-3}.

The ideal climate conditions are found in Brazilian semi-arid region of the São Francisco River basin, where vineyards are being extensively cultivated. The most important varieties are Petite Syrah and Superior seedless for wine and table grapes, respectively (Figure 3.1).

Figure 3.1. Wine and table grapes cultivated in semi-arid region of São Francisco River basin, Brazil.

A regulated deficit irrigation approach is ideal to compensate the natural water shortage preventing the soil to become too wet. Excess of soil moisture will create massive biomass production with relatively low berry yields, being an unacceptable standard. Regulated deficit will ensure relatively more berries than leaves and higher sugar content (Klaasse et al., 2007). Proper irrigation technologies such as drip systems provide the necessary flexibility to meet all these on-farm management demand criteria. Most vineyards are therefore equipped with drip systems. The high output value of grape cultivation makes it economically viable to invest in these high-tech systems in the Low-Middle São Francisco River basin (Teixeira et al., 2007).

Mango orchard climatology

Another economically important fruit crop is mango. It belongs to the genus Mangifera which consists of about 30 species of tropical fruiting trees in the Flowering plant family Anacardiaceae. Mango trees (Mangifera indica L.) are large, reaching up to 35 to 40 m in height, with a crown radius up to 10 m. The mango is reputed to be the most commonly eaten fresh fruit worldwide. Native to southern Asia, especially eastern India, Burma, and the Andaman Islands, the mango has been cultivated, praised and even revered in its homeland since ancient times. Later, mango was propagated in other parts of the world, including the Americas. Its fruit has the advantage of being juicy and relatively large in size, besides being a rich nutrient source.

Mango trees less than 10 years old may flower and fruit regularly every year. Blooming is strongly affected by weather. Dryness stimulates flowering and rainy weather discourages it. Hence, a dry season period is mandatory for commercial orchards. The timing and amount of rainfall is not very critical as it is for table grapes. The best climate for mango is to receive 750-2500 mm during a relatively short rainy season of 4 months, followed by 8 months of dry season. Absorbed solar radiation by the leaves affects the vegetative growth and fruit maturation periods. The leaves situated inside the canopies receive low levels of solar radiation, reducing the carbohydrates availability what promotes effect in fruit development and final productivity (Singh, 1977). Air temperature, as well as wind speed, is important in the evapotranspiration process. The warm air near the rough canopies transfers energy to the leaves, thereby enhancing the water vapour transfer away from irrigated orchards into the atmosphere. Air temperature is also important for photosynthesis,

because this process involves biochemical reactions and the enzymes involved are a function of air temperature (Nunez-Elisea and Davenport, 1995), being the ideal range is from 24 to 30° C. The values above 48° C are harmful to productivity. Low air temperature values are also unfavourable to yield and when they are near 0° C, severe damages and even the death of the trees can occur. The dry matter production is influenced by air temperature being affected under low values by reduction of canopies. Very cold or very hot air are unfavourable to pollen grain formation with consequent small fruits without commercial value (Nunez-Elisea and Davenport, 1995). The air humidity is important, because high values are favourable for fungus diseases, and when associated with high air temperatures can adversely affect the fruit production (Lonsdale and Kotze, 1993). Arid and semi-arid regions are favourable for mango growing because the fruits are well exposed to the sun, becoming well coloured, and are relatively free of disease (Singh, 1977). Strong winds during the fruiting season cause many fruits to fall prematurely (Schaffer et al., 1994). The ET$_a$ of the rough mango trees canopies depends in a large part on the turbulence of the air, which in turn is affected by the roughness of the tall trees and their architectures (Teixeira et al. 2008b).

The climate of the semi-arid region of the São Francisco River basin is thus very favourable. However, because the orchards are in conditions of low precipitation and high evapotranspiration demands, irrigation becomes necessary. Figure 3.2 shows a *Tommy Atkins* mango orchard in a commercial mango producer farm in this region.

Figure 3.2. Commercial mango orchard in the semi-arid region of the São Francisco River basin, Brazil.

Dark coloured irrigated mango orchards in the Low-Middle São Francisco River basin, consume high amounts of water – as a consequence of large solar radiation. Mango trees are resistant to soil dryness conditions, because the root systems can attain great depths. Even with the trees being able to survive eight months without rainfall, the low amounts of precipitation make irrigation, however, a necessity for commercial orchards.

3.2   Land use statistics

Vineyard land use statistics

The evolution of harvested areas in the world for the main 14 grape producing countries during 1999 to 2005 is presented in Table 3.1.

Table 3.1: Evolution of the total area (10^3 ha) under vineyards in the world. The acreage encompasses wine grapes, table grapes and raisins. Source (O.I.V., 2007).

Northern hemisphere							
Country/Year	1999	2000	2001	2002	2003	2004	2005	Total
Spain	1,180	1,237	1,211	1,202	1,207	1,200	1,180	1,202
France	914	917	914	898	888	889	894	902
Italy	909	908	892	872	862	849	842	876
China	-	304	363	421	455	471	487	417
USA	384	405	426	415	415	398	399	406
Portugal	260	246	248	251	249	245	246	249
Romania	253	248	247	243	239	217	217	238
Germany	106	105	104	102	102	102	102	103
Total	4,006	4,370	4,405	4,404	4,417	4,371	4,367	4,394

Southern hemisphere							
Country/Year	1999	2000	2001	2002	2003	2004	2005	Total
Argentina	208	201	205	208	211	213	219	209
South Africa	115	117	126	129	132	133	134	127
Chile	158	174	181	184	185	189	191	180
Australia	123	140	148	159	157	164	167	151
Brazil	-	-	-	-	72	74	78	75
New Zealand	12	14	15	17	19	21	24	17
Total	616	646	675	697	776	794	813	759

The majority of the vineyards grow dominantly between 30 to 50 degrees north and between 20 to 40 degrees south. The world's most southerly vineyards can be found in the Central Otago region of New Zealand's South Island near the 45th parallel. The most northerly vineyards are located in Flen (Sweden) just above the 59th parallel, and

these locations are clear exceptions. The geographical distribution of the main wine and table grape producing regions in the world is shown in Figure 3.3. The major cultivated areas in the Northern hemisphere can be found in Europe (Spain, France and Italy) while for the Southern hemisphere Argentina, South Africa, Chile and Australia are the most important wine and grape producing countries.

Brazil is a small player, but the Brazilian production has been expanding over recent years. According to the total values of Table 3.1, for the period of 1999-2005 the cultivated area increased by 11% in the Southern hemisphere and the Northern hemisphere experienced the opposite situation with a reduction of 5%.
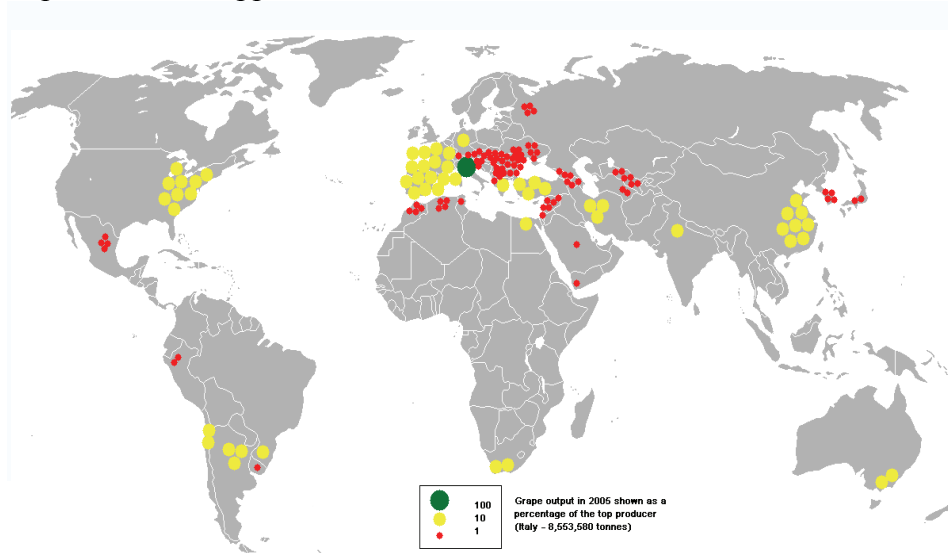
Figure 3.3. Main areas with vineyards in the world in 2005 (Source: FAO, 2007)

Approximately 71% of the total world grape production is used for wine, 27% for fresh fruit, and 2% for dried fruit (e.g. raisins). A portion goes to grape juice production to be used as a sweetener for canned fruits "with no added sugar" and "100% natural". Hence the majority of the global grape production is meant for the wine industry.

Mango orchards land use statistics

The evolution of harvested areas with mango orchards in the world for the main 10 producing countries is shown in Table 3.2. From this table it can be seen that the areas with mango orchards in the world increased by 22% from 1999 to 2005. Indonesia almost doubled the cultivated area (99%), followed by Guinea (64%) and Brazil (38%).

Table 3.2: Evolution of total area with mango orchards (10^3 ha) in the world during the period from 1999 to 2005. Source: FAO, 2007.

Country/Year	1999	2000	2001	2002	2003	2004	2005	Total
India	1,400	1,490	1,520	1,580	1,600	1,661	1,711	10,962
China	419	479	389	394	409	419	434	2,943
Thailand	245	270	270	270	270	270	285	1,880
Indonesia	137	144	144	185	159	312	273	1,354
Mexico	155	154	162	162	174	166	183	1,156
Pakistan	152	154	160	160	163	166	164	1,119
Philippines	132	134	137	151	155	159	164	1,032
Nigeria	122	125	125	125	125	133	138	893
Brazil	61	68	67	67	86	88	84	521
Guinea	45	45	60	78	80	75	74	457
Total	2,868	3,063	3,034	3,172	3,221	3,449	3,510	22,317

The crop was introduced to West Africa early in the 16th Century and also into Brazil by the Portuguese. The large global mango players are shown in Figure 3.4. The mango is naturally adapted to tropical lowlands between 25° N and 25° S and up to elevations of 915 m. It is grown as a dooryard tree at slightly cooler altitudes but is apt to suffer cold damage.

Mango orchards are widely cultivated in frost-free tropical and warmer subtropical climates throughout the Indian subcontinent; North, South and Central America; the Caribbean; South and Central Africa; Australia; and Southeast Asia.

World mango production

Legend: Top 1.6 million   Middle 288,031   Bottom 51,000   (No data)
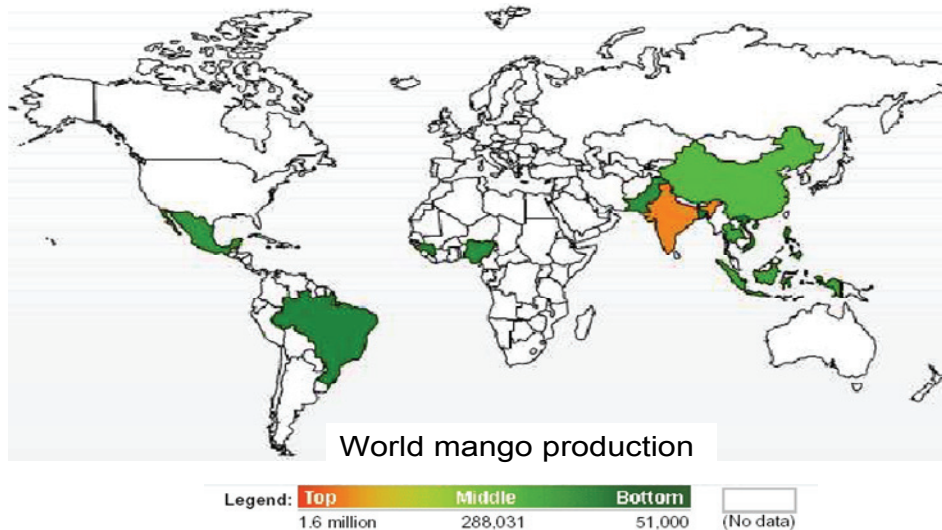
Figure 3.4. Ranking of 10 countries with the highest mango production in 2005. Source: NationMaster.com

India, with 70% of its fruit-growing area being mango orchards, produces 65% of the world's production. This country far outranks all others as an exporter of processed mangos, shipping 2/3 of the total production. Following India in volume of exports are Thailand; Pakistan and Bangladesh; Brazil; and Mexico. The Philippines have risen to 6th place. Tanzania is 7th, the Dominican Republic, 8th and Colombia, 9th. From Table 3.2 it can be seen that the areas with mango orchards in the world increased in average 22% from 1999 to 2005.

3.3 Global and Brazilian production
Wine and table grape production

Wine is produced from <u>fermenting</u> crushed grapes. Various grape varieties are used to create a large range of wines. The first twelve main wine producing countries are shown in Figure 3.5. Europe is the leading wine producer, representing 73%, followed by America (18%) and Asia, Africa and Oceania each with 3% of the total amount.
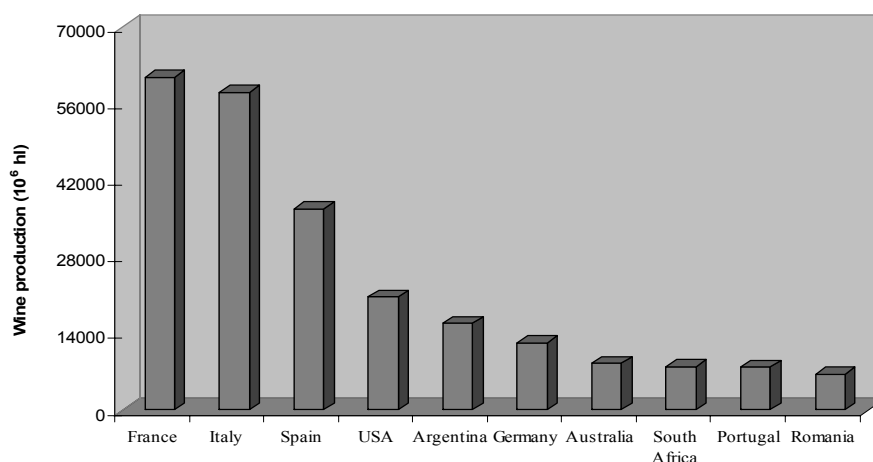
Figure 3.5. The major wine producing countries in 2005 (Source: O.I.V., 2007).

The productions of the nine leading wine producing countries in the Southern hemisphere are presented in Table 3.3. Argentina and Australia are the leaders in Southern hemisphere. Wine production in this hemisphere has further increased from 14.8% of the world share in 1996 to 18.5% in 2006. The Southern hemisphere wine producers export their products specifically to the United Kingdom, the United States and Canada, with an increase in production around 24% from 2001 to 2005. The Brazilian wine production in 2005 represented around 6% of the total in South America, and according to the Organisation Internatinale de la Vigne et du Vin (O.I.V.), will present a strong increase during the next years, as new plantations start to be harvested.

Table 3.3: Evolution of wine production in countries in the Southern hemisphere (in 10^3 hl) (Sources: O.I.V. and FAO, 2007)

Country	2001	2002	2003	2004	2005	Total
Argentina	15,835	12,695	13,225	15,464	15,640	72,859
Australia	10,731	12,168	10,835	14,679	12,740	61,153
South Africa	6,471	7,189	8,853	9,279	11,579	43,371
Chile	5,452	5,623	6,682	6,301	7,886	31,944
Brazil	2,968	3,212	2,620	3,925	3,199	15,924
New Zealand	533	890	550	1,192	1,200	4,365
Uruguay	873	714	840	1,126	1,126	4,679
Peru	373	408	458	445	435	2,119
Total	43,236	42,899	44,063	52,411	53,805	236,414

Brazil already ranks fifth in the Southern hemisphere. The semi-arid region of São Francisco River basin is highlighted. Wine farms in

the Low-Middle São Francisco River basin have produced 8 to 15 t ha^{-1} of grapes per growing season according to the weather conditions, or even more, however compromising the final wine quality. The main variety is Petite Syrah which had a market price around US$ 0.90 L^{-1}, producing 1 litre of wine from 1.25 kg of grapes in 2003 (Teixeira et al., 2007).

The ranking for the ten most table grape producing countries in the world is shown in Figure 3.6. The world highest production of table grapes is also for Italy and France.
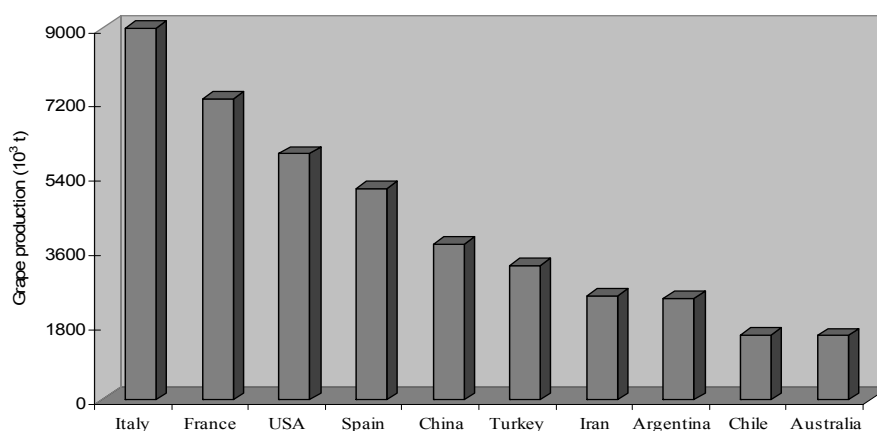
Figure 3.6. Ranking of the top 10 countries with highest table grape production in 2005 (Source: FAO, 2007)

The table grape production of the 9 leading countries in the Southern hemisphere is presented in Table 3.4. While the world table grape production increased 10% during the period 1990-2000, in Brazil it increased 29%. Although there was a decrease of 5% in relation to 2004, an increasing trend of 16% is observed considering the period from 2001 to 2005.

Table 3.4: Evolution of table grape production in countries in the Southern hemisphere (in 10^3 t). Source: OIV, 2007.

Country	2001	2002	2003	2004	2005	Total
Argentina	2,244	2,360	2,301	2,651	2,830	12,386
Chile	1,801	1,750	1,985	1,900	2,250	9,686
Australia	1,546	1,754	1,497	2,015	2,027	8,839
South Africa	1,328	1,522	1,664	1,762	1,683	7,959
Brazil	1,058	1,149	1,067	1,291	1,233	5,798
Peru	128	136	146	155	197	762
New Zealand	71	119	76	166	142	574
Uruguay	113	94	108	147	124	586
Total	8,289	8,884	8,844	10,087	10,486	46,590

The grape productivity data including wine and table grapes for Brazil in 2005 are shown in Table 3.5. The gross return for the entire country was approximately US $ 791,100,000 or US $ 10,800 ha^{-1}. Pernambuco and Bahia, followed by Minas Gerais rank the highest in terms of gross return. When analysing the gross return in terms of price of kilograms of fruits, the last state presented the highest value. The areas with vineyards of these states are inside the São Francisco River basin, which showed a significant expansion over the last decade. Nowadays the total vineyard area in Pernambuco and Bahia states is approximately 8,180 ha. Although Rio Grande do Sul has been traditionally the leader in cropped area as well in yield, this state stayed behind in terms of productivity when compared to the areas inside the São Francisco River basin. This can be attributed to differences in climatic conditions.

Table 3.5: Productivity data of vineyards (table grapes and wine grapes) in 2005 for the top production states as well as for Brazil: Harvested area- HA; Yield; Crop water productivity by land (CWP_L) and gross return (GR). Source: IBGE, 2007.

State/Region	HA (ha)	Yield (t)	CWP_L (kg ha^{-1})	GR (US$ ha^{-1})	GR (US$ kg^{-1})
Rio Grande do Sul	42,450	611,868	14,414	7,203	0.5
São Paulo	10,906	190,660	17,482	11,976	0.69
Pernambuco	4,872	150,827	30,958	34,179	1.1
Paraná	5,603	99,253	17,714	8,690	0.49
Bahia	3,685	109,408	29,690	26,604	0.9
Santa Catarina	4,224	47,971	11,357	4,268	0.38
Minas Gerais	935	14,389	15,389	17,232	1.12
Total	73,203	1,234,564	16,865	10,807	0.64

49

The trend of wine and table grape production in Brazil from 2001 to 2005 is shown in Figure 3.7. Despite the yield fall in 2003, one can see the increment of both wine and grape productions for all period, with highlight to the year of 2004. There were increases of cultivated areas in Pernambuco and Bahia of 1.07% and 0.44%, respectively, during this period.
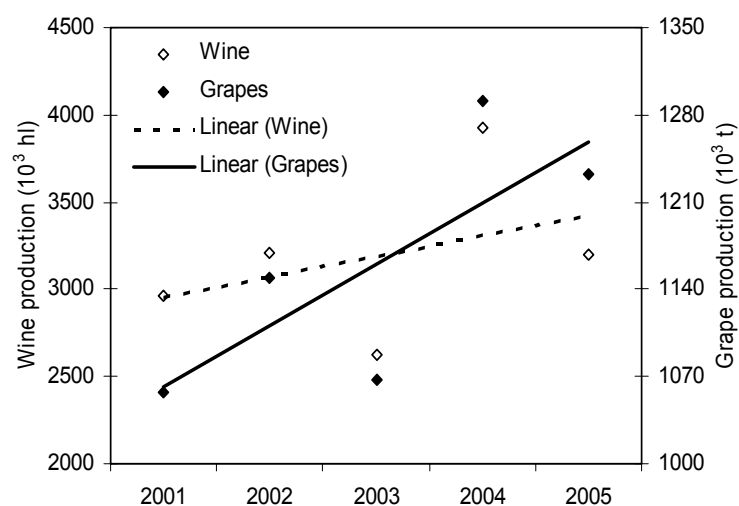
Figure 3.7. Evolution of table grape and wine production in Brazil from 2001 to 2005. Source: IBGE., 2007.

The São Francisco Valley started the commercialisation of table grapes with the cultivar Superior Seedless, with an average annual yield of 20 t yr^{-1}. The table grape crop became a high economic activity since the 1970's, when advanced technologies allowed the acquirement of competitive and better quality grapes in different consumers markets. More than 95% of the vineyard production (wine and table grapes) in the Northeast is found in this valley.

As shown in Table 3.5, Pernambuco state (Petrolina-PE) presented better physical and economic land productivity performance than Bahia state (Juazeiro-BA). Nowadays, table grapes are regarded as one of the main exported fruits in the São Francisco River basin, ranking second place after mango. The basin is responsible for almost all of the export of seedless table grapes in Brazil. The export market is increasing as a consequence of the international market's preference for seedless grapes.

Mango production

For 2005, the mango production of the main country producers are shown in Figure 3.8. India with 1,711,000 ha of mangos produced 65% of the world's total in 2005, with productivity of 6.5 t ha^{-1}.
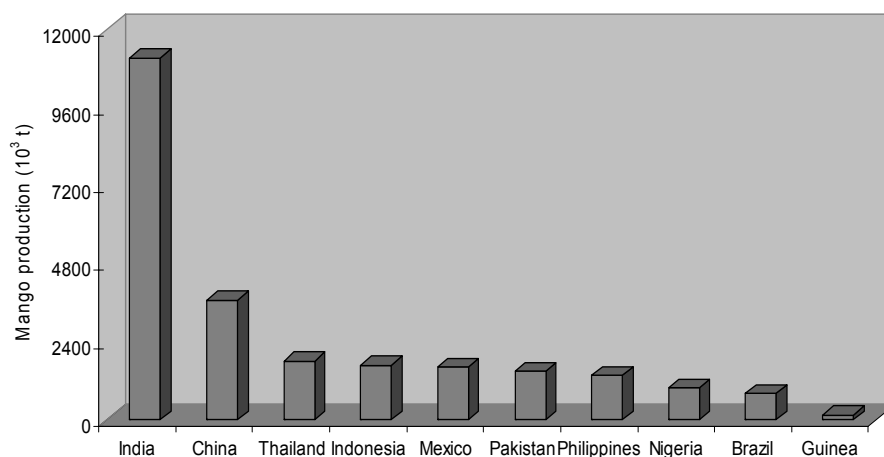
Figure 3.8. Ranking of 10 countries with higher mango production in 2005. Source: FAO, 2007.

Mango yield varies with the cultivar and the age of the trees. Currently, the world market is dominated by the cultivar *Tommy Atkins*, first cultivated in 1940 in Southern Florida, USA. Other cultivars, such as *Kent* and *Keitt* are also important, however *Tommy Atkins* quickly became an export favourite worldwide. Despite its fibrous flesh and fair taste, growers have embraced the cultivar for its exceptional production and disease resistance, the shelf-life of its fruit, their transportability as well as their size and beautiful colour. The evolution of yield of the ten leading mango producing countries in the world is presented in Table 3.6.

Table 3.6: Evolution of mango production (10^3 t) in the world during the period from 1999 to 2005. Source: FAO, 2007.

Country/Year	1999	2000	2001	2002	2003	2004	2005	Total
India	9,780	10,500	10,060	10,640	10,780	10,987	11,140	73,887
China	3,127	3,211	3,273	3,513	3,751	3,582	3,673	24,130
Thailand	1,462	1,633	1,700	1,700	1,700	1,700	1,800	11,695
Indonesia	1,508	1,559	1,557	1,523	1,362	1,573	1,679	10,761
Mexico	1,385	1,432	1,515	1,615	1,576	1,566	1,606	10,695
Pakistan	827	876	923	1,403	1,526	1,438	1,478	8,471
Philippines	456	538	782	842	1,254	1,358	1,348	6,578
Nigeria	886	848	882	956	1,006	968	984	6,530
Brazil	729	730	730	730	730	782	812	5,243
Guinea	83	83	120	156	160	147	145	894
Total	20,243	21,410	21,542	23,078	23,845	24,101	24,665	158,884

The highlights are for Philippines that almost tripled its production (296%) and Pakistan (79%). The Brazilian production from 1999 to 2005 had an increment of 11%, while the world average increment was of 22%. Nowadays, Brazil is responsible for 2.5% of the world production, and is after Mexico the second largest mango producing country in the Americas. Most Brazilian mangos are produced in the state of Bahia, São Paulo, Pernambuco and Minas Gerais, followed by Rio Grande do Norte, Ceará and Paraíba. Table 3.7 shows the productivity data for Brazilian states as well as for the country in 2005. Northeast Brazil had a harvested area of 43,792 ha, while Southeast Brazil, which is considered the second producer region of the country, presented a total of 22,054 ha.

Table 3.7: Productivity data of mangos in 2005 for the top production states as well as for Brazil. Harvested area- HA; Yield; Crop water productivity by land (CWP_L) and gross return (GR). Source: IBGE, 2007.

State/Region	HA (ha)	Yield (t)	CWP_L (kg ha^{-1})	GR (US $ ha^{-1})	GR (US$ kg^{-1})
Bahia	20,213	396,662	19,624	5,391	0.27
São Paulo	15,408	204,607	13,279	2,170	0.16
Pernambuco	8,368	152,694	18,247	4,131	0.23
Minas Gerais	5,992	62,406	10,415	2,848	0.27
Rio Grande do Norte	3,092	38,775	12,540	3,668	0.29
Ceará	4,812	38,181	7,935	1,198	0.15
Paraíba	2,721	23,064	8,476	1,148	0.14
Total	68,141	1,002,211	14,708	3,412	0.23

The production of mangos in Northeast represented 70% of the total Brazilian production in 2005, while for the Southeast the fraction was 28%. It is interesting to note that although Pernambuco presented lower harvested area and total yield than São Paulo, the yield per unit land in the first state exceeded the counterpart values of the second state. The reason should be related to the better climate conditions together with agricultural management. The trend of mango productions in Brazil from 2001 to 2005 is shown in Figure 3.9. One can see the continuous increment in mango production during this period, mainly between 2004 and 2005.
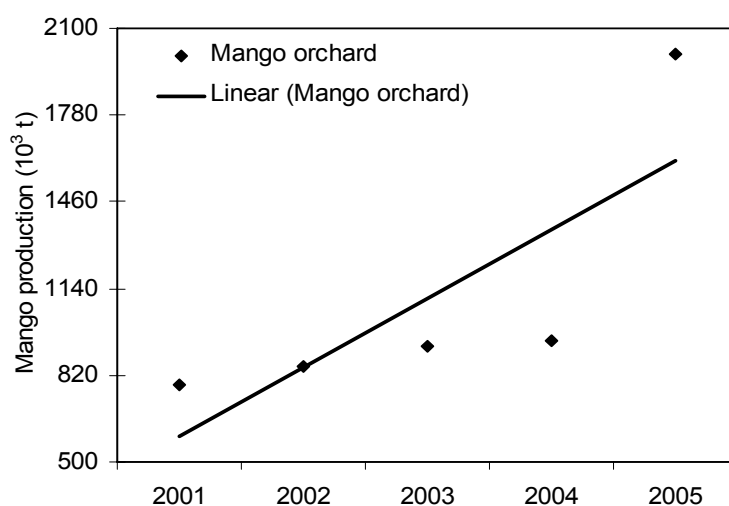
Figure 3.9. Evolution of mango production in Brazil from 2001 to 2005. Source: IBGE, 2007.

The bulk of the crop was for domestic consumption, however, exports to Europe have been increasing since 1973. Between 2001 and 2005 Northeast Brazil increased the mango production by 44%. Bahia and Pernambuco represented an average 27 and 12% of the national production, respectively. These states together had a gross return of US $ 144,000,000.00 being 62% of the total in Brazil. Around 39% of the mango production in Northeast Brazil is in the São Francisco Valley for both states; however Bahia (Juazeiro) presented better mango productivity performance than Pernambuco (Petrolina) in 2005, in relation to harvested area, yield and the gross return. The main variety cultivated in the São Francisco River basin is the Tommy Atkins, with

the price around US $ 1.02 kg-1 for export in 2005 (Teixeira et al., 2008a).

3.4 Crop water productivity

Grape water productivities

The review described in the previous sections revealed that there is information available on the areas under grapes and the yields that are obtained under practical circumstances. Data on yield will gain in importance, if this information is merged with water variables to arrive at crop water productivity based on water consumed (kg m-3). Data sets related to vineyard actual evapotranspiration (ETa) are scarce in the international literature. Nevertheless, it would be useful to make an assessment of the vineyards water depletion under different cultural managements. A first crude estimation of vineyard ETa would be the application of the crop coefficient approach suggested by FAO for areas with minimal ground information (Allen et al., 1998):

$$ET_a = K_s K_c ET_0 \qquad\qquad (3.1)$$

where ET_0 is the reference evapotranspiration, K_c is the unstressed crop coefficient and K_s is the water stress coefficient. Although this computational method is far from being perfect, it yields to a first estimate of water consumption in irrigated vineyards. For the further separation of ET_a into actual transpiration (T_a) and actual soil evaporation (E_a), the dual crop coefficient approach of FAO56 can be used with the basal crop coefficients (K_{cb}). Standard vineyard tabulated values of these coefficients are shown in Table 3.8.

Table 3.8: Standard published crop coefficient values for vineyards (after Allen et al., 1998).

Growth stage	K_c wine grape	K_{cb} wine grape	K_c table grape	K_{cb} table grape
Early stage	0.30	0.15	0.30	0.15
Mid stage	0.70	0.65	0.85	0.80
Harvest	0.45	0.40	0.45	0.40

Application of these crop coefficient values after local climatic calibration makes it possible to assess ET_a and vineyard water productivity if combining water fluxes with statistical production data. Teixeira et al. (2007) found the crop coefficients of Equation 3.1 considering two

growing seasons for wine and table grapes under semi-arid conditions of Northeast Brazil. The average values were then applied to estimate the water productivity for vineyards (wine and table grapes together) in some municipal districts in the Brazilian states of Pernambuco and Bahia, inside the São Francisco Valley with yield data of 2005 (Table 3.9). For ET_0, interpolated values from 7 agro-meteorological stations for the same year were used.

Table 3.9: Water productivity parameters for vineyards for 2005: Actual evapotranspiration (ET_a); actual transpiration (T_a); Harvested area (HA); production; crop water productivity per cultivated land (CPW_L); gross return (GR); and crop water productivity per actual evapotranspiration and transpiration (CWP_{ET} and CWP_T – physical values; $CWP\$_{ET}$ and $CWP\$_T$ – monetary values)

Variable/Region	ET_a (mm)	T_a (mm)	HA (ha)	Production (t)	CWP_L (kg ha^{-1})	GR (10^3 US $)	CWP_{ET_a} (kg m^{-3})	CWP_{T_a} (kg m^{-3})	$CWP\$_{ET_a}$ (US$ m^{-3})	$CWP\$_{T_a}$ (US$ m^{-3})
Pernambuco										
Lagoa Grande	1,268	1,078	730	20,110	27,534	24,100	2.17	2.55	1.90	2.24
Orocó	1,320	1,122	12	312	26,000	359	1.97	2.32	0.03	0.03
Petrolina	1,320	1,122	3,200	108,800	34,000	126,883	2.58	3.03	9.61	11.31
Sta Maria da Boa Vista	1,327	1,128	620	18,260	29,451	21,640	2.22	2.61	1.63	1.92
Belém do São Francisco	1,340	1,139	12	360	30,000	180	2.24	2.63	0.01	0.02
Petrolândia	1,340	1,139	20	360	18,000	200	1.34	1.58	0.01	0.02
Mean	1,319	1,121	766	24,700	27,498	28,894	2.08	2.45	2.19	2.58
Bahia										
Casa Nova	1,300	1,105	192	5,760	30,000	5,435	2.31	2.71	0.42	0.49
Curaçá	1,340	1,139	360	10,800	30,000	10,791	2.24	2.63	0.81	0.95
Juazeiro	1,201	1,021	2,814	84,420	30,000	79,664	2.50	2.94	6.63	7.80
Sento Sé	1,300	1,105	180	5,400	30,000	5,096	2.31	2.71	0.39	0.46
Sobradinho	1,300	1,105	6	210	35,000	198	2.69	3.17	0.02	0.02
Glória	1,201	1,021	5	100	20,000	28	1.67	1.96	-	-
Paulo Afonso	1,201	1,021	5	110	22,000	49	1.83	2.16	-	-
Bom Jesus da Lapa	1,201	1,021	24	480	20,000	560	1.67	1.96	0.05	0.05
Mean	1,256	1,068	448	13,410	27,125	12,728	2.16	2.54	1.01	1.19

* Crop coefficients used for ET_a calculations were averaged values obtained from field experiments in wine and table grapes and the reference evapotranspiration (ET_0) were interpolated values from 7 agro-meteorological stations for 2005.

In Pernambuco state, Petrolândia ranked lowest of both, physical and economic vineyard water productivity. The best performances for the physical values are for Petrolina and Belém do São Francisco. As in the last municipal district the harvest area was only 12 ha, the total production (360 t) contributed to small values of economic water productivities. In Bahia state the best physical values were for the vineyards in Sobradinho and Juazeiro, while the lowest ones are for Glória and Bom Jesus da Lapa. In Sobradinho only 6 ha were harvested resulting in low production (210 t) and consequently small economic values of water productivities. It can be concluded that if there is an intention to expand areas with vineyards in Low-Middle São Francisco River basin, the municipal districts Belém do São Francisco (Pernambuco) and Sobradinho (Bahia) should have priorities because in these municipal districts the water for grape crops is wisely used.

Although Petrolina presented better vineyard water productivity performance than Juazeiro, the averaged physical parameters for Pernambuco were a little bit lower than for Bahia. On the other hand the economic values for the first state were 45% higher than for the second state. The reason could be better yield and quality of the grapes as a result of water management in Pernambuco. The coefficient of variation for Pernambuco (CV = 20%) was however a little higher than for Bahia (CV = 18%). According to the CV values, both states showed scope for improvements in regional water productivity. The reason for the higher values of physical CWP in Bahia during 2005 was the lower value of ETa. The low economic CWP can be ascribed to the lower yield and by that the gross return.

Figure 3.10 shows the relationship between vineyard water productivities based on ETa and on cultivated land. The trend for Pernambuco (R^2 = 0.99) is slightly stronger than for Bahia (R^2 = 0.96). Pernambuco municipalities showed a steeper slope than for Bahia, which is an evidence of water management being more effective at higher yield values. The high correlation shows that the variation in vineyard water productivity is entirely explained by the variations in land productivity. Hence, a higher grape yield is equivalent to good on-farm water management practices.
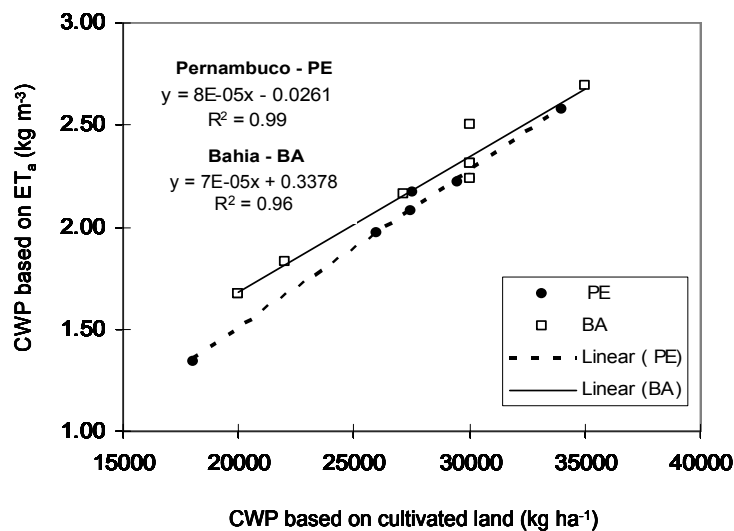
Figure 3.10. Relationships between vineyard water productivity based on actual ET and based on cultivated land for Pernambuco and Bahia states.

Despite the good on-farm water management practices, in general, water conservation programs in vineyards are not a common ingredient in Brazilian semi-arid viticulture. This may change if the country will get the same water shortage as witnessed in for instance South Africa and Australia. Considering vineyard water productivity based on ETa defined as weight of fruits for wine grapes, Jairmain et al. (2007) found higher values in South Africa (4.70 kg m-3), being 82% more than those for Petrolina and Juazeiro in Table 3.9. Walker et al. (2004) reported vineyard water productivity based on Ta of wine grapes (Shiraz and Cabernet) in Australia in the range from 2.50 to 3.30 kg m-3 under well-watered conditions, similar to the values for Petrolina and Juazeiro, however under mild water deficit they found values from 2.00 to 5.10 kg m-3, being 25% more. This is an indication that a similar reduction of 25% in crop water consumptive use could be worth considered. The physical values of CWP for table grapes in São Francisco Valley were a bit lower than those found in Australia under drip (Yunusa et al., 1997a) and furrow irrigation (Yunusa et al., 1997b). In this last country, CWP based on ETa of drip irrigated table grapes were 8.60 kg m-3 for Grafted and 4.30 kg m-3 for Own-rooted vineyards, while when based on Ta were 16.50 and 11.50 kg m-3, respectively. In the furrow irrigated grapes with cover crop, CWP resulted in 1.33 and

4.05 kg m-3 when based on ETa for two different growing seasons, respectively, corresponding to values of 8.40 and 21.11 kg m-3 when based on Ta. Klaasse et al. (2007) and Jairmain et al. (2007) also reported a higher mean value of CWP based on ETa of 3.70 kg m-3 for table grapes in South Africa.

All the international studies in the southern hemisphere discussed above confirm that vineyard water productivity will change according to soil moisture availability, climatic conditions and cultural management. The lower Brazilian semi-arid values of vineyards CWP are related to the lower yields associated with higher daily water consumptions in comparison with other producing regions, although the total production of 2.5 growing seasons compensate these differences and for one year the total yield is in good agreement with other producing countries in the Southern hemisphere. The vineyard water productivity values in the Low Middle São Francisco River basin in term of gross return are high, however the differences between municipal districts show scope for improvements, mainly in Pernambuco state, where the variation is greater.

Mango water productivity

Information on water productivity for mango (kg m^{-3}) is scarcer than for vineyards. The crop coefficients from Teixeira et al. (2008a) were used to infer ET_a and T_a for mango orchards under semi-arid conditions of Northeast Brazil. The average values for two growing seasons were applied to estimate the mango water productivity in some municipal districts of Pernambuco and Bahia states, inside the São Francisco Valley with yield data of 2005 (Table 3.10).

In Pernambuco state, Orocó ranked the lowest concerning physical and economic values for mango water productivity. The best performances for physical values were for Santa Maria da Boa Vista and Petrolina, although in the first municipal district there were fewer harvested areas than in Petrolina and then lower total production and economic values. Increment of the total cropped area in Santa Maria da Boa Vista is then favourable. In Bahia state the best performance for physical and economic values was for Juazeiro, while the lower physical values were for Bom Jesus da Lapa. Priority should be given to Sobradinho in Bahia state that presents a similar physical values as Petrolina in Pernambuco, however, because only 45 ha was harvested;

the economic values were very low. So, from the point of view of mango orchard expansion, the Sobradinho municipality is also a good option.

Table 3.10: Water productivity parameters for mangoes: Actual evapotranspiration (ET_a); actual transpiration (T_a); Harvested area (HA); production; crop water productivity per cultivated land (CPW_L); gross return (GR); and crop water productivity per evapotranspiration (CWP_{ET} and CWP_T – physical values; $CWP\$_{ET}$ and $CWP\$_{Ta}$ – monetary values)

Variable/Region	(mm)	(mm)	(ha)	(t)	(kg ha⁻¹)	(10³ US $)	(kg m⁻³)	(kg m⁻³)	(US$ m⁻³)	(US$ m⁻³)
Pernambuco										
Lagoa Grande	1,284	937	120	2,160	18,000	288	1.40	1.92	0.02	0.03
Orocó	1,335	975	10	160	16,000	37	1.20	1.64	0.01	0.01
Petrolina	1,335	975	6,300	126,000	20,000	28,867	1.50	2.05	1.84	2.96
Santa Maria da Boa Vista	1,343	980	300	7,500	25,000	1,707	1.86	2.55	0.11	0.17
Belém de São Francisco	1,356	990	300	5,400	18,000	2,598	1.33	1.82	0.16	0.26
Petrolândia	1,356	990	63	1,260	20,000	245	1.47	2.02	0.02	0.02
Mean	1,335	975	1,182	23,747	19,500	5,623	1.50	2.06	0.36	0.58
Bahia										
Casa Nova	1,315	960	1,426	35,650	25,000	11,478	1.90	2.60	0.74	1.20
Curaçá	1,356	990	1,460	36,500	25,000	11,751	1.84	2.53	0.74	1.19
Juazeiro	1,216	888	7,000	175,000	25,000	56,342	2.06	2.82	3.94	6.34
Sento Sé	1,315	960	400	10,000	25,000	3,220	1.90	2.60	0.21	0.34
Sobradinho	1,315	960	45	900	20,000	290	1.52	2.08	0.02	0.03
Glória	1,216	888	33	462	14,000	72	1.15	1.58	0.01	0.01
Paulo Afonso	1,216	888	10	140	14,000	27	1.15	1.58	0.00	0.00
Bom Jesus da Lapa	1,216	888	432	4,320	10,000	683	0.82	1.13	0.05	0.08
Mean	1,270	927	1,351	32,872	19,750	10,483	1.92	2.62	0.70	1.13

* Crop coefficients used for ET_a calculations were averaged values obtained from field experiments in mango orchard and the reference evapotranspiration (ET_0) were interpolated values from 7 agro meteorological stations for 2005.

Pernambuco presented lower values for the physical and economic components of mango water productivity than Bahia because the higher yield in the last state together lower ETa. However, the coefficient of variation for Pernambuco (CV = 14%) was lower than for Bahia (CV = 24%), showing more scope for improvements in regional mango orchard water management in the second state. The reason for the higher CV in Bahia can be due to a bigger area with mango orchard than in Pernambuco (Table 3.10) creating more lack of uniformity in cultivation and irrigation practices.

Figure 3.11 shows that the relationship of mango orchard water productivity values based on ET_a with the values per cultivated land for Pernambuco is a little stronger than for Bahia. The tendency line of Bahia had a slightly bigger offset of the relation as the yield was higher and ET_a was lower than for Pernambuco's municipalities.
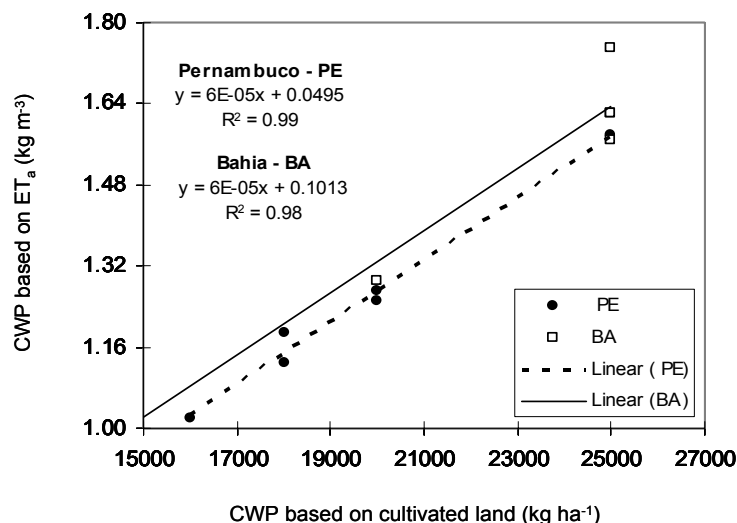
Figure 3.11. Relationships between mango water productivity based on actual ET and based on cultivated land for Pernambuco and Bahia states.

Differences in grape and mango water productivities

The irrigated area including vineyards and mango orchards in Petrolina-Juazeiro pole is now around 100,000 ha from which 80% started to be explored in the 1980's under surface and sprinkler irrigation. However in the last decades the drip and micro sprinkler irrigation are becoming the standard methods as a consequence of advantages as higher irrigation efficiency; fertirrigation; lower operational costs; better water productivity which can improve the yield and quality of fruits to attend

61

the standards for external markets. The analyses of economic water productivities based on ETa in vineyards and mango orchards according to Tables 3.9 and 3.10 indicated that in the 2005 year base, grapes ranked the best with the maximum value 9.61 US$ m-3 for Petrolina, while mangos presented a maximum value of 3.94 US$ m-3 for Juazeiro. At the same year the CWP based on land cultivated area was better for grapes than for mango.

Considering the water consumptions for one good commercial growing season of vineyards and mango orchards situated in three representative farms from Teixeira et al (2007) and from Teixeira et al. (2008a) and the averaged actual price values in the Low-Middle São Francisco River basin, Table 3.11 was constructed.

Table 3.11: Crop water productivity: based on cultivated land and actual evapotranspiration for wine grapes, table grapes and mangos in Low-Middle São Francisco River basin.

Crop	Land productivity - CWP_L (US$ ha^{-1})	Water productivity - CWP_{ET_a} (US$ m^{-3})
Wine grape	6,515	1.20
Table grape	33,600	6.50
Mango orchard	48,405	5.50

* Data are for one growing season of wine grape, table grape and mango orchard from 3 representative farms in Low-Middle São Francisco River basin.

For one growing season, the highest values of gross return per hectare were for mango orchard, while wine grape rank the lowest values of both per land and per water consumption. One should consider however that the growing seasons of grapes are much shorter than for mango orchard, around three months for seedless table grapes and four months for wine grapes, while one growing season of mango orchard is around one year making the seasonal ETa very high. As the growing season for table grapes is short, the seasonal ETa is also small contributing to high CWP based on actual evapotranspiration comparing to mango orchard. On the other hand, one can have grapes harvested till 2.5 times a year, increasing the gross return in annual scale.

Considering all results of CWP tables, an important conclusion is that the values for fruit crops are higher than those for annual crops found in literature. The agricultural water usage in the fruit farms is thus highly productive. From the point of view of water productivity, although table grapes have higher economic values of water productivity based on water consumption, the overall cost of production are bigger than for wine

62

grapes and mango orchards, due to several cultivation practices during the crop stages and higher susceptibility to fungus diseases, making the application of agrochemical very often. On the other hand, for mango orchards more land areas are necessary to accommodate large spaces between trees. So, if one has little land and no limited financial resources for the overall cost of production, it is preferable to cultivate table grapes.

Considering the annual scale, the gross return for grapes is higher than for mangos (see Tables 3.9 and 3.10) while for one growing season the opposite situation is verified (Table 3.11). This is due to several crop cycles of table grapes during a year in different plots. Although wine grape presented lower CWP than table grape, it has the advantage that mechanized cultivation practices are easier applied, because in general, the vertical trellis systems are used in wine grape, as the quality of the fruits is not as crucial as in table grape. In table grape the overhead trellis systems is used because the exigencies of external markets for the quality of the fruits. Also wine grape has fewer problems with fungi diseases making it possible to be cultivated even during the rainy season. On the other hand, if the financial resources are limited and land availability is unrestricted, mango orchard is the best option because of fewer cultivation practices and lower susceptibility to pests and diseases in relation to grapes. Also ample mechanization can be applied in mango orchards due to the large space between the rows of trees. These are some issues to consider when choosing which kind of fruit to cultivate commercially.

Analysing different water productivity performances of grapes and mangos in different regions of the semi-arid of the São Francisco River basin and considering regional water management, an important thing for allocation of water resources to vineyards or mango orchards is to have tools to evaluate the performance of different irrigation perimeters from field to regional scale. Field data together with remote sensing can be transformed in water use, water productivity and economic indicators at large scales. The basic parameters required for these analyses are evapotranspiration, gross and effective rainfall, irrigation water supply, crop yield and crop prices.

63

4. Descriptions of ground and remote sensing data

4.1 Field experiments and agro-meteorological stations

The experimental sites, agro-meteorological stations and satellite images used in this study were located in the Lower-Middle São Francisco River basin, which is shown in Figure 1.5. The four field experiments involved measurements of radiation, energy and water balances as well as the microclimate in the major irrigated crops and natural vegetation. Table 4.1 shows the specification of the irrigation and systems installed in each plot.

Table 4.1: Field energy balance experiments used for water productivity analyses and for calibration and validation of SEBAL in the Low- Middle São Francisco River basin.

Vegetation	Location (latitude, longitude)	Area (ha)	Irrigation system	Method of measurements
Wine grape	9°02' 24.53" S; 40°11' 13.49"W	4.13	Drip	Bowen ratio
Table grape	9°18' 40.84" S; 40°22' 29.47"W	5.13	Micro sprinkler	Bowen ratio
Mango	9°22' 32.20" S; 40°33' 54.23"W	11.92	Micro sprinkler	Eddy correlation
Caatinga	9°03' 30.71" S; 40°19' 45.21"W	N/A	Not irrigated	Eddy correlation

Table 4.2 shows the months and years covering the growing seasons used for water productivity and biomass production analyses of irrigated crops – wine grape, table grape, mango orchard and natural vegetation – caatinga.

Table 4.2: Duration of the experimental periods used for the energy and water balance analyses.

VG	2002	2003	2004	2005
	Months	Months	Months	Months
	1 2 3 4 5 6 7 8 9 10 11 12	1 2 3 4 5 6 7 8 9 10 11 12	1 2 3 4 5 6 7 8 9 10 11 12	1 2 3 4 5 6 7 8 9 10 11 12
WG	x x x x x x x x x x			
TG	x x x x	x x x x		
MG			x x x x x x x x x x x x x x x	x x x x x x x x x x x x
CT			x x x x x x x x x x x x	x x x x x x x x x x x x x x

* VG – vegetation; WG – wine grape; TG – table grape; MG – mango orchard; CT – caatinga.

65

In wine grape, the data were collected at the Vitivinícola Santa Maria farm near the town of Lagoa Grande-PE. The table grape plot was located in the Vale das Uvas farm near the town of Petrolina-PE. The experiments with mango orchard were carried out at the Fruitfort farm, near the town of Petrolina-PE. The tower in Natural Vegetation (caatinga) was located near the town of Lagoa Grande-PE.

Figure 4.1 shows the São Francisco River basin and the location of the field experiments together with the agro-meteorological stations. The green areas represent irrigated crops while the darker ones consist of natural vegetation and the thin blue lines are drainage lines. The experimental data set, together with satellite images and agro-meteorological stations, were used for analyses of actual evapotranspiration (ET_a), biomass production (BIO) and crop water productivity (CWP) in natural vegetation and irrigated crops as well as to calibrate and validate SEBAL algorithm for basin water management.
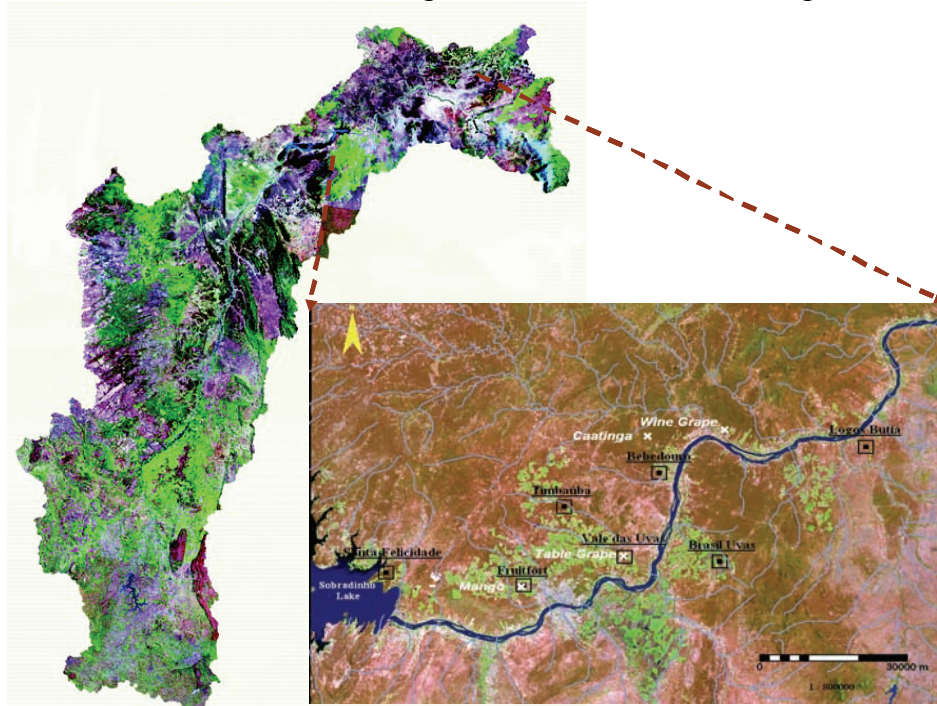

Figure 4.1. The São Francisco River Basin and the semi-arid region around the town of Petrolina-PE investigated. The agro-meteorological stations (black) and the flux towers (white) on irrigated crops (wine grape, table grape, mango orchard) and natural vegetation (caatinga) are indicated.

The weather data were taken from seven automatic agro-meteorological stations. The locations of the stations are described in Table 4.3. They were equipped with pyranometers, anemometers, net radiometers, sensors for air temperature and relative humidity, pluviometers and soil heat flux plates. The data was available for every 30 minutes and were used for the regional calculation of ET_0 by FAO Penman-Monteith method allowing the extrapolation of daily to seasonal or annual ET_a (Allen et al., 2007a).

Table 4.3: Agro-meteorological stations used to describe regional scale climatic variables interpolations.

Station	Latitude	Longitude	State
Fruitfort	09°22'22.99"S	40°33'40.47"W	Pernambuco
Vale das Uvas	09°18'50.93"S	40°22'22.98"W	Pernambuco
Bebedouro	09°08'12.35"S	40°18'31.51"W	Pernambuco
Timbaúba	09°12'28.75"S	40°29'05.21" W	Pernambuco
Santa Felicidade	09°20'40.24"S	40°48'59.42"W	Bahia
Brasil Uvas	09°19'26.71"S	40°11'48.67"W	Bahia
Logos Butiá	09°05'01.79"S	39°55'28.78"W	Bahia

The wine grape experiment

The wine grape was the cultivar *Petite Syrah*, being 10 years old at the time of the experiment installation in 2001. Two complete growing seasons in 2002 were used for wine water productivity analyses (Table 4.2). The plants were spaced at 1.20 m x 3.50 m, trained vertically to a bilateral cordon and spur pruned. The cordon wire was at a height of 1.60 m with no foliage wires (a sprawl type canopy developed). There was no cover crop between the rows, which were oriented in a north-south direction. The shoots were allowed to grow freely over the wires. Vertical trellis systems in wine grape are preferred instead the overhead horizontal type because it makes the mechanical practices easier. The daily drip irrigated area of 4.13 ha was bordered on all sides by other wine grapes. There was one drip emitter between two plants in the rows at a discharge rate of 4 L h^{-1}, suspended on the wire. Although it is common in many wine production areas not to irrigate vines at budbreak, or shortly thereafter, the irrigation manager started the irrigation soon after pruning with a fixed and large amount of water without quantifying the water demand. The soil is sandy with a water retention capacity that increases with depth, presenting a cracked rock layer below 0.60 m evidenced by the time of installing the tensiometers. Because the

vineyard was pruned two times in 2002, the wine water productivity analyses involved two growing seasons during this year. The duration of the first growing season (GS1) was 132 days, from 7 February to 19 June 2002, while the second one (GS2) comprised 136 days, from 08 July to 22 November 2002 (Table 4.2). Grapes were picked to produce wine in both periods.

The Bowen ratio surface energy balance method was used to measure the partitioning of net available energy into sensible and latent heat fluxes (Figure 4.2). The sensors were installed at the centre of the plot. The gradients of air temperature and vapour pressure above the crop were calculated using wet and dry thermocouples of cupper/constantan at 0.50 and 1.50 m above the canopy. The surface albedo ($\alpha_0 = R_R/R_G$) was measured through incident (R_G) and reflected (R_R) global solar radiation acquired with pyranometers faced up and down (model Eppley 19579, Rhode Island, USA and Eltec, Brazil). The net radiation (R_n) was measured at 1m over the canopy with two net radiometers (model NR-Lite, Kipp & Zonnen, Delft, the Netherlands), each one installed above a row of plants. The soil heat flux (G) was obtained with four heat flux plates (HFT3-L, REBS, Radiation and Energy Balance Systems, Seattle, WA and Hukseflux, Delft, the Netherlands) at 2 cm soil depth and 0.50 m from the plants. Two plates were buried at the west and the other two at the east side of two rows of plants. The values of G were the average of the four plates. The soil heat flux was not corrected for the heat storage above the plates; however as the surface above 2 cm is very thin, it was assumed that these corrections could be neglected.

Wind speed was measured with anemometers (R.M., Young wind Sentry 03101, Michigan, U.S.A) at two levels, i.e. 1.00 and 2.00 m above the canopy. Air temperature (T) and relative humidity (RH) at 0.50 m above the leaves were obtained with a probe from Vaisala (model HMP 35A, Helsinki, Finland), inside the shelter at the first level of the thermocouples. Soil moisture profiles were monitored weekly with tensiometers located between the drip emitters and the vine trunks. The soil moisture sampling depths were 20, 40 and 60 cm and considered to represent the effective root zone for vineyards in local soil and cultural conditions. Tensions were converted into soil moisture by using laboratory measurements of soil water retention curves. Applied water by irrigation was obtained by simple weekly readings of water meters attached to the drip pipes. Two days of wine grape site in 2001 coinciding with Landsat satellite overpass were used in the process of calibration and validation of SEBAL.

Figure 4.2 Measurements of gradients of air temperature, vapour pressure and wind speed; incident and reflected shortwave; net radiation; acquisition data system; and soil moisture in Bowen ratio system of wine grape.

The table grape experiment

The table grape cultivar was the *Superior seedless* and the vineyard was only 2 years old at the start of the measurement campaign. The plants were spaced at 3.50 m x 4.00 m, with the rows oriented in the usual north-south direction. The vineyard had an overhead horizontal trellis system at 1.80 m height. The cover crop consisted of a mixture of legumes and grasses, and was incorporated into the soil after budbreak. The plot investigated is 5.13 ha, surrounded by other table grapes. The crop was daily micro sprinkler irrigated, with one in-line micro sprinkler between two vines on the ground at a discharge rate of 44 L h^{-1} which wetted 70% of the soil surface. As in wine grape, the farmer started the irrigation soon after pruning with large amounts of water, thereby promoting high rates of direct soil evaporation and cover crop transpiration at initial stages. The soil is sandy throughout the vertical profile, but its water retention does not increase with depth. Water

holding capacity is higher in the upper soil layer (0-20 cm) due to high organic matter content. The measurements involved two growing seasons (GS1 and GS2), during the same period but in different years: both from 08 July to 07 October, in 2002 and in 2003 (Table 4.2). The duration of the growing seasons were 90 days only, being extremely short as compared to vineyards in California, South Africa and Australia, among others. The grapes were brought to the export market at the end of GS2 in 2003 allowing only this last growing season to be used for grape water productivity analyses. The crop was left resting between the two seasons, to avoid possible direct damage in fruits and high incidence of fungi diseases due to rainfall. At the stage of vegetative growth, non-fruitful shoots and lateral shoots growing in the fruiting zone were removed and at fruit growth stage the berries were protected with a white cover from direct solar radiation.

The same method, measurement procedures and manufacturer's equipment as for wine grapes were set up for table grapes with few differences (Figure 4.3). Two net radiometers were installed, with one instrument at 1.00 m over the canopy and the other at 1.00 m above the ground surface to measure intercepted radiation by the canopy. Two heat flux plates (model HFT3-L, REBS, Radiation and Energy Balance Systems, Seattle, WA) were used, one at the east and the other at the west side of two rows of plants at 2 cm soil depht. The values of G were the average of the two plates. As for table grapes, it was also assumed that corrections for soil heat flux for the heat storage above the plates could be neglected. T and RH near the leaves were measured by a probe from sky instruments (SKH 2013, Sky instruments LTD, Llandrindod Wells, UK) installed on the arm of the datalogger's shelter at 0.50 m below the trellis system and only one level anemometer was installed at 1.00 m above the canopy. Soil moisture profiles and applied water by irrigation were monitored weekly with tensiometers located between the emitters and the vine trunks along two rows at same soil depths as for wine grapes and with water meters in micro sprinkler pipes. For calibration and validation of the SEBAL algorithm, two days of table grape site in 2003 were used coinciding with the satellite overpass days.

Figure 4.3 Measurements of net radiation over and under canopy; air temperature and relative humidity; wind speed; and automatic data collection in Bowen ratio system of table grape.

In both vineyards above, the micrometeorological sensors were connected to a datalogger (model CR10X, Campbell Scientific, Logan, UT, USA) programmed to make readings each 5s storing averages for 10 minutes. In wine grape an additional datalogger from Licor (model LI-1000, Nebraska – USA) was installed while in table grape a multiplexer (model AM416, Campbell Scientific, Logan, UT) was used to increase the capacity of data acquisition systems (Figures 4.2 and 4.3).

The mango orchard experiment

The measurements in mango plot were in cultivar *Tommy Atkins*, 18 years old (in 2003), spaced in a regular square pattern at 10 m x 10 m, with an average height of 5.5 m, estimated mean leaf area index (LAI) of 5.6 and daily micro-sprinkler irrigation in an area of 11.92 ha, with one in-line micro sprinkler between two trees on the ground at a discharge rate of 44 L h^{-1} which wetted 70% of the soil surface. The orchard was bordered on all sides by other mango crops with similar height. The sensors were installed at the centre of the plot. There was no cover crop. The sandy soil is classified as Latossoil Red-Yellow with low retention capacity. The groundwater depth is approximately 2.5 m. The mango water productivity studies comprised two growing seasons. The duration of the first period was 390 days, from 01 October 2003 to 24 October 2004. The analyses continued into a second period of 370 days, elapsing from 25 November 2004 to 29 November 2005 (Table 4.2). During the experiments, all components of the energy balance were measured. Both eddy correlation and Bowen ratio surface energy balance methods were used for the partition of the heat fluxes (Figure 4.4).

The eddy correlation system measured the sensible and latent heat fluxes with a three-axis sonic anemometer (Model CSAT3, Campbell Scientific, Logan, UT) and a krypton hygrometer (Model KH20, Campbell Scientific, Logan, UT) connected to a datalogger (model CR10X, Campbell Scientific, Logan, UT, USA). The sensors were set at a height of 8.5 m (thus 3 m above the crown of the mango tree) with a horizontal separation of 0.15 m and a sampling frequency of 16 Hz. Corrections to the λE due to sensible and latent flux (Webb et al., 1980), oxygen absorption (Tanner et al. 1993) and frequency losses (Moore, 1986) were applied using software developed by van Dijk et al. (2004). The fluxes were computed for 30 minutes and later averaged for daily periods. The net radiation (R_n) was acquired with one net radiometer (model NR-Lite, Kipp & Zonnen, Delft, the Netherlands) above a row of plants at a height of 7.5 m. The soil heat flux (G) was measured with two heat flux plates (model HFT3-L, REBS, Radiation and Energy Balance Systems, Seattle, WA) at 2 cm soil depth and below the projected tree crown at 100 cm from the trunk. The flux plates were buried one at the west and the other at the east side of a row of trees. The values of G were obtained as the average of the two measurements. As for vineyards, it was also assumed that corrections for the heat storage above the soil heat flux plates could be neglected. The gradients of air temperature and

vapour pressure above the crop were calculated with wet and dry thermocouples of cupper/constantan at 1.0 and 3.0 m above the canopy. Data of T and RH near the leaves were acquired by a probe from Sky instruments (SKH 2013, Sky instruments LTD, Llandrindod Wells, UK). Low frequency data of R_n, G, T and RH were measured at each 5s interval and averages of 10 min were stored in another datalogger, being the same model as for eddy correlation measurements, equipped with a multiplexer (model AM416, Campbell Scientific, Logan, UT).

The soil moisture was monitored weekly in the orchard with tensiometers at depths varying between 20, 40, 60, 80, 100 and 120 cm, considered to be inside of the effective root zone for mango trees under local conditions. Suctions were converted into soil moisture by using soil water retention curves. For calibration and validation of the SEBAL algorithm, two days of mango orchard site in 2004 and 2005 and one day in 2006 and 2007 were used coinciding with the satellite overpass days.
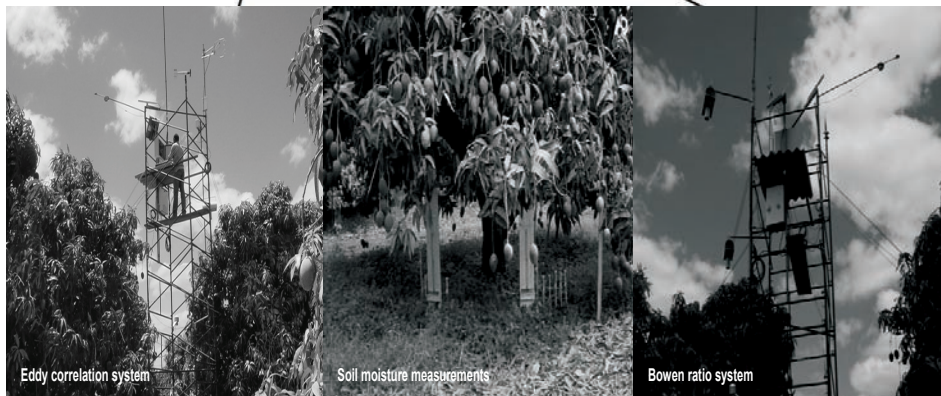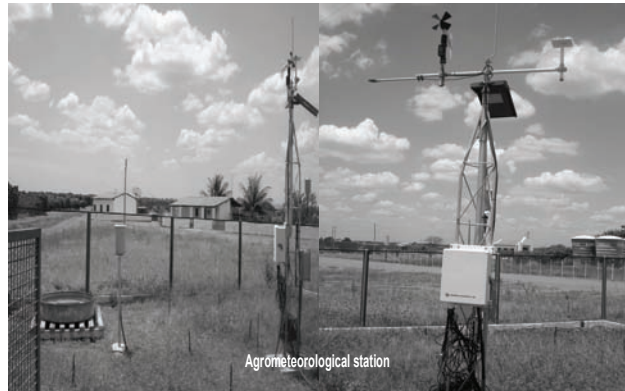
Figure 4.4 Measurements of radiation and energy balance; soil moisture; and reference evapotranspiration in mango orchard.

The natural vegetation experiment

Caatinga is a vegetation type whose location is mainly found in the northeast of Brazil. The dry period is characterized by brown vegetation. During the rainy period, the vegetation turns a verdant green. This natural vegetation is a mixture of species and the more frequent are *Caesalpinia microphylla* Mart., *Manihot pseudoglaziovii* Pax et. K Hoffman, *Croton conduplicatus* Kunth and *Sapium lanceolatum*. Some species have a loss of leaves in the dry season and others store water. The vegetation is distributed in an irregular way. Patches of bare soil and clumps of vegetation are interspersed. Agriculture is difficult without irrigation in this area. With irrigation systems in place one can plant fruits successfully and thereby replacing the natural vegetation by crops. Caatinga is defined as bushes that possess small leaves or thorns.

In Caatinga's site, the fluxes were measured with an eddy correlation system (Figure 4.5). The mean height of the vegetation was 8 m. The EC system over caatinga, was installed at 11 m above the ground surface, and consists of the same sonic anemometer as described as for mango orchard for determination of H, but for λE the gas analyzer (LI7500-Licor, Nebraska – USA) was used. The system had the same sampling frequency and datalogger as for mango orchard.

The data comprised measurements from 2003 to 2007, but only the years of 2004 and 2005 with different rainfall amounts were taken for seasonal analyses of water fluxes and biomass production (Table 4.2). All components of short and long wave solar radiation were measured at 10m above the ground with pyranometers and pyrgeometers (Kipp & Zonnen, Delft, the Netherlands) with sensors faced up and down.

R_n was acquired with a net radiometer at a height of 10 m and one soil heat flux plate placed at 2 cm below the soil surface was used for G. The same manufacturers for the net radiometer and soil heat flux plate, as in the mango orchard, were used. As for irrigated crops, it was also assumed that corrections for soil heat flux to account the heat storage above the plate could be neglected. Microclimatic measurements of T and RH were taken above the vegetation with a probe from Vaisala (model HMP 45C-L, Helsinki, Finland), at the same height of the radiation sensors. The low frequency data in caatinga were collected at each minute and averages of 10 minutes were stored in another datalogger (CR23X, Campbell Scientific, Logan, UT, USA). The satellite overpass days used for caatinga's site were two days in 2003, 2004 and

2005 and one day in 2006 and 2007. These days were used for calibration and validation processes of SEBAL.
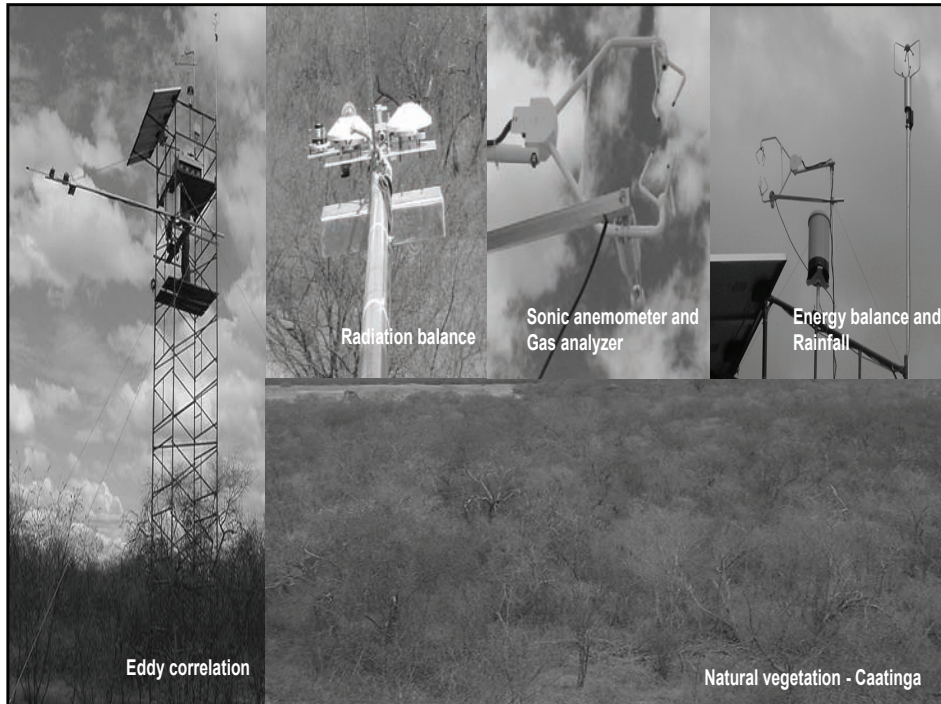
Figure 4.5 Measurements of radiation and energy balance over natural vegetation (Caatinga).

Table 4.4 resumes the data collection in all field experiments as well in agro-meteorological stations at the vicinities of each site.

Table 4.4: The field data over the period July 2001 to January 2007 in the four energy balance field experiments and agro-meteorological stations

Site	Instrumentation
Wine grape	• Tower - Bowen ratio system: gradients of air temperature and humidity. • Radiation: short wave radiation (downward and upward) and net of all wave radiation above the canopy. • Microclimatic conditions: air temperature and relative humidity at canopy level and gradient of wind speed above the canopy. • Soil heat flux at a depth of 2cm. • Soil moisture at the depths of: 20, 40 and 60cm
Table grape	• Tower - Bowen ratio system: gradients of air temperature and humidity. • Radiation: short wave radiation (downward) and net of all wave radiation above and under the canopy. • Microclimatic conditions: wind speed above the canopy (one level), air temperature and relative humidity at canopy level. • Soil heat flux at a depth of 2cm. • Soil moisture at the depths of: 20, 40 and 60cm
Mango orchard	• Tower - Bowen ratio and eddy correlation systems: gradients of air temperature and humidity; fluctuations of wind speed, air temperature and absolute humidity; and frictional velocity. • Radiation: short wave radiation (downward and upward) and net of all wave radiation. • Microclimatic conditions: wind speed above the canopy (one level), air temperature and humidity at canopy level. • Soil heat flux at a depth of 2cm. • Soil moisture at the depths of: 20, 40, 60, 80, 100, 120cm.
Caatinga	• Tower - Eddy correlation system: fluctuations of wind speed, air temperature and absolute humidity; and frictional velocity. • Radiation: short wave radiation (downward and upward), long wave radiation (downward and upward) and net of all wave radiation. • Microclimatic conditions: wind speed above the vegetation (one level), air temperature and humidity at leaves level. • Soil heat flux at a depth of 2cm. • Air pressure • rainfall above the vegetation

77

4.2   Satellite images

For this thesis regional radiation and energy balance calculations were done from Landsat Thematic Mapper (TM) and Enhanced Thematic Mapper (ETM+). The cloud free satellite images used are in Table 4.5.

Table 4.5: Satellite data over the period September 2001 to January 2007

Date	DOY	Satellite
10 September 2001	253	Landsat 7
04 October 2001	277	Landsat 5
06 July 2003	187	Landsat 5
24 September 2003	267	Landsat 5
12 October 2004	286	Landsat 5
14 November 2004	328	Landsat 5
15 October 2005	288	Landsat 5
16 November 2005	320	Landsat 5
30 July 2006	211	Landsat 5
22 January 2007	022	Landsat 5

* DOY – Day of the year

The Landsat images have a 16 overpass days at around 09:30 hours local time but only a maximum of two images per year were free of clouds. They were used together with the results of field experiments and interpolated weather data from the network of seven agro-meteorological stations.

Landsat-5 Thematic Mapper (TM) and Landsat-7 Enhanced Thematic Mapper (ETM+) are sun-synchronous, near-polar satellites that provide spectral radiance measurements in narrow bands. The bands 1 to 5 and 7 provide data for the visible and near infrared bands. The pixel size for these bands is 30 m by 30 m. TM band 6 provides data for longwave (thermal) radiation. The pixel size for this band is 60m by 60m for Landsat 7 and 120m by 120m for Landsat 5. Both Landsat satellites have a swath width of 185 km and orbit 705 kilometres (about 435 miles) above the Earth. Table 4.6 shows the characteristics of the Landsat sensors.

Table 4.6: Lansat satellite sensor characteristics

Satellite	Sensor	Bands	Bandwidth (μm)	Resolution (m)	Swathwidth (km)
Landsat 5	TM	1	0.45 to 0.52	30	185
		2	0.52 to 0.60	30	185
		3	0.63 to 0.69	30	185
		4	0.76 to 0.90	30	185
		5	1.55 to 1.75	30	185
		6	10.4 to 12.5	120	185
		7	2.08 to 2.35	30	185
Landsat 7	ETM+	1	0.45 TO 0.52	30	185
		2	0.52 to 0.60	30	185
		3	0.63 to 0.69	30	185
		4	0.76 to 0.90	30	185
		5	1.55 to 1.75	30	185
		6	10.4 to 12.5	60	185
		7	2.08 TO 2.35	30	185
		8 (pan)	0.50 TO 0.90	15	185

The TM sensor records reflect or emit radiation from the Earth's surface in the blue-green (band 1), green (band 2), red (band 3), near-infrared (band 4), mid-infrared (bands 5 and 7), and the far-infrared (band 6) portions of the electromagnetic spectrum.

The Landsat 7 satellite contains an improved Thematic Mapper sensor called the Enhanced Thematic Mapper (ETM+). The sensor records data in the same seven bands as the TM sensor aboard Landsat 5, but has an additional sensor that records data in a wide bandwidth (encompassing bands 2, 3, and 4) in a panchromatic mode (black and white). This panchromatic sensor has twice the resolution of the multispectral bands (Table 4.6). Unfortunately, an instrument malfunction occurred on May 31, 2003.

For Landsat 5 and 7 the spectral radiance for each band (L_b) is computed

$$L_b = \left[\frac{L_{MAX} - L_{MIN}}{QCAL_{MAX} - QCAL_{MIN}} \right] x (DN - QCAL_{MIN}) + L_{MIN} \quad (4.1)$$

where DN is the digital number of each pixel, L_{MAX} and L_{MIN} are calibration constants, $QCAL_{MAX}$ and $QCAL_{MIN}$ are the highest and lowest range of values for rescaled radiance in DN. The units for L_b are W m^{-2} sr^{-1} μm^{-1}.

For Landsat 5, $QCAL_{MAX} = 255$ and $QCAL_{MIN} = 0$. For Landsat 7 with header file data on gains and biases, a simpler equation for L_b is given:

$$L_b = (\text{Gain x DN}) + \text{Bias} \qquad (4.2)$$

where Gain and Bias refer to the values given in the header file.

Table 4.7 gives the values for L_{MAX} and L_{MIN} for Landsat 5 TM.

Table 4.7: The values of LMIN and LMAX (Equation 4.1) for TM measurements

Band Number	L_{MIN} W m^{-2} sr^{-1} µm^{-1}	L_{MAX} W m^{-2} sr^{-1} µm^{-1}
1	-1.500	152.100
2	-2.800	296.800
3	-1.200	204.300
4	-1.500	206.200
5	-0.370	27.190
6	1.238	15.600
7	-0.150	14.380

5. Crop water parameters of irrigated vineyards

5.1 Introduction

General aspects of vineyard water productivity in the world and in Brazil were dealt in details in Chapter 3. The vineyards growing under warm conditions of semi-arid region of São Francisco River basin exhibit an agronomic behaviour being different from those in temperate climates. While in these last climates a typical winter season induces dormancy in grapes, the continuous physiological processes in the semi arid climate of Northeast Brazil are accelerated and the propagation is very fast allowing the first production after 1.5 years. With proper irrigation and cultural management practices, the farmers in São Francisco Valley can produce grapes and wine in any time of the year, allowing on average 2.5 production cycles per year and the harvests in periods with higher prices, although for seedless table grapes the rainy period is avoided due to the direct damage to the fruits and the high occurrence of diseases.

In the increasing irrigated areas of São Francisco River basin it is deemed necessary to study the energy and water balances of vineyards for understanding and predicting the crop water productivity - CWP. As wine and table grapes are cultivated in different trellis and irrigation systems in the basin, it is important to quantify various grape water parameters under these differences, being the actual evapotranspiration (ET_a) the most important of them. ET_a from vineyards can be obtained accurately using weighing lysimeters (Evans et al., 1993; Williams et al., 2003; Williams and Ayars, 2005), eddy correlation technique (Oliver and Sene, 1992; Sene, 1994; Trambouse et al., 1998; Ortega-Farias et al., 2006) and the Bowen ratio energy balance method (Heilman et al, 1994, 1996; Rana et al., 2004; Yunusa et al., 2004, Azevedo et al., 2007). These studies reveal a significant variation in vineyard water consumption due to different irrigation strategies and cultural practices. While certain farmers prefer the production of high quantities of berries, others like a high quality product introducing significant water stress levels by partial root zone drying and deficit irrigation. The extrapolation of field measurements to irrigation schemes, regions and river basins are, therefore, cumbersome (Williams and Ayars, 2005). The ratio of actual to reference evapotranspiration (ET_a/ET_0) normalizes ET_a for climatic influences. This relation reflects the canopy development and vineyard water status as the crop stages progress (Snyder et al., 1989) and is useful to scale water fluxes from instantaneous or daily, seasonal or annual values in regional water balance studies (Allen et al., 2007a,b).

As Brazil is a developing country on fast track with a growing export of wines and fresh grapes, on-farm water management in vineyards is the cornerstone for a productive use of scarce water resources at the basin scale. The objective of this chapter is the determination of water parameters related to evapotranspiration such as the ratio ET_a/ET_0, evaporative fraction, soil evaporation and canopy transpiration, bulk surface and canopy resistances and water productivity for wine and table grapes growing under different trellis and irrigation systems. Up-scaling of these data sets will be dealt in Chapter 8 to analyze incremental evapotranspiration due to irrigation and for appraising the options for increasing total vineyard water productivity at the regional scale.

5.2   Methodology

The site and instrumental for measurements of ET_a was dealt in details in Chapter 4. The energy balance equation of a vineyard can be expressed by means of bulk energy and heat fluxes (Equation 2.1). The vineyard latent heat flux (λE_v) was obtained by a partitioning parameter:

$$\lambda E_v = \frac{R_{n_v} - G}{1 + \beta} \tag{5.1}$$

where R_{n_v} is the vineyard net radiation, H_v the sensible heat flux from the vineyard and G is the soil heat flux. β is the Bowen ratio:

$$\beta = \gamma \left(\frac{\Delta T}{\Delta e} \right) \tag{5.2}$$

and γ (kPa °C^{-1}) is the psychrometric constant, ΔT(° C) the temperature gradient measured by the dry thermocouples and Δe (kPa) is the water vapour pressure gradient measured by the difference between dry and wet thermocouples over the height interval above the vineyard canopy surface.

The ET_a was derived from the latent heat of vaporization (λ), density of water and λE_v. With measured values of R_{n_v} and G together with the estimations of λE_v, H_v was obtained as a residual in Equation 2.1.

The reference evapotranspiration (ET_0) was calculated in this study following FAO-56 standardized guidelines (Allen et al., 1998), using weather data from an automatic agro-meteorological station near the table grape plot (at a distance of 200m), also equipped with a pluviometer to measure rainfall. For the further separation of ET_a into actual transpiration (T_a) and actual soil evaporation (E_a), the lower envelop of ET_a/ET_0 values was considered as the basal crop coefficients (K_{cb}). Hence the Equations 2.12 and 2.13 were applied.

Initial and end values of K_{cb} were derived at these stages when foliage development was minimal. The mid-stage K_{cb} values were taken from Allen et al. (1998). Tabulated values for mid-stage K_{cb} of 0.80 for table grape and 0.65 for wine grape were adjusted for the specific weather conditions:

$$K_{cb} = K_{cb}(\text{tabular}) + \{0.04(u_2 - 2) - 0.04(RH_{min} - 45)\}\{h_v / 3\}^{0.3} \quad (5.3)$$

where u_2 and RH_{min} are respectively the averaged wind speed and minimum relative humidity at the agro-meteorological station (at a height of 2 m) and h_v (m) is the mean plant height for the mid-stage periods.

The surface roughness parameters of the vineyards were estimated from the flux profile relationships. The atmospheric surface-layer similarity theory was used (Stull, 1988; Monteith and Unsworth, 1990) applying universal integrated stability functions of temperature (Ψ_h) and momentum (Ψ_m) throughout Equations 2.6 to 2.11 for relating fluxes to atmospheric state profiles and surface properties (Businger et al., 1971).

The friction velocity, u_* (m s^{-1}), which is a velocity scale related to mechanically generated turbulence, was calculated from two-level (z_1, z_2) wind speed measurements (u_1, u_2):

$$u_* = \frac{k(u_2 - u_1)}{\ln\left[\dfrac{z_2 - d}{z_1 - d}\right] - \psi_m(\dfrac{z_2 - d}{L}) + \psi_m(\dfrac{z_1 - d}{L})} \quad (5.4)$$

The surface roughness length for moment transfer (z_{0m}) that together the roughness length for heat and vapour transfer ($z_{0h} = 0.1\ z_{0m}$) controls u_* and r_a was obtained from Equation 2.10 and the aerodynamic resistance, r_a (s m^{-1}), between the surface roughness and the canopy level

from where atmospheric state variables were measured was calculated from Equation 2.11

In Equation 5.4, u_1 and u_2 are the wind speed values at heights z_1 and z_2 (2.6 m and 3.6 m for wine grapes and 2.8 m and 3.8 m for table grapes), d is the zero plane displacement height (2/3 of the mean canopy height), k is the von Karman's constant (0.41) and L is the Obukhov length, which for vineyards was obtained by an iterative numerical method starting with a value of 10^6 m. The wind speed in table grapes was measured only at 2.8 m. The values at 3.8 m, necessary for solving u_* in Equation 5.4, were estimated by means of H_v and field measurements of ΔT considering initially neutral conditions solving r_a in Equation 2.3. The first values for u_* were then calculated by Equation 2.11 using the height levels of 3.8 m and 2.8 m. The resulted values of u_* were used in Equation 5.4 to obtain the wind speed at 3.8 m (u_2). Initially, a neutral condition in the logarithm wind profile equation was used to derive the first value of u_*, which could be subsequently improved with L.

The canopy latent heat flux (λE_c) was acquired from T_a. The continuous measurement of net radiation over and under the canopy made it possible to obtain the available energy to the soil surface (R_{n_g}) for table grape, as well to derive the amount absorbed by the canopy ($R_{n_c} = R_{n_v} - R_{n_g}$). With known values of λE_v, λE_c and r_a, the bulk surface (r_s) and canopy (r_c) resistances were estimated inverting the general Penman-Monteith equation (Farah, 2001):

$$\lambda E_{v.c} = \frac{\Delta(AE) + \rho_a c_p (D)/r_a}{\Delta + \gamma(1 + (r_{s,c})/r_a)} \tag{5.5}$$

where $\lambda E_{v,c}$ is the latent heat flux from the vineyard (subscript v) or from the canopy (subscript c); Δ (kPa °C^{-1}) is the slope of the saturated vapour pressure curve, AE is the available energy [(R_{n_v} - G) or ($R_{n_v} - R_{n_g}$)], ρ_a (kg m^{-3}) is the moist air density, c_p (J kg^{-1} K^{-1}) is the air specific heat at constant pressure, D (kPa) is the water vapour pressure deficit, γ (kPa °C^{-1}) is the psychrometric constant, and $r_{s,c}$ (s m^{-1}) is the bulk surface (subscript s) or canopy (subscript c) resistance to water vapour transport.

The Leaf Area Index (LAI) was derived for table grape with the values of intercepted radiation (Teixeira and Lima Filho, 1997) and consideration of the inversion of Beer's law:

$$\text{LAI} = 0.17 - 1.24 \ln\left[\frac{R_{n_g}}{R_{n_v}}\right] \tag{5.6}$$

Crop water productivity (CWP) in vineyards is commonly expressed in yield per unit of applied water, including rainfall and irrigation (Peacock et al., 1977; Araujo et al., 1995; Srinivas et al. 1999). In the present study it was calculated for the growing seasons (GS) applying Equation 2.19. The economic indicators used were the standard gross value of production over the irrigation supply (CWP$_I$), over actual evapotranspiration ($\text{CWP\$}_{ET_a}$) and over actual transpiration ($\text{CWP\$}_{T_a}$).

5.3   Analysis of results

Soil moisture and weather conditions

The values of soil moisture (θ) are shown in Figure 5.1. Soil moisture at 20 cm (θ_{20}) showed more variations with time than at deeper soil layers in both vineyards. This is an expected result because of the dynamic of infiltration and sub-sequent depletion by root water uptake and soil evaporation. The maximum values of θ in the wine grape were found at 60 cm depth pinpointing that moisture assembled in the lower root zone and was not easily drained away. This could be related to the increasing retention properties and reduced permeability at θ_{60}. For table grape the values were over against that maximal at 20 cm, which revealed typical free drainage conditions.

85
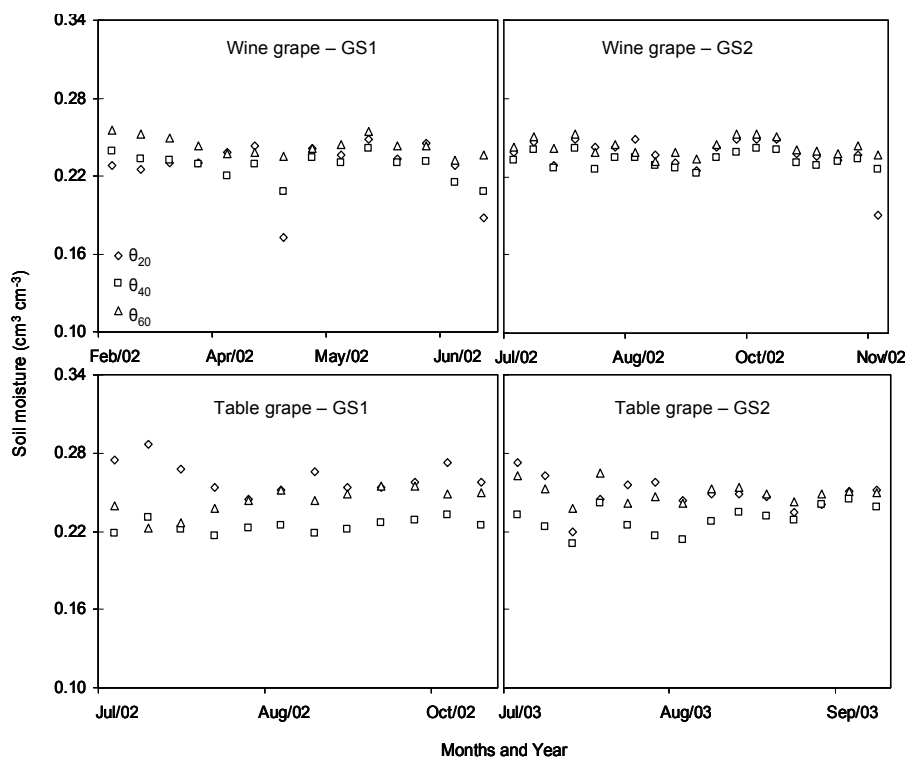
Figure 5.1 Soil moisture (θ_i) at different depths (i = 20, i = 40 and i = 60cm), during the first (GS1) and second (GS2) growing seasons of wine and table grapes.

Considering all depths, θ varied during most days between 0.19 to 0.29 cm^3 cm^{-3} in both vineyards, which was similar to the range those from Ortega-Farias et al. (2006) in Chile. A regular θ trend line reflects a constant supply and removal of irrigation water. Water excess can arise if supply exceeds removal by root water uptake, what in wine grape, could adversely affect the production and quality of wine. This excess not only enhances the loss of water resources but also valuable nutrients can be leached out the root zone.

July and October were the coldest and the warmest months of the year, respectively. The difference between the values of mean air temperature (T) near the canopies and at the agro-meteorological station was small (see Figures 5.2a and b). The seasonal average near-canopy T in wine grape was with 26.5° C, slightly higher than the 25.2° C for table grape. The lower values in the last vineyard could be ascribed to the

86

higher soil cover caused by the overhead trellis system and to wetter conditions promoted by micro sprinkler irrigation.

The higher values of wind speed (u) in the study region normally happen during the driest period, between August and October, with long term values reaching 3.0 m s^{-1} in September. The lowest values in the present study occurred during the rainy period with monthly average of 1.6 m s^{-1}. The daily variations of u over the vineyards and at agro-meteorological station are depicted in Figures 5.2c and d. During 2002 and 2003, averaged daily values were above 0.8 m s^{-1} and lower than 3.0 m s^{-1} for both vineyards. The above-canopy wind speed measurements accounted for 80% of those from the agro-meteorological station, which can be ascribed to differences in surface roughness.

The high values of T together with the dryness of the air induced high vapour pressure deficit (D) conditions outside the rainy period. The monthly averaged relative humidity in the region ranges from 55 to 70%. The 24 hours averaged values of D for the vineyards study period are plotted in Figures 5.2e and f. Wetter air near the canopy could be attributed to irrigation that raises the air humidity. This effect was greater in micro sprinkler irrigation system of table grape than for the drip irrigation conditions in wine grape.

According to Figures 5.2g and h, incident global solar radiation (R_G) decreased in the first half of the year of 2002 and increased during the second halves of the years 2002 and 2003. The reference evapotranspiration (ET_0) followed R_G. Higher values of R_G in the second half of 2002 established slightly bigger values for T and ET_0, in comparison with the same period in 2003. ET_0 was 4.4 mm d^{-1} and 5.0 mm d^{-1} on average for the first and second halves of 2002, while it averaged 4.1 mm d^{-1} during the second half of 2003. The total of precipitation during the first half of 2002 was 41.4 mm, and in the second half of the same year, it was 49.3 mm. It rained only 17.3 mm during the growing season of table grape in 2003.
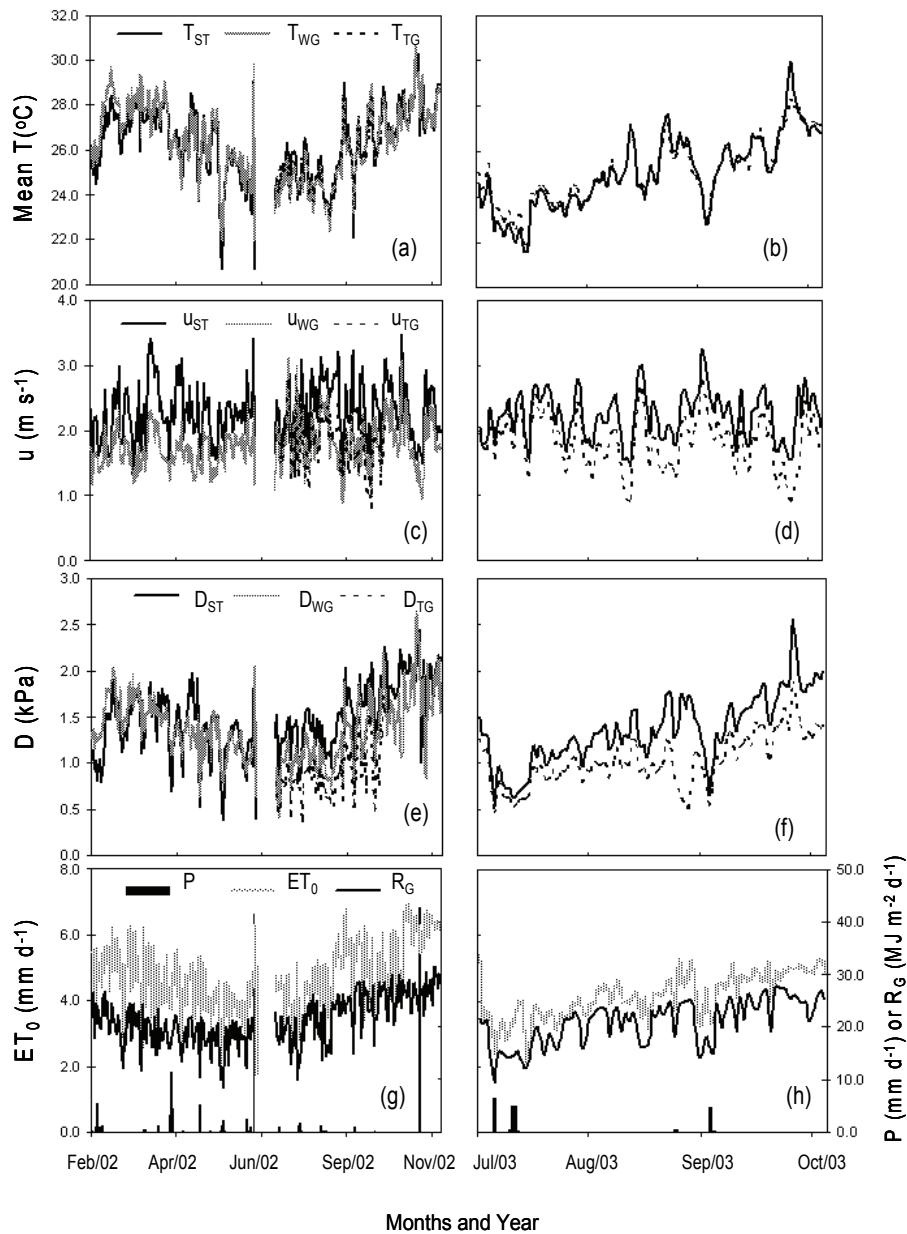
Figure 5.2 Averaged daily values of weather variables during the study period in 2002 and 2003 from agro-meteorological station (subscript ST) and near the canopies of wine grape (subscript WG) and table grape (subscript TG): (a) and (b) - Mean air temperature (T), (c) and (d) - Wind speed (u); (e) and (f) – Water vapour pressure deficit (D); (g) and (h) - Incident global solar radiation (R_G), reference evapotranspiration (ET_0) and precipitation (P).

88

Vineyard energy partitioning

The values of the components of the energy balances – and the latent heat flux from the vineyards (λE_v) in particular – varied according to R_G. The diurnal variations of these components for the period of measurements are depicted in Figure 5.3. Maximum midday λE_v values were around 400 - 500 W m^{-2} for both vineyards. The fluxes had a very smooth behaviour during daytime hours, with an exception for G in wine grape, which presented midmorning and midafternoon peaks and lower values at midday due to the canopy architecture, what is in agreement with Heilman et al. (1994).

Figure 5.3 Diurnal averages for the energy balance components during the first (GS1) and second (GS2) growing seasons of wine and table grapes: Vineyard net radiation (R_{n_v}); vineyard latent heat flux (λE_v); vineyard sensible heat flux (H_v) and soil heat flux (G).

89

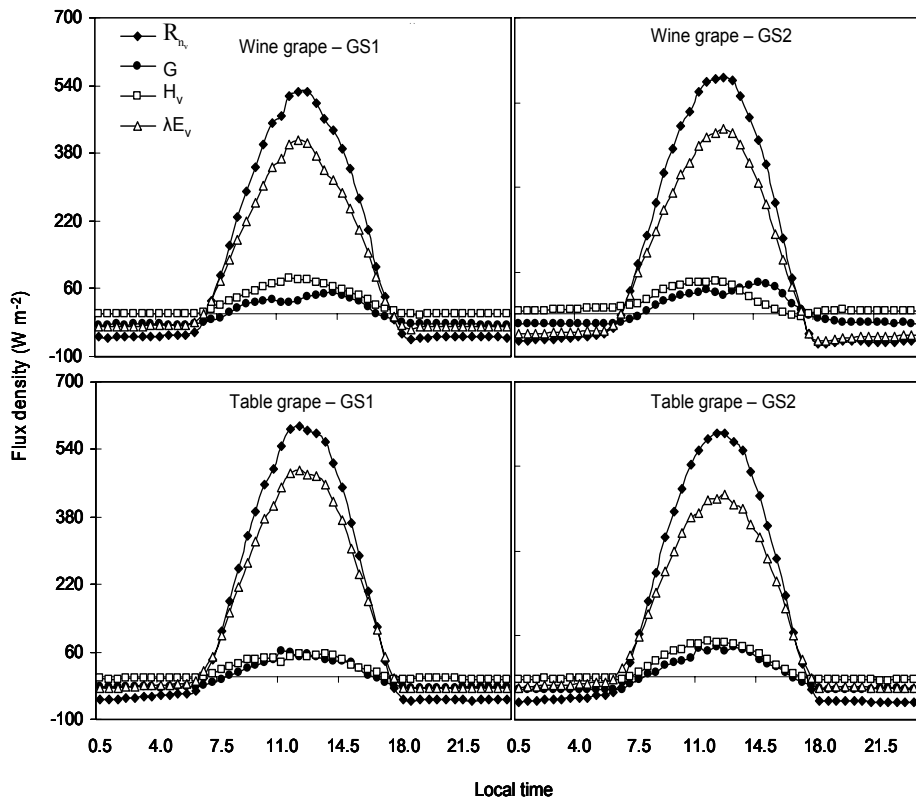Daily averages of vineyard energy balances components for wine grape in 2002 are presented in Table 5.1. The R_{n_v} was on average 46% of R_G for both growing seasons. A fraction of approximately 50% is in agreement with earlier crop science radiation studies (e.g. Makkink, 1957; Oliver and Sene, 1992).

The H_v accounted for 18 % of R_{n_v} for both growing seasons of wine grape, being a modest heat flux. During GS1 the daily averaged G was negative because heat was released from the warm soil body. The opposite situation occurred during GS2. The largest portion of R_{n_v} was converted into λE_v, which represented around 83% and 78% in GS1 and GS2, respectively, corresponding to an evaporative fraction [$E_F = \lambda E_v/(R_{n_v} - G)$] around 81%.

Table 5.1: Daily averages of the vineyard energy balance components for wine grape at Lagoa Grande-PE, Brazil, for the first growing season (GS1) from 07/02 to 19/06 and for the second growing season (GS2) from 08/07 to 21/11, both in 2002: vineyard net radiation (R_{n_v}), vineyard latent heat flux (λE_v), vineyard sensible heat flux (H_v), soil heat flux (G) and evaporative fraction (E_F) are presented.

DOY	R_{n_v} (MJ m^{-2} d^{-1})	λE_v (MJ m^{-2} d^{-1})	H_v (MJ m^{-2} d^{-1})	G (MJ m^{-2} d^{-1})	E_F (-)
GS 1					
057	11.69	9.20	2.09	0.40	0.81
077	10.63	8.34	2.00	0.29	0.81
097	10.01	8.13	1.91	-0.01	0.81
117	10.07	8.35	2.14	-0.42	0.80
137	9.65	8.16	1.91	-0.42	0.81
157	8.05	7.17	1.64	-0.76	0.81
170	7.45	6.62	1.57	-0.73	0.81
Mean	9.65	8.00	1.89	-0.24	0.81
GS 2					
208	8.59	6.48	1.69	0.42	0.79
228	9.43	6.98	1.80	0.65	0.80
248	11.67	9.63	1.71	0.33	0.85
268	12.59	9.73	2.18	0.68	0.82
288	12.69	9.64	2.43	0.62	0.80
308	14.06	11.39	1.92	0.74	0.86
325	14.32	11.23	2.42	0.67	0.82
Mean	11.91	9.30	2.02	0.59	0.82

*DOY – Day of the year. The values were taken at 20 days intervals.

Daily averages of energy balance components for table grape in 2002 and 2003 are presented in Table 5.2. R_{n_v} represented a fraction of 55% of R_G, being higher than for wine grape; the overhead trellis and micro sprinkler irrigation systems promoted lower both, albedo and longwave emission, increasing R_{n_v}. The measured albedo in wine grape in the actual study varied between 0.19 and 0.24, while the estimated values for table grapes were from 0.17 to 0.21. The values for wine grapes are higher than for micro sprinkler irrigated table grape (0.18 to 0.23) reported by Azevedo et al. (1997), while the estimated table grapes values in the actual study were lower than those of these last authors.

Table 5.2: Daily averages of the vineyard energy balance components for table grape crop at Petrolina-PE, Brazil from 08/07 to 06/10 of the first growing season (GS1) in 2002 and for the second growing season (GS2) in 2003: net radiation (R_{n_v}), vineyard latent heat flux (λE_v), vineyard sensible heat flux (H_v), soil heat flux (G) and evaporative fraction (E_F) are presented.

DOY	R_{n_v} (MJ m^{-2} d^{-1})	λE_v (MJ m^{-2} d^{-1})	H_v (MJ m^{-2} d^{-1})	G (MJ m^{-2} d^{-1})	E_F (-)
GS 1					
204	9.73	9.00	0.78	-0.06	0.92
219	10.29	9.19	1.20	-0.10	0.88
233	10.25	9.33	1.17	-0.25	0.89
249	12.79	11.66	1.24	-0.11	0.90
264	13.09	11.96	1.40	-0.27	0.89
280	13.32	12.20	1.12	0.00	0.92
Mean	11.58	10.56	1.15	-0.13	0.90
GS 2					
204	7.35	6.75	0.76	-0.17	0.90
219	9.49	8.40	1.40	-0.32	0.86
233	10.82	9.50	1.71	-0.39	0.85
249	11.70	10.24	1.88	-0.41	0.85
264	12.50	10.29	2.07	0.14	0.83
280	13.76	11.66	1.70	0.40	0.88
Mean	10.94	9.47	1.58	-0.12	0.86

*DOY – Day of the year. The values were taken at 15 days intervals.

Near neutral conditions predominated above the table grape, with H_v representing around 12% of R_{n_v}. The averaged G was negative during both seasons, accounted for only 1% of R_{n_v}. The largest portion of R_{n_v} was also partitioned into λE_v which represented 91% and 87% in

2002 and 2003, respectively, corresponding to a mean E_F of 88%. Higher values of energy partition as λE_v are explained by moister both, microclimatic and soil conditions in table grape than in wine grape. According to Scott et al. (2003), E_F also reflects the moisture conditions in the root zone. High values reveal that the crop is not water stressed, and that the soil is wet, what is confirmed by the Figure 5.1.

Differences in the partition of the energy balance with different trellis and training systems in vineyards were also reported by Novello et al. (1992), Heilman et al. (1996), Katerji et al. (1994) and Rana et al. (2004).

Vineyard water fluxes

For GS1 of wine grape, the average 24-hourly λE_v of 8.00 MJ m^{-2} d^{-1} corresponded to an ET_a of 3.3 mm d^{-1}. This value is similar to Heilman et al. (1996) in Texas (3.6 mm d^{-1}) who also used a Bowen ratio system for energy balance measurements. During GS2, the average 24-hourly λE_v increased to 9.30 MJ m^{-2} d^{-1} being equivalent to 3.8 mm d^{-1}. The accumulated values of ET_a were 438 mm and 517 mm, for respectively GS1 and GS2, showing the seasonal effects (Table 5.3).

The average daily λE_v values of 10.56 and 9.47 MJ m^{-2} d^{-1} for table grape represented ET_a of 4.4 mm d^{-1} in 2002 and 3.9 mm d^{-1} in 2003, respectively. Higher daily values than for wine grape are due to the micro sprinkler irrigation system, bigger soil cover and the transpiration from the cover crop of legumes and grasses at initial stages. Consequently, the ratios of ET_a, T_a and E_a to ET_0 were higher and resistance values were lower than for wine grape (Table 5.3). As the growing season of table grape is around 90 days only, the seasonal crop water consumption is with a mean value of 372 mm lower than for wine grape (478 mm).

A review of international literature about water use in vineyards showed an average ET_a from nine field experiments of 3.0 mm d^{-1} (Oliver and Sene, 1992; Evans et al., 1993; Heilman et al., 1996; Yunusa et al., 1997b; Trambouse et al., 1998; Williams et al., 2003; Yunusa et al., 2004; Rana et al., 2004, Williams and Ayars, 2005).

Table 5.3: Water-use variables for wine and table grapes during the first (GS1) and second (GS2) growing seasons in 2002 and 2003: reference evapotranspiration (ET_0); actual evapotranspiration (ET_a); actual transpiration (T_a); actual soil evaporation (E_a); ratios ET_a/ET_0, T_a/ET_0 and E_a/ET_0; aerodynamic (r_a), surface (r_s) and canopy (r_c) resistances; and leaf area index (LAI).

Variable	Wine grape GS1	Wine grape GS2	Table grape GS1	Table grape GS2
Duration (days)	132	136	90	90
ET_0 (mm)	586	671	435	382
ET_a (mm)	438	517	393	352
T_a (mm)	385	462	312	293
E_a (mm)	53	56	81	59
ET_a (mm d^{-1})	3.3	3.8	4.4	3.9
ET_a/ET_0	0.75	0.77	0.90	0.92
T_a/ET_0	0.66	0.69	0.72	0.77
E_a/ET_0	0.09	0.08	0.18	0.15
r_a (s m^{-1})	114	109	63	66
r_s (s m^{-1})	131	125	64	82
r_c (s m^{-1})	-	-	49	89
LAI	-	-	0.70	1.60

The mean values of daily water consumption obtained in semi arid region of São Francisco River basin are, in general, greater than those from literature, however, Williams and Ayars (2005) reported similar daily values of ET_a for cv. Thompson Seedless in Sao Joaquin Valley of California, when there was neither gibberelic acid (GA3) application nor trunk girdling, comparing with the 3-years-old Superior Seedless of the actual study. By the other hand, as the growing seasons in the São Francisco Valley are shorter, the seasonal water consumption is lower. A water balance study in vineyards in South Africa (Jairmain et al., 2007) showed that the average value of seasonal ET_a for wine grape is around 621 mm and for table grape is in the range from 519 to 827 mm. The length of the growing seasons in South Africa is between 6 to 8 months with only one harvest per year.

ET_a can be corrected for climatic influences by normalizing it with ET_0, producing the ratios ET_a/ET_0. The ET_a/ET_0 values can be variable with the crop properties and stress conditions caused by water deficit and salinity. Under pristine conditions, the crop will be at potential evapotranspiration (ET_p) and K_c values (ET_p/ET_0) can be taken (Allen et al., 1998). The weekly interval averaged ET_a/ET_0 data for the second growing seasons of wine and table grapes, outside the rainy

period of the year, were fitted with polynomial functions expressed in degree days (Basal T = 10° C) rather than in calendar days, for incorporation of T effects on the growing stages of the vineyards (Figure 5.4). The ratios of water fluxes to ET_0 at the initial stage are highly related to the cover crop and irrigation. For wine grape, the mean weekly values of ET_a/ET_0 in GS1 were in the range from 0.65 to 0.82, while for GS2 they were from 0.63 to 0.87. For table grape, the weekly averaged values of this ratio for both growing seasons varied between 0.77 and 0.91. On average, 89 to 90 % of the total ET_a was used for T_a and 10 to 11% for E_a in wine grape. For table grape, 79 to 83 % of ET_a was used for T_a and 17 to 19% for E_a.
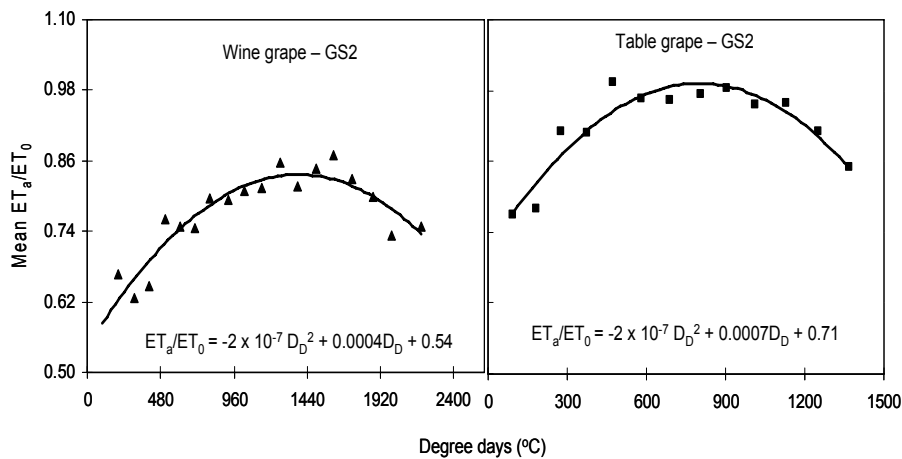
Figure 5.4. The seasonal variation of ET_a/ET_0, as a function of degree days - D_D (Basal T = 10^oC), during the second growing seasons of wine grape – 2002 (a) and table grape – 2003 (b), by the Bowen ratio method. Weekly intervals were averaged.

The behaviours of daily ratios of ET_a/ET_0, T_a/ET_0 and E_a/ET_0 are demonstrated in Figure 5.5. Actual growing conditions of this study can also include few non-pristine environmental circumstances.
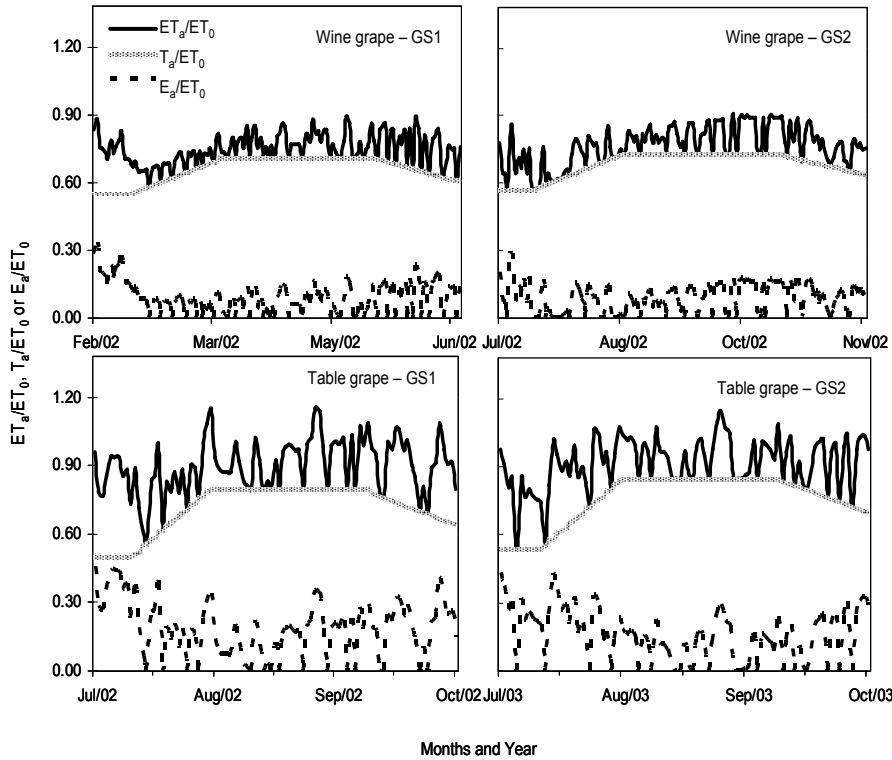
Figure 5.5. Seasonal variation of the daily ratios of water fluxes to reference evapotranspiration (ET_0) during the first (GS1) and second (GS2) growing seasons of wine and table grapes: actual evapotranspiration (ET_a), actual transpiration (T_a) and actual soil evaporation (E_a) to ET_0.

The values of ET_a followed the ET_0. For table grape, ET_a rates sometimes exceeded ET_0, during the crop stages, resulting in daily ET_a/ET_0 values exceeding 1. Soil evaporation caused by the micro sprinkler irrigation, played a role in these high values, as can be seen by the behaviour of E_a/ET_0. This effect was more pronounced in GS1, when the crop was younger.

The seasonal behaviour of the daily water fluxes are shown in Figure 5.6 for both growing seasons of wine and table grapes. It can be seen that in general, ET_a decreases from the start to the middle of the year and increase again in the second half.
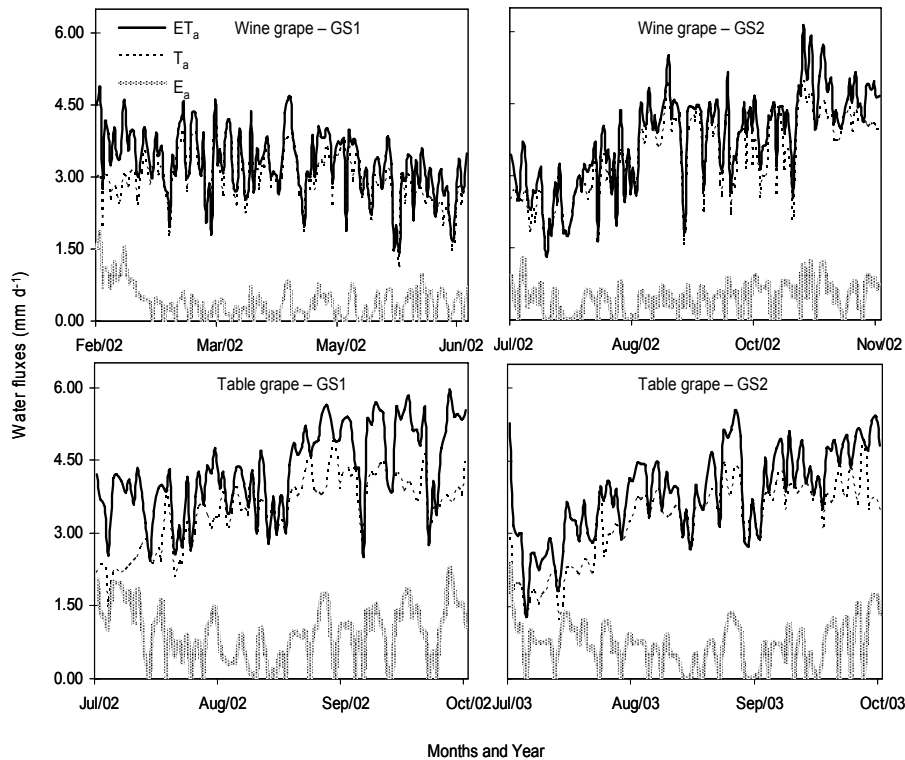
Figure 5.6. Seasonal variation of the daily water fluxes, during the first (GS1) and second (GS2) growing seasons of wine and table grapes: actual evapotranspiration (ET_a), actual transpiration (T_a) and actual soil evaporation (E_a).

By the bigger fluctuations in E_a in micro sprinklers (Table grape) it is noticed that this irrigation system have a higher portion of non-beneficial water flux than drip systems. Maximum T_a values were around 5.0 mm d^{-1} for both vineyards, while the biggest differences were those for E_a with maximum values of 1.8 mm d^{-1} and 2.4 mm d^{-1} for wine and table grapes, respectively, during the growing seasons.

Vineyard resistances

Data availability of net radiation above (R_{n_v}) and under (R_{n_g}) the canopy for table grape allowed the calculation of intercepted net radiation ($R_{n_i} = R_{n_g} / R_{n_v}$) and the estimation of leaf area index (LAI) for

96

the two growing seasons applying Equation 5.6. The mean values of LAI (Table 5.3) pinpointed a situation of a young maturing vineyard., being the value of for GS2 (1.60) close to that found by Rana et al. (2004) for table grapes in Italy and by Yunusa et al. (2004) for mature Sultana grapes, growing in a T-trellis system in Australia. Klaasse et al (2007) reported LAI values between 2.5 and 3.0 for the table grapes and around 1.0 for wine grapes, in Hex River Valley, West Cape Province (South Africa). According to Katerji et al. (1994), LAI for vineyards in rows with a dominant vertical plant structure present values around 0.70-0.80. There were no measurements of R_{n_i} to allow LAI estimations in wine grapes in the actual study.

The seasonal variations of aerodynamic (r_a), surface (r_s) and canopy (r_c) resistances are shown in Figure 5.7. Averaged values are found in Table 5.3. In wine grape the values of r_a stayed in the range from 78 to 170 s m^{-1}, while for table grape, the range was from 30 to 160 s m^{-1}. The lower r_a values for table grape can be related to the aerodynamic smoother horizontal trellis systems. Both higher LAI and soil cover cause a shelter effect (e.g. Verhoef et al., 1997).

The r_s values in wine grape were between 35 and 240 s m^{-1}. For table grape the range was from 10 to 140 s m^{-1}. Heilman et al. (1994) found maximum values of r_s of 50 and 75 s m^{-1}. The canopy resistance (r_c) for table grape in both years stayed between 20 and 182 s m^{-1}. Assuming that the stomatal resistance (r_{st}) can be roughly estimated by (0.5 x LAI x r_s) as reported in several handbooks (Allen et al., 1998), the mean values of r_{st} become 22 s m^{-1} and 66 s m^{-1}, for GS1 and GS2 of table grape, respectively. Winkel and Rambal (1990) described r_{st} response of different French vineyards. The minimum values were 73 s m^{-1} for Carignane, 93 s m^{-1} for Merlot and 114 s m^{-1} for Shiraz. According to them, the main reason for these differences could be attributed to different conditions of D, soil cover, θ and evaporative demand.
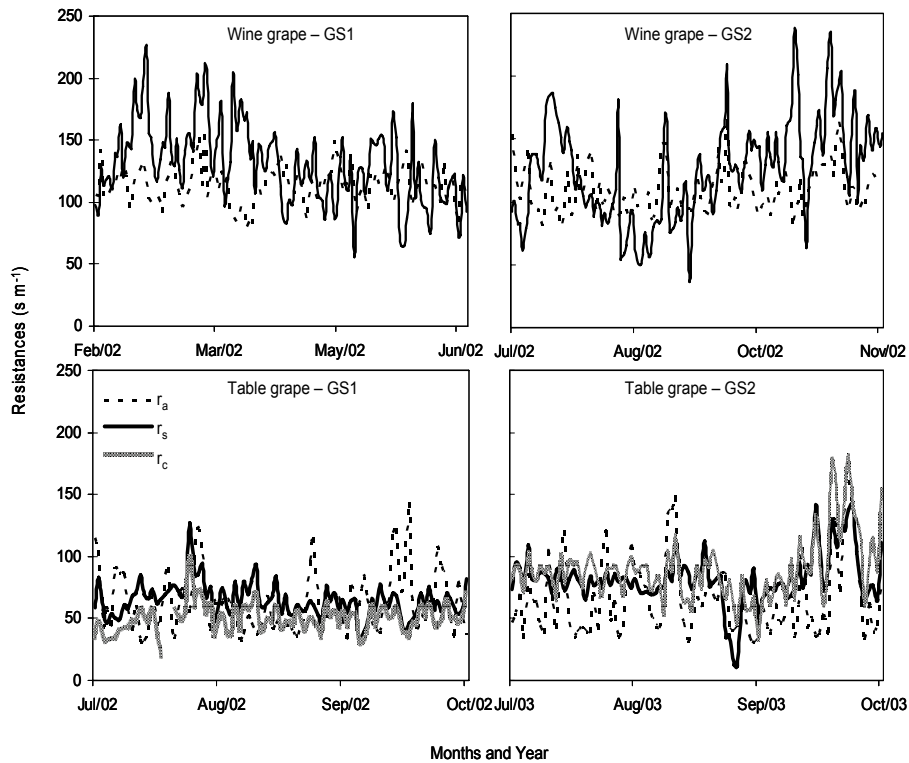
Figure 5.7. Seasonal trends of calculated aerodynamic (r_a), surface (r_s) and canopy resistances (r_c), during the growing seasons of wine and table grapes.

Ben-Asher et al. (2006) measured r_{st} of grapes under saline irrigation conditions in Israel, and they showed minimum values of 135 s m^{-1}. The low values of r_s, r_c and r_{st} in micro sprinkler irrigated table grape of semi arid region in Brazil are due wet conditions for both, soil and air near the canopies. The magnitude of the differences between r_s and r_c comparing the two growing seasons can be explained because for the younger vineyard in 2002, the lower R_{n_i} promoted the soil component to represent a relative large fraction of r_s (Figure 5.7).

The different magnitudes of grape water parameters between the two vineyards discussed above were due to differences in crop stages, age and varieties, trellis and irrigation systems, soil cover and cultural management.

98

Vineyard water productivity

A summary of all crop water productivity parameters for both vineyards is presented in Table 5.4. Large portion of applied irrigation water turned into percolation losses. The values of deep percolation (P_D) were computed as the differences between rainfall, irrigation and ET_a, and there were no corrections made for soil storage changes. It is worrisome to note that the percolation rates had the same magnitude as ET_a.

Table 5.4 Yield for growing seasons (Y_{GS}), actual evapotranspiration (ET_a), actual transpiration (T_a) Irrigation (I), precipitation (P), deep percolation (P_D), crop water productivity (CWP) based on I, ET_a and T_a for wine (litres of wine) and table (kilograms of fruits) grapes.

Variable	Wine grape GS1	Wine grape GS2	Table grape GS2
Period	7 February to 19 June 2002	8 July to 21 November 2002	8 July to 6 October 2003
Y_{GS} (kg ha^{-1})	4,222	8,143	11,200
Y_{GS} (L ha^{-1})	3,376	6,514	na
ET_a (mm)	438	517	352
T_a (mm)	385	462	293
IRR (mm)	874	960	827
P (mm)	41	49	17
P_D (mm)	477	492	492
CWP_I (kg m^{-3})	0.48	0.85	1.35
CWP_{ET_a} (kg m^{-3})	0.96	1.58	3.18
CWP_{T_a} (kg m^{-3})	1.10	1.76	3.82
CWP_I (L m^{-3})	0.39	0.68	na
CWP_{ET_a} (L m^{-3})	0.77	1.26	na
CWP_{T_a} (L m^{-3})	0.88	1.41	na
$CWP\$_I$ (US\$ m^{-3})	0.35	0.62	2.77
$CWP\$_{ET_a}$ (US\$ m^{-3})	0.70	1.15	6.51
$CWP\$_{T_a}$ (US\$ m^{-3})	0.80	1.28	7.82

Wine yield values are inside in what is expected to be normal practices in this region. The differences in between GS1 and GS2 pinpointed seasonal effects. GS1 was cloudier and the duration of the days during the stages of flower and maturation of fruits were shorter than GS2. As a consequence, GS1 yielded lower economical water productivity than GS2. Although the productivity for one growing season of wine grape is lower than in regions where the climate is temperate, the total production of two growing seasons in one year is in good agreement with for instance South Africa (Jairman et al., 2007).

The yield in 2002 for table grape was not marketable. Only the growing season in 2003 was analyzed for water productivity purposes. The yield of fresh table grapes was in agreement with the public perception in the São Francisco River basin. At a double season, the yield could increase to 22.4 t ha^{-1}. The CWP_{ET_a} values for marketable table grape were found to be lower than previous table grape studies with drip and furrow irrigation (Yunusa et al., 1997b). Klaasse et al. (2007) reported a value of CWP_{ET_a} of 3.70 kg m^{-3} in South Africa. The economic water productivity performance for table grape are in order of magnitude higher than for wine grape, however, the overall production costs for table grape are significantly more; hence the differences in net income between table and wine grapes tend to reduce. The difference between $CWP\$_{ET_a}$ and $CWP\$_{T_a}$ is higher for table grape than for wine grape, showing the better performance of drip irrigation system in comparison with micro sprinkler irrigation.

5.4 Conclusions

Albedo, evaporative fractions, beneficial/non-beneficial water consumption, aerodynamic resistance, bulk surface resistance and canopy resistance for vineyards in semi-arid region of São Francisco River basin were derived from the field data set and compared with the international literature. The results allowed expressing water consumption in more specific bio-physical parameters, rather than only by crop coefficients that lump together other crop water parameters.

Considering totals for two growing seasons, the actual evapotranspiration of table grape was less (352 to 393 mm) than for wine grape (438 to 517 mm). Water fluxes from vineyards in this semi arid region are essentially driven by solar radiation. The partitioning of available energy into latent heat flux in the two vineyards studied was found extremely constant throughout the crop stages due to a systematic

100

over-irrigation that induces a continuous deep percolation flux. Micro-sprinklers increase the moisture content in soil and lower atmosphere, which turns the fraction of non-beneficial actual evapotranspiration to 18%, comparing to 10 % in drip systems.

The vineyard water productivities are extremely high when comparing with annual crops, both bio-physically as well as economically with values exceeding 3 kg harvestable fresh product per unit of water depleted in the case of table grapes. Analyzing the specific plots, the economic water productivity based on actual evapotranspiration ($CWP\$_{ET_a}$) exceeded 1.00 US\$ m^{-3} (for wine grape), up to 6.51 US\$ m^{-3} (for table grape).

The crop water productivity analyses of two vineyards revealed that water is wisely used, however by sampling two specific plots of wine and table grape crops under different cultural management, it can be seen that the regional irrigation management requires full attention as significant percolation can adversely affects environments in terms of rising water tables and return flow of polluted water to the river.

6. Crop water parameters of mango orchard

6.1 Introduction

General aspects of mango water productivity in the world and in Brazil were dealt in details in Chapter 3. The overview indicated that the water use of fruit crops varies considerably, being unknown how much variability exists from orchard to orchard. Differences in cultivation practices or the method used in calculating evapotranspiration is of fundamental importance for extrapolation of research results to other regions (Williams and Ayars, 2005).

The relationship between irrigation, actual evapotranspiration (ET_a), yield and percolation is essential for applying and maintaining good water management practices. ET_a measurements by energy balance techniques in fruit crops, vineyards and vegetables have been made in grapes (Heilman et al., 1996), mango orchard (Azevedo et al., 2003), garlic (Villalobos et al. 2004), grapes (Yunusa et al., 2004), pecans (Samis et al., 2004), citrus (Rana et al., 2005), peach (Paço et al., 2006), olives (Testi et al., 2006) and grapes (Teixeira et al., 2007), however, the agro-hydrological processes in a mango orchard are only rarely described in the international literature. Despite the economical and nutritious importance of its fruits, little research has been attributed to the mango water productivity.

Irrigation of mango orchards can be associated with environmental problems. Molle et al. (1999) reported that mango orchards in Thailand are receiving 20 pesticide treatments and 5 fertilizer applications per season. Although the attention to irrigated orchards leaking root zones is growing, knowledge on evapotranspiration – percolation relationships is nevertheless limited. Thus the environmental impact of non-consumed irrigation water requires more attention. This chapter addresses ET_a measurements which, in conjunction with soil moisture storage changes, and rainfall, allowed the isolation of percolation fluxes (instead of deriving ET_a from percolation estimates, it was assessed percolation from ET_a estimates).

The general objective of this study was to find useful recommendations for a rational and strategic water management in irrigated mango orchards. The specific objectives of this chapter are:
- The evaluation of the performance of the eddy correlation technique for measuring actual evapotranspiration in tropical fruits

- Assessment of daily and seasonal actual mango evapotranspiration and related crop water parameters for two complete growing seasons having different rainfall regimes
- Determination of the field scale water balance for irrigation performance and environmental analysis
- Quantifying water productivity indicators at field scale that can be used in subsequent up scaling studies that will be dealt in Chapter 8.

6.2   Methodology

The experimental setup was described in Chapter 4. During the experiments, all components of the energy balance were acquired by both, the Bowen ratio (BR) and eddy correlation (EC) methods, but only EC measurements were used for water productivity analyses in this chapter. The BR method was explained in Chapter 5. By using EC method, the latent heat flux (λE) was calculated by the following expression:

$$\lambda E = L_v \overline{w'\rho_v'} \tag{6.1}$$

where L_v is the vaporization latent heat and ρ_v' is the instantaneous deviation of water vapour density in relation to the mean value (kg m^{-3}). The quantity $\overline{w'\rho_v'}$ is the co-variance between the vertical wind speed and water vapour density and the bars means average (Stull, 1988).

The sensible heat flux (H) was calculated by the following expression:

$$H = \rho_a c_p \overline{w'T'} \tag{6.2}$$

where w' is the instantaneous deviation of vertical wind speed (w) in relation to mean value, and T' is the instantaneous deviation of T in relation to mean value. The quantity $\overline{w'T'}$ is the co-variance between the vertical wind speed and air temperature and the bar means average (Stull, 1988).

Because of the lack of energy closure, a hybrid combination of radiation and flux measurements was deployed in this chapter. By this combination method using EC measurements and the Bowen ratio of the fluxes ($\beta = H/\lambda E$), the latent heat flux was derived using the Equations 5.1 for the mango orchard. The ET_a was calculated transforming the λE

into millimetres of water. The calculation of ET_a at a daily time scale was obtained by summation of all 30 minute values for 24 hour periods.

The reference evapotranspiration (ET_0) was calculated following Allen et al. (1998) using weather data from an agro-meteorological station in the vicinity of the orchard (500 m). Half hourly measurements of average air temperature (T), relative humidity (RH), wind speed (u), net radiation (R_n) over grass and soil heat flux (G) under grass were used. For the further separation of ET_a into actual transpiration (T_a) and actual soil evaporation (E_a), the lower envelop of ET_a/ET_0 values was considered as the basal crop coefficients (K_{cb}) and then the Equations 2.12 and 2.13 were applied for mango orchard.

The soil moisture was weekly monitored in the orchard with tensiometers at depths of 20, 40, 60, 80, 100 and 120 cm. These depths are considered to be inside the effective root zone for mango trees under local conditions. Suctions were converted into soil moisture by using measured soil water retention curves.

The aerodynamic resistance r_a (s m^{-1}) was estimated with Equation 2.11 and values of friction velocity (u_*) from EC measurements:

$$u_* = \sqrt{-\overline{w'u'}} \tag{6.3}$$

where u_* is in m s^{-1}; w' and u' are instantaneous departures from the average vertical and horizontal wind speed with respect to the mean values, respectively; the quantity $\overline{w'u'}$ is the co-variance between the vertical and horizontal wind speed; and the bar means average.

The universal integrated stability functions of temperature (Ψ_h) and momentum (Ψ_m) for relating mango orchard fluxes to atmospheric state profiles and surface properties were applied throughout Equations 2.6 to 2.11 (Businger et al., 1971):

Microclimatic data of T and RH were used together mango orchard energy balance components to estimate the bulk surface resistance to water vapour transport (r_s) applying the Penman-Monteith equation (Equation 2.5) for the mango orchard. The value of r_s was obtained from the model inversion using 30 minute data. The 30 minute data values of r_s were averaged.

The combined percolation and drainage term could be obtained from the remaining soil water balance terms as the difference between inputs (precipitation - P, irrigation - I and change in moisture storage -

ΔW) and outputs (ET$_a$). Since sub-surface drainage systems were absent, and flow to surface drains was negligible, the combined percolation/drainage flux could essentially be considered to represent deep percolation (P$_D$):

$$P_D = P + I - ET_a \pm \Delta W \tag{6.4}$$

The changes in soil water storage (ΔW) were positive when water is added to the root zone, otherwise they were negative:

$$\Delta W = W(t-1) - W(t) \tag{6.5}$$

The water storage W in the root zone was derived from the layer-wise soil moisture values (θ$_i$). At moment t, the storage across the depth (δz$_i$) of the six sensors (i = 1…6) could be computed as:

$$W(t) = \delta z_1 \theta_1 + \delta z_2\, \theta_2 + \delta z_3 \theta_3 + \delta z_4\, \theta_4 + \delta z_5 \theta_5 + \delta z_6 \theta_6 \tag{6.6}$$

For mango crop water productivity analyses the Equation 2.19 was applied for the growing seasons of mango orchard. As economic indicators, the indexes used were the standard gross value of production (fruits) over the irrigation supply (CWP\$$_I$), over actual evapotranspiration and over actual transpiration (CWP\$$_{ET_a, T_a}$).

6.3   Analysis of results

Soil moisture and weather conditions

The values of layer-wise soil water content (θ) from 20 to 120 cm depth are presented in Figure 6.1. The near-surface θ values were from 0.04 to 0.12 cm^3 cm^{-3} only, which showed a visually dry soil surface. Underneath the dryer surface layer, the soil was wetter with measured θ values peaking at 0.38 cm^{3}cm^{-3}. These levels can be interpreted as representing the soil porosity when the volumetric soil water content reaches its maximum in sandy soil.
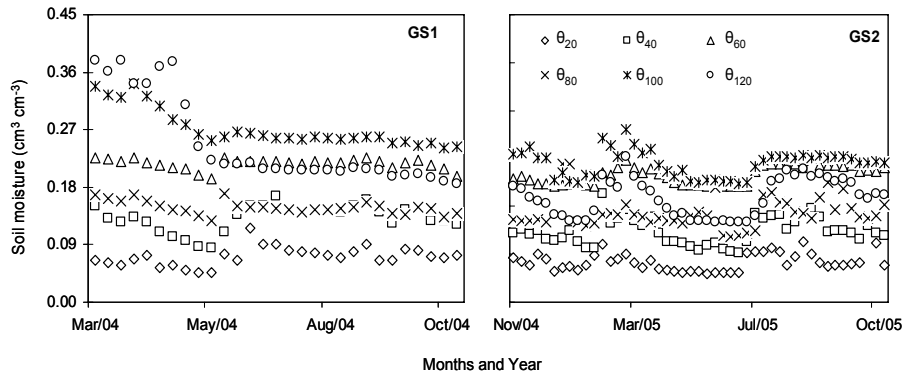
Figure 6.1. Soil water content (θ_i) at different depths (i = 20cm, i = 40 cm, i = 60 cm, i = 80 cm, i = 100 cm, i = 120cm) during the first growing season in 2003-04 (GS1) and second growing season in 2004-05 (GS2) growing seasons of mango orchard.

The highest θ values occurred at the end of February in 2004 and are related to the preceding storm events. After this period, soil moisture was approximately constant throughout the growing seasons. The values at 120 cm were most often lower than at 60 cm and 100 cm, which reveal typical downward percolation conditions. The magnitude of the percolation was investigated from the soil water balance. As the effective root zone of mango orchard is 120 cm, it could be concluded from the θ values that the mango orchard was not stressed by water shortage during most of the days.

Figure 6.2 shows the daily averaged weather variables during the two growing seasons studied. Mean T reached the maximum value in November and December with approximately 30° C, while the minimum values occurred during June (22° C).

The mean RH presented the inverse behaviour of the mean T. The values for water vapour pressure deficit (D), calculated for each half hour and averaged for 24 hours – which expresses the inverse of RH – presented the same temporal tendency as T through the growing seasons. Wind speed (u) at 3 m above a standardized grass field presented maximum values from July to November (3.6 m s^{-1}) and the minimum values from January to April (0.8 m s^{-1}). The wind speed over the rough mango trees were around 12% greater than over grass due to the height of the anemometer above the orchard.
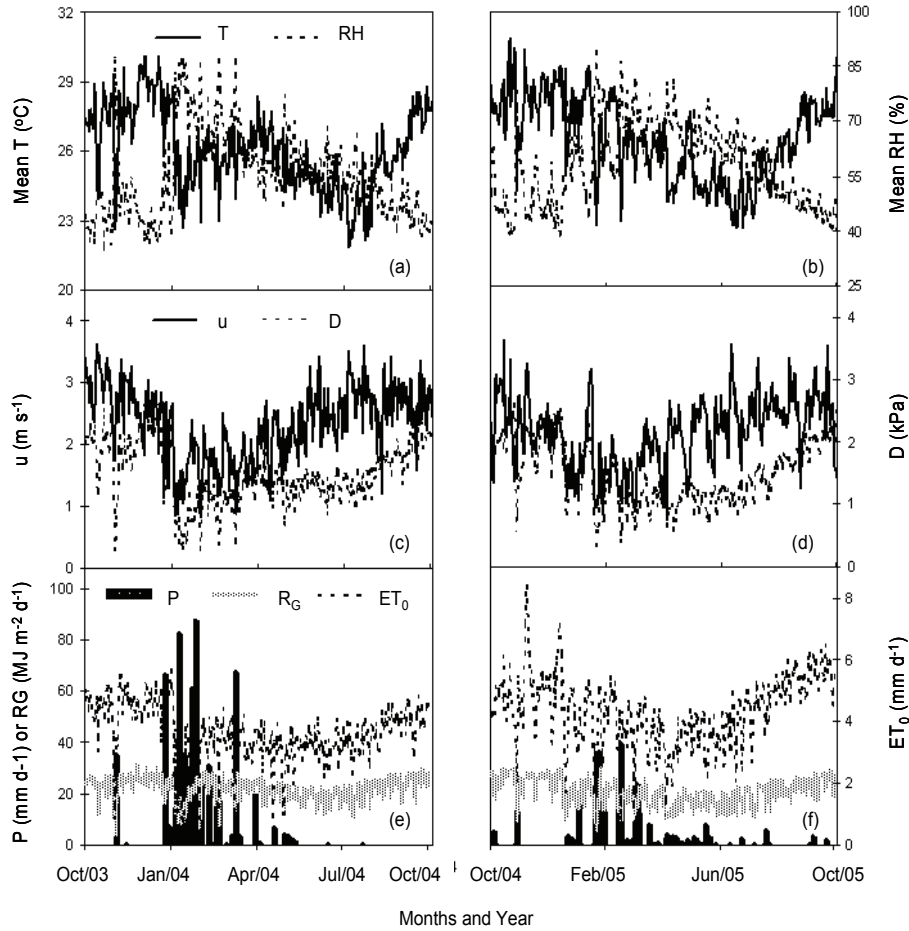
107

Figure 6.2. Averaged daily values of weather variables during the study period from 2003 to 2005: (a) and (b) - Mean air temperature (T) and relative humidity (RH), (c) and (d) - Wind speed (u) and water vapour pressure deficit (D); (e) and (f) – Incident global solar radiation (R_G), reference evapotranspiration (ET_0) and precipitation (P)

Values of the incident global solar radiation (R_G) were as expected in the southern hemisphere: lower from April to July and higher from August to January, when they started to decline again. Reference evapotranspiration (ET_0) followed the oscillation of R_G. Precipitation (P) was concentrated between January and April. The year 2004 was unusually wet. The accumulated rainfall for GS1 was 887 mm, for GS2 it was only 384 mm, while the longer term annual average is 570 mm.

108

Energy balance closure

Despite eddy correlation (EC) being among the most advanced "in situ" measurement technologies that directly provide λE, it is widely known to have problems. While in EC method there is a lack of energy balance closure, in Bowen ratio (BR) method this closure is forced. The comparison between the fluxes obtained by the BR and EC systems is shown in Figure 6.3 for averaged half hours and GS1 and GS2 together.
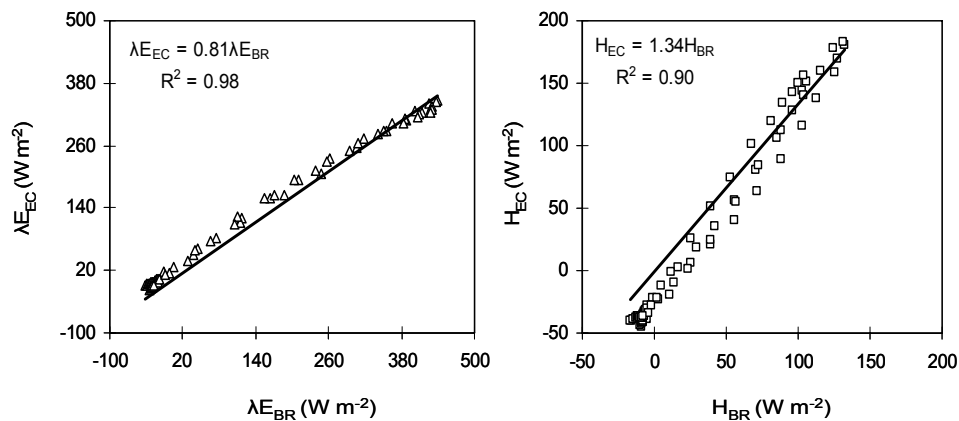

Figure 6.3. Comparison between the latent heat fluxes obtained by the eddy correlation technique (λE_{EC}) and with those from the Bowen ratio method (λE_{BR}): Averages values for each half hour for the two growing seasons were used.

The agreement on latent heat fluxes ($R^2 = 0.98$) was more satisfactory than on sensible heat fluxes ($R^2 = 0.90$). The data also showed that in average EC had 19% lower latent heat fluxes than the BR method while for sensible heat fluxes, EC measurements were in average 34% higher than those for BR method. The main reason for differences between the BR and EC methods can be due that in the first method the closure of energy balance is forced, however, another problem in BR method arises by the assumption of the similarity between H_{BR} and λE_{BR} turbulent diffusion coefficients in energy balance equations. Overestimations of λE_{BR} values were also observed by Azevedo et al. (2003) when comparing BR measurements with soil water balance method. Dugas et al. (1991) reported values of λE_{EC} being 23 to 33% less than those of λE_{BR}.

109

The data quality from EC system was verified by studying the energy balance closure: fluxes ($\lambda E_{EC} + H_{EC}$) and available energy ($R_n - G$) were compared for the whole period of measurements (2003-2005) at a daily time scale (Figure 6.4). Since the main objective of this research is irrigation management and water productivities, there was less interest in studying hourly energy balance closures, daily total values were sufficient. The energy balance ratio, i.e. the ratio of turbulent energy fluxes to available energy was 88%. The RMSE for 24 hour values of 1.7 MJ m^{-2} d^{-1}, evidenced the good quality of the dataset.
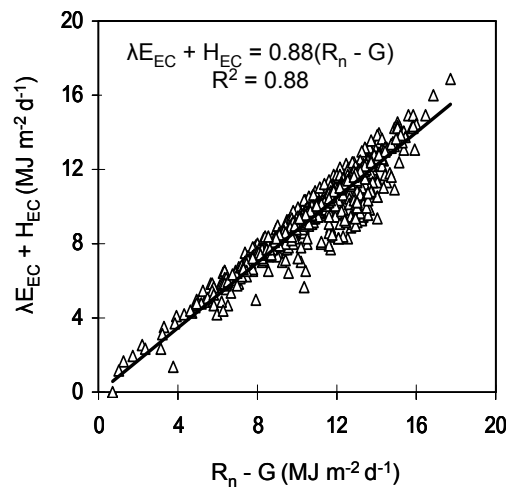

$$\lambda E_{EC} + H_{EC} = 0.88(R_n - G)$$
$$R^2 = 0.88$$

Figure 6.4. Relationship between latent heat (λE_{EC}) plus sensible heat (H_{EC}) fluxes and available energy ($R_n - G$) for the eddy correlation system.

A closure error of 10 to 30 % seems to occur frequently with eddy correlation - based latent heat flux estimates. A summary paper of 22 flux sites indicated a general lack of closure, with a mean imbalance in the order of 20% (Wilson et al., 2002). Available energy ($R_n - G$) systematically exceeding measured fluxes ($\lambda E_{EC} + H_{EC}$) were also published by Twine et al. (2000), Paço et al. (2006) and Testi et al. (2006). The lack of energy balance closure can also be associated with measurement errors in R_n and G, but not completely explained by this uncertainty, because eddy correlation systems have their own sources of error (Twine et al., 2000). Further to systematic biases in the instrumentation, the general hypothesis is that lack of energy balance closure can be explained by sampling errors related to different footprints, neglected energy sinks, loss of low and/or high frequency

contributions to the turbulent heat flux and advection of scalars (e.g. Paw U et al., 2000).

To circumvent this common problem, several agro-meteorological studies have found a practical solution to force the closure of the surface energy balance in EC systems. Simmons et al. (2007) used the residual method to obtain ET_a by measuring the sensible heat fluxes with a sonic anemometer and the available energy in a flood-irrigated pecan orchard, while Chebouni et al. (2006) used EC measurements and the ratio $H_{EC}/\lambda E_{EC}$ over irrigated wheat in the Yaqui Valley in northwest Mexico. It was decided to analyse the results combining this last ratio with the measured available energy (e.g. Twine et al., 2000). Whilst the lack of energy balance closure underestimates λE_{EC}, forcing the closure by this combination method it was assumed this underestimation to be corrected (e.g. Hoedjes et al., 2002).

The preference for the combination method was because:
- it directly produces evaporative fraction, being a key expression for energy partitioning
- it ensures a closed energy balance
- it mainly utilizes highly advanced eddy correlation systems
- it has a good consistency with the theoretically best latent and sensible heat fluxes measurements

All the energy balance and ET_a data discussed hereafter are based on the combination method with the latent and sensible heat fluxes obtained from EC measurements. Therefore the subscripts EC are not used anymore in the next sections.

Mango orchard energy partitioning

Figure 6.5 shows the diurnal trend in the fluxes of individual energy balance components for the mango orchard. λE was always in excess of H during daylight hours. H was – in turn – higher than G. At night the results from eddy correlation (EC) showed near zero λE.
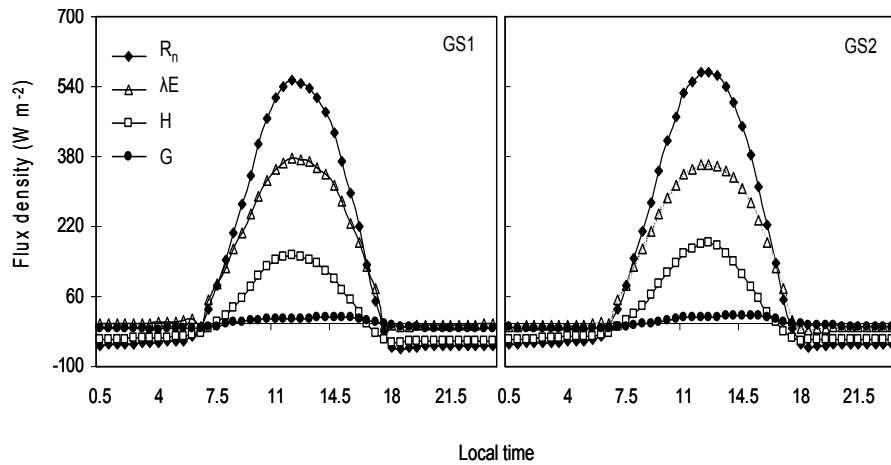
111

Figure 6.5. Diurnal averages for energy balance components during the growing seasons in 2003-04 (GS1) and in 2004-05 (GS2) for mango orchard: net radiation (R_n); latent heat flux (λE); sensible heat flux (H) and soil heat flux (G).

Daily averages of energy balances are given in Table 6.1. H accounted for 11 and 15 % of R_n during the GS1 and GS2 respectively. The significant Leaf Area Index of mango orchard (LAI~5 to 6) caused solar R_G to hardly penetrate through the canopy. As a consequence, G at daily scale was small and negative with 24 hours averaged values of 3% and 2% of R_n in the GS1 and GS2, respectively. Negative values for G were the result of conditions of a large LAI in conjunction with frequent micro sprinkler irrigation that kept the soil thermal conductivity high. The largest fraction of R_n was used as λE, which represented on average 89 % during the GS1 and 80 % in GS2. The corresponding evaporative fractions ($E_F = \lambda E/(R_n - G)$) were 0.86 and 0.79. During an earlier mango energy balance study in Petrolina in 1998, the E_F was found to be 0.73 in August, 0.86 in September, 0.78 in October and 0.80 in November (Lopes et al., 2001), similar to our results. The values of E_F remained high during most of the time of the growing seasons what reflected a constant supply of irrigation water. An average E_F of 0.83 is according to Scott et al. (2003) equivalent to a degree of soil moisture saturation in the root zone of 67 %, which at a maximum moisture value of 0.38 cm^3 cm^{-3} suggests average θ in the root zone of 0.25 cm^3 cm^{-3}. The latter can be confirmed from the soil moisture measurements (see Figure 6.1). Testi et al. (2004) studied the partition of energy balance in a young olive orchard, under different soil water conditions. They also

112

concluded that the amount of R_n used as λE and H depends on θ. The rainy period elapsed from January to April and after that, farmers refrained from irrigation, inducing a drop of E_F to a value around 0.70 during the branch development stages.

Table 6.1: Daily averages of the energy balance components for mango orchard during the growing seasons in 2003-04 (GS1) and in 2004-05 (GS 2): net radiation (R_n), latent heat flux (λE), sensible heat flux (H), soil heat flux (G) and evaporative fraction (E_F)**.**

DOY/YEAR	R_n (MJ m^{-2} d^{-1})	λE (MJ m^{-2} d^{-1})	H (MJ m^{-2} d^{-1})	G (MJ m^{-2} d^{-1})	E_F (-)
GS 1					
303/03	9.66	8.43	0.80	-0.13	0.86
333/03	10.84	9.49	1.20	-0.29	0.85
363/03	10.64	9.13	1.14	-0.22	0.84
028/04	9.73	8.30	1.91	-0.60	0.80
058/04	12.18	10.28	2.93	-1.41	0.76
088/04	11.69	10.15	1.84	-0.31	0.85
118/04	11.96	10.46	1.25	0.00	0.87
148/04	9.75	8.45	1.29	-0.20	0.85
178/04	8.91	8.09	0.74	-0.37	0.87
208/04	8.70	8.01	0.76	-0.33	0.89
238/04	9.71	8.49	1.04	-0.28	0.85
268/04	11.51	11.19	-0.07	-0.33	0.95
298/04	12.21	11.65	-0.24	-0.38	0.93
Mean	10.58	9.39	1.12	-0.37	0.86
GS 2					
326/04	12.47	10.61	0.71	-0.25	0.83
354/04	12.17	10.17	1.19	-0.15	0.83
016/05	11.67	8.71	2.20	-0.02	0.75
044/05	12.13	9.37	2.57	-0.30	0.75
072/05	11.87	9.10	2.59	-0.38	0.74
100/05	12.41	9.43	2.90	-0.44	0.73
128/05	9.04	8.11	1.19	-0.29	0.87
156/05	8.78	7.85	0.83	-0.07	0.89
184/05	8.43	7.67	0.66	-0.07	0.90
212/05	10.03	8.40	0.49	0.25	0.86
240/05	10.62	8.56	1.64	-0.03	0.80
268/05	12.04	9.14	2.60	-0.20	0.75
302/05	12.35	8.62	2.13	-0.38	0.68
Mean	11.08	8.90	1.67	-0.18	0.79

*DOY – Day of the year. The values were taken at 30 and 28 days intervals for GS1 and GS2 respectively.

Mango orchard water fluxes

The summary of water use variables for the two growing seasons of mango orchard is shown in Table 6.2.

Table 6.2: Summary of water-use variables for mango orchard during the growing seasons in 2003-04 (GS1) and in 2004-05 (GS2): mean values of reference evapotranspiration (ET_0); actual evapotranspiration (ET_a); actual transpiration (T_a) and soil evaporation (E_a); aerodynamic (r_a) and surface (r_s) resistances.

DOY/YEAR	ET_0 (mm d^{-1})	ET_a (mm d^{-1})	T_a (mm d^{-1})	E_a (mm d^{-1})	r_a (s m^{-1})	r_s (s m^{-1})
GS 1						
303/03	4.87	3.41	2.49	0.92	32	191
333/03	4.70	3.87	2.90	0.97	34	160
363/03	4.18	3.79	3.59	0.20	44	193
028/04	3.67	3.40	2.99	0.41	38	116
058/04	3.82	4.18	3.24	0.93	44	107
088/04	3.78	4.08	3.21	0.86	35	112
118/04	3.52	4.24	3.00	1.25	43	121
148/04	3.34	3.43	2.84	0.59	41	119
178/04	3.56	3.36	3.03	0.33	31	135
208/04	3.41	3.29	2.90	0.39	30	121
238/04	3.74	3.49	3.13	0.35	33	123
268/04	4.27	4.57	3.32	1.25	34	122
298/04	4.44	4.63	3.14	1.49	34	145
Mean	3.95	3.83	3.06	0.75	36	136
GS 2						
326/04	4.66	4.33	2.15	2.18	36	152
354/04	5.02	4.17	2.82	1.35	36	155
016/05	4.87	3.74	3.19	0.55	39	180
044/05	4.14	3.78	3.06	0.72	42	149
072/05	3.92	3.65	2.94	0.71	46	120
100/05	3.74	3.81	2.81	1.00	46	111
128/05	3.06	3.21	2.30	0.91	39	113
156/05	3.42	3.20	2.56	0.63	37	120
184/05	3.36	3.13	2.52	0.61	34	116
212/05	3.88	3.46	2.91	0.55	33	108
240/05	4.59	3.55	3.32	0.23	31	124
268/05	5.30	3.73	3.16	0.57	32	140
302/05	5.58	3.54	2.47	1.08	32	163
Mean	4.27	3.64	2.79	0.85	39	135

*DOY – Day of the year. The values were taken at 30 and 28 days intervals for GS1 and GS2 respectively

114

Despite GS1 having an above average rainfall; the difference in water fluxes between growing seasons was mainly caused by cloud cover and levels of R_G. Outside the short rainy season, R_G is abundant. As a consequence of the wetter soil due to rainfall (the 80 to 120 cm depth layers were systematically wetter in GS1) ET_a in 2003-04 was 1492 mm, higher than the 1346 mm measured in 2004-05. The average ET_a over the two growing seasons was 1419 mm with an average daily rate of 3.7 mm d^{-1}.

With the ratios ET_a/ET_0, T_a/ET_0 and E_a/ET_0, the values of actual transpiration (T_a) and soil evaporation (E_a) for the several crop stages of the growing seasons could be determined. Table 6.2 shows the seasonal variation of water-use variables in mango orchard. T_a for both seasons in general followed the fluctuations in ET_a.

The Figure 6.6 shows the seasonal trend of daily values of actual evapotranspiration (ET_a) in mango orchard. The ET_a values followed the atmospheric demand in both growing seasons, being higher from October (2003) to March (2004), and from August to November (2004) in GS1, while in GS2, the peak values were from January to April and from August to November, both in 2005. Maximum daily values of ET_a for GS1 were around 6.3 mm d^{-1}. During GS2 the maximum daily values were about 5.1 mm d^{-1}. The minimum daily values were around 0.6 mm d^{-1} for both growing seasons.
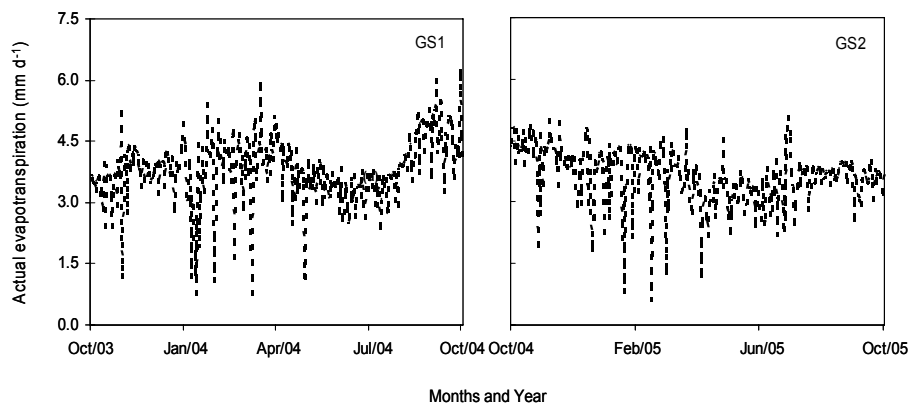

Figure 6.6. Daily variation for actual evapotranspiration, during the growing seasons in 2003-04 (GS1) and in 2004-05 (GS2) for mango orchard.

Azevedo et al. (2003) showed averaged daily values of mango orchard ET_a of 4.4 mm d^{-1} for the crop stages from flowering to fruit maturation using both, Bowen ratio and soil water balance methods in

115

Petrolina-PE, Brazil. It should be noted that the study of Azevedo et al. reflects drip irrigation, while the actual mango orchard was irrigated by micro sprinklers. The mean crop heights were similar for both studies (around 5 m) and the trees were spaced 8.0 x 5.0 m in the previous study, while in the present field, trees stand in a regular square pattern at 10 m x 10 m. The mango orchard LAI in the first study was approximately 12 to 15 while the larger spacing in the actual study yielded values of LAI of 5.2 to 6.0 for the same crop stages, being another reason for the lower ET_a values in the actual study.

Annual mango orchard ET_a in South Africa was found by Mostert and Wantenaar (1994) to be 1197 mm. The winter ET_a was 2.2 mm d^{-1} on average, while the summer ET_a was with 4.4 mm d^{-1}, exactly double. Molle et al. (1999) reported on an annual mango plot water consumption of 1630 mm in a raised bed system, including crop consumptive use and evaporation from pounding water. With regard to other orchards, the actual ET_a results for mango orchard were greater than for peach (Paço et al., 2006) and lower than for citrus (Rana et al. 2005). Paço et al. (2006) using EC measurement system in a peach orchard in Portugal found ET_a values ranging from 1.4 to 3.6 mm d^{-1} in 1998 and from 2.1 to 3.3 mm d^{-1} in 1999 with mean values of 2.5 and 2.6 mm d^{-1}, respectively. Rana et al. (2005) using the same system in a citrus orchard under Mediterranean conditions (Southern Italy) found values ranging from 3.0 to 8.0 mm d^{-1}. The EC system was also used by Sammis et al. (2004) to study water consumption of flood-irrigated pecans in USA; they found an averaged total ET_a of 1420 mm for 2001 and 2002 that was similar to the total ET_a of mango orchard for GS2 in the present study.

The 20 day interval averaged ET_a/ET_0 data for the dryer growing season (2004-05) were fitted with a polynomial function expressed in degree days (Basal T = 10° C) rather than in calendar days, for incorporation of T effects on the growing stages of mango trees (Figure 6.7). The period before the pruning date was included because the farmers also applied large amounts of water during post harvest periods, which must be considered for the final mango water productivity analyses.
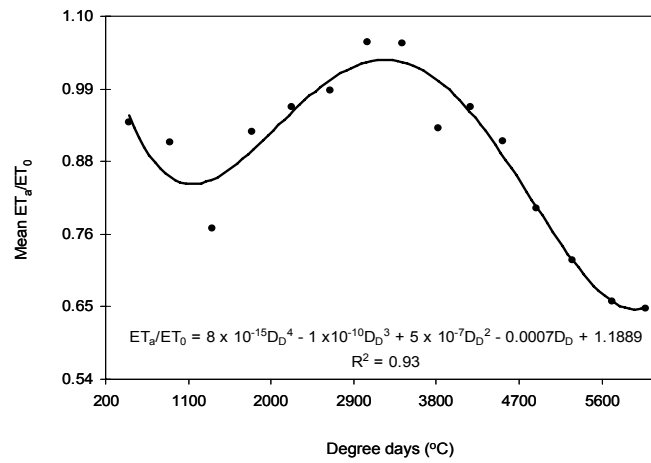
Figure 6.7. The seasonal variation of averaged daily ET_a/ET_0, as a function of degree days - D_D (Basal T = 10° C), during the growing season of 2004-05 of mango orchard.

The values of ET_a largely followed the ET_0. During the rainy periods at the start of the year, ET_a rates exceeded ET_0, resulting in daily ET_a/ET_0 values bigger than 1 for both growing seasons (Figure 6.8).
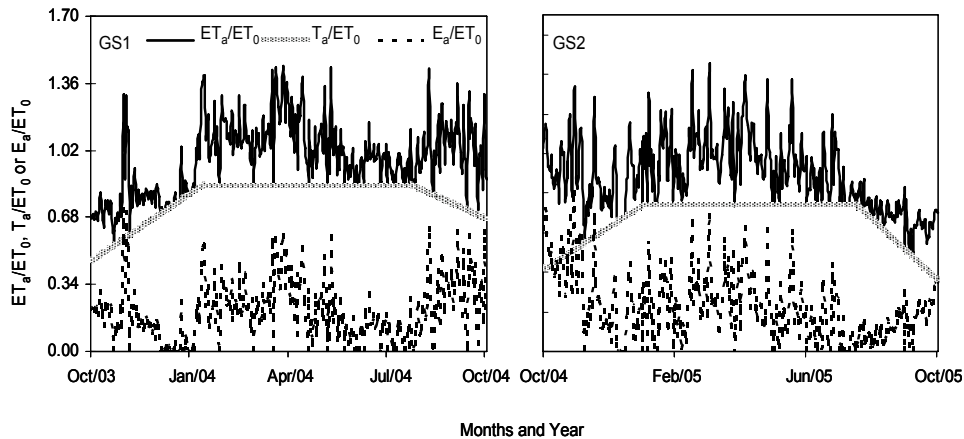

Figure 6.8. Seasonal variation of the ratios of water fluxes to reference evapotranspiration (ET_0) in mango orchard during the first growing season in 2003-04 (GS1) and during the second growing season in 2004-05 (GS2) growing seasons: actual evapotranspiration (ET_a), actual transpiration (T_a) and actual soil evaporation (E_a) to ET_0.

Soil evaporation played a role in these high values, as can be seen by the behaviour of E_a/ET_0. This effect was more pronounced in 2004, when unusually strong storms occurred. The highest daily values of

117

ET_a/ET_0 were from the end of January to the end of March reaching peaks of 1.40. This time of both years (2004 and 2005) was the rainy period when the crop was at the branch development and flowering stages. The minimum ET_a/ET_0 values occurred when the crop was in a transition stage from previous post-harvest to vegetative growth, coinciding with periods without rain. The maximum daily values of T_a/ET_0 (K_{cb}) were 0.85 and 0.75 for GS1 and GS2, respectively. The minimum value for initial stages was 0.46 during GS1, while for GS2, was 0.41. The basal crop coefficients during the harvest season were 0.67 and 0.36 for the first and second growing seasons, respectively. Seasonal E_a/ET_0 behaviour showed that soil evaporation contributed about 20% to the total mango orchard ET_a (see also Table 6.2).

For both growing seasons of mango orchard, higher ET_a/ET_0 values were found than by Azevedo et al. (2003) who reported values around 0.71 during the crop stages studied. They also fitted a polynomial curve, but with ET_a/ET_0 values as a function of the days after flowering (DAF). The higher ET_a/ET_0 values in the actual study had the same reasons as mentioned for ET_a, but in addition it should be noticed that Azevedo et al. used a conventional agro-meteorological station in contrast with the automatic weather station data to calculate ET_0 in the present study. The maximum ET_a/ET_0 values found for citrus by Rana et al. (2005) were around 1.20, while Sammis et al. (2004) and Paço et al. (2006) found values in the range of 0.20 to 1.10 for pecan and from 0.40 to 0.60 for peach orchards, respectively.

Mango orchard resistances

A more in-depth physical explanation of mango orchard water fluxes can be obtained if the aerodynamic (r_a) and bulk surface (r_s) resistances are derived. Figure 6.9 shows the seasonal variation of these resistances for the growing seasons of 2003-04 (GS1) and 2004-05 (GS2) calculated from microclimatic data and λE measurements. The highest values of r_a coincided with the lowest values of r_s and they occurred during the rainy periods. The relatively low r_a values of approximately 35 s m^{-1} can be directly ascribed to the tall trees with 5.5 m averaged height. In Teixeira et al. (2008b), the friction velocities from the eddy correlation measurements are interpreted in r_a values, and it is confirmed that the r_a is low due to a high surface roughness length to momentum transfer (z_{0m} was 0.50 to 0.54 m).
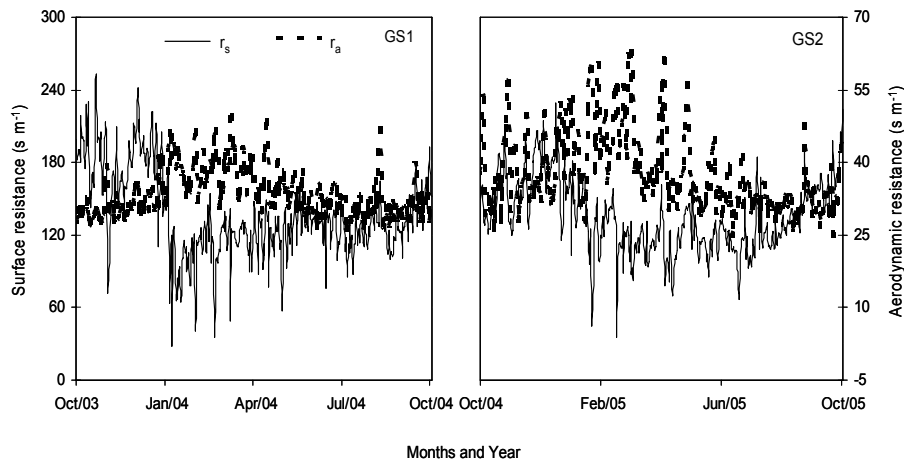
118

Figure 6.9. Seasonal trends of surface (r_s) and aerodynamic (r_a) resistances for the first growing season in 2003-04 (GS1) and for the second growing season in 2004-05 (GS2) of mango orchard.

The seasonal behaviour of r_s followed the dryness of the lower part of the atmosphere with some peaks associated with high values of D in both seasons. The value of r_s were on average 135 s m^{-1}, which explains that the mango ET$_a$ is lower than for grass as the reference crop (for which r_s is assumed to be 70 s m^{-1}). These r_s values can be related to absence of a ground cover crop and the relatively dry air. Yet, r_s can also vary with θ and soil hydraulic conductivity close to the roots. The increase of r_s with high values of D has been reported by Testi et al (2006) for olive orchard in Spain. According to Rana et al. (2005), r_s is not a constant, they confirm that it varies depending on D, but also with the available energy to the crop. Alves and Pereira (2000) used the so called climatic resistance that is directly proportional to D for lettuce crop, to explain variations in λE. If there is sufficient soil moisture to avoid water stress, conditions of high D together with low values of r_a promote high rates of ET$_a$, which make the values of r_s lower and this is the case of irrigated mango orchards growing in the semi-arid conditions of São Francisco River basin.

The main reasons for differences in orchard water variables between the actual study and some others cited above can be attributed to different species, varieties, climate, soil type, irrigation systems and frequency of irrigation, cultural management, methods of determination of evapotranspiration and also the plant density that affect the soil cover.

119

Soil water balance

Irrigated soils in the central São Francisco River basin have experienced declines in productivity, which may be a reflection of changes in soil chemical properties due to management (Heck et al., 2003). The water flow in the unsaturated zone needs to be properly understood for assessing sustainability. The monthly soil water balance for the mango orchard is presented in Table 6.3. The percolation flow can be as high as 50 mm per week (or 200 per month) following periods of rain storms. This flow can be regarded as happening at a depth of 140 cm below natural ground surface.

Table 6.3: Monthly soil water balance of irrigated mango trees during the first (from 060/04 to 298/04) and second (from 298/04 to 291/05) growing seasons: rainfall (P); actual evapotranspiration (ET_a), Irrigation (I), change in soil water content (ΔW) and deep percolation (P_D) or capillary rise (CR).

DOY/YEAR	P	ET_a	I	ΔW	D_p (-) or CR (+)
	(mm)	(mm)	(mm)	(mm)	(mm)
GS 1					
060/04 - 091/04	76.2	128.1	0.0	19.3	32.5
092/04 - 121/04	20.8	125.7	0.0	32.1	72.7
122/04 - 152/04	19.6	107.1	87.2	-28.9	29.2
153/04 - 182/04	0.0	97.8	109.4	-2.5	-9.1
183/04 - 213/04	0.3	102.2	113.1	-0.2	-11.0
214/04 - 244/04	0.5	114.7	126.2	-1.7	-10.3
245/04 - 274/04	0.0	141.4	118.1	8.1	15.2
275/04 - 298/04	0.0	108.9	121.0	4.9	-17.0
Total	117.4	925.9	675.0	31.1	102.2
GS2					
299/04 - 335/04	22.1	157.3	137.0	10.2	-12.0
336/04 - 366/04	0.0	125.7	104.8	11.0	9.9
001/05 - 031/05	31.5	116.2	127.5	12.7	-55.5
032/05 - 059/05	153.7	103.2	170.0	-24.8	-195.7
060/05 - 090/05	96.0	115.2	71.9	1.5	-54.2
091/05 - 120/05	23.9	110.7	0.0	9.7	77.0
121/05 -151/05	24.9	92.9	0.0	0.7	67.2
152/05 - 181/05	15.2	94.8	80.6	4.6	-5.6
182/05 - 212/05	3.0	105.8	169.1	-28.3	-38.0
213/05 - 243/05	7.4	110.5	128.6	5.1	-30.6
244/05 - 273/05	0.0	111.3	117.3	2.7	-8.7
274/05 - 291/05	4.1	63.6	88.2	-3.5	-25.2
Total	381.8	1307.2	1195.0	1.6	-271.4

*DOY – Day of the year. The values were taking when having simultaneous measurements of θ and ET_a

120

The seasonal variation of soil water balance is showed in Figure 6.10. The largest fluctuations in percolation are found during the rainy season – January to April. The highly permeable soils have a great drainage capacity that ensures that soil moisture is not rising and that water excess percolates downwards. This is in agreement with the general soil water requirements of mango orchard; hence it has been a good choice to cultivate this fruit crop in the soils and climate of the semi-arid region of São Francisco River basin. The latter is confirmed from the soil moisture changes. Table 6.3 shows that the changes across a month are 30 mm at maximum.
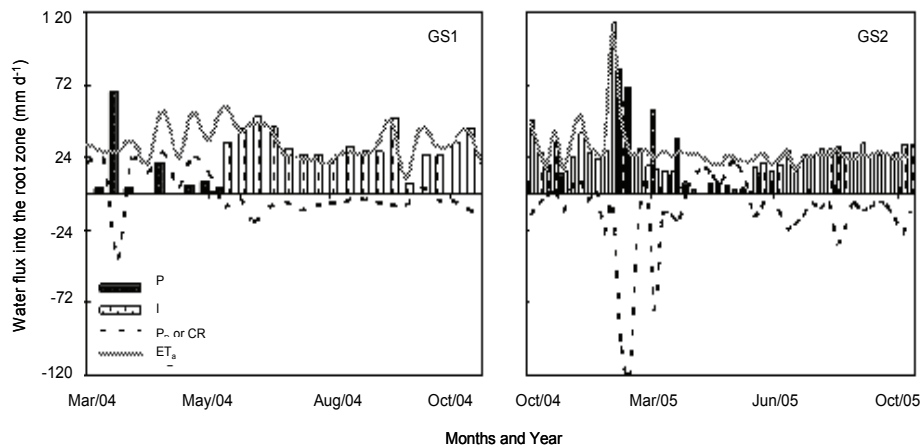

Figure 6.10. Soil water balance into the root zone for the first growing season in 2003-04 (GS1) and for second growing season in 2004-05(GS2) of mango orchard: precipitation (P); irrigation (I); deep percolation (P_D); capillary rise (CR) and actual evapotranspiration (ET_a).

The soil water balance as defined in Equation 6.4 could be computed only for the period in which soil moisture of the layers and ET_a were measured. The percolation flows were rather conserved outside the rainy season. During driest periods, capillary rise provided extra water to the root zone. This last process could be established only if the 120 cm deep moisture layer was wetter than the 100 cm layer. This indeed sometimes occurred, especially after the end of the rainy period during GS1, when the time without irrigation was longer than in GS2 (see Figures 6.1 and 6.10).

Seasonal P_D for one growing season could be computed as being around 300 mm, considering the rate of 0.8 mm d^{-1}, from the data during GS2 (Table 6.3), and a mean duration for the two growing seasons of 380

121

days. This is a substantial return flow of the irrigation system that to a large degree can be manageable. Irrigation conservation could reduce the percolation rates. An example of stress induced soil water content is described in Nadler et al. (2006). The limited distance of 5.5 km from the river ensured that most return flow is drained to the São Francisco River. The significant percolation flow transports the solutes down to the groundwater. Both groundwater quality and the soil health need to be controlled.

Mango water productivity

The mango water productivity indicators are summarized in Table 6.4 according to the growing seasons.

Table 6.4: Crop water productivity (CWP) based on cultivated land (L), irrigation (I), actual evapotranspiration (ET_a) and actual transpiration (T_a) of mango orchard, together with economic values of these indices (US$).

GS	CWP_L (Kg ha^{-1})	CWP_I (Kg m^{-3})	CWP_{ET_a} (Kg m^{-3})	CWP_{T_a} (Kg m^{-3})	$CWP\$_L$ (US$ ha^{-1})	$CWP\$_I$ (US$ m^{-3})	$CWP\$_{ET_a}$ (US$ m^{-3})	$CWP\$_{T_a}$ (US$ m^{-3})
GS1	41,593	4.76	2.79	3.57	42,425	4.86	2.85	3.65
GS2	48,405	4.30	3.60	5.38	49,373	4.39	3.68	5.50

The statistical average mango yield in Petrolina-PE during 2005 was 20 t ha^{-1}. The mango yield in Fruitfort farm (CWP_L) was in average 45 t ha^{-1}. The difference between the two growing seasons can likely be ascribed to the water stress during flowering in GS1. According to Table 6.4 the bio-physical water productivities are generally higher than for arable crops (essentially CWP_{ET_a} from 0.5 to 1.5 kg m^{-3} for wheat and rice; see Zwart and Bastiaanssen, 2004) but comparable to grapes (CWP_{ET_a} is 3.8 kg m^{-3}; see Teixeira et al., 2007) that contain a high moisture content of the fresh product (approximately 75-80%). An CWP_{ET_a} of 3 to 4 US$ m^{-3} per unit of water depleted is almost a factor 20 more than for irrigated annual crops. The agricultural water usage in the semi-arid region of the São Francisco River basin is thus highly productive, besides also providing jobs in the agri-business, which is a stimulus for rural development of the region.

6.4 Conclusions

Because of the importance of the water management in fruit crops, daily and seasonal water use patterns of a large commercial mango orchard were collected. The results presented in this chapter are important for irrigation management, water allocation, water savings and environmental sustainability of irrigated mango orchards.

Despite the aerodynamically rough surface with the crowns of mango trees exceeding 5 m, the actual evapotranspiration of the mango orchard was less than for grass as a reference crop ($ET_a/ET_0 = 0.91$). The underlying reason is the presence of a relatively large bulk surface resistance ($r_s = 135$ s m^{-1}) due to presence of older leaves, shadow in the crown, distance between trees for mechanical access and the absence of a ground cover crop.

In the commercial farm investigated, soil moisture and the evaporative fraction were in general kept at ideal levels, especially considering the values for the entire growing seasons. The drawback of a wet light textured soil is the capacity to percolate excessive water resources. The seasonal percolation flow was 300 mm, and this can be a threat to groundwater contamination and soil salinity build up, if drainage is not given proper attention.

The bio-physical and economical water productivities of mango are very high. An economic water productivity based on actual evapotranspiration of US\$3 m^{-3} to US\$4 m^{-3} is in order of magnitude much better than for annual crops. Hence from the water resources point of view, water allocation to irrigated mango orchards is desirable. Although this water usage is highly productive, the environmental consequences must be considered keeping irrigated horticulture in pace with sustainability requirements. The challenge is to find a balance between water productivity and environmental pollution.

7. Energy fluxes and vegetation-atmosphere parameters in irrigated and natural ecosystems

7.1 Introduction

Water managers in the semi-arid region of the Low-Middle São Francisco River basin are faced with several challenges. Water policy makers have to work out strategies for integrated water management, which rely on a proper knowledge of the physical conditions of this sub-basin. The water depletion is caused mainly by actual evapotranspiration (ET_a) from a range of crops and natural vegetation types, soil, build-up areas and water bodies. A proper knowledge of ET_a for various land covers is essential for managing scarce water resources and for keeping long-term ET_a in balance with precipitation. Experimentally, ET_a can be determined by using weighing lysimeters, eddy correlation technique and the Bowen Ratio energy balance method. ET_a in irrigated crops and natural vegetation can be determined by analyzing the available energy at the land surfaces, the relevant potential differences (gradients of air temperature or air specific humidity), and the aerodynamic and bulk surface resistances (e.g. Gash and Shutteworth, 2007). Examples of energy balance measurements by means of the Bowen ratio method above vegetated surfaces can be found in for instance Heilman et al. (1994, 1996). Eddy correlation technique is considered to be a standard procedure for determining the latent heat flux in field conditions (e.g. Oliver and Sene, 1992; Lund and Soegaard, 2003), albeit this method is not free from errors.

The commonly used Penman-Monteith equation is an appropriate mathematical framework to compute ET_a at local and regional scales (e.g Dolman, 1992; Riddersma and De Ridder, 1996; Bastiaanssen and Bandara, 2001). Despite that an extensive literature describes the theoretical mechanisms of turbulent transport above and within crop canopies; fewer studies have examined the actual soil-vegetation-atmosphere-transfer parameters within landscapes of irrigated crops being interchanged with semi-arid natural land cover. Some earlier examples of ET_a research in composite arid zone landscape are provided by for instance Kustas et al. (1994) for Walnut Gulch in Arizona, Chehbouni et al. (2001) for Mexico and Kite and Droogers (2000) for Turkey.

The objectives of this chapter are (i) to review and improve parameterizations of the radiation and energy balances in irrigated crops

and natural vegetation using field measurements, (ii) to predict 24-hour energy balance from instantaneous values and (iii) to derive analytical relationships that can be used to predict evaporation resistances from irrigated crops (vineyards and mango orchard) and natural vegetation (caatinga)

7.2 Methodology

The experiments with irrigated crops (wine grape, table grape and mango orchard) and natural vegetation (caatinga) were dealt in details in Chapter 4. The overall calculations of radiation and energy balances are described in many text books. First the components of net radiation (R_n) will be discussed, as R_n is the main supplier of energy required to drive the evapotranspiration process. The longwave radiation received from the atmosphere ($R_L\downarrow$) can be computed from the Stephan Boltzmann equation for all cases with direct measurements of air temperature (T), when the apparent emissivity of the atmosphere (ε_a) is known. Various empirical solutions exist to describe ε_a (Brunt, 1939; Swinbank, 1963). During a comparative study executed by the University of Idaho (Allen et al., 2000), the empirical equation developed by Bastiaanssen (1995) performed most favourably, provided that it is calibrated against local observations (see also Allen et al., 2007a). Thus:

$$\varepsilon_a = a \, (-\ln\tau_{sw})^b \qquad\qquad (7.1)$$

where τ_{sw} is the shortwave atmospheric transmissivity and a and b are regression coefficients.

All radiation components of the caatinga site were measured, which made it feasible to isolate ε_a from measured $R_L\downarrow$ and T values. The a and b coefficients of Equation 7.1 could be calibrated and this equation was applied to retrieve daily values of ε_a and $R_L\downarrow$ in the irrigated sites. The incoming longwave radiation ($R_L\downarrow$) could be computed from the Stephan Boltzmann equation for all irrigated crops, after making the proper correction for atmospheric emissivity:

$$R_L\downarrow = \varepsilon_a \, \sigma \, T^4 \qquad\qquad (7.2)$$

where σ (5.67×10^{-8} W m^{-2} K^{-4}) is the Stefan-Boltzmann constant and (K) the air temperature.

Values of surface albedo (α_0) were obtained by measurements from incoming global solar radiation (R_G) and outgoing solar radiation R_R in wine grape, mango orchard and caatinga. For table grape R_R was estimated from the regression equation between net short wave radiation (R_G - R_R) and R_n developed by Azevedo et al. (1997) for the same crop in semi arid conditions of the São Francisco River basin.

Using the 24-hour values of short wave components (R_G - R_R), R_n and $R_L\downarrow$ the 24-hour values of $R_L\uparrow$ could be estimated as the residuals in radiation balances for irrigated fruit crops where this radiation parameter was not measured.

The 24-hour values of the net radiation ($R_{n_{24}}$) can be described by the 24-hour values of net shortwave radiation, with a correction term for net longwave radiation at the same time scale. De Bruin (1987) and de Bruin and Stricker (2000) reported on the use of the following equation:

$$R_{n_{24}} = \left(1 - \alpha_{0_{24}}\right)R_{G_{24}} - a\tau_{sw_{24}} \qquad (7.3)$$

where a is the regression coefficient of the relationship between net long wave radiation ($R_{nl_{24}}$) and atmospheric transmissivity ($\tau_{sw_{24}}$) at daily scale.

Equation 7.3 has the advantage that the emmisivities during daytime and nighttime necessary for solving the Stephan Boltzmann equation can be omitted. Thus, $R_{n_{24}}$ can be quantified if net shortwave radiation is measured and the adjusting factor, a, is known.

The latent heat fluxes (λE) in vineyards were acquired by the Bowen ratio systems with the gradients of temperature and water vapour pressure, R_n above the canopies and the soil heat fluxes (G). The sensible heat fluxes (H) was then derived as residuals in the energy balance equation (Teixeira et al., 2007). Using data from the eddy correlation systems (EC) in mango orchard and caatinga, H and λE were obtained (Stull, 1988).

The Penman-Monteith equation is described in Chapter 2 (Equation 2.5). The drag force between land and atmosphere in this equation is accounted for the aerodynamic resistance (r_a), and this parameter requires the roughness length for heat and vapour (z_{0h}), the displacement height (d) and the friction velocities (u_*) as specified in Equation 2.11. For vineyards the friction velocity was calculated using flux profile relationships (u_{FP*}) with two-level near-ground wind speed measurements. The eddy correlation data of mango orchard and caatinga

could be used to acquire the friction velocity (u_{EC*}) directly without wind speed measurements at multiple heights. The roughness length for moment transfer (z_{0m}) was then obtained from either u_{FP*} or u_{EC*} applying Equation 2.10 and z_{0h} was considered as a function of z_{0m}.

Ratios of the d to the height of the vegetation (h_v) were usually reported to lie in the range of 0.6 (Garrat, 1978), although several authors assumed (Hicks, 1973) or calculated (Riou et al., 1987) a negligible d for extensive vineyards. In the actual study it was considered d = 0.66 h_v (Allen et al., 1998) and solve z_{0m} as the unknown in Equation 2.10. Early measurements in closed canopies reported z_{0m} = 0.13h_v, (e.g. Monteith, 1973). The roughness parameters for vegetation under incomplete canopy cover were less studied and the z_{0m}/h_v relationship seems to vary more than for closed canopies (e.g. Hicks, 1973; Garratt, 1978; Riou et al. 1987). Garrat (1978) found z_{0m}/h_v of 0.05 for a natural savannah; Driese and Reiners (1997) reported averaged z_{0m}/h_v values of 0.04, 0.04 and 0.13 for natural sagebrush, saltbush and greasewood, respectively. Van Dijk et al. (2004) found a value of z_{0m}/h_v = 0.03 for a rain fed cropping system with maize and cassava. Originally the relationship between z_{0h} and z_{0m} was denoted by the dimensionless quantity kB^{-1}:

$$kB^{-1} = \ln (z_{0m}/z_{0h}) \qquad\qquad (7.4)$$

In many hydro-meteorological models containing a sub-model for the vegetation-atmosphere interaction, the results of Thom (1972) and Garrat and Hicks (1973) are used and kB^{-1} for vegetation is taken as a constant at about 2.0. Following them and also the standard work of Allen et al. (1998), it was assumed a kB^{-1} value of 2.3, being equivalent to z_{0h} = 0.1 z_{0m}.

The surface resistance parameters in the Penman-Monteith equation are combined into one parameter, the 'bulk' surface resistance (r_s) which operates in series with r_a. Microclimatic data of T and relative humidity (RH) were used together R_n, λE and G to estimate r_s inverting Equation 2.5. The effects of D and θ in the r_s values of irrigated fruit crops and natural vegetation growing in semi arid conditions of the Low-Middle São Francisco River basin were evaluated and specific relationships were found.

7.3   Analysis of the results

Energy fluxes and their parameterizations

The daily values of the radiation balances are presented in Table 7.1. R_n averaged 46% of R_G for wine grape, 55% for table grape, 51% for mango orchard, and 53% for caatinga. The rule of thumb of R_n being approximately 50% of R_G (e.g. Makkink, 1957; Oliver and Sene, 1992) was herewith confirmed to be a first realistic estimate.

Table 7.1: Daily averages of the radiation balance for irrigated crops (Wine Grape - WG, Table Grape - TG, Mango orchard - MG) for the first (GS1) and second (GS2) growing seasons; and for natural vegetation (Caatinga - CT) for two years (2004 and 2005): global solar radiation (R_G), reflected solar radiation (R_R), incident longwave radiation ($R_L\downarrow$), emitted longwave radiation ($R_L\uparrow$), and ratio of reflected solar radiation (R_R/R_G) and net radiation (R_n/R_G) to global solar radiation.

Vegetation/Period	R_G (MJ m^{-2} d^{-1})	R_R (MJ m^{-2} d^{-1})	$R_L\downarrow$ (MJ m^{-2} d^{-1})	$R_L\uparrow$ (MJ m^{-2} d^{-1})	R_R/R_G (-)	R_n/R_G (-)
WG_GS1	20.10	4.20	34.56	40.69	0.21	0.48
WG_GS2	23.87	5.15	32.95	41.36	0.22	0.43
TG_GS1	20.96	3.85	32.37	37.88	0.18	0.55
TG_GS2	20.49	3.83	32.57	38.27	0.19	0.54
MG_GS1	21.19	3.29	34.09	41.42	0.16	0.50
MG_GS2	21.92	3.30	33.97	41.50	0.15	0.51
CT_2004	21.60	3.08	33.51	40.47	0.14	0.54
CT_2005	20.84	2.70	34.16	41.52	0.13	0.52

For all sites, there was a consistent relationship between the half hourly values of R_n and R_G (Figure 7.1). The slopes of all equations ranged between 0.60 and 0.75.
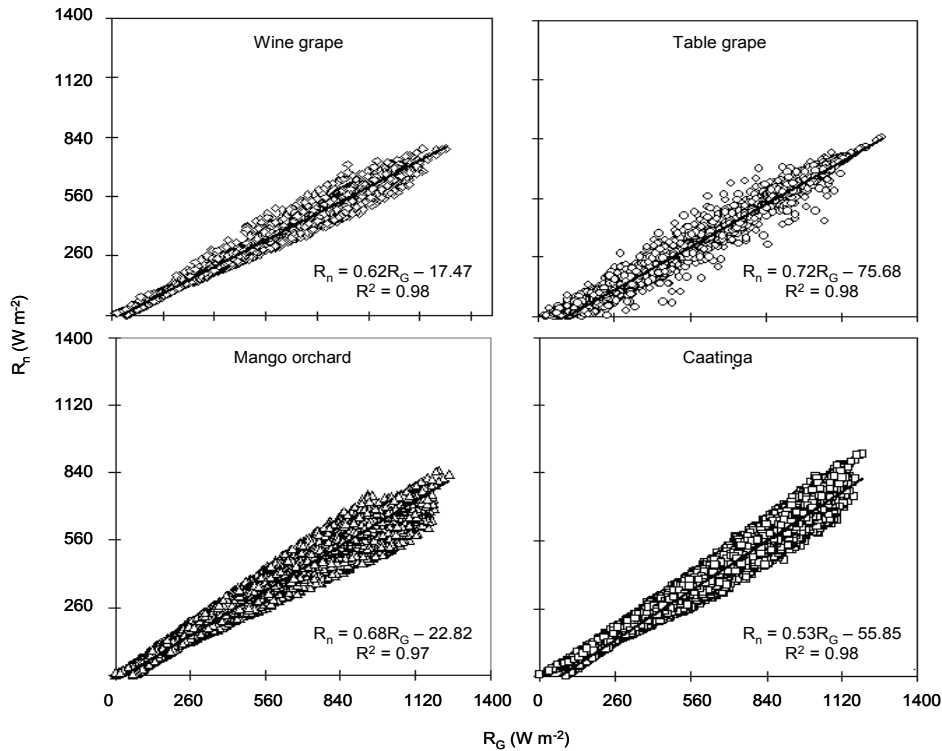
Figure 7.1. Relationship between net radiation (R_n) and global solar radiation (R_G) for 30 minutes time intervals during daylight hours for irrigated fruit crops (wine grape, table grape and mango orchard) and natural vegetation (Caatinga).

Similar results were obtained by Oliver and Sene (1992) from a rainfed vineyard in Spain, as well as for mature Sultana grapes, growing in a T-trellis system (Yunusa et al., 2004) and other ecosystems both in Australia (Hughes et al., 2001).

The high correlations imply that R_n can be estimated from R_G only. This is relevant because net radiometers are only occasionally available and sometimes there are technical problems associated with R_n measurements during a period of an experiment. The spatial variation of R_G across vast river basins can nowadays be well described from satellites by means of cloud cover data, which aids the description of the spatial variation of R_n.

The relationship between R_G and R_n is, to a large extent, affected by the surface albedo (α_0). A dark land surface absorbs more R_G, and has a higher R_n than a bright surface. The seasonal behaviour of α_0 is shown in Figure 7.2 for all vegetation types studied.
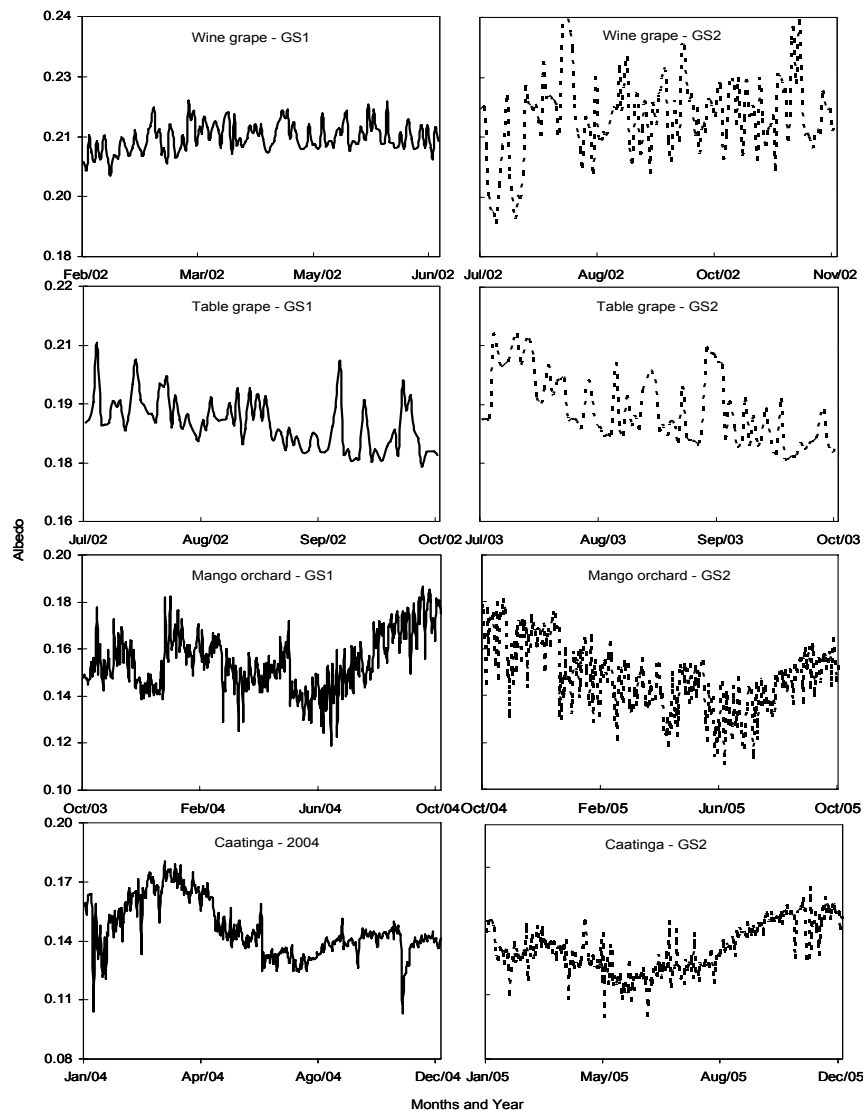
130

Figure 7.2. Seasonal variation of the surface albedo (α_0) for the first (GS1) and second (GS2) growing seasons of irrigated crops – wine grape, table grape and mango orchard; and for two years of natural vegetation – Caatinga.

The oscillation in daily averaged values is mainly due to the crop stages, cultural practices and irrigation for irrigated crops and rainfall regime in natural vegetation. The cover crop in table grape caused high α_0 values before bud break. After this stage α_0 varied due to several cultural practices reaching the lower values at the senescence stages.

131

Differences between the values for wine and table grapes are further due to the different trellis systems and cultural management. Mango trees displayed variation in α_0 according to their crop stages and time of the year. However, more variation occurred during the rainy season when the leaves were alternatively wet and dry due to interception. Higher values occurred as the leaf area increased under these conditions. This is a normal feature (Oliver and Sene, 1992).

The variability of α_0 in caatinga can be mainly attributed to variation in surface moisture conditions due to rainfall. The amounts of precipitation in caatinga site were 720 and 340 mm for 2004 and 2005 respectively, concentrated from January to April. The long term average is about 570 mm yr^{-1}. Monteith and Unsworth (1990) reported α_0 values between 0.15 - 0.26 for natural vegetation, higher than those for caatinga, possibly because of different surface moisture conditions and background reflectivity. However, the caatinga values were similar to those (0.12 to 0.13) reported for tropical rain forest (Oguntoyinbo, 1970; Pinker et al., 1980; Shuttleworth, 1988). The modification of α_0 with moisture conditions is in agreement with several authors (Campbell and Norman, 1998; Lobell and Asner, 2002; Van Dijk et al., 2004; Li et al., 2006).

R_R represented on average 22% of R_G for wine grape, 19% for table grape, 16% for mango orchard and 14% for caatinga, respectively (Table 7.1). Wine grape was the highest reflector out of the four agro-ecosystems investigated. This can be explained by the use of the vertical trellis system together with the exposure of the brightly reflecting soils to R_G. More oscillation in the values during the second growing season (GS2) of wine grape could be attributed to the sun position in relation to the rows and cloud free conditions in the second half of the year. The averaged albedo data for all vegetation of the current study were smaller than for those found in a rainfed vineyard (0.27) by Oliver and Sene (1992) on whitish calcareous soils.

The longwave radiation measurements over caatinga made it possible to estimate the 24 hour apparent atmospheric emissivity ($\varepsilon_{a_{24}}$), which was in turn related to atmospheric transmissivity - $\tau_{sw_{24}}$ (Equation 7.1) as well as to actual vapour pressure - $e_{a_{24}}$ (Figures 7.3a and 7.3b), for the same time scale. The second relation (Figure 7.3b) followed the classical parameterization that is commonly applied for irrigated crops (Allen et al., 1998). The relationship with $\tau_{sw_{24}}$ was better ($R^2 = 0.75$) than for $e_{a_{24}}$ ($R^2 = 0.64$). This can be most probably because the first

parameter describes the overall conditions in the atmospheric column, rather than those at one given level near to the surface.
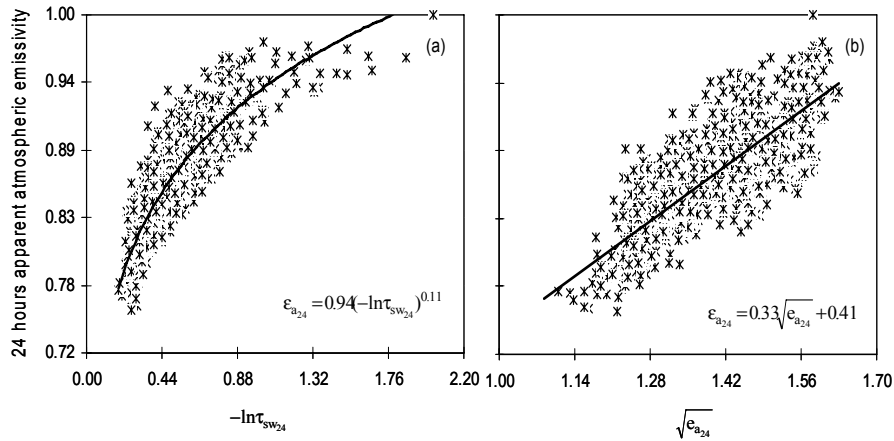

Figure 7.3. Relationships between apparent atmospheric emissivity ($\varepsilon_{a_{24}}$) with atmospheric transmissivity ($\tau_{sw_{24}}$) (a) and with actual air vapour pressure ($e_{a_{24}}$) (b) for 24 hours time scale.

The coefficients found for Equation 7.1 in Figure 7.3a are in between the values obtained for Idaho (a = 0.85 and b = 0.09; Allen et al., 2000) and Egypt (a = 1.08 and b = 0.26; Bastiaanssen, 1995). The availability of $\varepsilon_{a_{24}}$ made it feasible to compute $R_L\downarrow$ at daily time scale.

Equation 7.2 was tested because it allowed the extrapolation of instantaneous to daily values of net radiation ($R_{n_{24}}$). Figure 7.4 shows that the fundamental basis of describing $R_{n_{24}}$ by means $\tau_{sw_{24}}$ is valid; the overall agreement (R^2 = 0.78 to 0.83) is acceptable for semi-arid conditions of the Low-Middle São Francisco River basin.
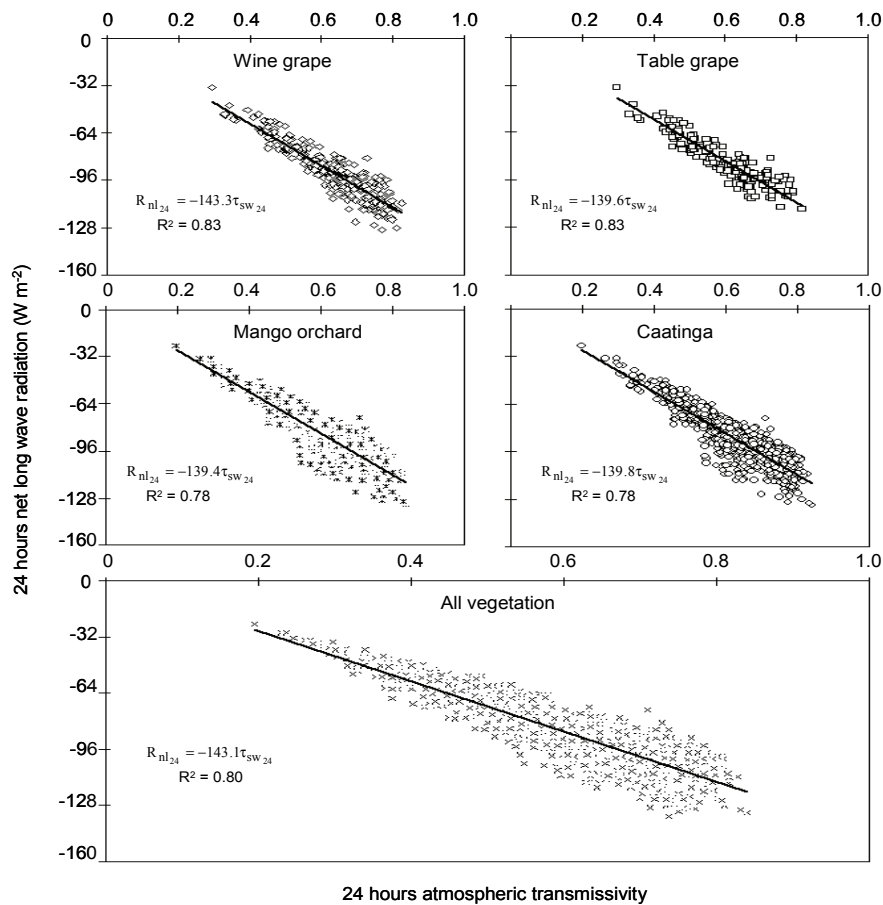
133

Figure 7.4. Relationships between net long wave radiation ($R_{nl_{24}}$) and atmospheric transmissivity ($\tau_{sw_{24}}$) on a 24 hour basis. $R_{nl_{24}} = -143.3\tau_{sw_{24}}$

In average, the $R_{n_{24}}$ coefficient for all agro-ecosystems was a = 143. In a grassland catchments area in the Netherlands, de Bruin and Stricker (2000) used a = 135, while the original value was a = 110. Apparently, the $R_{n_{24}}$ coefficient in semi-arid climates is much higher than for northern latitudes such as the Netherlands. The difference could be ascribed to differences in macroclimatic conditions. Because of the air temperature dependency on longwave radiation via the Stephan Boltzmann equation, it was investigated further whether the variations of the $R_{n_{24}}$ coefficient could be explained by variations in 24 hours air temperature (T_{24}). The relationship is shown in Figure 7.5. Higher T_{24}

134

values will result in more negative values of both longwave radiation and of the coefficient a.

$$a = 6.99T_{24} - 39.93$$

(y-axis) 24 hours R_n coefficient
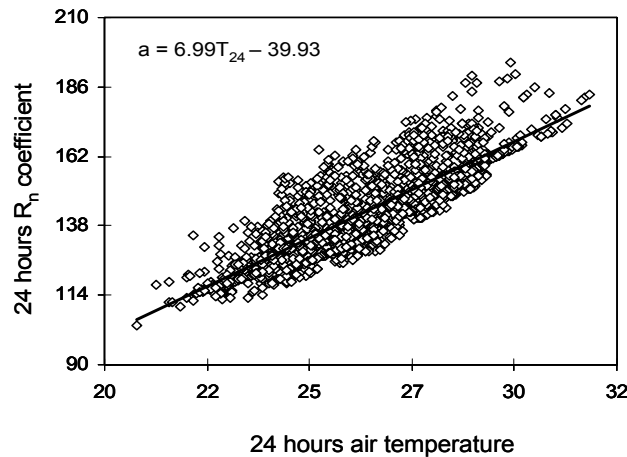
(x-axis) 24 hours air temperature

Figure 7.5. Relationship between the 24 hours coefficient for net radiation and 24 hours averaged air temperature near the canopies of irrigated crops (Wine grape, table grape and mango orchard) and natural vegetation (Caatinga).

The relationship of Figure 7.5 is useful when used together with interpolated values of air temperature to obtain the spatial variation of the energy balance, which will be dealt in the next chapter.

Average daily values of the energy balance for the entire growing seasons in irrigated crops and for two years in natural vegetation are summarized in Table 7.2. Near neutral atmospheric conditions predominated above the irrigated crops with the sensible heat flux (H) accounting for 13 to 20% of R_n. Most of R_n was partitioned into latent heat flux (λE), averaging, 79%, 89%, and 77%, for wine grape, table grape and mango orchard, respectively. The correspondent values of the evaporative fraction (E_F) ranged from 0.73 to 0.89. Not surprisingly, the intensively irrigated table grapes exhibited the highest λE and E_F values.

Due to the vertical trellis system that resulted in more exposed soil, lower values of E_F were found for wine grapes than for table grapes. The experiments in wine grape involved growing seasons with different solar angles. The 24 hours averaged value of G in wine grape was negative for the first half of the year, while during the second half G was positive. This indicates heating of the ground during the second growing season, as a result of the apparent movement of the sun associated to the vertical trellis system (see Table 7.2). Changes from negative to positive

135

values of G were also reported by Li et al. (2006) for the steppe of Mongolia, when seasonal energy partition was analyzed. Differences in the partition of the energy balance with different trellis and crop-training systems in vineyards were also reported by Novello et al. (1992), Heilman et al. (1996) and Rana et al. (2004).

While the values of λE for mango orchard exceeded those for wine grapes (not for table grapes), the E_F values were lower. These differences could be ascribed to the lower α_0 of mango orchard that resulted in higher R_n values. For both seasons of table grape and mango orchard G was negative, while for natural vegetation for both years it was nearly zero. Negative values indicated that the ground was an energy source to the atmosphere.

Table 7.2: Averaged daily (24 hours) energy balance in irrigated crops (Wine Grape - WG, Table Grape - TG, Mango orchard - MG) for the first (GS1) and second (GS2) growing seasons and in natural vegetation (Caatinga - CT) for two years (2004 and 2005): net radiation (R_n), latent heat flux (λE), sensible heat flux (H), soil heat flux (G) and evaporative fraction ($E_F = \lambda E/ (R_n-G)$)

Vegetation/Period	R_n (MJ m^{-2} d^{-1})	λE (MJ m^{-2} d^{-1})	H (MJ m^{-2} d^{-1})	G (MJ m^{-2} d^{-1})	E_F (-)
WG_GS1	9.77	8.07	1.90	-0.20	0.81
WG_GS2	10.31	7.73	2.08	0.50	0.79
TG_GS1	11.60	10.57	1.32	-0.29	0.89
TG_GS2	10.96	9.46	1.58	-0.08	0.86
MG_GS1	10.58	8.45	1.38	-0.37	0.77
MG_GS2	11.09	8.19	1.72	-0.18	0.73
CT_2004	11.56	4.62	5.69	0.03	0.40
CT_2005	10.78	2.67	6.88	0.03	0.25

The caatinga natural ecosystem characteristics were manifested by low values of both E_F and λE. Despite the relatively high values of R_n, the λE was low implying in a greater part of available energy being partitioned as H. During the dry season, the air above caatinga received more heat than water vapour, resulting in warmer air layers. During the rainy seasons, R_n was essentially converted into λE, however these periods were short and for the annual scale, H exceeded λE.

A classical problem in energy balance modelling is the conversion from instantaneous components of this balance to daily values. The most common procedure is to compute instantaneous E_F, and consequently to apply the same value for the entire day (e.g. Brutsaert and Sugita, 1992; Bastiaanssen, 1995; Su, 2002; Wang et al., 2007).

Literature on temporal variation of E_F has reported that the constant-value approach has an acceptable accuracy (e. g. Crago, 1996). Farah and Bastiaanssen (2004) demonstrated that there could be a deviation on a particular day, but that it can be used accurately to acquire ET_a on weekly to monthly time scales. The seasonal variations of E_F together the precipitations (P) are shown in Figure 7.6. During the growing seasons, vineyards were daily irrigated resulting to fairly constant values of E_F as they were cultivated in periods with absence or low amounts of rains. In mango orchard the high values of E_F after the rains are evident as the growing seasons are longer involving the rainy periods. The natural vegetation with the ability to respond quickly to rainfall caused the values of E_F high soon after the rains. The biggest effect was during 2004, when unusual precipitation occurred from January to April.
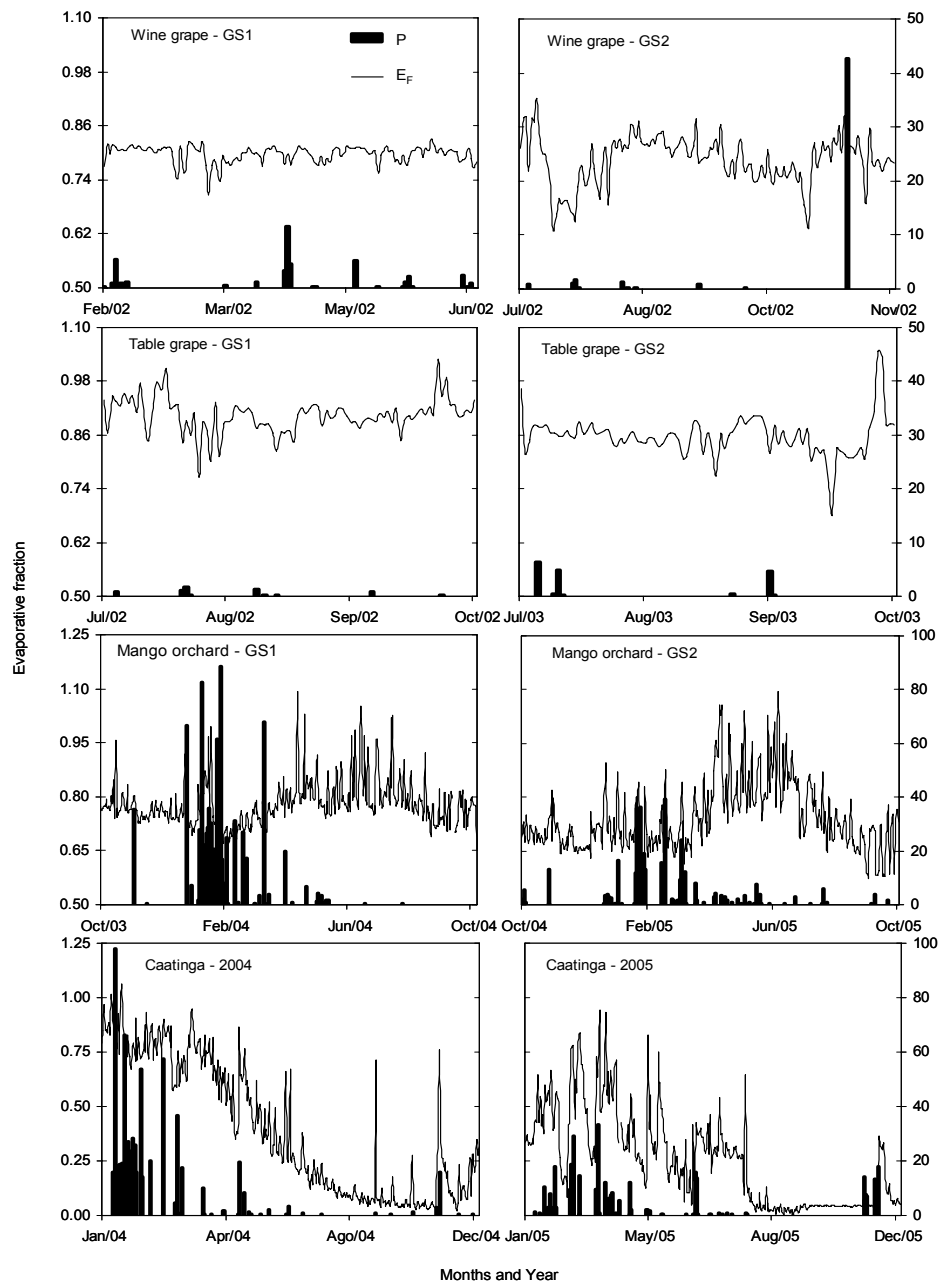
Figure 7.6. Seasonal variation of the evaporative fraction (E_F) and precipitation (P) for irrigated crops (Wine grape, table grape and mango orchard) and natural vegetation (caatinga).

138

The 24 hours ($E_{F_{24}}$) and daylight ($E_{F_{daylight}}$) values of evaporative fraction were calculated with the averaged values of R_n, λE and G for these time scales fulfilling $R_n > 0$ for daylight conditions. For midday ($E_{F_{12}}$), the instantaneous values at 12.00 hour were considered (Figure 7.7). The scatter in the graph with $E_{F_{12}}$ is larger than for $E_{F_{daylight}}$, because the latter represents a time integrated value that to a large extent affects $E_{F_{24}}$. Yet, the values of $E_{F_{24}}$ higher than those of $E_{F_{daylight}}$ for mango and caatinga. While for these two last vegetation a correction is necessary to acquire $E_{F_{24}}$ from $E_{F_{12}}$, for vineyards this is not. The implication is that E_F constancy varies with agricultural and natural ecosystems is an important finding for energy balance models at different time scales.
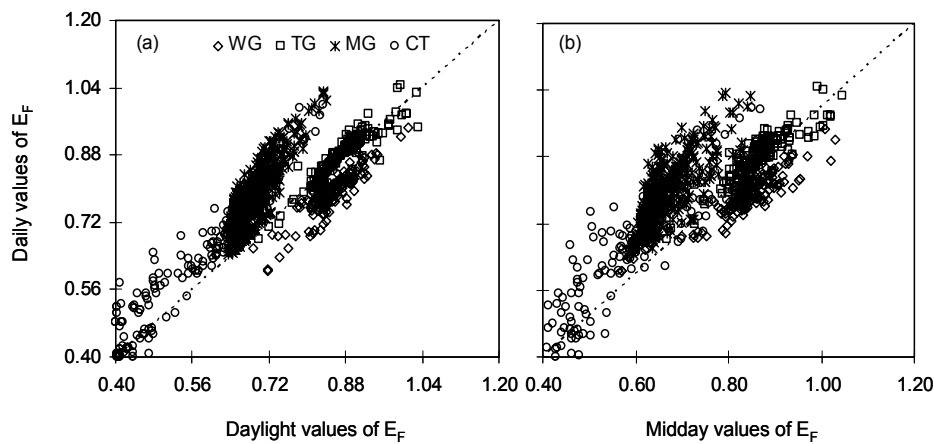

Figure 7.7. Relationships between the values EF_{24} vs. $EF_{daylight}$ (a) and of EF_{24} vs. EF_{12} values (b) for wine grape (WG), table grape (TG), mango orchard (MG) and caatinga (CT).

Values of λE_{night} from eddy correlation measurements (mango orchard and caatinga) were higher than those from the Bowen ratio method (vineyards). This implies that grapes have more condensation than the first two types of vegetation. Whether this is a true observation or a consequence of the different micro-meteorological measurements has not been further investigated. The values of λE_{night} in mango orchard and caatinga contributed to a higher $E_{F_{24}}$.

Soil-vegetation parameterizations

The seasonal-averaged measurements of the key vegetation parameters related to water fluxes are shown in Table 7.3. Due to the tall and aerodynamically rough canopy architecture, mango orchard presented the greatest values of u_*. The averaged value was 0.49 m s^{-1}, much greater than for wine grape (0.21 m s^{-1}). The average z_{0m} value for wine grape was 0.08 m and for table grape 0.24 m. Sene (1994) reported values ranging from 0.04 to 0.06 m for rainfed wine grape growing under semi-arid conditions in Castilla La Mancha with larger spacing within and between the rows (5 m x 5 m). Van den Hurk et al. (1996) showed for the same region in Spain (but at a different plot) values from 0.01 m to 0.06 m, varying proportionally to the leaf area index (LAI). The maximum value seems to be in good agreement with the actual wine grape results. Table grape has a rougher surface than wine grape, and thus a larger z_{0m} that generates more turbulent movement above the canopy.

Although the mean value of z_{0m} for table grape was higher than for wine grape, the variations along the growing seasons were lower. The standard deviation for z_{0m} was 0.04 m in wine grape vineyard and only 0.01 m in the table grape vineyard (Figure 7.8). The vertical trellis system with a low LAI in wine grape showed results that depended on the wind direction. The rows of vineyards were north-eastern oriented. When the wind blew more parallel to the rows (115°), z_{0m} values were 50% of those when the wind direction was near south-east (130°). Table grape was insensitive to changes in wind direction (see Table 7.3). Hicks (1973) reported that the drag coefficient doubled as the wind direction swung from parallel to normal of the vine rows in vertical trellis. When they blew normal to the rows, z_{0m} was found to be about 13% of the vineyard height, behaviour typical for rough and closed canopies. In the present study, the horizontal overhead trellis of table grape covered almost all the soil beneath the canopy few days after bud break creating a rougher surface.

Table 7.3: Average values of the vegetation parameters of irrigated crops (Wine Grape - WG, Table Grape - TG, Mango orchard - MG), for the first (GS1) and second (GS2) growing seasons and of natural vegetation (Caatinga - CT) for 2004 and 2005: aerodynamic (r_a) and surface (r_s) resistances; friction velocity (u_*); roughness length for momentum transfer (z_{0m}); mean vegetation height (h_v); vapour pressure deficit (D), wind speed above the canopies (u) and wind direction (WD).

Vegetation/ Period	r_a (s m^{-1})	r_s (s m^{-1})	u_* (m s^{-1})	z_{0m} (m)	h_v (m)	D (kPa)	u (m s^{-1})	WD (Degrees)
WG_GS1	114	131	0.21	0.11	1.6	1.8	1.9	128
WG_GS2	109	125	0.21	0.06	1.6	2.1	2.1	116
TG_GS1	63	64	0.38	0.23	1.8	1.3	2.0	118
TG_GS2	66	82	0.40	0.24	1.8	1.2	2.1	138
MG_GS1	36	133	0.50	0.50	5.5	1.3	2.6	126
MG_GS2	37	133	0.48	0.54	5.5	1.3	2.4	124
CT_2004	53	1542	0.39	0.43	8.0	1.5	2.8	135
CT_2005	58	2332	0.39	0.33	8.0	1.5	2.9	132

*The height of the anemometers was 1m above the canopies of vineyards, while they were at 3m above the canopies in mango orchard and caatinga.

The z_{0m} values in the mango orchard averaged 0.52 m. The big crowns of the trees enhanced the momentum flux. The higher values of wind speed (u) above the canopy, if compared with vineyards, were due to the higher level of the anemometer. Despite the taller mixed species of caatinga (8 m) in relation to the mango trees (5.5 m), results showed lower aerodynamic roughness values of z_{0m} (0.38 m) and u_* (0.39 m s^{-1}). The reason can be explained by the patchwork of bushes and the irregular spacing among them in the natural vegetation. During an international land surface flux campaign on Sahelian bushland with irregular spacing among stripes of bushes, the values for z_{0m} were also found to be at the lower side (0.22 to 0.27 m: Troufleau et al., 1997).

The z_{0m} values for mango orchard and for caatinga showed both effects from the rainy period (between January and March) which increased in leaf areas and thereby the surface roughness. More distinct differences in roughness parameters for natural vegetation were visible during 2004 than in 2005 (Figure 7.8). This was related to the unusual high rainfall amount in 2004.

According to Sene (1994), sparse crops typically present z_{0m} values in the range 5-10% of h_v while for uniform crops the values are typically about 13%. With the present averaged values of z_{0m} of $0.06h_v$ for wine grape, $0.13h_v$ for table grape, $0.09h_v$ for mango orchard and $0.05h_v$ for caatinga, one can conclude that table grape is an exception due

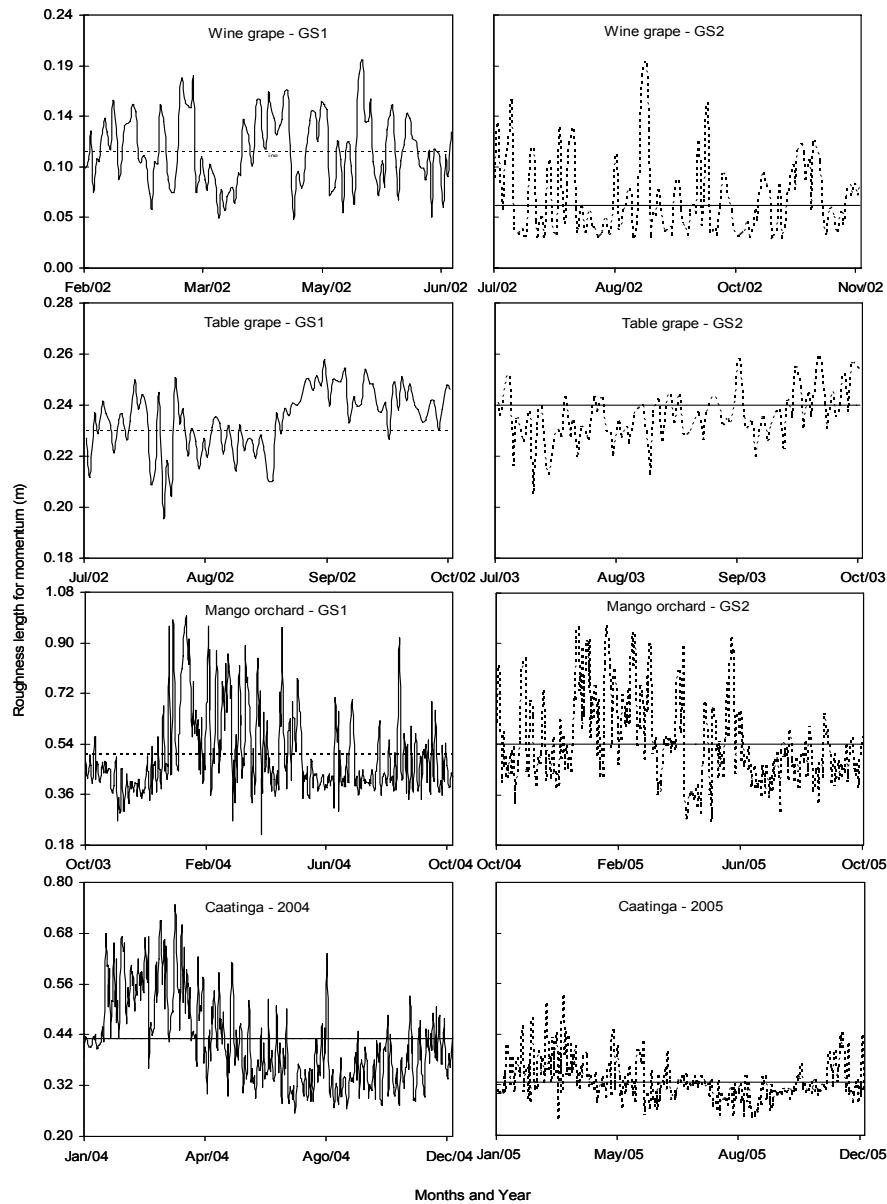to its deviating canopy architecture. On average, z_{0m} was approximately 9% of the h_v.

Figure 7.8. Seasonal variation of roughness length for momentum transfer (z_{0m}) for the first (GS1) and second (GS2) growing seasons of irrigated crops: wine grape, table grape and mango orchard; and for 2004 and 2005 of natural vegetation: caatinga. Horizontal bars are averaged values.

142

The seasonal-averaged values of resistances to water fluxes are shown in Table 7.3. Wine grape had the highest averaged value of r_a (112 s m^{-1}), followed by table grape (65 s m^{-1}), caatinga (55 s m^{-1}) and mango orchard (36 s m^{-1}). The low values for mango orchard are due to the aerodynamically rough canopy architecture evidenced by the highest values of u_* and z_{0m}. The maximum values of r_s among the vegetation types studied are detected in caatinga (average of 1937 s m^{-1}). The low moisture conditions during the dry season caused the stomata to close preventing the vegetation from cell moisture depletion and wilting. Wine grape and mango orchard present similar r_s values around 130 s m^{-1}, for while table grape r_s values were as low as 74 s m^{-1}. Table grape has almost a double LAI compared to wine grape. The lower value of D in micro sprinkler irrigation system also contributed to smaller values of r_s in table grape than for drip irrigated wine grape.

The daylight variation of r_s and D are shown in Figure 7.9. Low values during the early morning represented the dominance of energetically dependent physiological control over λE.
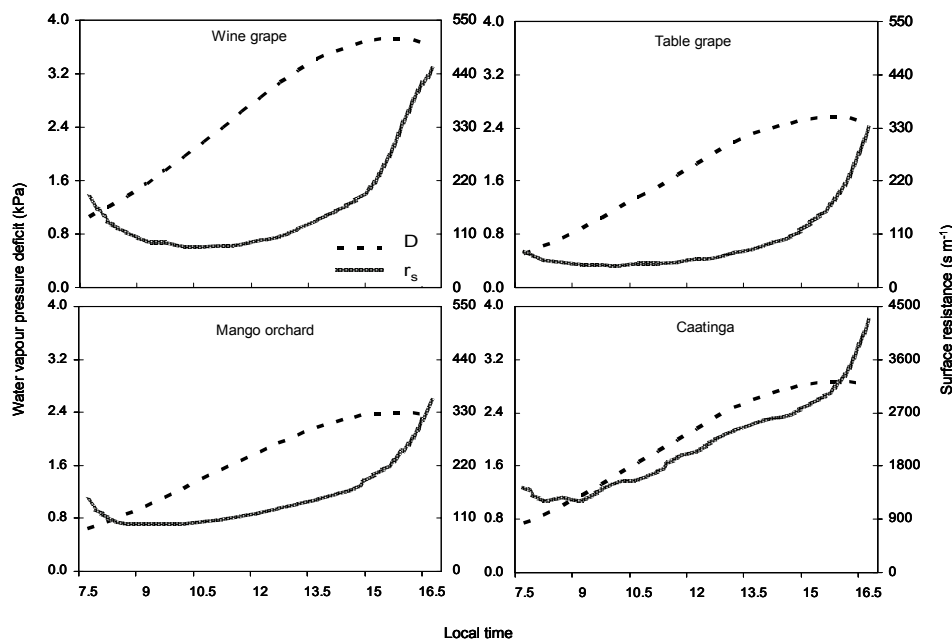

Figure 7.9. Daylight fluctuation of bulk surface resistances - r_s and vapour pressure deficit - D for irrigated crops (wine grape, table grapes and mango orchard) and natural vegetation (caatinga).

143

The greatest variation occurring at this time of the day is because r_s is close to its minimum value, partially due to dew (van Dijk et al., 2004). The low and near-minimum values for r_s only hold when all environmental conditions are optimal at the same time. Such pre-requisite does not last long, and a quick rise of r_s during morning hours is envisaged. The progressive soil moisture constraints and rising T and D induce stomatal closure. The higher values of r_s during the late afternoon are mainly related to the constraints induced by high T and D, in conjunction with lower levels of R_G. It is thus a combined effect, and no single responsible variable can be determined. The globally accepted standard ecological theories first presented by Jarvis (1976) and Stewart (1989) are herewith confirmed.

Figure 7.9 suggests that the daylight behaviour of $r_s = f(D)$ is most tight for caatinga. The likely reason for this is the control of θ on stomatal regulation.
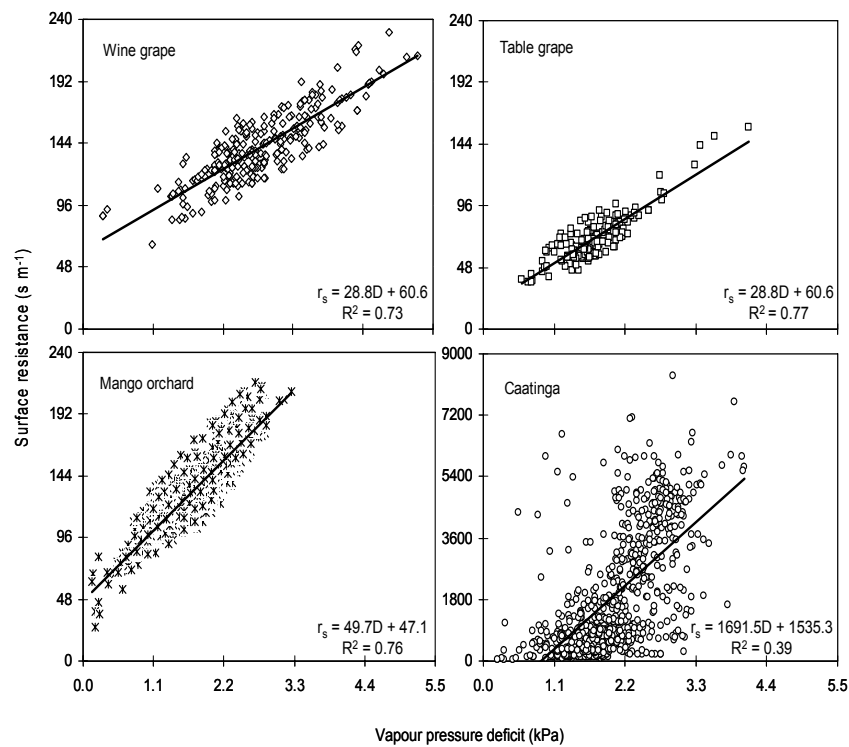

Figure 7.10. Daylight relationships between surface resistance (r_s) and vapour pressure deficit (D) for irrigated crops (Wine grape, table grapes and mango orchard) and natural vegetation (Caatinga).

While the irrigated crops experience diurnal cycles in root zone water availability, caatinga responds stronger to rainfall regime. The relationships between r_s and D at a daily time scale throughout the measuring period are shown in Figure 7.10. Except caatinga ($R^2 = 0.39$), irrigated vineyards and mango showed a good correlation. While there were higher water vapour gradients between the stomata and the near-surface atmosphere in dry periods, these gradients at the same time induced partial stomatal closure. There is thus a negative feedback system in agro-ecosystems that dampens any significant variation in λE.

The effect of θ on r_s was evident when studying their relationships for irrigated fruit crops (Figure 7.11).
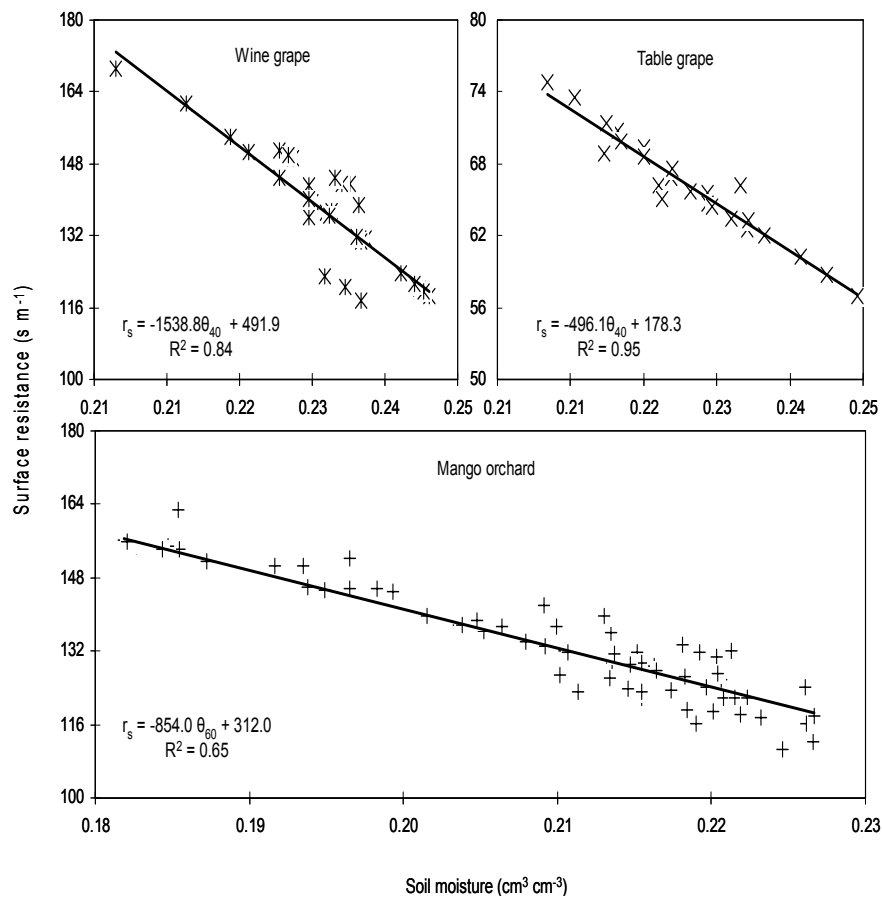

Figure 7.11. Weekly relationships between surface resistance (r_s) and soil moisture in irrigated vineyards for 40 cm soil depth (θ_{40}) and mango orchard for 60 cm soil depth (θ_{60}).

145

The r_s of caatinga was dominantly controlled by seasonal soil moisture variability. In irrigated fruit crops it was controlled by both θ ($R^2 = 0.65$ to 0.95) and D ($R^2 = 0.73$ to 0.77). Mango orchard was more responsive to D ($R^2 = 0.76$) than to θ ($R^2 = 0.65$). Hence, water fluxes and water productivity in this orchard are largely influenced by D levels. The role of on-farm irrigation management in vineyards need thus to be done more alert than in mango orchards. One can practice very precise irrigation applications, but the water balance in mango orchards will be influenced by D. The r_s response to θ was published for alfalfa by van Bavel (1996) and for wheat by Hatfield (1985). Larger changes of r_s occur at small changes of θ in wet soils. At an average θ of 0.20 cm^3 cm^-^{3}, the sensitivity of wine grape was $dr_s/d\theta = 1539$, $dr_s/d\theta = 496$ for table grape, $dr_s/d\theta = 854$ for mango orchard, $dr_s/d\theta = 350$ for alfalfa (van Bavel, 1996), and $dr_s/d\theta = 80$ for wheat (Hatfield, 1985).

The highest slopes of $dr_s/d\theta$ reveal the strongest response to changes in available soil water. Wine grape thus exhibits the strongest response of r_s to minor changes of θ, followed by mango orchard, table grape, alfalfa and finally wheat.

7.4   Conclusions

The diurnal and seasonal variation of the radiation and energy balance components in irrigated crops and natural vegetation in the Brazilian semi-arid region of the Sao Francisco River basin have been investigated. These investigations allowed a better understanding of the energy fluxes and the physical vegetation properties that affect these exchange processes, what are important for appraising the impact of land use changes on the regional scale water balance. From radiation measurements, it could be concluded that net radiation can be estimated by means of a linear expression with global solar radiation depending on the type of vegetation. The presented equation to estimate apparent emissivity of the atmosphere from atmospheric transmissivity had a better correspondence with field measurements than the standardized FAO equation based in actual water vapour pressure. The atmospheric emissivity estimation is fundamental for the estimation of instantaneous net radiation fluxes.

The daily values of evaporative fraction for all irrigated crops varied between 0.71 (mango orchard) to 0.90 (table grape), revealing that most net available energy is converted into actual evapotranspiration. This implies that the atmospheric boundary layer over wet irrigated

146

perimeters receives small quantities of sensible heat, and stays thus relatively cold. The values of evaporative fraction for caatinga, the natural vegetation, were in an annual scale with 0.25 to 0.40 much smaller than for irrigated crops. A distinct seasonal variation of in caatinga was found because of the water availability linked to precipitation pattern during the year.

It was demonstrated that daytime and daily energy balances can be estimated from instantaneous measurements, provided that net radiation and soil heat flux are known across time integrated periods. The energy balances for mango orchard and caatinga showed that a slight correction is required if the instantaneous value of evaporative fraction is to be used as a representative value for a 24-hour period.

Parameterizations of the aerodynamic (r_a) and the bulk surface (r_s) resistances facilitated the analysis of the comprehensive evapotranspiration from heterogeneous land surfaces. The variability of r_a can be mainly explained by the friction velocity which on turn depended on the surface roughness length for momentum transport (z_{0m}). In wine grape, the vertical trellis system affected the roughness parameters according to the wind direction. The overhead trellis system in table grape was – due to the sheltering effect – less sensitive to wind direction. The experimental data showed that for sparse canopies, z_{0m} being 9 % of the vegetation height is a doable operational rule for the semi arid region of the Low-Middle São Francisco River basin. For large spacing between clumps of caatinga, z_{0m} is reduced in comparison with irrigated fruit trees.

The r_s values for wet surfaces are dominantly affected by atmospheric water vapour pressure deficit (D) and soil moisture (θ). There was a negative physiological feedback from D on evapotranspiration rates: while high D values increased the gradient of water vapour transport, it at the same time created an extra blockade on the vapour flow path by partially closing the stomata. Natural vegetation also showed a link between r_s and D but less than for irrigated crops; for long period, r_s in natural vegetation is determined predominantly by rainfall regime. The availability of analytical methods to assess r_a and r_s makes the one-step Penman-Monteith equation suitable for actual evapotranspiration and water productivity estimations. By further developing of methods to parameterize crop production at the regional scale, it will become feasible to estimate water productivity variations and detect areas where water saving in agriculture could be realized.

147

8. Reviewing SEBAL input parameters for assessing actual evapotranspiration and water productivity

8.1 Introduction

Intensification of agriculture has caused widespread changes of land cover in the Low-Middle São Francisco River basin during the last decades. Water scarcity in this sub-basin sometimes leads to the depletion of water resources resulting to aquifer mining and stream flow reduction. In addition, agricultural drainage and urban sewage adversely affect the water quality, both locally and further downstream. Irrigated lands have cleared natural vegetation systems inducing a loss of biodiversity. Water use of irrigated crops exceeds that of natural rainfed ecosystems, promoting a reduction of stream flow, because more precipitation is converted into actual evapotranspiration (ET_a). With increasing water scarcity and decreasing water quality, all water users (urban, industrial, agricultural, and ecological) will be calling for an appropriate and fair share of the São Francisco River water.

The accurate determination of ET_a significantly reduces uncertainties in the water balance of a (sub-) basin (Cleugh et al, 2007), providing water managers with information on (i) water resources being consumed and thus not longer available for downstream users, and (ii) water productivity, i.e. the consumption of water in terms of biomass production per unit of water (e.g. Molden et al., 2007c). Field scale ET_a measurements on vineyards, mango orchards and natural vegetation (caatinga) were made in the semi-arid region of the São Francisco River basin. Micro-meteorological methods were used that provide point values for specific sites which were described in Chapter 4. A direct extrapolation of these data to large scale can lead to biased estimates, because a few flux sites cannot provide a fair sample of water fluxes in a bigger area (Wylie et al, 2003). Therefore, data from flux stations are only a first estimate of ET_a from contrasting ecosystems (Leuning et al., 2005). The spatial and temporal distribution of ET_a can be mapped from remote sensing techniques without going through excessive ground data collection (e.g. Franks and Beven, 1999). According to Nagler et al. (2007), remotely sensed vegetation indices, obtained as a time series over a growing season, together with micrometeorological data can be used to extrapolate plot level measurements of ET_a and water productivity over larger landscapes units. One of the remote sensing algorithms is the

Surface Energy Balance Algorithm for Land (SEBAL), which has been applied to a variety of ecosystems. Although this algorithm was designed to calculate the energy balance at regional scale using a minimum of ground data, local parameterization of any remote sensing equations can improve the accuracy in the model (Duchemin et al., 2006).

This chapter combines satellite data, field measurements of the surface radiation and energy balances and agro-meteorological stations to review the various SEBAL steps aiming to analyse whether the additional river water resources are wisely used. During the calibration and validation processes, the accuracy of individual empirical relationships, as well as the final estimate of large scale ET_a, biomass production and crop water productivity is assessed. The reviewed parameters are; surface albedo, surface temperature, surface and atmospheric emissivities, roughness length for momentum transport, net radiation, soil heat flux, air temperature gradient, sensible heat flux, latent heat flux, and photosynthetically active radiation. The relevant equations were adapted and validated for the semi-arid conditions of São Francisco Valley, and then applied to each individual Landsat image for water productivity analyses.

8.2   Methodology

8.2.1   Outline of SEBAL principles for Landsat images

Radiation balance

SEBAL requires spatially distributed, visible, near-infrared and thermal infrared data together with routine weather data. The algorithm computes net radiation (R_n), sensible heat flux (H) and soil heat flux (G) for every pixel of a satellite image and the latent heat flux (λE) is acquired as a residual in energy balance (Equation 2.1). This is accomplished by first computing the surface radiation balance, followed by the surface energy balance. The schematic overview to convert spectral radiance into the net radiation using Landsat images is presented in Figure 8.1.
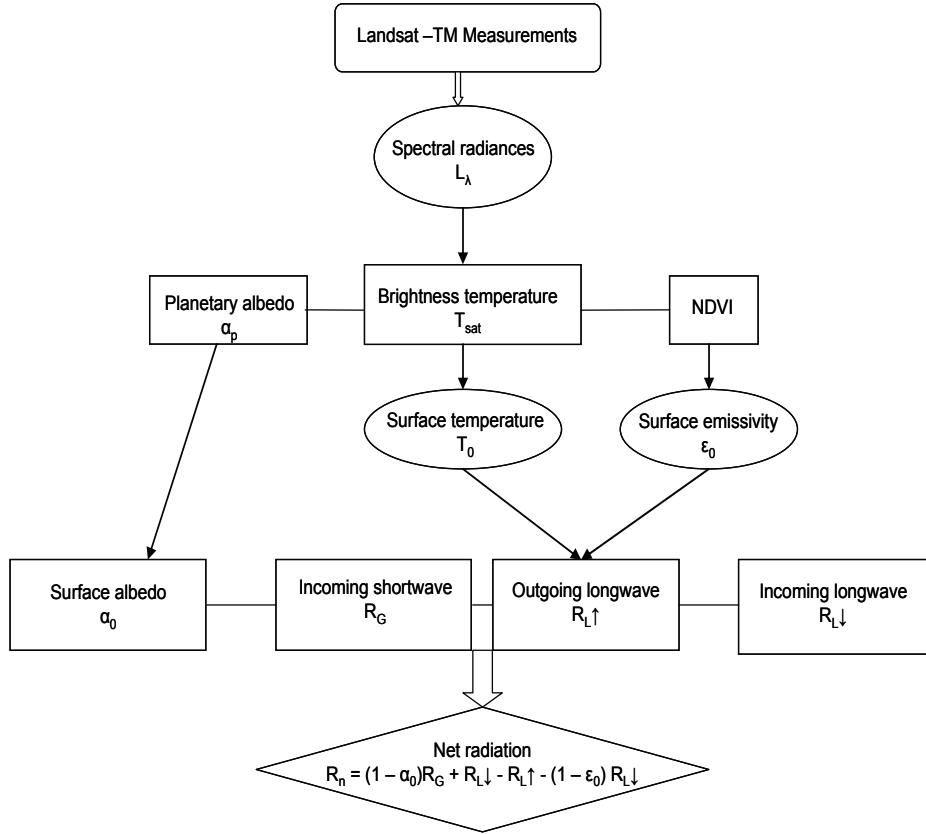
Figure 8.1. Schematic flowchart for the radiation balance.

In the radiation balance, the net shortwave radiation available at the earth surface depends of the incoming global solar radiation (R_G) and the surface albedo (α_0). The second parameter is calculated from satellite-measured spectral radiances for each narrow band, followed by mathematical expressions for spectral integration and atmospheric corrections. Regional R_G in the present research was computed using interpolated measurements from pyrometers of agro-meteorological stations.

The planetary albedo for each satellite band (α_{p_b}) is calculated as:

$$\alpha_{p_b} = \frac{L_b \pi d^2}{R_{a_b} \cos \varphi} \qquad (8.1)$$

where L_b is the spectral radiance for wavelengths of the band b, d is the relative earth-sun distance; R_{a_b} is the mean solar irradiance at the top of the atmosphere (or atmospheric irradiance) for each band (W m^{-2} μm^{-1}) and φ the solar zenith angle. The broadband planetary albedo (α_p) is calculated as the total sum of the different narrow-band α_{p_b} values according to weights for each band (w_b).

$$\alpha_p = \sum w_b \alpha_{p_b} \tag{8.2}$$

The weights for the different bands are computed as the ratio of the amount of incoming shortwave radiation from the sun in a particular band and the sum of incoming shortwave radiation for all the bands. The bands 1 to 5 and 7 provide data for the visible and near infrared bands used for surface albedo calculations.

The spectral radiance in band 6 (L_6) of Landsat is converted into a radiation temperature applicable at the top of the atmosphere (T_{sat}) by inversion of Plank's law in the 10.4-12.5 μm band width:

$$T_{sat} = \frac{K_2}{\ln(\frac{K_1}{L_6+1})} \tag{8.3}$$

where L_6 is the uncorrected thermal radiance from the land surface and K_1 (607.76 and 666.09 for Landsat 5 and 7, respectively) and K_2 (1260.56 and 1282.71 for Landsat 5 and 7, respectively) are conversion coefficients.

The resulting broadband planetary albedo and radiometric temperature need to be corrected atmospherically for acquiring the land surface counterparts.

Outgoing longwave radiation ($R_L\uparrow$) is obtained using the Stefan-Boltzmann equation (Allen et al., 1998) with an empirically determined surface emissivity (ε_0) and surface temperature (T_0) acquired by the satellite after atmospheric correction. The incoming longwave radiation ($R_L\downarrow$) is calculated also using the Stefan-Boltzmann equation with an empirically determined atmospheric emissivity (ε_a) and data of air temperature (T). The final term in radiation balance equation, $(1-\varepsilon_o) R_L\downarrow$, represents the fraction of $R_L\downarrow$ that is lost from the surface due to

reflection (Figure 8.1). The local calibrations of radiation balance terms are explained in detail in the next sections.

Energy balance

The second step of the SEBAL is to compute the regional values of G and H. The first term is calculated by the ratio G/R_n. Most literature describes this last ratio being a function of leaf area index - LAI or of the Normalize Difference Vegetation Index - NDVI (e.g. Clothier et al., 1986; Choudhury, 1989). The role of T_0 in the physical description of heat diffusion is recognized by incorporating it into the parametric expression G/R_n. H is obtained by near-surface temperature gradients (ΔT).

According to the Figure 8.2, the first value for friction velocity (u_*) is computed for neutral atmospheric stability, using data from agro-meteorological stations. The near-surface wind speed is converted to a value at the blending height, i.e. a height above the stations where the effects from the land surface roughness can be eliminated. A height of 200 meters can be considered (u_{200}). The first estimate of u_* is used – conjunctively with surface roughness estimates – to infer aerodynamic resistance (r_a). Corrections for atmosphere stability are obtained iteratively for each pixel. A series of iterations is required to determine new values of u_{*_corr} and r_{a_corr} before obtaining numerical stability.

SEBAL computes ΔT by assuming its linear relationship with T_0, and the coefficients of this relationship are acquired following an internal calibration procedure (Allen et al., 2007a). This calibration is image and occasion dependent. The algorithm uses two "anchor" pixels at which a value for H can be estimated on the basis of *a priori* knowledge (Figure 8.2) of the fluxes over dryland (hot pixel) and wet terrain (cold pixel). The sensible heat fluxes in these sites (H_{hot} and H_{cold}) can be calculated applying the energy balance equation for the anchor pixels.
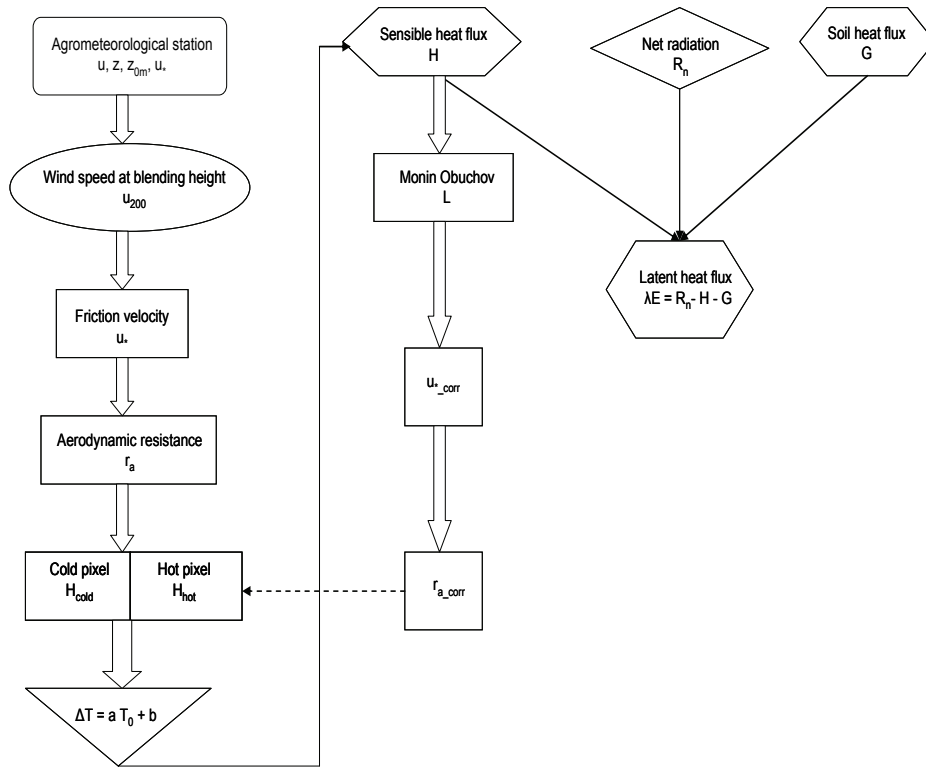
Figure 8.2. Schematic flowchart for the energy balance of the SEBAL algorithm.

The instantaneous estimation of λE can be scaled to longer periods by using the evaporative fraction $[E_F = \lambda E/(R_n - G)]$ following Bastiaanssen et al. (2005) or applying the ratio ET_a/ET_0 following Allen et al. (2007a). The essential SEBAL steps are elucidated in Allen et al. (2007a) and in Koloskov et al. (2007).

Crop water productivity

The calculation of regional crop water productivity (CWP) based on actual evapotranspiration requires ET_a and biomass production (BIO) to be spatially known. BIO is obtained from photosynthetically active radiation (PAR) and light use efficiency (ε) for specific type of vegetations. The yield is estimated from BIO and specific apparent harvest indexes (AHI). The flowchart is shown in Figure 8.3.
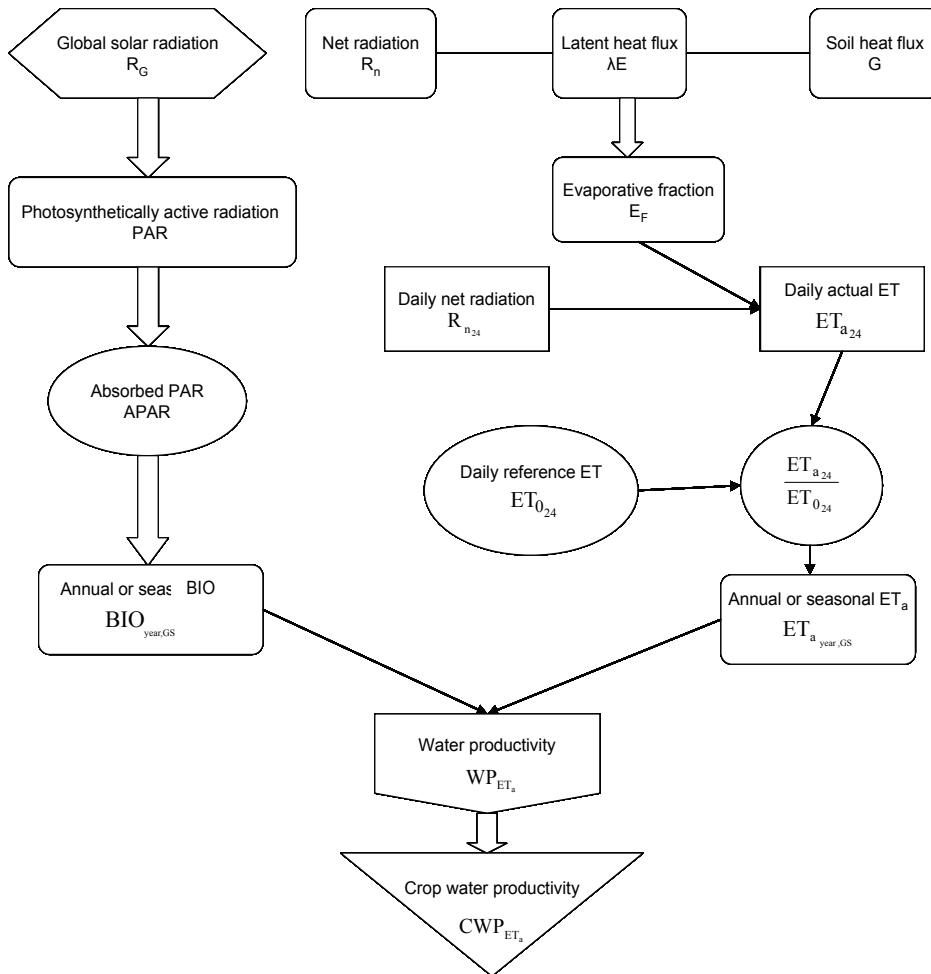
Figure 8.3. Schematic flowchart for calculation of bio-physical crop water productivity based on actual evapotranspiration (CWP_{ET_a}).

With data from ago-meteorological stations, the interpolated daily values of the reference evapotranspiration ($ET_{0_{24}}$) yielded a grid of reference data. Following Allen et al. (2007a,b), the annual (subscript year) and seasonal (subscript GS) actual evapotranspiration ($ET_{a_{year,GS}}$) were calculated with the reference evapotranspiration for these time scales ($ET_{0_{year,GS}}$) as:

$$ET_{a_{year,GS}} = \left(\frac{ET_{a_{24}}}{ET_{0_{24}}} \right)_{avg} ET_{0_{year,GS}} \tag{8.4}$$

where the values $\left(\dfrac{ET_{a_{24}}}{ET_{0_{24}}} \right)_{avg}$ are the calibrated and averaged daily ratios

for the year or growing season (GS).

The limited availability of cloud free Landsat images is the main argument for using Equation 8.4 as a simplified method to estimate annual or seasonal regional ET_a including natural vegetation and irrigated land. The interpolated daily values of global solar radiation data for 24 hours ($R_{G_{24}}$) can be used to estimate the regional scale Photosyntetically Active Radiation (PAR$_{24}$) for the same time scale (PAR$_{24}$):

$$PAR_{24} = aR_{G_{24}} \quad (W \ m^{-2}) \tag{8.5}$$

where a is the constant of the regression equation that reflects the portion of $R_{G_{24}}$ that can be used by leaf chlorophyll for photosynthesis.

The values of Absorbed Photosyntetically Active Radiation for 24 hours (APAR$_{24}$) can be approximated directly from PAR$_{24}$:

$$APAR_{24} = f \, PAR_{24} \ (W \ m^{-2}) \tag{8.6}$$

The factor f (i.e. APAR$_{24}$/ PAR$_{24}$) can be directly estimated from the NDVI (e.g. Asrar et al., 1992). Bastiaanssen and Ali (2003) considered for a mixture of arable crop types the following coefficients:

$$f = -0.161 + 1.257 \ NDVI \ (W \ m^{-2}) \tag{8.7}$$

The annual and seasonal accumulated biomass productions (BIO$_{year,GS}$) were obtained as:

$$BIO_{year,GS} = \sum \left(\varepsilon_{max} E_{F_{24}} APAR_{24} 0.864 \right). \ (kg \ ha^{-1}) \tag{8.8}$$

where ε_{max} is the maximum light use efficiency, which according to Monteith (1972) varies only with c3 and c4 crops (if not water stressed).

The CWP at farm level is expressed in this thesis as wine and fruit production per cubic meter water consumed (Teixeira et al., 2007, 2008a):

$$\text{CWP}_{\text{ET}_a} = \left(\frac{\text{BIO}_{\text{GS}}}{\text{ET}_{a_{\text{GS}}}} \right) \text{AHI} \quad (\text{kg m}^{-3} \text{ or L m}^{-3}) \qquad (8.9)$$

where AHI is the apparent harvest index required for the conversion of total dry matter into fresh yield.

In this thesis, AHI values were acquired by dividing fresh fruit productions measured by the farmers for the growing seasons by BIO_{GS} from satellite images for three representative farms of grapes and mangos, in the plots where the flux towers were installed. For wine grapes the fruit yields were converted into wine productions, by considering that 1.25 kilograms of grapes yielded 1 litre of wine (Teixeira et al., 2007).

The satellite values of $\dfrac{\text{ET}_{a_{24}}}{\text{ET}_{0_{24}}}$, $\text{E}_{\text{F}_{24}}$ and NDVI were calibrated with field measurements in irrigated crops (Teixeira 2007, 2008a) and natural vegetation (Teixeira et al. 2008b). After calibrations and interpolations of the satellite images, the annual and seasonal values of ET_a and BIO were obtained using Equations 8.4 and 8.8, respectively. The three representative commercial farms of wine grapes, table grapes and mangos were analyzed in terms of CWP.

8.2.2 Field measurements

The region with the field experiments and the network of agro-meteorological stations used in this study were dealt in details in Chapter 4 and shown in Figure 4.1 and described in Table 4.4. Routine weather data from the seven automatic agro-meteorological stations were used for SEBAL calculations and to compute the reference evapotranspiration (ET_0) by the FAO Penman-Monteith method (Allen et al., 1998). Table 8.1 summarizes the averaged daily meteorological ground conditions during the overpasses days of the Landsat satellite, as well the vegetated surface types considered for each image. These days covered periods with high (6.2 mm d^{-1}) and low (3.8 mm d^{-1}) values of ET_0. The average value of this last parameter for all days was 5.1 mm d^{-1}.

157

Table 8.1: Daily values of weather variables on Landsat overpass days. The averaged data of seven agro-meteorological stations and land surface types used for calibration and validation are presented: extra-terrestrial solar radiation (R_a); global solar radiation (R_G), air temperature (T), relative humidity (RH), vapour pressure deficit (D), wind speed at 3 m above the ground (u) and reference evapotranspiration (ET_0). All values represent 24 hour periods.

Day/Year	Surface type	R_a (MJ m^{-2} d^{-1})	R_G (MJ m^{-2} d^{-1})	T (^{o}C)	RH (%)	D (kPa)	u (m s^{-1})	ET_0 (mm d^{-1})
253/2001	WG	35.7	25.0	27.4	52	1.8	3.0	4.4
277/2001	WG	37.1	24.5	29.2	46	2.2	3.2	4.5
187/2003	TG,CT	28.7	21.5	23.5	54	1.3	1.9	3.8
267/2003	TG,CT	38.3	22.2	25.8	48	1.7	2.4	5.0
286/2004	MG,CT	37.1	26.7	28.1	46	2.1	3.4	6.0
318/2004	MG,CT	39.4	28.0	31.4	39	2.8	2.5	6.2
288/2005	MG,CT	37.0	27.4	28.1	45	2.1	3.0	5.8
320/2005	MG,CT	39.4	28.0	28.2	48	2.0	2.6	6.0
211/2006	MG,CT	31.1	21.8	27.0	53	1.7	2.0	4.0
022 /2007	MG, CT	40.7	27.7	29.6	46	2.3	1.4	5.2
Mean	-	36.5	25.3	27.4	52	1.8	3.0	5.1

* Irrigated crops: Wine grape (WG), table grape (TG) and mango orchard (MG)
* Natural vegetation: Caatinga (CT)

8.3   Analysis of the results

8.3.1   Calibration and validation of SEBAL equations

Satellite measured variables

The atmosphere disturbs the signal reaching the satellite sensor. The satellite registered radiances are, therefore, affected by the atmospheric interaction in the radiative transfer path. Part of R_G is scattered back to the satellite before it reaches the earth surface. A correction is deemed necessary to estimate α_0. Following Menenti et al. (1989), a simplified linear relationship of the following type has been sought for correcting all atmospheric disturbances:

$$\alpha_0 = a\ \alpha_p + b \qquad\qquad (8.10)$$

Combination of field measurements of α_0 with Landsat calculations of α_p resulted in physical meaningful results: a = 0.61 and b = 0.08. The coefficient a is the two-way transmittance through the

atmosphere, leading to an average single pathway atmospheric transmissivity of $a^{0.5} = 0.78$. The latter is a value for clear sky radiation (e.g. Allen et al., 1998). The regression analysis is shown in Figure 8.4a.

Equation 8.10 was applied to all Landsat images for determining the spatial variation of α_0. The Landsat overpass measurements yielded instantaneous values of surface albedo ($\alpha_{0_{inst}}$) that were systematically lower than those for 24 hour ($\alpha_{0_{24}}$). Hence, a second regression equation was necessary to retrieve the daily from instantaneous values (Figure 8.4b). The relationship depicted in Figure 8.4b has been considered in the computations of the 24-hour values of net radiation required for the determination of daily ET_a.
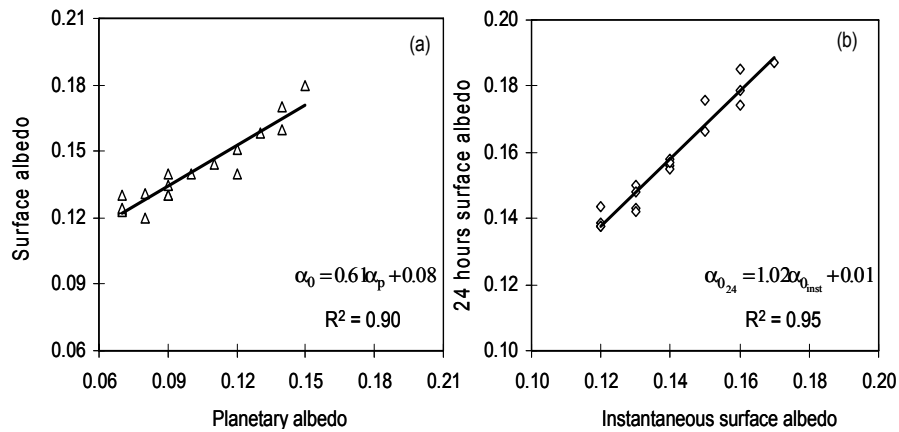
Figure 8.4. Relationship between surface albedo from the field energy balance experiments and their counterparts from satellite overpass measurements: (a) instantaneous values of α_0 and α_p; (b) daily and instantaneous values of α_0.

From field energy balance experiments, the vertical temperature difference (ΔT) between two heights was derived using data of H, air temperature above the canopies, and the aerodynamic resistance - r_a (Smith et al., 1989).

$$\Delta T = \frac{H\ r_a}{\rho_a\ c_p} \tag{8.11}$$

where ρ_a (kg m^{-3}) and c_p (J kg^{-1} K^{-1}) are the air density and air specific heat at constant pressure, respectively.

International experiments have demonstrated that, other than for a thin surface such as bare soil or a short canopy, a difference of several degrees can be observed between radiometric and aerodynamic surface temperature (Troufleu et al, 1997). The latter implies that the radiometric temperature from Landsat is an ill-provision of aerodynamic surface temperature required for solving H. Cleugh and Dunin (1995) compared aerodynamic surface temperatures with canopy radiometric temperatures founding excellent agreement for dense fully-closed wheat. However when this crop is sparse, large differences were observed, especially when LAI was lower than 2. For sparse or composite vegetation, the radiometric surface temperature was found to be much higher than aerodynamic temperature from flux inversion (Kalma and Jupp, 1990).

The thermal radiation measured by satellite sensors thus need to be corrected for both atmosphere emission and the difference between radiometric and aerodynamic surface temperature. To correct these conjugated effects the field results from Equation 8.11 were used to fit a linear relationship between T_0 ($T_0 = T + \Delta T$) and T_{sat}:

$$T_0 = a\,T_{sat} + b \tag{8.12}$$

The coefficients of the Figure 8.5 were applied in Equation 8.12 to all Landsat images to obtain the spatial variation of T_0 to be used in solving H.
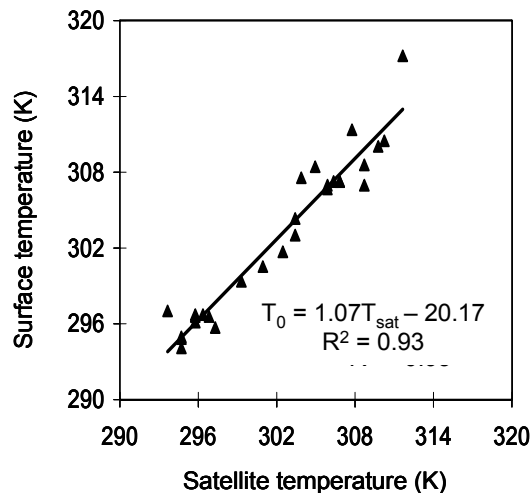

Figure 8.5. Relationship between surface temperature from the field energy balance experiments and their counterparts from satellite overpass measurements.

160

It is realized that a physically based atmospheric correction would include transmittance and reflectance of spectral radiances (e.g. Schmugge et al., 1998), but for practical reasons Equations 8.10 and 8.12 are doable.

Land measured variables

Measured $R_L\downarrow$ over caatinga – in combination with T – allowed the inspection of the apparent emissivity of the atmosphere (ε_a). The SEBAL – based equation described in Chapter 7 (Equation 7.1) was applied for the satellite overpass time. The regression coefficients became a = 0.942 and b = 0.103. The Stefan Boltzman equation was thereafter applied together interpolated values of T from the seven agro-meteorological stations, to all Landsat images to obtain the regional $R_L\downarrow$ (Figure 8.1).

Field values of $R_L\uparrow$ – jointly with estimates of T_0 – gave the opportunity to quantify the thermal infrared emissivity (ε_0). Following van der Griend and Owe (1993), the field values of ε_0 were correlated with NDVI (Figure 8.6):

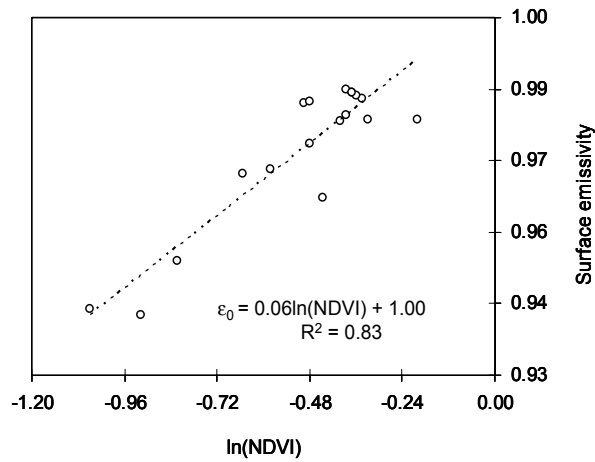$$\varepsilon_0 = a\ \ln NDVI + b \tag{8.13}$$

Figure 8.6. Relationship between broadband surface emissivity of vegetated surfaces and NDVI.

161

The original coefficients are a = 0.047 and b = 1.009, hence slightly different (Bastiaanssen, 1995). The values of ε_0 were used for the estimation of $R_L\uparrow$ in the regional radiation balance (Figure 8.1).

Field values of roughness length for momentum transfer (z_{0m}) in natural vegetation and irrigated crops are described in Chapter 7. To estimate z_{0m} by remote sensing Allen et al (2007a) suggested a simplified expression based on α_0 and NDVI. The inclusion of both satellite indices helps to distinguish between vegetation having different architecture but similar values of NDVI. For example table grape can present the same NDVI values as mango orchard, but at a substantially lower LAI.

The simplified approach below was tested for the mixture of agricultural and natural ecosystems:

$$z_{0m} = \exp\left[\left(a\frac{NDVI}{\alpha_0}\right) + b\right] \tag{8.14}$$

The regression coefficients were a = 0.26 and b = -2.21 (Figure 8.7). The coefficient of determination is rather encouraging ($R^2 = 0.92$) for describing a difficult land surface parameter by some simplified remote sensing variables.
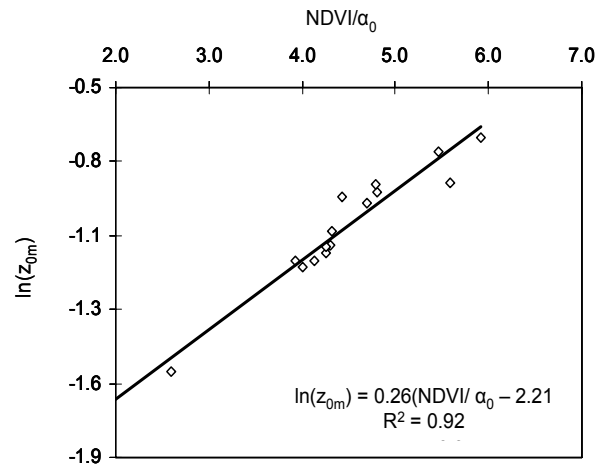

Figure 8.7. Relationship between the roughness length for momentum transport (z_{0m}) and the ratio of the Normalized Difference Vegetation Index (NDVI) to surface albedo (α_0).

162

Equation 8.14 was scaled up and the results used in calculating regional friction velocity (u_*) and then H.

Field measurements of G and R_n were used together with satellite measurements of T_0, α_0, and NDVI to test the following multiple regression equation:

$$\frac{G}{R_n} = T_0\left(a\alpha_0 + b\right)\left(1 - 0.98\text{NDVI}^4\right) \tag{8.15}$$

The results reveal a = -0.11, b = 0.02 to be the best set of locally calibrated coefficients. These coefficients were obtained from the multiplying the regression of G/R_n with α_0, T_0 and NDVI by the factor 0.04 (Figure 8.8).
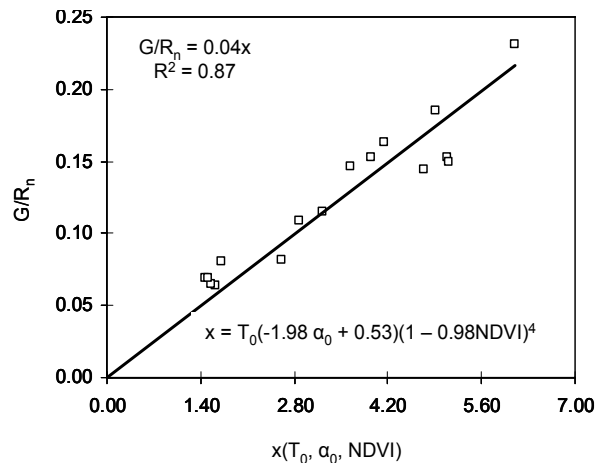

Figure 8.8. Relationship between the ratio of soil heat flux (G) over net radiation (R_n); and surface temperature (T_0), surface albedo (α_0) and the Normalized Difference Vegetation Index (NDVI)

The original coefficients are different with a = 0.0074 and b = 0.0038 for the condition where they were found (Bastiaanssen, 1995). The differences can be explained by the conditions of daily irrigation and bigger LAI of irrigated fruit crops in the Low-Middle São Francisco River basin, Brazil. G is a difficult term to evaluate and care should be taken in its computation by Equation 8.15. The values should be checked against actual measurements on the ground for specific conditions.

The computation of H by SEBAL algorithm requires two "anchor" pixels, referred to as the hot and the cold pixels. In this thesis,

163

the hot and cold pixels were represented by the natural vegetation (caatinga) and irrigated crop (mango orchard), respectively. To compute H from Equation 8.11, the near surface temperature difference (ΔT) for each pixel is given as ($T_1 - T_2$), the temperature difference between two heights (z_1 and z_2). The regionalization of ΔT occurred by assuming a linear relationship with T_0:

$$\Delta T = aT_0 + b \tag{8.16}$$

where a and b are the fitting coefficients.

The generalized annual curves of ET_a/ET_0 for the time of satellite overpass (9:30) of these two contrasting vegetation types have been used to estimate H (and thus ΔT) at these specific locations (Figure 8.9). There were two complete years of flux data in mango orchard and caatinga, however, data of 2005 were used because during the year of 2004 unusual storms occurred. These ET_a/ET_0 curves were applied for other years together the values of ET_0 in the satellite overpass days.
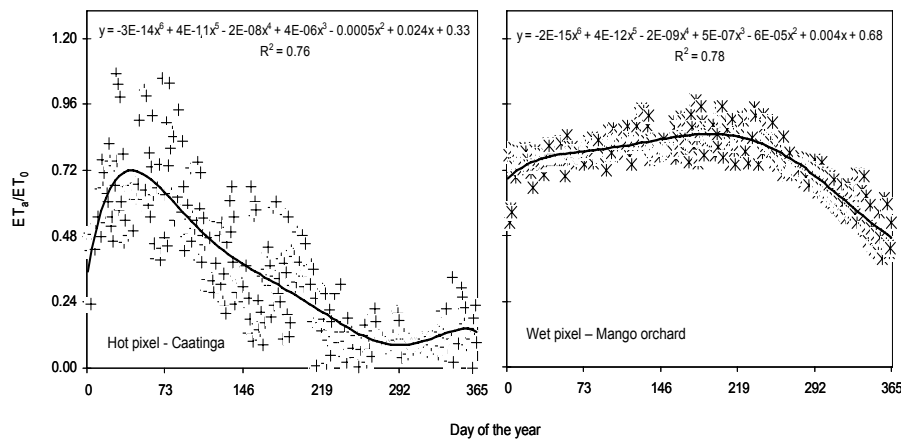

Figure 8.9. Curves of (ET_a/ET_0) for the cold (mango orchard) and hot (caatinga) pixels. Data for 2005 were taken.

Figure 8.9 shows that the λE of natural vegetation (caatinga) is not negligible, but has sometimes an ET_a/ET_0 of 0.20 during the dry period and even more than 0.90 during the rainy period. The advantage of using known land use together with ET_a/ET_0 values is that the assumptions of zero H or λE are not strictly required as originally (Bastiaanssen, 1995), which makes it possible to calculate regional ET_a also during the rainy period.

164

In the cold pixel (irrigated mango orchard) the value of H_{cold} could be approximated as:

$$H_{cold} = R_{n_{cold}} - G_{cold} - \left(\frac{ET_a}{ET_0}\right)_{cold} ET_0 \qquad (8.17)$$

where $\left(\dfrac{ET_a}{ET_0}\right)_{cold}$ is the ratio valid for the mango orchard according to the time of the year (Figure 8.9), $R_{n_{cold}}$ is the net radiation, G_{cold} is the soil heat flux and ET_0 is the reference evapotranspiration at satellite overpass for the place where the flux tower was in the irrigated mango orchard. The energy balance terms were taken from satellite results, while for ET_0 the weather values at the agro-meteorological stations were interpolated.

At the hot pixel, the values of H_{hot} was calculated in the same way using values of $\left(\dfrac{ET_a}{ET_0}\right)_{hot}$ valid for caatinga according to the time of the year (Figure 8.9), net radiation ($R_{n_{hot}}$), soil heat flux (G_{hot}) and reference evapotranspiration (ET_0) for the place where the flux tower was in the natural vegetation:

$$H_{hot} = R_{n_{hot}} - G_{hot} - \left(\frac{ET_a}{ET_0}\right)_{hot} ET_0 \qquad (8.18)$$

The values of H_{cold} and H_{hot} were used to infer ΔT applying Equation 8.11 in an iterative process starting with neutral conditions till stabilization of ΔT at the cold and the hot pixels after successive atmospheric stability corrections for r_a. The calculations of the regression coefficients of ΔT versus T_0 (Equation 8.16) were done in a spreadsheet and were variable for each Landsat image acquisition day. The a and b values based on degrees Kelvin varied from 0.543 to 1.156 and from -160.8 to -348.2, respectively, found for the images of January (lowest a and highest b) and November (highest a and lowest b), representing the wettest and the warmest months of the year, respectively. Equation 8.16 and the image date specific regression coefficients were applied to all Landsat images for acquirement of H.

The SEBAL procedure has been applied to all 10 different Landsat images using the calibrated relationships. The energy balance results were validated with field measurements. Figure 8.10 shows scatter plots for instantaneous satellite and field measurements for R_n; for λE; for H; and for G involving all vegetation types studied.

The results showed excellent agreements on R_n and λE. The coefficient of determination for R_n was $R^2 = 0.94$, with a root mean square error (RMSE) of 17.5 W m^{-2} and an average deviation of 1%. The results for λE were $R^2 = 0.93$, average deviation of 10 % and a RMSE of 33.8 W m^{-2}. The differences occurred typically for the higher values of λE. The latter was a result of the bias that was observed at the lower end H-values.
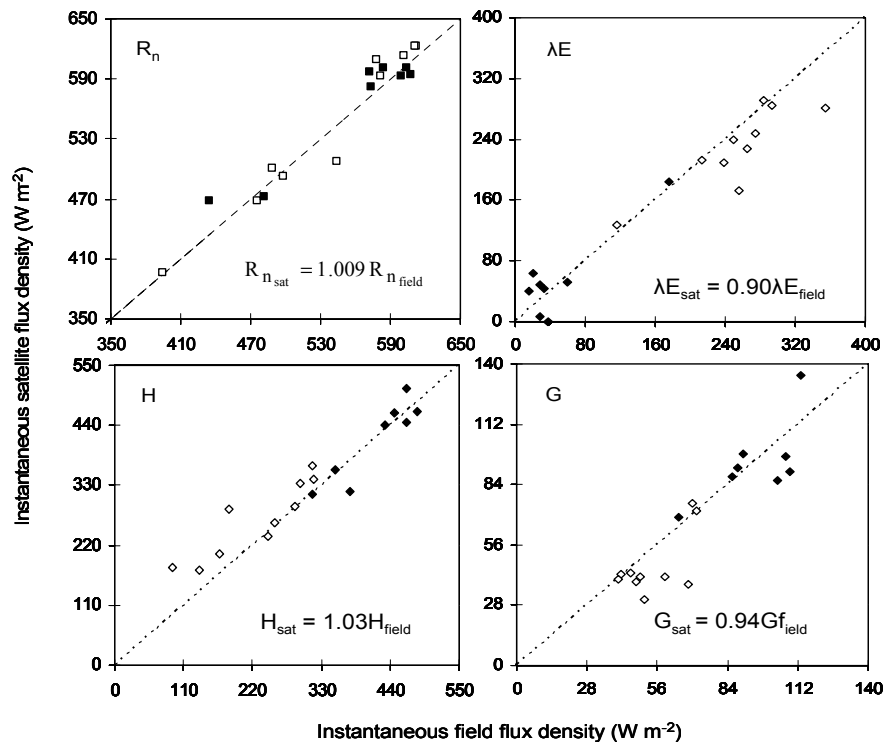

Figure 8.10. Relationship between instantaneous energy balance components obtained from SEBAL (subscript sat) and from field energy balance measurements (subscript field): R_n - net radiation; λE - latent heat flux; H - sensible heat flux; and G - soil heat flux. The black and white symbols represent natural vegetation and irrigated crops, respectively

166

Good agreements were achieved for H and G. For H, the R^2 was of 0.83. Part of the deviations could be attributed to the estimations of z_{0m}. The RMSE was of 41.8 W m^{-2}, with an average deviation 3%. Deviations were higher in the lower end of H values – thus centered on the irrigated pixels. For G, the local calibration yielded a R^2 of 0.81, with the RMSE of 13.3 W m^{-2} and an average deviation 6% occurring typically at the lower end of G values.

As instantaneous values of actual evapotranspiration are not interesting for water managers, the daily 24 hours values were computed as well. A straightforward regression equation was applied to the Brazilian data set to scale the instantaneous ET_a retrieving daily values according to:

$$ET_{a_{24}} = bE_{F_{isnt}} R_{n_{24}}$$ (8.19)

where $ET_{a_{24}}$ and $R_{n_{24}}$ are the actual evapotranspiration and the net radiation for 24 hours and b is a correction coefficient, which was found to be 1.18 (Figure 8.11a). The $E_{F_{inst}}$ represents the instantaneous values of evaporative fraction at satellite overpass. The net radiation for 24 hours was calculated with albedo values ($\alpha_{0_{24}}$), global solar radiation ($R_{G_{24}}$) and atmospheric transmissivity ($\tau_{sw_{24}}$) for this time scale, applying the Equation 7.3, with the regression coefficient a as function of T (Figure 7.5). Interpolated values of T were used to scale up $R_{n_{24}}$.

The evaporative fractions for instantaneous and daily time scales were calculated by the following equation:

$$EF_{inst,24} = \frac{\lambda E_{inst,24}}{R_{n_{inst,24}} - G_{inst,24}}$$ (8.20)

where the subscripts inst and 24 meaning instantaneous and daily fluxes, respectively. G_{24} is very small and was considered zero.

After the application of the coefficient 1.18 in Equation 8.19, the relation between the satellite and field measurements of daily ET_a presented then a better R^2 and a RMSE of 0.38 mm d^{-1} with a very small deviation of 1% (Figure 8.11b).
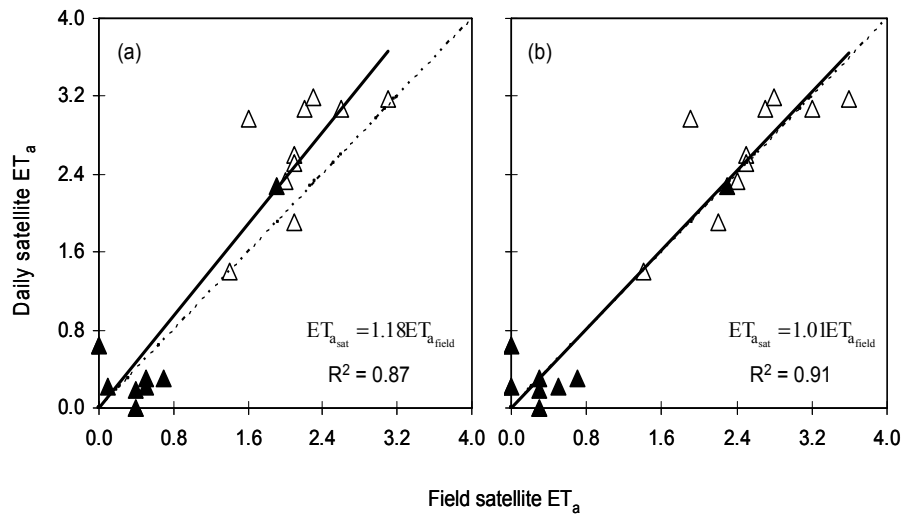
Figure 8.11 Relationships between daily actual evapotranspiration obtained from SEBAL and field measurements ($ET_{a_{sat}}$ and $ET_{a_{field}}$): (a) considering E_F similar for instantaneous and daily scales and (b) applying the correction factor for E_F. The black and white symbols are for natural vegetation and for irrigated crops, respectively.

According to Bastiaanssen et al. (2008), the SEBAL model has been validated in grapes, peaches and almonds from Spain, Turkey and California. These validations revealed that accumulated values of ET_a predicted by the model are within several percent from the measured values. Considering that the field measurements have their own sources of errors, the accuracy of the present study is very satisfactory. The results of regional ET_a and PAR were then scaled up and used for biomass production and crop water productivity analyses in semi arid region of the Low-Middle São Francisco River basin and discussed in the next sections.

8.3.2 Applications of calibrated SEBAL

Regional energy Partition

The 24 hours energy partition was expressed by Equation 8.20 taking G_{24} zero for this time scale. The EF_{24} for three different periods of the year (before, just after, and during the rainy season) are presented in Figure 8.12.
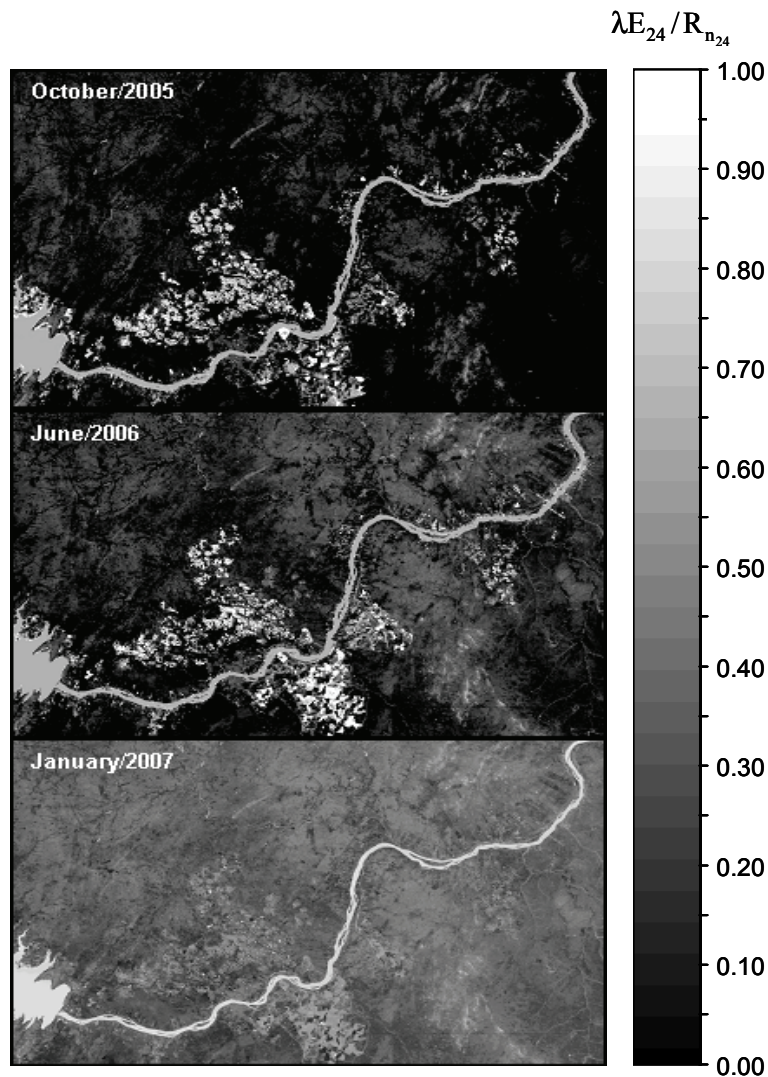
Figure 8.12. Daily energy partition ($E_{F24} = \lambda E_{24} / R_{n_{24}}$): for the dry season in October of 2005; for the end of the rainy season in June of 2006 and for the rainy season in January of 2007 .

The natural vegetation (caatinga) converted large portions of the available energy into sensible heat flux (H), causing values of $H_{24} / R_{n_{24}}$ higher than 0.90 during the driest period of the year (October/2005), while the irrigated agricultural fields presented high values of $\lambda E_{24} / R_{n_{24}}$. In general, irrigation intervals were small during this period (daily irrigation), and the water supply was rather uniform

169

reducing heat losses to the atmosphere. As a consequence, values of $E_{F_{24}}$ for irrigated crops were near 1.00, while for caatinga this indicator varied from 0.00 to 0.20.

$E_{F_{24}}$ had intermediate values just after the rainy season , because antecedent precipitation during January to April provided sufficient water storage in the caatinga root zone still keeping this natural ecosystem wet and green, despite the quick rise of the atmospheric demand (June/2006). During this period $E_{F_{24}}$ in natural vegetation reached to 0.35, while irrigated crops presented values about 0.80.

During the rainy season, the evapotranspiration rates from caatinga were – in some cases – similar to those from irrigated areas. A high portion of the daily available energy in natural vegetation was converted into λE_{24} (January/2007), making the values of $E_{F_{24}}$ around 0.50 for both kind of vegetation as the most of the farmers stopped irrigation during this period and rainfall kept the soil wet for all ecosystems.

Bastiaanssen (2000) found similar $E_{F_{24}}$ values for irrigated cotton and perennial vegetation (vineyards and orchards) varying from 0.40, when the crops started to be irrigated to 0.70-0.90 during the irrigation season in Gediz basin (Turkey). Li et al. (2006) reported that for a grazing steppe in central Mongolia, seasonal values of $E_{F_{24}}$ followed the variation in leaf areas and rainfall events during the dry-wet cycles, similar with the results for caatinga. Farah et al. (2004) showed $E_{F_{24}}$ values of 0.70 during the wet season and 0.10 during the dry season, for a tropical watershed in the Kenyan Rift Valley with natural meadows. The magnitudes of the energy partitioning in the actual study were thus plausible.

Regional actual evapotranspiration

Figure 8.13 presents the histograms for daily ET_a values in the semi-arid region of the Low-middle São Francisco basin. The averaged values for 10 individual days in different years and seasons are shown.
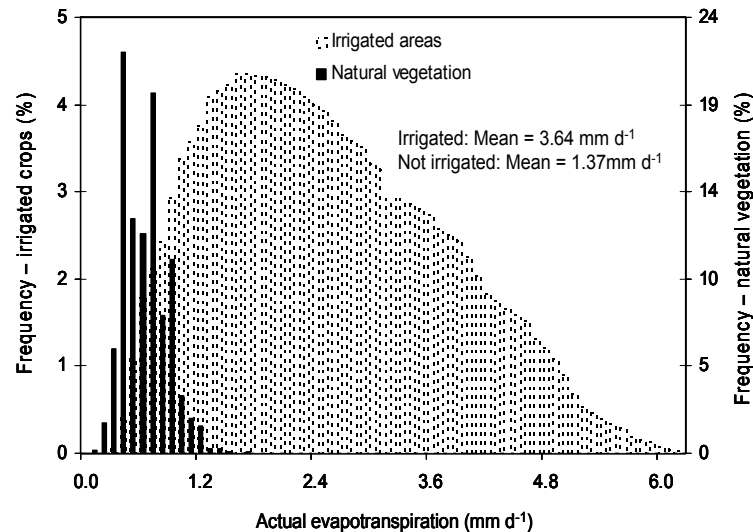
Figure 8.13. Histograms of daily ET_a for irrigated and not-irrigated areas averaged according to the 10 Landsat TM images acquired during different moments of the growing seasons and across different years.

The Landsat pixels were divided in classes of irrigated and natural vegetation lands to highlight the incremental evapotranspiration due to irrigation by using a simplified multi-spectral classification. The effect of soil moisture was strong during the dry season. Pixels with ET_a lower than 1.0 mm d^{-1} occurred frequently under drier conditions. These pixels represent natural vegetation (caatinga). The distribution of ET_a in caatinga was more skewed and tended towards the lowest values. Values of 1.0 to 5.0 mm d^{-1} coincided with irrigated crops, with higher values for table grapes. While the average value for all irrigated areas was 3.6 mm d^{-1}, natural vegetation had a mean value of 1.4 mm d^{-1}. Irrigated crops thus evaporated around 2.2 mm more than caatinga.

Landsat images for the dry seasons of 2004 and 2005 (October and November) were integrated with those representing the wet seasons of 2006 (June) and 2007 (January) to derive annual ET_a values. The regression equations of ET_a/ET_0 between field data of 2004 and 2005 and satellite values involving the period 2001 - 2007 and the same DOY (Day of the year) for irrigated mango orchard and natural vegetation were applied to calibrate the images of 2006 and 2007 (Figure 8.14).
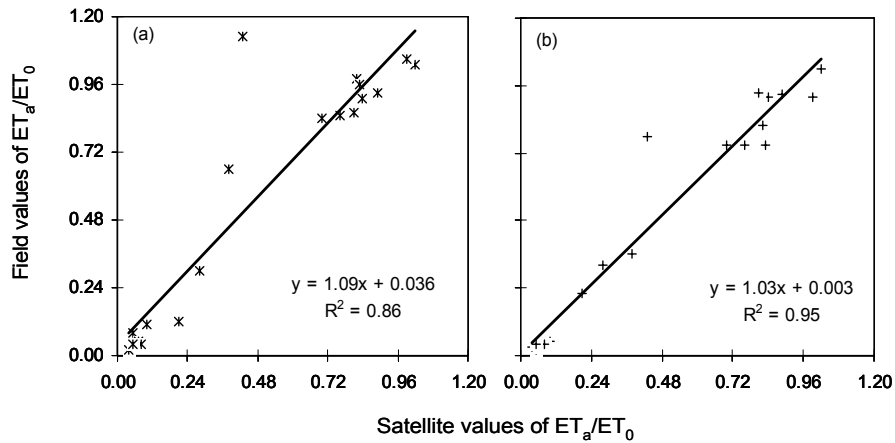
171

Figure 8.14. Relationship between the field and satellite values of ET_a/ET_0 for irrigated mango orchard and natural vegetation. Values from images involving the period 2001 - 2007 were compared with field data for 2004 (a) and 2005 (b) with the same DOY (Day of the year).

After calibration, successive interpolations were performed to retrieve the monthly values of ET_a/ET_0 for 2004 and 2005 and then the annual values. The mean annual values for this ratio of these years were averaged to obtain the average regional annual ET_a by using the grids of ET_0 and Equation 8.4 (Figure 8.15). Although this is a simple method to obtain averaged annual values, it is probably the best possible way to assess time integrated regional scale ET_a at high resolution for different land use classes in Low-Middle São Francisco River basin.

The highest accumulated regional ET_a values were found for table grapes, being around 800 to 1300 mm yr^{-1}. Mango orchards had lower values than vineyards, ranging from 600 to 1100 mm yr^{-1} while in caatinga they were between 200 and 600 mm yr^{-1}. The annual values for natural vegetation were close to the amounts of annual rainfall.
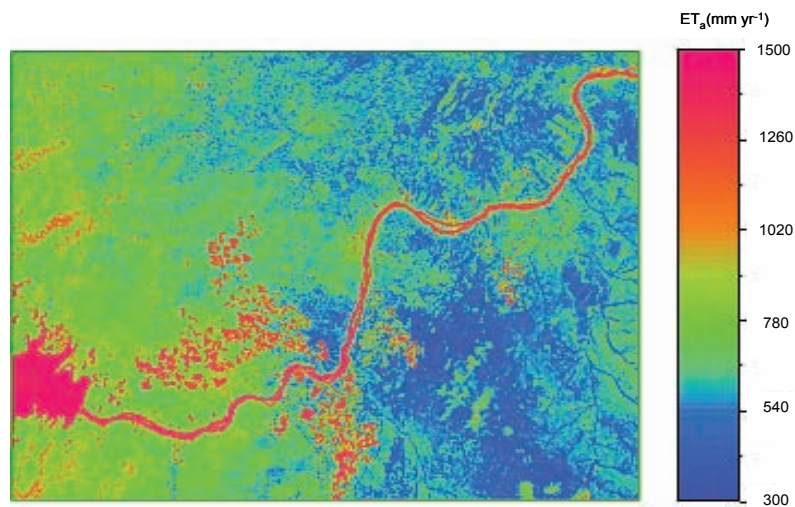
172

Figure 8.15. Averaged total annual ET_a for the region comprised by the net of agro-meteorological stations in Low-Middle São Francisco River basin. Field values of ET_a and ET_0 for 2004 and 2005 were used for calibration of satellite counterparts.

The total rainfall in 2004 in caatinga site was with 720 mm above the long term value of 570 mm yr^{-1}. The year 2004 was thus exceptionally wet. 2005 was a dry year with 337 mm of rainfall. The average conditions of these two years were considered representative for a long term condition.

Caatinga has the ability of turning into a verdant green ecosystem during the rainy season. By the end of this wet period, natural vegetation showed moderately high values of ET_a/ET_0 (~0.30 - 0.35) due to the ability of the roots in using soil moisture from deeper layers and in conserving this water.

Incremental evapotranspiration

The monthly and annual SEBAL results of ET_a in conjunction with field measurements in irrigated land (mango orchard) and natural vegetation (caatinga) are shown in Table 8.2. The total annual ET_a from satellite measurements for caatinga during 2004 was with 644 mm slightly lower than the measured rainfall (720 mm). The annual ET_a for the year of 2005 in caatinga was much lower (376 mm), but slightly higher than the measured rainfall (337 mm). This confirmed that during

173

dry years, bush lands extract moisture from the soil profile that is stored during preceding wetter years.

The difference between estimations of ET_a based on satellite data and the field measurements for natural vegetation in 2004 was only 4.7%. For the second year in 2005, this difference reduced to 4.1%. The significantly lower ET_a of caatinga during 2005 as compared to 2004 agreed well with the reduction of rainfall. For mango orchard, the differences between SEBAL and field measurements were 0.6% and 0.5% only, for 2004 and 2005, respectively (Table 8.2). The magnitudes of these differences after calibrations are better than earlier validation reports of SEBAL where they pointed that accumulated ET_a values can be estimated with 95% accuracy (Bastiaanssen et al., 2005).

Table 8.2. Monthly actual ET from field and satellite measurements for irrigated crop – mango orchard (MG) and natural vegetation – caatinga (CT), together with monthly rainfall amounts during the years of 2004 and 2005. The field data represent point values. The satellite data are a reflection of thousands of pixels.

Year/Month	MG_Field (mm)	CT_Field (mm)	MG_Satellite (mm)	CT_Satellite (mm)	Rainfall (mm)
2004					
Jan	104.6	100.9	104.0	94.2	397.8
Feb	118.7	131.1	118.6	123.8	187.0
Mar	128.1	130.3	127.7	124.6	61.2
Apr	125.7	104.9	125.9	99.7	13.5
May	107.3	70.8	107.8	68.7	29.7
Jun	97.8	37.7	97.8	36.0	6.1
Jul	102.2	24.3	113.1	26.4	0.8
Aug	114.7	15.0	115.5	14.3	0.5
Sep	141.4	10.9	142.0	10.0	0.8
Oct	140.3	9.8	140.9	9.5	1.5
Nov	130.1	17.2	126.4	15.4	20.3
Dec	125.7	23.2	125.2	20.9	0.5
Year	1437	676	1445	644	720
2005					
Jan	116.2	69.5	116.2	64.6	48.5
Feb	103.2	63.4	103.5	62.4	78.0
Mar	115.2	82.2	114.2	78.4	89.9
Apr	110.7	44.1	110.0	42.4	24.4
May	89.9	32.0	92.8	32.2	2.0
Jun	97.7	28.5	94.7	26.7	31.5
Jul	105.8	30.3	105.0	29.6	2.8
Aug	110.5	7.2	110.3	6.7	1.3
Sep	111.3	3.6	113.2	3.0	0.0
Oct	108.6	6.5	111.8	6.8	0.0
Nov	78.4	6.6	81.6	6.0	26.9
Dec	78.8	18.5	79.1	17.6	31.8
Year	1226	392	1232	376	337

Since caatinga showed an ET_a of 644 mm and mango orchard 1445 mm in 2004, the increment is 801 mm or a factor 2.24. For 2005, this difference between 376 (caatinga) and 1232 mm (mango orchard) is 856 mm, or a factor 3.27. Hence, it can be concluded that irrigated mango orchards evapotranspirate more than double the amount for caatinga in a year and that the incremental ΔET on average is around 828 mm yr^{-1}.

Some summary statistics of land use and ET_a for the Low-Middle São Francisco River basin are given in Table 8.3. The mango orchards and vineyards areas represent 20% and 9% of the total irrigated area respectively, resulting in a total evaporative depletion of 0.36 km^3 yr^{-1}. Because the incremental ΔET for the first crop is 2.2 mm d^{-1} and for vineyards it is 2.5 mm d^{-1}, the additional volume of water used for ET_a in these two main irrigated fruit crops in the sub-basin is around 0.22 km^3 yr^{-1}. For all irrigated crops, the total evaporative depletion increases to 0.75 km^3 yr^{-1} (93,180 ha and ΔET of 2.2 mm d^{-1}). The latter volume represents the net depletion; the difference between diversion and return flow that is truly consumed and not longer available for downstream urban and environmental users.

Table 8.3. Main land cover types, area and averaged daily and annual actual evapotranspiration in Low-Middle São Francisco basin from field and SEBAL measurements.

Surface type	Area (ha)	Area (%)	$ET_{a_{24}}$ (mm d^{-1})	$ET_{a_{year}}$ (km^3 yr^{-1})
Vineyards	8,180	9	3.9[1]	0.12
Mango orchards	18,607	20	3.6[2]	0.24
Irrigated crops	93,180	100	3.6[3]	1.22
Not irrigated	11,505,520	-	1.4[4]	58.79

[1]: source - Teixeira et al. 2007, [2]: source - Table 8.2, [3] and [4]: source - Landsat images of Figure 8.13.

In an earlier study in the Nilo Coelho area (Bastiaanssen et al., 2001), inside the Low-Middle São Francisco River basin, ET_a outside the irrigated areas was 70% of the annual rainfall. The total ET_a for irrigated fruit crops resulted in 0.15 km^3 yr^{-1}, while the rainfall totalized 0.08 km^3 yr^{-1} in these plots. The ET_a due to rainfall was then 0.06 km^3 yr^{-1}. The resulting incremental ET_a (0.09 km^3 yr^{-1}) was 60 % of the amount that is diverted from the Sobradinho reservoir. Applying this percentage to the actual net withdrawal of 0.75 km^3 yr^{-1} the amount diverted from the river

175

was estimated as 1.25 km^3 yr^{-1}. Assuming that around 80% of the losses – i.e. the difference between diversion and ET$_a$ – are recaptured back into the river, the net withdrawal from the river becomes 0.85 km^3 yr^{-1} with a return flow of 0.40 km^3 yr^{-1} and 0.10 km yr^{-1} being seepage to deep aquifers.

Regional water productivity

Irrigated crops in semi-arid Brazil produce large amounts of biomass as a result of the conjugated effects of abundant solar radiation, favourable air temperature and moist soils during the irrigation periods and rainy seasons. The Photosynthetically Active Radiation (PAR) during October and November is very high and this radiation is intercepted by the crop leaves for photosynthesis and dry matter production. The natural vegetation (caatinga) is only green during the rainy periods. The contrast between caatinga and irrigated ecosystems becomes apparent when analyzing the regional distribution of biomass production.

To use Equation 8.8, the values of E$_F$ were calibrated and interpolated in the same was as for ET$_a$/ET$_0$ applying the regression equations of Figure 8.16 to the images of 2006 and 2007.
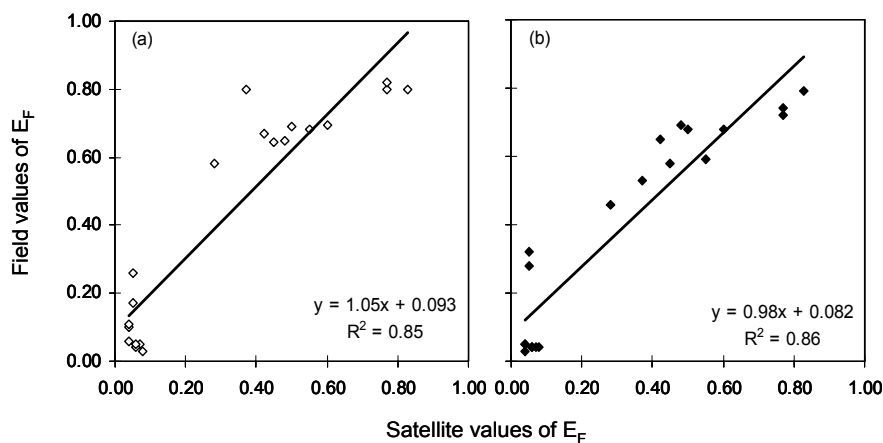

Figure 8.16. Relationship between the field and satellite values of E$_F$ for irrigated mango orchard and natural vegetation. Values from images involving the period from 2001 to 2007 were compared with field data for 2004 (a) and 2005 (b) with the same DOY (Day of the year).

176

To calculate APAR for the same period, NDVI values of the images of 2006 and 2007 were calibrated using the regression equation between this vegetation index and field values of daily surface albedo for 2004 and 2005 for vegetated areas (Figure 8.17).
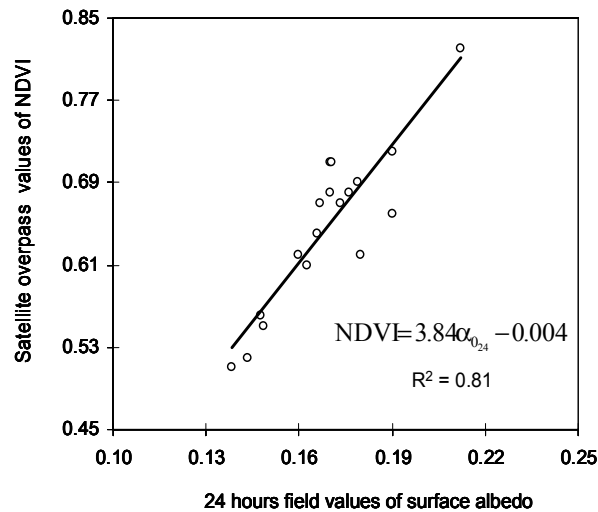

Figure 8.17. Relationship between satellite overpass values of NDVI and 24 hours field values of surface albedo ($\alpha_{0_{24}}$) for irrigated crops and natural vegetation.

After that, the estimated field values of NDVI were correlated with satellite values in the same way as it was for ET_a/ET_0 and E_F (Figure 8.18). The regression equations were applied to the images of 2006 and 2007 for vegetated areas maintaining the NDVI values for areas not vegetated.
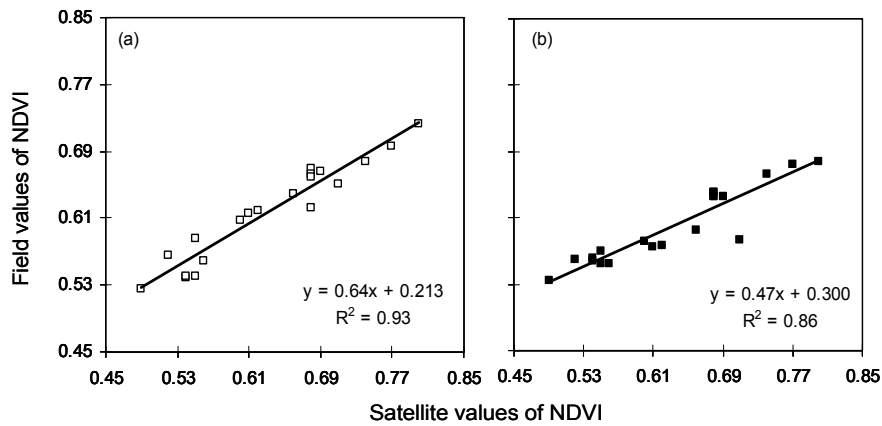
Figure 8.18. Relationship between the field and satellite values of NDVI for irrigated mango orchard and natural vegetation. Values from images involving the period from 2001 to 2007 were compared with field data of 2004 (a) and 2005 (b) with the same DOY (Day of the year).

After the successive interpolations of E_F and APAR, the annual values were used to estimate the total biomass production (BIO_{Year}) by the Equation 8.8 (Figure 8.19). The combination of pixels of 2004 (above long term rainfall) and 2005 (below long term rainfall) gave average conditions.
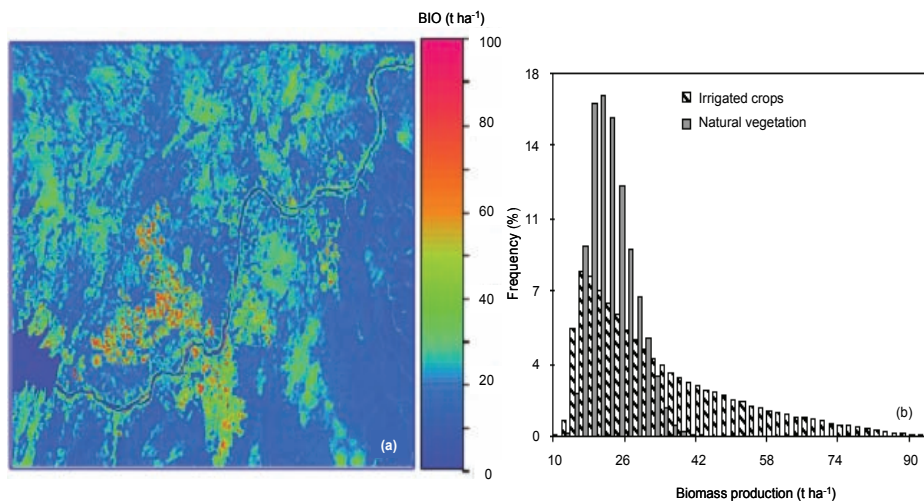

Figure 8.19. Map (a) and histograms (b) of mean annual total biomass production (t ha^{-1}) averaged for 2004 (wet year) and 2005 (dry year) in the Low Middle São Francisco River basin.

178

The most frequent BIO_{year} values for all ecosystems were in the range of 14.0 to 34.0 t ha^{-1}. The highest values were found in irrigated mango orchards (50 - 100 t ha^{-1}) and vineyards (30 - 100 t ha^{-1}). As was for BIO_{year}, to calculate BIO_{GS} the same procedure of calibration and interpolation was done for the growing seasons of wine grapes (2002), table grape (2003) and mango orchard (2003-2005). The regression analyses between field and satellite values of ET_a/ET_0, E_F and NDVI are shown in Figure 8.20. These equations were applied to the images for different years but with the DOY inside the period of the growing seasons.
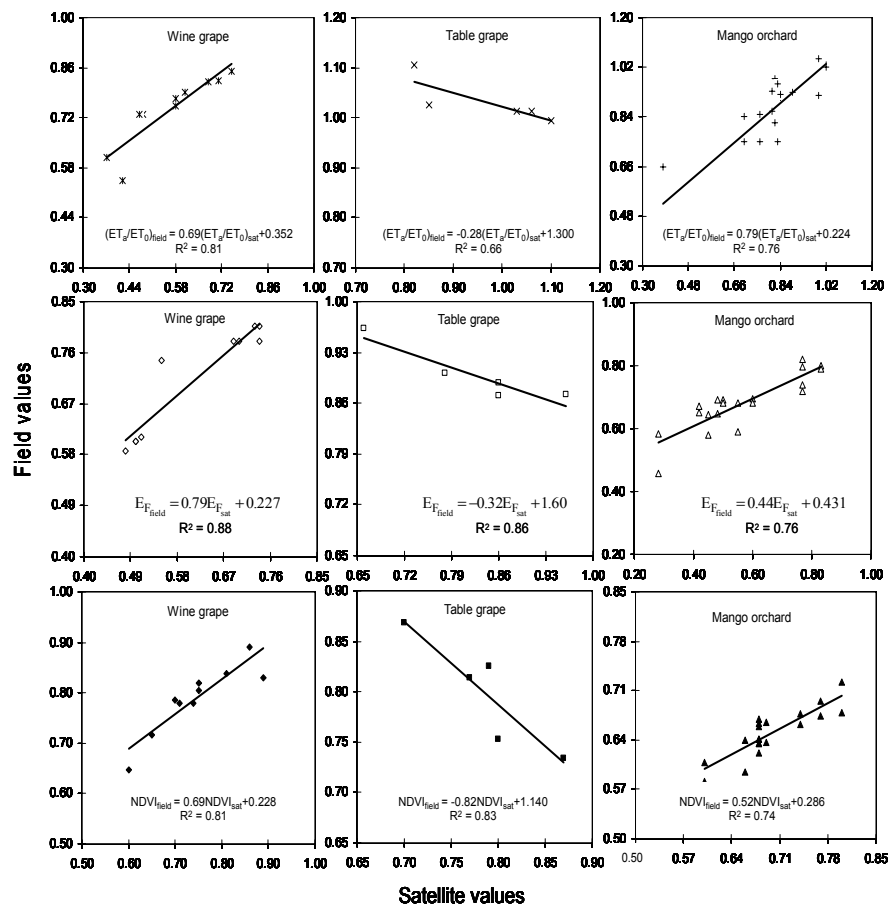

Figure 8.20. Relationship between field and satellite values of ET/ET_0, E_F and NDVI for irrigated crops. Values from images (subscript sat) involving the period from 2001 to 2007 were compared with field data of the growing seasons (subscript field) of wine grape (2002), table grape (2003) and mango orchard (2003-2005) with the same DOY (Day of the year).

179

By combining yield data of wine grape, table grape and mango orchard from farmer measurements and satellite estimates of accumulated biomass production for the growing seasons (BIO_{GS}), the Apparent Harvest Indices (AHI) were obtained (Table 8.4). The AHI describe the ratio of fresh yields to the total produced dry matter.

Table 8.4: Apparent Harvest Indices (AHI) obtained from farmer surveys and SEBAL-based biomass production

Term	Unit	Wine grapes	Table grapes	Mango
Measured yield	kg ha^{-1}	6,183	11,200	44,999
Estimated biomass	kg ha^{-1}	9,815	17,552	54,418
AHI	-	0.63	0.64	0.83

The AHI values were subsequently applied to the three representative commercial farms of wine, grapes and mangos, where the flux towers were. The main reason for the higher values of AHI for mangos is due to the size of the fruits that increases the physical values of production.

Crop Water Productivity

The CWP_{ET_a} maps for wine grapes, as well as the histograms for the two growing seasons (GS1 and GS2) in Vitivinícola Santa Maria farm, are shown in Figure 8.21. The crop water productivity analyses were done in terms of wine.
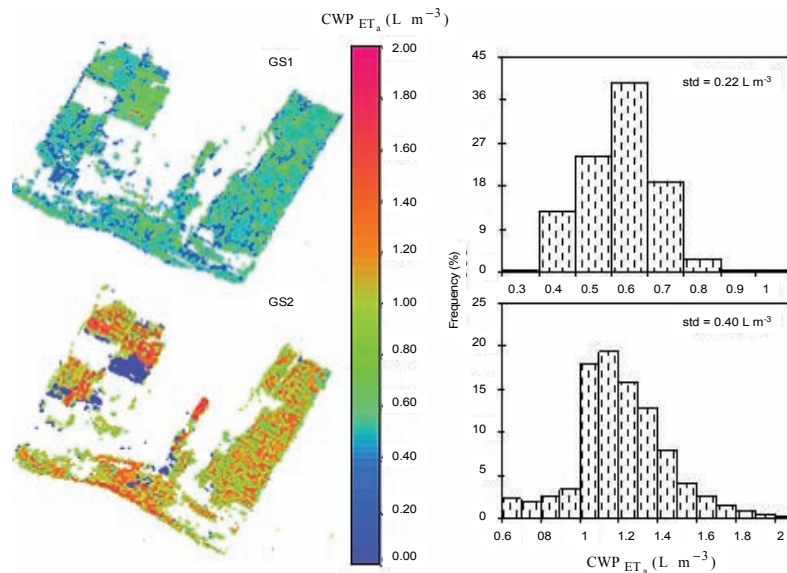
180

Figure 8.21. Crop water productivity based on actual evapotranspiration (CWP_{ET_a}) in Vitivinícola Santa Maria farm for the first (GS1) and second (GS2) growing seasons of wine grapes in 2002, Lagoa Grande-PE, Brazil.

For GS1, irrigated wine grapes presented CWP_{ET_a} values between 0.40 and 0.80 L m^{-3} for 98% of pixels. The average was 0.60 L m^{-3} (i.e. 0.75 kg m^{-3} of water consumed) with a standard deviation (std) of 0.22 L m^{-3}. For GS2, 90% of the pixels were in the range from 0.70 to 1.70 L m^{-3} averaging 1.15 L m^{-3} (i.e. 1.44 kg m^{-3} of water consumed) and a std of 0.40 L m^{-3}. The average Coefficient of Variation (CV) for the two seasons was 36 %. When the crop water productivity was based on actual transpiration $-CWP_{T_a}$ applying the ratios T_a/ET_a for wine grape described in Chapter 5, the averaged values for the two growing seasons became 0.69 and 1.29 L m^{-3} (i.e. 0.86 and 1.61 kg m^{-3}).

The differences in CWP values of bottled wine between GS1 and GS2 could be explained by the bio-physical processes. GS1 was cloudier and the duration of flowering and maturation of fruits stages were shorter than for GS2. The lower std in GS1 could be ascribed to more uniformity with respect to the crop stages than for GS2.

Considering CWP_{ET_a} defined as weight of fruits, Jairmain et al. (2007) found higher values in South Africa (4.70 kg m^{-3}). Walker et al. (2004) reported CWP_{T_a} of wine grapes (Shiraz and Cabernet) in

181

Australia in the range from 2.50 to 3.30 kg m^{-3} under well-watered conditions, and from 2.00 to 5.10 kg m^{-3} under mild water deficit.

Considering the average price of 0.91 US$ L^{-1} for the Shiraz wine in 2002 and in the study region, the corresponding monetary values of crop water productivity based on actual evapotranspiration (CWP$\$_{ET_a}$) ranged from 0.36 to 1.55 US$ m^{-3}. It could be concluded that the values of CWP in the actual study for wine grapes are relatively low compared to those found in literature, showing the scope for improvement.

The CWP$_{ET_a}$ map for table grapes together with the histogram for the second growing season (GS2) in Vale das Uvas farm is shown in Figure 8.22.
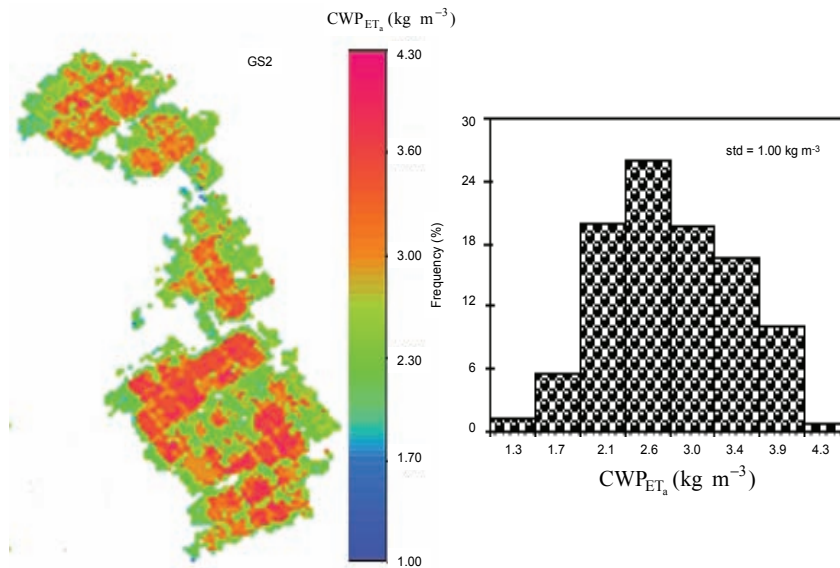

Figure 8.22. Crop water productivity based on actual evapotranspiration (CWP$_{ET_a}$) in Vale das Uvas farm for the second growing season (GS2) of seedless table grapes in 2003, Petrolina-PE, Brazil.

For table grapes, 99% of the values were between 1.70 and 4.00 kg m^{-3}, averaging 2.80 kg m^{-3} with a std of 1.00 kg m^{-3}. The CV was also high (36 %) as in the case of wine grapes, what showed relatively large spatial variations for both vineyards. When the crop water productivity was based on actual transpiration by using the ratios T_a/ET_a for table grape described in Chapter 5, the CWP$_{T_a}$ values were in the

range from 2.04 to 5.17 kg m^{-3}. These results reflected the message that more uniformity on CWP in vineyards is desirable.

The physical values of CWP for table grapes in the current study were lower than those found in Australia under drip (Yunusa et al., 1997a) and furrow irrigation (Yunusa et al., 1997b). In this last country, CWP$_{ET_a}$ of drip irrigated table grapes were 8.60 kg m^{-3} for grafted and 4.30 kg m^{-3} for own-rooted vineyards, while CWP$_{T_a}$ were 16.50 and 11.50 kg m^{-3}, respectively. In the furrow irrigated grapes, CWP resulted in 1.33 and 4.05 kg m^{-3} when based on ET$_a$ for two different growing seasons, respectively, corresponding to CWP$_{T_a}$ of 8.40 and 21.11 kg m^{-3}. Klaasse et al. (2007) and Jairmain et al. (2007) reported a mean value CWP$_{ET_a}$ of 3.70 kg m^{-3} for table grapes in South Africa.

The lower Brazilian values of vineyards CWP are related to the lower yields associated with higher daily water consumptions. In Chapter 5 it was discussed that although the CWP$_{ET_a}$ and CWP$_{T_a}$ values for one growing season in Low-Middle São Francisco River basin are lower than in regions where the climate is temperate, the total production of 2.5 growing seasons compensate these differences and for one year the total yield is in good agreement with South Africa and Australia (but the total water consumption for the growing seasons in these last countries is substantially higher). One of the reasons for significant non-uniformity in vineyards is the presence of multiple varieties with different crop stages and cultural management practices. Nevertheless, the variations are high when compared with for instance wheat (Zwart and Bastiaanssen, 2007) that have a CV of typically 14 % (ranging 5 to 30%).

As the growing season of seedless table grape (3 months) is shorter than that for wine grape (4 months) in Low-Middle São Francisco River basin; the seasonal ET$_a$ for wine grapes was higher, contributing to a lower CWP values among other factors. However, the difference between CWP$_{ET_a}$ and CWP$_{T_a}$ was higher for micro sprinkler irrigated table grapes than for the drip irrigated wine grapes, showing the better performance of the drip irrigation system. With the price of seedless grapes being 2.20 US\$ kg^{-1} in 2003, CWP\$$_{ET_a}$ ranged from 3.74 to 8.80 US\$ m^{-3}, providing more economic gross value of production than for wine grapes.

The results of the crop water productivity analyses for mangos in Fruitfort farm are shown in Figure 8.23. The bulk of the CWP$_{ET_a}$ values

were found between 2.20 and 3.80 kg m^{-3} in GS1 (95% of the pixels). The average value was 2.80 kg m^{-3} with a std of 0.88 kg m^{-3} (CV = 31%). For GS2, 97 % of the pixels were in the range between 3.40 to 5.00 kg.m^{-3} averaging 4.00 kg m^{-3} with a std of 0.62 kg m^{-3} (CV = 16%). The seasonal averaged CV was lower than in the case of vineyards, showing more uniformity for Fruitfort farm. Considering the T_a/ET_a relationships for the two growing seasons described in Chapter 6, and applying these ratios to the entire farm, CWP_{T_a} became 2.82 to 4.86 kg m^{-3} for GS1 and 5.08 and 7.47 kg m^{-3} for GS2.

The main reason for the lower values of CWP found for GS1 could be ascribed to irrigation management during the rainy period. The farmer stopped irrigation for a too long time following rain showers, causing some water stress. Considering the mango price of 1.02 US$ kg^{-1} in 2005 and in the study region, the correspondent monetary values based on actual evapotranspiration ($CWP\$_{ET_a}$) varied between 2.24 to 5.10 US$ m^{-3}.
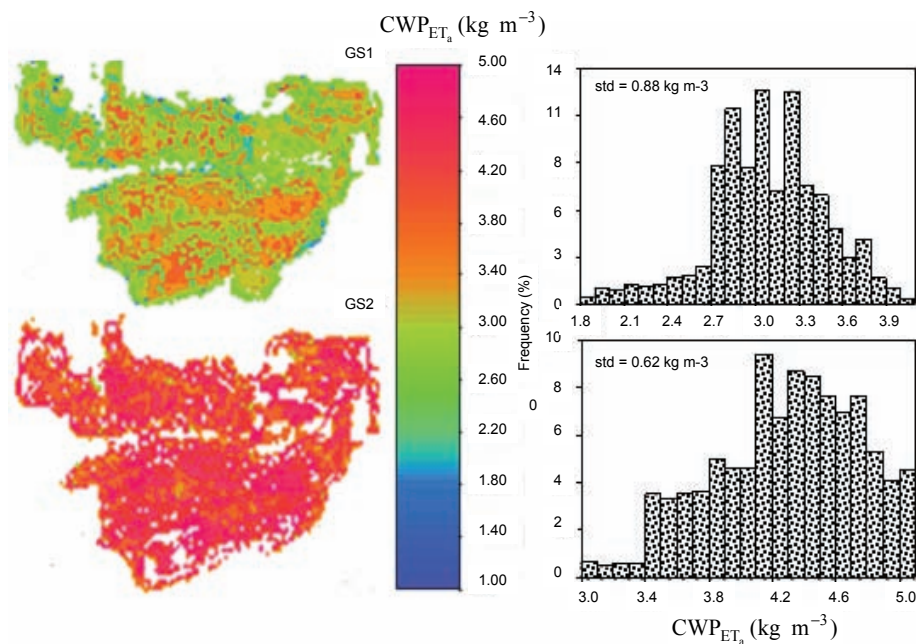

Figure 8.23. Crop water productivity based on actual evapotranspiration (CWP_{ET_a}) in the Fruitfort farm for the first (GS1) and second (GS2) growing seasons of mango orchard from 2003 to 2005, Petrolina-PE, Brazil.

The averaged crop water productivity variables for vineyards (wine and table grapes together) and mango orchard in 2005 involving all producer farms in Petrolina-PE are summarized in Table 8.5.

Table 8.5: Annual total crop water productivity parameters for vineyards and mango orchards: harvested area (HA); yield; crop water productivity per cultivated land (CWP_L); gross return (GR) and crop water productivity per actual evapotranspiration (CWP_{ET_a} – physical value; $CWP\$_{ET_a}$ – monetary value) in Petrolina-PE, Brazil.

Irrigated crop	HA (ha)	Yield (t)	CWP_L (kg ha^{-1})	GR (US $)	CWP_{ET_a} (kg m^{-3})	$CWP\$_{ET_a}$ (US$ m^{-3})
Vineyards	3,200	108,800	34,000	126,883	2.16	8.08
Mango orchards	6,300	126,000	20,000	28,867	1.27	1.84

The values of CWP_{ET_a} for table grapes and mangos in Vale das Uvas and Fruitfort farms, respectively, indicated a good performance, mainly in the case of the last farm. The lower economic value for table grapes in 2003 in relation to Table 8.5 is due the increase in price in 2005 (3.04 US$ kg^{-1}). At a favourable market price, the gross margin of production for table grapes is order of magnitude higher than for wine grape.

Economic water productivities from 2.50 to 7.50 US$ m^{-3} per unit of water depleted in table grapes and mango orchard are much higher than for irrigated annual crops. Sakthivadivel et al. (1999) reported typical values for arable crops to be 0.10 to 0.20 US$ m^{-3}. Further to that, orchards have intensive cultivation practices such as pruning and hand-picking, besides chemical protection and weed control. While large scale arable crops such as wheat, maize, potatoes, soybean and cotton can be intensively mechanized, fruit cultivation require more labour.

8.4   Conclusions

Field energy balances in natural vegetation and irrigated crops have been used to calibrate the SEBAL algorithm. The satellite images covered the semi arid region of the Low-Middle São Francisco River basin, Northeastern Brazil, from 2001 to 2007. The ground data consisted of radiation and energy balances from four field experiments and seven agro-meteorological stations. It is one of the first datasets that could be

used to validate individual steps of SEBAL since the development of the model.

The coefficients of determination were for: surface albedo ($R^2 = 0.90$), daytime integration surface albedo ($R^2 = 0.95$), surface temperature ($R^2 = 0.93$), apparent emissivity of the atmosphere ($R^2 = 0.75$), surface emissivity ($R^2 = 0.83$), instantaneous net radiation ($R^2 = 0.94$), integration of net radiation ($R^2 = 0.80$), surface roughness for momentum transport ($R^2 = 0.92$), soil heat flux/net radiation fraction ($R^2 = 0.87$), instantaneous soil heat flux ($R^2 = 0.80$), instantaneous sensible heat flux ($R^2 = 0.83$), integration of evaporative fraction ($R^2 = 0.91$), instantaneous latent heat flux ($R^2 = 0.93$), integration of actual evapotranspiration ($R^2 = 0.91$) and photosynthetically active radiation ($R^2 = 0.99$). The apparent emissivity of the atmospheric is one of the most problematic parameter, and this has been known for some time.

The direct comparison between field measured latent heat flux and the application of calibrated equations in the SEBAL algorithm to estimate actual evapotranspiration revealed that it is essential to distinguish between instantaneous and daily time scales. For instantaneous values it is required to apply the hot and cold pixel calibration for every individual image. For daily scale, the values of the instantaneous evaporative fraction need to be adjusted.

It is useful to use curves of the ratio of actual to reference evapotranspiration instead the average values of the pixel with the lowest and highest surface temperatures in the calibration processes as this ratio change along the year.

Using satellite images it was showed that the differences between SEBAL calculations and field measurements of monthly actual evapotranspiration was less than 1 % and 5% for irrigated mango orchard and caatinga ecosystems, respectively, being lower than reported in international SEBAL studies as a consequence of the local calibration processes. These accuracies are sufficient for further studies on the effect of land use changes on downstream river flow in the entire semi-arid region of the São Francisco River basin.

The satellite based annual actual evapotranspiration for natural vegetation is around 500 mm much lower than for mango orchards (1329 mm).Total withdrawal from river is estimated to be 1.25 km^3 yr^{-1}, total ET$_a$ from irrigated land 1.22 km^3 yr^{-1}, incremental ET$_a$ due to withdrawals 0.75 km^3 yr^{-1}, return flow 0.40 km^3 yr^{-1}, seepage to deep aquifers of 0.10 km yr^{-1} and hence a net depletion of 0.85 km^3 yr^{-1}.

The total grape production appeared to be lower than the average yield in other grape regions in the world. However, the annual production per hectare is comparable due to the multiple (2.5) growing seasons. The bio-physical Crop Water Productivities based on evapotranspiration (CWP_{ET_a}) in wine and table grapes averages 0.80 L m^3 and 2.80 kg m^{-3}, respectively, while for mango orchard it was 3.40 kg m^{-3}.

The analyses of economic water productivities in vineyards and mango orchards indicated that irrigated fruit crops have till 20 times more value per unit water consumed than irrigated annual crops. Table grapes rank the best (from 3.74 to 8.80 US\$ m^{-3}), followed by mangos (from 2.24 to 5.10 \$ m^{-3}) and wine grapes (from 0.36 to 1.55 \$ m^{-3}). The agricultural water usage in the fruit farms is thus highly productive, and it creates a considerable amount of jobs. Indeed, the towns of Petrolina-PE and Juazeiro-BA, in Low-middle São Francisco river basin, have increased in terms of exports and job creation, and this is a good example of converting marginal savannah land into a booming rural development; however the irrigation management requires full attention as significant percolation have adversely affected environments in terms of rising water tables and return flow of polluted water to the river, being necessary to promote more efficient water use, water-resources management, and planning for the expansion of irrigated areas.

9. Summary and conclusions

9.1 Summary

Problem statement

The São Francisco River basin is a vast and complex system encompassing several Brazilian states. The basin is marked by socio-economic disparities. Wealthy areas with high population densities coexist alongside areas with severe poverty and low population densities. The cities Petrolina and Juazeiro, situated in semi-arid region of the Pernambuco (PE) and the Bahia (BA) states, respectively, are prosperous due to the introduction of irrigated horticulture. Water withdrawals for irrigation can – however – introduce water stress in downstream areas. Rising conflicts are expected as populations expand, economies grow, and the competition for water resources intensifies. There is also a concern about the adverse environmental effects of agriculture. Water quality can be affected by the leaching of nutrients and pesticides from agro-ecosystems, leading to declining biodiversity.

Basin-level dialogues involving water basin agencies, water user associations and local communities will be required. The success of any dialogue will depend on the knowledge base and the general trust in data sources. The incremental evapotranspiration due to the conversion of natural ecosystems to irrigated crops needs to be well understood for appraising the net withdrawals and impact on downstream water users. Remote sensing measurements together with agro-meteorological data can be used to determine the water consumption from a field or a region. A better knowledge on the spatial variation of actual evapotranspiration (ET_a), actual crop yield (Y_a) and water productivity (WP) in irrigated horticulture provides valuable information for achieving local water conservation practices without loosing good productivity levels of irrigated crops.

The main objective of this study in Low-Middle São Francisco River basin is to investigate the accuracy of parameterizations for actual evapotranspiration and biomass production. The second objective is to determine parameters associated with energy and water transfer from irrigated crops and natural vegetation that are useful for water resources management. The third objective is to assess the crop water productivity parameters in irrigated vineyards and mango orchards.

Background on evapotranspiration and water productivity

Based on field and satellite measurements, the theoretical frameworks to calculate ET_a, Y_a and WP were discussed in Chapter 2. The ET_a at field scale can be estimated from energy balance methods. The crop coefficients (K_c) for irrigated crops can be derived from the ratio of potential evapotranspiration (ET_p) to reference evapotranspiration (ET_0). The unstressed crop coefficient K_c describes evaporation difference between a given crop and the reference grass field, under conditions of unlimited water supply.

A first estimation of ET_a would be the application of the crop coefficient approach suggested by FAO (Allen et al., 1998) multiplying ET_0 by K_c and by K_s. This last coefficient is the water stress coefficient. With the availability of the evaporation resistances, ET_a can also be derived from agro-meteorological data by means of Penman-Monteith equation

The SEBAL algorithm is a good tool to be used together with a network of agro-meteorological stations for retrieving ET_a at regional scale. Crop yield for the growing seasons (Y_{GS}) can be measured in the fields and used together with biomass production (BIO) from remote sensing measurements to calculate the apparent harvest index (AHI) that is applicable to the farm levels. Crop water productivities (CWP) at basin scale are derived with AHI available and satellite determinations of BIO and ET_a.

Global overview of grape and mango water productivities

In Chapter 3 the overall situation from the perspective of area, production statistics and water productivity of these fruit crops were described. It was demonstrated that Europe (Italy and France) is the leading wine producing continent, followed by America and Asia, Africa and Oceania. The worldwide production of table grapes is also led by Italy and France. In Brazil, the semi-arid region of the São Francisco River basin is highlighted by both wine and table grape production mainly in the cities of Petrolina (Pernambuco state) and Juazeiro (Bahia state). The trend of table grape and wine production in Brazil showed that the increment is evident being important to conduct the researches on vineyard water productivity described in this thesis.

It was shown that India is the leading mango producing country. Brazilian mangos are nowadays responsible for 2.5 % of the world

mango production, and it is the second largest producing country in the Americas. The trend of mango production in Brazil from evidenced the continuous increment what also shows the importance in conducting the researches on mango water productivity described in this thesis.

Study area and measurements

The Low-Middle São Francisco River basin was selected as study area. Daily and seasonal water and energy balances were measured in situ. A network of seven agro-meteorological stations was used for the sake of regionalization. Interpolated weather data from these agro-meteorological stations were used to assist the calculations of the surface energy balance terms and the regional ET_0. The field experiments were described in Chapter 4.

The Bowen ratio surface energy balance method (BR) was used to measure the partition of net available energy into sensible (H) and latent (λE) heat fluxes in vineyards. In mango orchard both eddy correlation (EC) and BR methods were used for the partition of the heat fluxes, however only EC measurements were used for water productivity purposes. In natural vegetation another EC system was used for determination of H and λE.

For regional analyses the remote sensing algorithm SEBAL was calibrated and validated with experimental data in irrigated crops and natural vegetation. Satellite-based computations of the radiation and energy balance components were performed with nine Landsat Thematic Mapper (TM) and one Enhanced Thematic Mapper (ETM+) cloud free satellite images (path/row 217/66). The Landsat data set has also been described in Chapter 4.

Crop water parameters of vineyards and mango orchard

Chapters 5 and 6 describe the crop water variables of wine grape, table grape and mango orchard. The partitioning of available energy the available energy into λE in all irrigated fruit indicated systematic over-irrigation that induced a continuous percolation.

Micro-sprinklers in table grape site increased the moisture content in soil and lower atmosphere, which turns the fraction of non-beneficial ET_a to 18%, comparing to 10% in drip system of wine grape site. In this last vineyard, the differences in yield of bottled wine between the first (3,376 L ha^{-1}) and the second growing seasons (6,514 L ha^{-1}) pinpoint

seasonal effects. Whereas the first growing season yielded an average economical water productivity of 0.70 US$ m^{-3} based on ET_a, the average value for the second growing season increased to 1.15 US$ m^{-3}. Only one growing season of table grape was analyzed for water productivity purposes, with an yield of 11,200 kg ha^{-1}. The economic water productivity performance for table grape was 6.51 US$ m^{-3} based on ET_a.

The micro sprinkler irrigation in mango orchard resulted in 20% of ET_a originated from E_a. The mango orchard yielded 41,600 kg ha^{-1} and 48,400 kg ha^{-1} of mangos for the first and second growing season, respectively, corresponding to economic values of water productivity of 2.85 US$ m^{-3} and 3.68 US$ m^{-3} based on ET_a. The difference between the two growing seasons could be ascribed to the water stress during flowering in the first growing season as the farmer stopped irrigation for a longer time after the rainy period.

.

Parameterizations in irrigated crops and natural vegetation

Energy fluxes and soil-vegetation parameterizations in natural vegetation and irrigated crops were discussed in Chapter 7. For all types of vegetation, there were consistent relationships between the half hourly values of net radiation (R_n) and global solar radiation (R_G). The daily values of E_F for all irrigated crops varied between 0.71 (mango orchard) to 0.90 (table grape. The E_F values the natural vegetation, were on an annual scale with 0.25 to 0.40 much smaller than for irrigated crops. It was demonstrated that daytime and daily energy balances can be estimated from instantaneous measurements.

In wine grape, the vertical trellis system affected the roughness parameters according to the wind direction. The overhead trellis system in table grapes was less sensitive to wind direction. The surface resistance (r_s) values for wet surfaces were dominantly affected by atmospheric vapour pressure deficit (D) and soil moisture (θ). In natural vegetation, r_s was predominantly influenced by rainfall.

Assessing regional water productivity

Chapter 8 applies the theory of the Surface Energy Balance Algorithm for Land (SEBAL). The algorithm was calibrated and validated for the semi-arid region of the Low-Middle São Francisco River basin. The improved theory was used to assess changes in ET_a due

to expansion of irrigated agriculture and to quantify BIO and CWP at large scale.

Analyzing three representative commercial farms of wine, grapes and mangos in the Low-Middle São Francisco River basin, the economic crop water productivity per unit of ET_a at farm level varied. Table grapes ranked best (from 3.74 to 8.80 US\$ m^{-3}), followed by mangos (from 2.24 to 5.10 \$ m^{-3}) and wine grapes (from 0.36 to 1.55 \$ m^{-3}).

9.2   Conclusions

General

The assessment of actual evapotranspiration and crop water productivity shows that the farmers, in general, irrigate crops without considering the crop water requirements inducing high rates of deep percolation.

Analytical tools

The availability of analytical methods to assess evaporation resistances makes it possible to apply the one-step Penman-Monteith equation for the actual evapotranspiration and the water productivity estimations for the local scale. As the surface resistance to water vapour transfer can be related to remote sensing variables the Penman-Monteith equation can also be applied for regional scale.

Some local calibrations of the empirical equations of SEBAL were necessary for specific conditions of the Brazilian semi-arid. Analysing annual satellite values of ET_a in conjunction with field measurements in irrigated land and natural vegetation the results indicated a difference 4.4% and 0.6% for caatinaga and mango orchard, respectively.

River basin management

There is ample potential for expanding irrigation without entering into conflicts with the power generation industry in São Francisco River basin. The return flow from additional irrigated land in the future can affect environments in terms of rising groundwater tables and return flow of polluted water to the river. The actual scenario of irrigated agriculture in the Low-Middle sub-basin is indicative of the importance of water

193

resources management. The conversion of caatinga is causing an incremental evapotranspiration about 22 m^3 ha^{-1}.

Perspectives for future researches

With the local calibration and validation of the SEBAL algorithm for estimating spatially distributed water consumptive use in conjunction with a network of agro-meteorological stations and a Geographic Information System, the water cycle in irrigated agriculture can be well described. The tools developed in this thesis can be operationally implemented to monitor the intensification of agriculture in the semi-arid region of Brazil and to monitor the adverse impact on downstream water users.

10. Samenvatting en Conclusies

10.1 Samenvatting

Doel van de studie

Het stroomgebied van de San Francisco rivier omvat verschillende staten in Brazilië. Het stroomgebied wordt gekenmerkt door sociaaleconomische tegenstellingen. Welvarende regio's met grote bevolkingsdichtheid grenzen aan gebieden met grote armoede en lage bevolkingsdichtheid. De tweelingsteden Petrolina en Juazeiro liggen in het semi-aride deel van respectievelijk Pernambuco en Bahia en zijn welvarend dank zij de introductie van geïrrigeerde landbouw. De onttrekking van water uit de San Francisco rivier kan watertekorten veroorzaken benedenstrooms van het geïrrigeerde gebied. Spanningen over watergebruik worden voorzien bij een verdere toename van de bevolking. Verdere problemen ontstaan door de uitspoeling van kunstmest en pesticide uit landbouwgebieden. Als gevolg verslechtert de kwaliteit van het water benedenstrooms van dit landbouwgebied waardoor de biodiversiteit terugloopt.

Overleg over watergebruik is nodig tussen de federale en provinciale overheden, waterschappen en steden. Het succes van zo'n dialoog hangt in sterke mate af van de kwaliteit van gegevens over watergebruik en verbruik. De toename van waterverbruik ten gevolge van de ontwikkeling van natuurlijke vegetatie naar geïrrigeerde landbouw behoeft een goede onderbouwing. Dit is nodig om de netto onttrekking van water en het benedenstrooms effect van deze onttrekking, te kwantificeren. Satelliet teledectie, in combinatie met meteorologische data, kunnen worden gebruikt om waterverbruik door een veld of een regio te kwantificeren. Een goede kennis van het actuele waterverbruik (ET_a) en actuele gewas productie (Y_a) zijn basis data voor de berekening van de productiviteit van waterverbruik. (WP). Deze data zijn nodig voor een verbetering van de productiviteit van geïrrigeerde landbouw.

Het primaire doel van deze studie in het midden van het stroomgebied van de San Francisco, is onderzoek naar de nauwkeurigheid waarmee data kunnen worden gemeten voor de berekening van waterverbruik en productie van biomassa. Het tweede doel van de studie is het kwantificeren van parameters van de energie- en

waterbalans van geïrrigeerde gewassen en natuurlijke vegetatie t.b.v. waterbeheer. Het derde doel is de evaluatie van de productiviteit van waterverbruik (WP) op lokaal en regionaal niveau in geirrigeerde wijngaarden en mango boomgaarden.

Evapotranspiratie en productiviteit van waterverbruik

In hoofdstuk 2 worden de theorie besproken voor het gebruik van satelliet gegevens voor de berekening van ET_a, Y_a en WP. De waarde van ET_a voor een veld kan worden berekend via de energie balans van dat veld. De gewascoëfficiënt (K_c) is gelijk aan de potentiële verdamping (ET_p) gedeeld door de referentie verdamping (ET_0). De ET_0 is het waterverbruik door een veld met (een fictief referentie gewas) gras met ongelimiteerde watervoorziening.

Het actuele waterverbruik (ET_a) is op verschillende manieren berekend. De eerste methode gebruikt de referentie verdamping en gewascoëfficiënten zoals gegeven door de FAO (Allen et al., 1988). Hierbij wordt de ET_0 vermenigvuldigd met bovengenoemde K_c en een zogenoemde waterschaarste coëfficiënt (K_s).
Na veldmetingen van de verdampingsweerstand kan de ET_a ook worden berekend met behulp van de Penman-Monteith vergelijking.

Verder kan een energie balans algoritme (SEBAL) worden gebruikt om de ET_a te berekenen voor een regio. De gewasopbrengst na een groeiseizoen (Y_{GS}) wordt in het veld gemeten. Deze kan worden gecombineerd met de biomassa productie (BIO) welke gemeten wordt via een satelliet. Zodoende kan de oogstindex (AHI) worden berekend. De productiviteit van water verbruik voor landbouw (CWP) kan daarna worden berekend voor het hele stroomgebied.

Waterverbruik voor druiven en mango in de wereld

Hoofdstuk 3 geeft een overzicht van het landbouwgebied, opbrengsten en productiviteit van druiven en mango in de wereld. Europa (Italië en Frankrijk) is het belangrijkste wijnproducerende werelddeel, gevolgd door Amerika, Azië, Afrika en Oceanen. Italië en Frankrijk zijn ook de belangrijkste producenten van consumptie druiven. De verbouw van druiven in Brazilië is geconcentreerd in het stroomgebied van de San Francisco rond de steden Petrolina (Pernambuco) en Jazeiro (Bahia). De jaarlijkse toename van het areaal met druiven in Brazilië is de

achterliggende rede voor het onderzoek naar waterverbruik in deze thesis.

Bovengenoemd overzicht toont dat India de belangrijkste producent is van mango. De mango productie in Brazilië bedraagt 2.5% van de wereld productie waarmee Brazilië op de tweede plaats staat van Noord- en Zuid Amerika. De jaarlijkse toename van het areaal met mango is de achterliggende rede voor het onderzoek naar waterverbruik in deze thesis.

Onderzoekgebied en de veldmetingen

Het midden van het stroomgebied van de San Francisco rivier werd gekozen als gebied voor dit onderzoek. Data voor de waterbalans voor elke dag en voor het seizoen werden ter plaatse gemeten. Een netwerk van zeven agiometeorologische stations werd ingericht voor het meten van data. Geïnterpoleerde data van deze stations werden gebruikt voor de berekening van de energie balans van het aardoppervlak en van de regionale waarde van ET_0. Een beschrijving is gegeven in hoofdstuk 4.

De oppervlakte energy balans methode, welke gebruik maakt van de Bowen ratio (BR), werd gebruikt om de verdeling van de beschikbare energie te meten tussen de sensibel heat flux (H) en de latent heat flux (λE) in wijngaarden. In mango boomgaarden werden zowel de eddy correlatie methode als de Bowen ratio methode gebruikt voor de verdeling van energie tussen de warmte floxen. Echter, voor de berekening van de productiviteit van watergebruik voor mango werd alleen de eddy correlatie methode gebruikt.

Voor de natuurlijke vegetatie werd de eddy correlatie methode gebruikt voor het meten van de sensibel heat flux (H) en de latent heat flux (λE). Voor regionale berekeningen werd het algoritme SEBAL gekalibreerd en gevalideerd met behulp van data voor geïrrigeerde gewassen en natuurlijke vegetatie. Voor de berekening van straling en de energiebalans werden negen beelden van de Landsat Thematic Mapper (TM) en een wolkeloos beeld van de Enhanced Thematic Mapper (ETM+ path/row 217/66) gebruikt. De Landsat data zijn beschreven in hoofdstuk 4.

Gewas en water gegevens voor wijngaarden en mangoboomgaarden

Hoofdstuk 5 en 6 beschrijven de karakteristieken van wijngaarden (voor wijn en handdruiven) en voor mangoboomgaarden. De verdeling van de beschikbare energie tussen de sensibel heat flux (H) en de latent heat flux (λE) toont dat systematisch te veel irrigatiewater wordt gegeven aan de gewassen. Als gevolg is er continu een neerwaartse stroming naar het grondwater. Micro sproeiers in velden met handdruiven bevochtigen alle grond. Uit metingen blijkt dat 18% van de ET_a bestaat uit E_a; dus waterverbruik waartegenover geen gewasproductie staat. Bij druppelirrigatie wordt een deel van de grond niet bevochtigd en daalt dit percentage naar 10%.

Daarnaast werden grote verschillen gemeten tussen de verschillende seizoenen. Bijvoorbeeld, in het veld met druppelirrigatie was de wijnproductie 3.4 l/ha (ofwel 0.70 US\$/m^3) in het eerste seizoen en 6.5 l/ha (1.15 US\$/m^3) in het tweede seizoen. Voor handdruiven zijn gegevens beschikbaar voor een seizoen. De opbrengst was 11200 kg/ha overeenkomend met een productiviteit van 6.51 US\$/m^3 (op basis van ET_a).

De microsproeiers onder de mangobomen resulteerden in een E_a gelijk aan 20% van ET_a. De opbrengst van mango was 41600 kg/ha voor het eerste en 48400 kg/ha voor het tweede seizoen overeenkomend met 2.85 en 3.68 US\$/m^3 (op basis van ET_a). Het verschil tussen de twee opbrengsten kan worden verklaard door watertekorten gedurende de bloeiperiode. De boer onderbrak toen de irrigatie voor een te lange periode na de regen.

Parameters voor geïrrigeerde gewassen en natuurlijke vegetatie

De componenten van de energiebalans voor natuurlijke vegetatie en geïrrigeerde gewassen zijn besproken in hoofdstuk 7. Voor alle soorten vegetatie werd een consistente verhouding gevonden tussen de netto straling per half-uur (R_n) en straling van de zon (R_G). De dag-waarde van E_F varieerde voor alle geïrrigeerde gewassen tussen 0.71 (mango) en 0.90 (handdruiven). Het jaar-gemiddelde van E_F voor de natuurlijke vegetatie was, met 0.25 tot 0.40, aanzienlijk lager dan voor geïrrigeerde gewassen. Een goed verband werd gevonden tussen de enkelvoudige (punt) meting van de energie balans en de dagwaarde van deze balans.

De richting van de rijen wijndruiven t.o.v. de windrichting heeft een meetbare invloed op de ruwheid. Bij het gesloten bladerdek van de handdruiven is dit verschil niet aanwezig. De oppervlakte ruwheid (r_s) van een nat oppervlak worden hoofdzakelijk bepaald door de atmospheric vapour pressure deficit (D) en de vochtigheid van de bodem (θ). De r_s-waarde voor natuurlijke begroeiing wordt sterk beïnvloed door de regenval.

Evaluatie van regionale productiviteit van waterverbruik

Hoofdstuk 8 beschrijft de theorie van de energie balans voor het landoppervlak (SEBAL). Het model werd gekalibreerd en gevalideerd voor het semi-aride midden van het San Francisco stroomgebied. Het model is gebruikt om de toename van ET_a te berekenen ten gevolge van de uitbreiding van het geïrrigeerde gebied.
SEBAL is ook gebruikt om BIO en CWP te berekenen op regionaal niveau. En analyse van gegevens van drie commerciële boerderijen toont een grote variatie van de productiviteit van waterverbruik (op basis van ET_a). Handdruiven geven de beste resultaten met 3.74 tot 8.80 US\$/m^3 gevolgd door mango met 2.24 tot 5.10 US\$/m^3 en wijndruiven met 0.36 tot 1.55 US\$/m^3.

10.2 Conclusies

Algemeen

Een evaluatie van het actuele waterverbruik en de productiviteit (op basis van ET_a) toont aan dat de boeren hun gewassen irrigeren zonder rekening te houden met de waterbehoefte van het gewas. Dit resulteert in een grote drainage flux naar het grondwater.

Berekeningsmethoden

Het gebruik van verschillende methoden om gewasweerstanden te berekenen, maakt het mogelijk om de een-staps Penman-Monteith methode te gebruiken voor berekeningen van ET_a en de water productiviteit op veld-niveau. Omdat de oppervlakteweerstand voor de overgang van waterdamp kan worden gerelateerd aan remote sensing gegevens, kan de Penman-Monteith methode ook toegepast worden op regionaal niveau.

Enige kaliberbepaling van empirische vergelijkingen in SEBAL zijn nodig voor toepassing in de semi-aride gebieden langs de San Francisco (Brazilië). Een vergelijking van het actuele waterverbruik op basis van satelliet metingen en veld metingen geven een verschil op jaarbasis van 4.4% voor natuurlijke vegetatie en 0.6% voor mangoboomgaarden.

Beheer van het stroomgebied

Er zijn voldoende mogelijkheden voor de uitbreiding van irrigatie langs de San Francisco rivier zonder in conflict te komen met andere watergebruikers zoals de energie sector. Drainage vanuit (additionele) geïrrigeerde gebieden kan leiden tot degradatie van het milieu t.g.v. stijgende grondwaterpeilen en oppervlakteafvoer van vervuild water naar de rivier. Deze ontwikkelingen zijn van belang voor toekomstig waterbeheer binnen het semi-aride deel van de rivier. De vervanging van natuurlijke vegetatie door geïrrigeerde gewassen geeft een toename van het waterverbruik van ongeveer $22m^3$/ha.

Aanbevelingen voor toekomstig onderzoek

Een gecombineerd gebruik van de gekalibreerde en gevalideerde versie van SEBAL, een netwerk van agro-meteorologisch stations, en een geografisch informatie systeem (GIS) kan het waterverbruik in geïrrigeerde landbouw goed kwantificeren. De methodes, zoals beschreven in deze thesis, kunnen worden toegepast voor het monitoren van intensieve landbouw in het semi-aride deel van Brazilië. De methode kan ook gebruikt worden voor de evaluatie van negatieve effecten op benedenstrooms watergebruikers.

Referelces

Akbari, M., Toomanian, N., Droogers, P., Bastiaanssen. W.G.M., Gieske, A., 2007. Monitoring irrigation performance in Esfahan, Iran, sing NOAA satellite imagery. Agricultural Water Management 88, 99-109.

Alcamo, J., Kreileman, E., Krol, M., Leemans, R., Bollen, J., van Minnen, J., Schäfer, M., Toet, S., de Vries, B., 1998: Global modelling of environmental change: an overview of IMAGE 2.1. In Global change scenarios of the 21st century. Results from the IMAGE 2.1 Model. Alcamo, J., Leemans, R., Kreileman, E. (eds.), Elsevier Science, Kidlington/Oxford, pp. 3-94.

Allen, R.G., Pereira, L.S., Raes, D., Smith, M., 1998. Crop evapotranspiration. Guidelines for computing crop water requirements. FAO Irrigation and Drainage Paper 56, Rome, Italy, 300 pp.

Allen, R.G., Hartogensis, O., de Bruin, H.A.R., 2000. Long-wave radiation over alfafa during the RAPID field campaign in southern Idaho. Research Report, Kimberly, Univ. of Idaho, Id.

Allen, R. G, Tasumi M., Morse, A., Trezza, R. 2005. A Landsat-based energy balance and evapotranspiration model in Western US rights regulation and planning. Irrigation and Drainage Systems, 19, 251-268.

Allen, R.G., Tasumi, M., Trezza, R., 2007a. Satellite-based energy balance for mapping evapotranspiration with internalized calibration (METRIC) – Model. Journal of Irrigation and Drainage Engineer ASCE 133, 380-394.

Allen, R.G., Tasumi, M., Morse, A., Trezza, R., Wright, J. L., Bastiaanssen, W.G.M., Kramber, W., Lorite, I., Robison, C.W., 2007b. Satellite-based energy balance for mapping evapotranspiration with internalized calibration (METRIC) - applications. Journal of Irrigation and Drainage Engineer ASCE. 133, 395-406.

Alves, I., Pereira, L.S., 2000. Modelling surface resistance from climatic variables. Agricultural Water Management 42, 371-385.

Amir J., Sinclair T.R., 1991. A model of temperature and solar radiation effects on spring wheat growth and yield. Field Crops Research 28, 47-58

Araujo, F., Williams L.E., Mattews, M.A., 1995. A comparative study of young "Thompson Seedless" grapevines (Vitis vinifera L.) under drip and furrow irrigation, II. Growth, water use efficiency, and nitrogen partionning. Scientia Horticulturae. 60, 251-265.

Asrar, G., Fuchs, M., Kanemasu, E.T., Hatfield, J.L., 1984. Estimating absorbed photosynthetically active radiation and leaf area index from spectral reflectance in wheat. Agronomy Journal 76, 300-306.

Azevedo, P.V., Teixeira, A.H., Silva, B.B. da, and Soares, J.M., Saraiva, F.A.M. 1997. Avaliação da reflectância e do saldo de radiação sobre um cultivo de videira européia. Revista Brasileira de Agrometorologia 5, 1-7.

Azevedo, P.V. de, Silva, B.B. da, Silva, V.P.R. da., 2003 Water requirements of irrigated mango orchards in northeast Brazil. Agricultural Water Management 58, 241-254.

Azevedo, P.V. de, Soares, J.M., Silva, V.P.R. da, Silva, B.B. da, Nascimento, T., 2007. Evapotranspiration of "Superior" grapevines under intermittent irrigation. Agricultural Water Management 95, 301-308.

Bastiaanssen, W.G.M., 1995. Regionalization of surface flux densities and moisture indicators in composite terrain: A remote sensing approach under clear skies in Mediterranean climates. Ph.D. dissertation, CIP Data Koninklijke Bibliotheek, Den Haag, The Netherlands. 273 p.

Bastiaansssen, W.G.M., Pelgrum, H., Wang, J., Ma, Y., Moreno J.F., Roerink, G.J., Wal van der T., 1998b. A remote sensing surface energy balance algorithm for land (SEBAL) 2. Validation. Journal of Hydrology, 212-213, 213-229.

Bastiaansen, W.G.M., Thiruvengadachari, S., Sakthivadivel, R., Molden, D.J., 1999. Satellite Remote Sensing for Estimating Productivities of Land and Water. International Journal of Water Resources Development 15, 181-194.

Bastiaansssen, W.G.M., 2000. SEBAL – based sensible and latent heat fluxes in the irrigated Gediz Basin, Turkey. Journal of Hydrology 229, 87-100.

Bastiaanssen, W.G.M., Bandara, P., 2001. Evaporative depletion assessments for irrigated watersheds in Sri Lanka, Irrigation Science 21, 1-15.

Bastiaansssen, W. G. M., Brito, R. A. L., Bos, M. G., Souza, R. A., Cavalcanti, E. B., Bakker, M. M., 2001. Low cost satellite data for monthly irrigation performance monitoring: Benchmarks from Nilo Coelho, Brazil. Irrigation and Drainage Systems 15, 53-79.

Bastiaanssen, W. G. M., Ahmed, M.-ud-D., Chemin, Y., 2002. Sattellite surveillance of evaporative depletion across the Indus Basin. Water Resources Research 38, 1273 – 1282.

Bastiaanssen, W.G.M., Ali, S., 2003. A new crop yield forecasting model based on satellite measurements applied across the Indus Basin, Pakistan. Agriculture, Ecosystems & Environment 94 (3), 321–340.

Bastiaanssen, W. G. M., Harshadeep, N., 2005. Managing scarce water resources in Asia: The nature of the problem and can remote sensing help? Irrigation and Drainage Systems 19 (3-4), 269-284.

Bastiaanssen, W. G. M., Noordman, E. J. M., Pelgrum, H. Davids, G., Allen, R. G., 2005. SEBAL for spatially distributed ET under actual management and growing conditions. Journal of Irrigation and Drainage Engineer 131, 85 – 93.

Bastiaanssen, W.G.M., Pelgrum, H., Soppe, R.W.O., Allen, R.G. , Thoreson, B.P. , Teixeira, A.H. de C., 2008. Thermal infrared technology for local and regional scale irrigation analysis in

horticultural systems. ISHS Acta Hort. 792, Proc. Vth IS on Irrigation of Horticultural Crops.

Batra, N., Islam, S., Venturini, V., Bisht, G., Jiang, L., 2006. Estimation and comparison of evapotranspiration from MODIS and AVHRR sensors for clear sky days over the Southern Great Plains. Remote Sensing of the Environment 103, 1-15.

Ben-Asher, J., Tsuyuki, I., Bravdo, B.A., Sagih, M. 2006. Irrigation of grapevines with saline water, I. Leaf Area Index, stomatal conductance , transpiration and photosynthesis, Agricultural Water Management 83, 13-21.

Beringer, J., Tapper, N.J., 2000. The influence of subtropical cold fronts on the surface energy balance of a semi-arid site. Journal of Arid Environments 44, 437-450.

Bloom, A.J., Chapin, F.S., Mooney, H.A., 1985. Resource limitation in plants: an economic analogy. Annual Review of Ecological Systems 16, 363–392.

Boegh, E., Thorsen, M., Butts, M.B., Hansena, S., Christiansen, J.S., Abrahamsen, P., Hasager, C.B., Jensen, N.O., Van der Keur, P., Refsgaard, J.C., Schelde, K., Soegaard, H., Thomsen, A., 2004. Incorporating remote sensing data in physically based distributed agro-hydrological modeling. Journal of Hydrology 287 (1-4), 279-299.

Bondeau, A., Smith, P.C., Zaehle, S., Schaphoff, S., Lucht, W., Cramer, W., Gerten, D., Lotze-Campen, H., Mu¨ ller, C., Reichstein, M., Smith, B., 2007. Modelling the role of agriculture for the 20th century global terrestrial carbon balance. Global Change Biology 13, 679–706.

Boogaard, H.L., Eerens, H., Supit, I., Diepen, C.A.v., Piccard, I., Kempeneers, P., 2002. Description of the MARS crop yield forecasting system (MCYFS), Joint Research Centre, Study contract number 19226-2002-02-F1FED ISP NL.

Booker, J. F., Michelson, A. M., Ward, F. A., 2005. Economic impact of alternative policy responses to prolonged and severe drought in the Rio Grande Basin. Water Resources Research 41 (2), 1-15.

Bos, M. G., 2004. Using depleted fraction to manage groundwater table in irrigated areas. Irrigation and Drainage Systems 18 (3), 201-209.

Bos, M.G., Burton, D.J., Molden D.J., 2005. Irrigation and drainage performance assessment. Practical guidelines. CABI Publishing, Cambridge, USA, 158 pp.

Bouman, B.A.M., Peng, S., Castañeda, A. R., Visperas, R.M., 2005. Yield and water use of tropical aerobic rice systems in the Philippines. Agricultural Water Management 72(2) 87-105.

Bruin de, H. A. R., 1987. From Penman to Makkink. In: Hooghart, J. C. (Ed.), Proceedings and information: TNO Commitee on Hydrological 39, 5-31. Gravennhage, The Netherlands.

Bruin de, H.A.R., Stricker, J.N.M., 2000. Evaporation of grass under non-restricted soil moisture conditions. Hydrological Sciences - Journal- des Sciences Hydrologiques, 45 (3), 391-406.

Brunsell, N.A., Gillies, R.R., 2003. Scale issues in land-atmosphere interactions: implications for remote sensing of the surface energy balance. Agricultural and Forest Meteorology 117, 203-221.

Brunt, D., 1939. Physical and dynamical meteorology. Cambridge University Press.

Brutsaert, W., Sugita, M., 1992. Application of self-preservation in the diurnal evolution of the surface energy budget to determine daily evaporation. Journal of Geophysical Research 97 (D17), 18377-18382.

Businger, J.A. Wyngaard, J.C., Izumi, Y., Bradley, E.F. 1971, Flux-profile relationships in the atmospheric surface layer. Journal of Atmospheric Science 28, 189-191.

Cai, X., Mckinney, C., Lasdon, S., 2002. A framework for sustainable analysis in water resources management and application to the Syr Darya Basin. Water Resources Research 38(6), 21–1/14.

Campbell, G.S., Norman, J.M., 1998. An Introduction to Environmental Biophysics, Springer, New York, 286pp.

Ceotto, E., Castelli, F., 2002. Radiation use efficiency in flue-cured tobacco (*Nicotiana tabacum* L.): response to nitrogen supply, climate variability and sink limitations. Field Crops Research 74, 117-130.

Chehbouni, A., Nouvellon, Y., Lhomme. J.,-P., Watts, C., Boulet, G., Kerr, Y.H., Moran, M.S., Goodrich, D.C., 2001. Estimation of surface sensible heat flux using dual angle observations of radiative surface temperature. Agricultural and Forest Meteorology 108, 55-65.

Chehbouni, A., J. Ezzahar, C. Watts, J-C. Rodriguez and J. Garatuza-Payan, 2006. Estimating area-averaged surface fluxes over contrasted agricultural patchwork in a semi-arid region, in (eds.) J. Hill and A. Roder, Advances in remote sensing and geoinformation processing for land degradation assessment, Taylor and Francis

Choudhury, B.J., 1989. Monitoring global land surface using Nimbus-7 37 GHz data. Theory and examples, International Journal of Remote Sensing 10, 1579–1605.

Cleugh, H.A., Dunin, F.X., 1995. Modeling sensible heat fluxes from a wheat canopy: evaluation of resistance energy balance model. Journal of Hydrology 164, 127-152.

Cleugh, H.A., Leuning, R., Mu, Q., Running, S.W., 2007. Regional evaporation estimates from flux tower and MODIS satellite data. Remote Sensing of Environment 106, 285-304.

Cleverly, J.R., Dahm, C.N., Thibaut, J.R., Gilroy, D.J., Coonrod, J.E.A., 2002. Seasonal estimates of actual evapotranspiration from Tamarix ramosissima stands using three-dimensional eddy covariance. Journal of Arid Environments 52, 181-197.

Clothier, B.E., Clawson, K.L., Pinter, P.J., Moran, M.S., Reginato, R.J., Jackson, R.D., 1986. Estimating of soil heat flux from net radiation during the growth of alfafa. Agricultural and Forest Meteorology 37, 319-329.

Consoli, S., O'Connel, N., Snyder, R., 2006. Estimation of evapotranspiration of different-sized navel-orange tree orchard using energy balance, Journal of Irrigation and Drainage Engineer 132(1), 2-20.

Coombe, B.G., 1987. Influence of temperature on composition and quality of grapes. Acta horticulturae 206, 23-35.

Costacurta, A., Roselli, G., 1980. Critères climatiques et edaphiques pour l'établissement des vignobles. Bulletin de L'O.I.V 53 (596), 783-786.

Crago, R.D. 1996. Comparison of the evaporative fraction and the Priestley-Taylor α for parameterizing daytime evaporation. Water Resources Research 32 (5), 1403-1409.

Dadhwal, V.K., Ray, S.S., 2000. Crop assessment using remote sensing. Part II. Crop condition and yield assessment. Indian Journal Agricultural Economics 55 (2), 54–67.

Daughtry, C.S.T., Gallo, K.P., Goward, S.N., Prince, S.D., Kustas, W. P., 1992. Spectral estimates of absorbed radiation and phytomass production in corn and soybean canopies. Remote Sensing of Environment 39, 141–152.

Dolman, A.J., 1992, A Note on Areally-Averaged Evaporation and the Value of the Effective Surface Conductance, Journal of Hydrology 138, 583–589.

Driese, K.L., Reiners, W.A., 1997. Aerodynamic roughness parameters for semi-arid natural shrub communities of Wyoming, USA. Agricultural and Forest Meteorology 88, 1-14.

Droogers, P., Kite, G.W., 1999. Water productivity from integrated basin modelling. Irrigation and Drainage Systems 13, 275-290.

Droogers, P., Kite, G.W., Murray-Rust, H., 2000. Use of simulation models to evaluate irrigation performance including water productivity, risk and system analysis. Irrigation Science 19, 139-145

Duchemin, J., Hadria, R., Er-Raki, S., Boulet, G., Maisongrande, P., Chehbouni, A., Escadafal, R., Ezzahar, J., Hoedjes, J., Karroui, H., Khabba, S., Mougenot, B., Olioso, A., Rodriguez, J.-C., Simonneaux, V., 2006. Monitoring wheat phenology and irrigation in Central Morocco: on the use of relationship between evapotranspiration, crops coefficients, leaf area index and remotely-sensed vegetation indices. Agricultural Water Management 79, 1 - 27.

Dugas, W.A., Fritschen, L.J., Gay, L.W., Held, A.A., Matthias, A.D., Reicosky, C., Steduto, P., Steiner, J.L, 1991. Bowen ratio, eddy correlation and portable chamber measurements of sensible and latent heat flux over irrigated spring wheat. Agricultural and Forest Meteorology 56, 1-20.

Eitzinger J., Trnka M., Hosch J., Zalud Z., Dubrovsky M., 2004. Comparison of CERES, WOFOST and SWAP models in simulating soil water content during growing season under different soil conditions. Ecological Modelling 171, 223–246.

Er-Raki, S., Chehbouni, A., Guemouria, N., Duchemin, B., Ezzahar, J., Hadria, R., 2007. Combining FAO-56 model and ground-based remote sensing to estimate water consumptions of wheat crops in a semi-arid region. Agricultural Water Management 87, 41 - 54.

Evans, R.G., Spayd, S.E., Wample, R.L., Kroeger, M.W., Mahan, M.O., 1993. Water use of Vits vinifera grapes in Washington. Agricultural Water Management 23, 109-124.

Farah, H.O., 2001. Estimation of regional evaporation under different weather conditions from satellite and meteorological data, Ph.D. thesis, Department of Water Resources, Wageningen University: 170 pp.

Farah, H.O., Bastiaanssen, W.G.M., 2004. Evaluation of the temporal variability of the evaporative fraction in a tropical watershed.

International Journal of Applied Earth Observation and Geoinformatics 5, 129-140.

Field, C.B., Randerson, J.T., Malmström, C.M., 1995. Global net primary production: combining ecology and remote sensing. Remote Sensing of Environment 51 (1), 74–88.

Fischer, G., van Velthuizen, H., Shah, M., Nachtergaele, F.O., 2002. Global Agroecological Assessment for Agriculture in the 21st Century: Methodology and Results, RR-02-02, FAO and IIASA, Laxenburg, Austria.

Franks, S.W., Beven, K., 1999. Conditioning a multiple patch SVAT model using uncertain time-space estimates of latent heat fluxes as inferred from remotely sensed data. Water Resources Research 35, 2751–2761.

Frouin, R., Pinker, R.T., 1995. Estimating photosynthetically active radiation (PAR) at the earth's surface from satellite observations. Remote Sensing of Environment 51, 98–107

Garrat, J.R., Hicks, B.B., 1973. Momentum, heat and water vapour transfer to and from natural and artificial surfaces. Quarterly Journal of Royal Meteorology Society 99, 680-687.

Garrat, J.R., 1978. Transfer characteristics for a heterogeneous surface of large aerodynamics roughness. Quarterly Journal of Royal Meteorology Society 104, 491-502.

Garrat, J.R., 1992. The atmosphere boundary layer. Cambridge atmospheric and space science series. Cambridge University Press, 316 pp.

Gash, J.H.C., Shuttleworth, W.J., 2007. Evaporation, selection, introduction and commentaries, Sahra benchmark papers in hydrology, IAHS, ISBN 978-901502-98-5.

Gervois, S., de Noblet-Ducoudre, N., Viovy, N., 2004. Including croplands in a global biosphere model: methodology and evaluation at specific sites. Earth Interactions 8, 1-25.

Gleick, P.H., 2000. 'The world's water 2000-2001', The Biennial Report on Freshwater Reources, Island Press, Washington, D.C.

Gosse, G., Varlet-Grancher, C., Bonhomme, R., Chartier, M., Allirand, J.M., Lemaire, G., 1986. Maximum dry matter production and solar radiation intercepted by a canopy. Agronomie 6, 47-56.

Gourbesville, P., 2008. Challenges for integrated water resources management. Physics and Chemistry of the Earth, 33, 284-289.

Gower, S.T., Kucharik, C.J., Norman, J.M., 1999. Direct and indirect estimation of leaf area index, fAPAR, and net primary production of terrestrial ecosystems. Remote Sensing of Environment 70, 29-51.

Green, F.C., Hebblethwaite, P.D., Ison, D.A., 1985. A quantitative analysis of varietal and moisture status effects on the growth of *Vicia faba* in relation to radiation absorption. Annals of Applied Biology 106, 143–145.

Groten, S.M.E., 1993. NDVI-crop monitoring and early yield assessment of Burkina Faso. International Journal of Remote Sensing 14, 1495-1515.

Gutman, G.G., 1999. On the use of long-term global data of land reflectances and vegetation indices derived from the advanced very high resolution radiometer. Journal of Geophysics Research 104, 6241 – 6255.

Hafeez, M., Khan, S., 2006. Tracking fallow irrigation water losses using remote-sensing techniques: A case study from the Liu Yuan Ku irrigation system, China. In I. R. Willet and Z. Gao, eds. Agricultural Water Management in China: Proceedings of a workshop held in Bijin China, 14 September 2005. Canberra: Australian Centre for International Agriculture Research.

Hamar, D., Ferencz, C., Lichtenberg, J., Tarcsai, G., Frencz-Arkos, I., 1996. Yield estimation for corn and wheat in the Hungarian Great Plain using Landsat MSS data. International Journal of Remote Sensing 17, 1689–1699.

Hatfield, J.L., 1985. Wheat canopy resistance determined by energy balance techniques, Agronomy Journal 77(2), 279-283.

Havstad, K.M., Kustas, W.P., Rango, A., Ritchie, J.C., Schmogge, T.J., 2000. Jornada experimental Range: A unique Arid Land Location for Experiments to Validate Satellite Systems. Remote Sensing of Environment 74, 13-25.

Heck, R.J., Tiessen, H., Salcedo, I.H., Santos, M.C., 2003. Soil chemical changes under irrigated mango production in the central São Francisco River Valley, Brazil, Journal of Environmental Quality 32, 1414-1421.

Heilman, J.L., Mcinnes, K.J., Savage, M.J., Gesh, R.W., Lascano, R.J., 1994. Soil and canopy energy balances in a west Texas vineyard. Agricultural and Forest Meteorology 71, 99-114.

Heilman, J.L., Mcinnes, K.J., Gesh, R.W., Lascano, R.J., Savage, M.J., 1996. Effects of trellising on the energy balance of the vineyard. Agricultural and Forest Meteorology 81, 79-93.

Hemakumara, H.M., Chandrapala, L.; Moene, A.F., 2003. Evapotranspiration fluxes over mixed vegetation areas measured from large aperture scintillometer. Agricultural Water Management 58, 109-122.

Hicks, B.B., 1973. Eddy fluxes over a vineyard. Agricultural Meteorology 12, 203-215.

Hoedjes, J.C.B., Zuurbier, R.M., Watts, C.J., 2002. Large aperture scintillometer used over a homogeneous irrigated area, partly affected by regional advection, Boundary Layer Meteorology 105, 99-117.

Hughes, G., Keatinge, J.D.H., 1983. Solar radiation interception, dry matter production and yield in pigeon pea (*Cajanus cajan* (L.) Millspaugh). Field Crops Research 6, 171–178.

Hughes, C.E., Kalma, J.D., Binning, P., Willgoose, G.R., Vertzonis, M., 2001. Estimating evapotranspiration for a temperate salt marsh Newcastle, Australia. Hydrological Processes 15, 957–975.

Humphreys, E.R., Black, T.A., Ethier, G.J., Drewitt, G.B., Spittlehouse, D.L., Jork, E.M., Nesic, Z. Livingston, N.J., 2003. Annual and seasonal variability of sensible and latent heat fluxes above a coastal Douglas-fir forest, British Columbia, Canada. Agricultural and Forest Meteorology 115, 109-125.

Hunsaker, D. J., Pinter Jr., P. J., Barnes, E. M., Kimball, B. A., 2003. Estimating cotton evapotranspiration crop coefficients with a multispectral vegetation index. Irrigation Science. 22, 95-104.

Hunsaker, D. J., Pinter, P., Kimball, B., 2005. Wheat basal crop coefficients determined by normalized difference vegetation index. Irrigation Science 24, 1-14.

Hutchinson, C.F., 1991. Uses of satellite data for famine early warning in sub-Saharan Africa. International Journal of Remote Sensing 12, 1405-1421.

Inman-Bamber, N.G., McGlinchey, M.G., 2003. Crop coefficients and water-use estimates for sugarcane based on long-term Bowen ratio energy balance measurements. Field Crops Research 83, 125-138.

Jacson, R.D., Reginato, R. J., Idso. S.B., 1977. Wheat canopy temperatures; A practical tool for evaluating water requirements. Water Resources Research 13, 651-656.

Jairmain, C., A. Klaasse, W.G.M. Bastiaanssen and A.S. Roux, 2007. Remote sensing tools for water use efficiency of grapes in the Winelands region, Western Cape, Proc. 13th Sanciahs Symposium, Capetown, September 6 - 7, 2007.

Jarvis, P.G., 1976. The interpretation of the variations in leaf water potential and stomatal conductance found in canopies in the field. Philosophical Transactions of The Royal Society of London, Series B 273, 593-610.

Jia, L., Su, Z., den Hurk, B.; Menenti, M., Moene, A., De Bruin, H. A. R., Yriassy. J. J. B. Y., Ibanez, M., Cuesta, A., 2003. Estimation of sensible heat flux using Surface Energy Balance System (SEBS) and ATSR measurements. Physics and Chemistry of the Earth 28, 75-88.

Jia, L., 2004. Modelling heat exchanges at the land-atmosphere interface using multi-angular thermal infrared measurements. PhD dissertation, Wageningen, the Netherlands, 199 p.

Kalma, J. D., Jupp, D.L.B., 1990. Estimating evaporation from pasture using infrared thermometry: evaluation of one layer resistance model. Agricultural and Forest Meteorology 51, 223-246.

Katerji, N., Daudet, F.A., Carbonneau, A., Ollat, N. 1994. Etude à l'échelle de la plante entière du fonctionnement hydrique et phosynthétique de la vigne: comparaison des systèmes de conduite traditionnel et an Lyre. Vitis 33, 197-203.

Keller, A., Keller, J., 1995. Effective Efficiency: A water use efficiency concept for allocating freshwater resources. Brief of the Center for Economic Policy Studies. Winrock International, Arlington, Va.

Kenny, G.J., Warrick, R.A., Campbell, B.D., Sims, G.C., Camilleri, M., Jamieson, P.D., Mitchell, N.D., McPherson, H.G., Salinger, MJ, 2000. Investigating climate change impacts and thresholds: An application of the CLIMPACTS integrated assessment model for New Zealand agriculture. Climate Change 46, 91–113.

Kimura, R., 2007. Estimation of moisture availability over the Liudaogou river basin of the Loess Plateau using new indices with surface temperature. Journal of Arid Environments 70, 237-252.

Kimura, R., Bai, L., Fan, J., Takayama, N., Hinokidani, O., 2007. Evapotranspiration estimation over the river basin of the Loess Plateau of China base don remote sensing. Journal of Arid Environments 68, 53-65.

Kite, G.W., Droogers., P. 2000. Comparing evapotranspiration estimates from satellites, hydrological models and field data. Journal of Hydrology 229, 3-18.

Kijne, J.W., Barker, R., Molden, D., 2003. Water productivity in agriculture: limits and opportunities for improvement, CABI, Wallingford, UK

Klaasse, A., Bastiaanssen, W.G.M., de Wit, M., 2007. Satellite analysis of water use efficiency in the winelands region of Western Cape, South Africa, WaterWatch report for West Cape Department of Agriculture, Wageningen, The Netherlands: 70 pp.

Koloskov, G., Mukhamejanov, Kh., Tanton, T.W., 2007. Monin–Obukhov length as a cornerstone of the SEBAL calculations of evapotranspiration. Journal of Hydrology 335 (1-2), 170-179.

Kumar, M., Monteith, J.L., 1981. Remote sensing of crop growth. In: Smith, H. (Ed.), Plants and the Daylight Spectrum. Academic Press, London, pp. 133–144.

Kumar, M., Monteith, J.L., 1982. Remote Sensing of Crop Growth, in Plants and the Daylight Spectrum. Academic Press, London, pp. 133-144.

Kustas W.P., Perry E.M., Doraiswamy P.C., Moran, M. S., 1994. Using satellite remote sensing to extrapolate evapotranspiration estimates in time and space over a semiarid rangeland basin, Remote Sensing of Environment 49, 275–286.

Kustas, W.P., Norman, J.M., 1996. Use of remote sensing for evapotranspiration monitoring over land surface. IAHS Hydrological Science Journal 4, 495-516.

Kustas, W.P.; Anderson, M.C., French, A.N., Vickers, D., 2006. Using a remote sensing field experiment to investigate flux-footprint relations and flux sampling distributions for tower and aircraft-based observations. Advances in Water Resources 29, 355-368.

Lee, X., Yu, Q., Sun, X., Liu, J., Min, Q., Liu Y., Zhang, X., 2004. Micrometeorological fluxes under the influence of regional and local advection: a revisit. Agricultural and Forest Meteorology 122, 11-124.

Leemans, R., van den Born, G.-J., 1994. Determining the potential global distribution of natural vegetation, crops and agricultural productivity. Water, Air, and Soil Pollution. 76, 133–161.

Leuning, R., Cleugh, H.A., Zegelin, S.J., Hughes, D., 2005. Carbon and water fluxes over a temperate *Eucalyptus* forest and a tropical wet/dry savannah in Australia: measurements and comparison with MODIS remote sensing estimates. Agricultural and Forest Meteorology 129, 151-173.

Li, S.-G., Eugster, W., Asanuma, J, Kotani, A., Davaa, G., Oyunbaatar, D., Sugita, M., 2006. Energy partitioning and its biophysical controls above a grazing steppe in central Mongólia. Agricultural Forest Meteorology 137, 89-106.

Lipiec, J., Arvidsson, J., Murer, E., 2003. Review of modelling crop growth, movement of water and chemicals in relation to topsoil and subsoil compaction. Soil and Tillage Research 73, 15–29

Liu, J., Chen, J.M., Cihlar, J., 2003. Mapping evapotranspiration based on remote sensing: An application to Canada's landmass. Water Resources Research 39(7), 1189.

Lobell, D.B., G.P. Asner, G.P., 2002. Moisture effects on soil reflectance, *Soil Science Society of America Journal 66*, 722-727.

Lobell, D.B., Asner, G.P., Ortiz-Monasterio, J. I., Benning, T. L., 2003. Remote sensing of regional crop production in the Yaqui Valley, Mexico: estimates and uncertainties. Agriculture, Ecosystems & Environment 94, 205-220.

Loomis, R. S., Amthor, J. S., 1999. Yield potential, plant assimilatory capacity, and metabolic efficiencies. Crop Science 39, 1584–1596.

Lonsdale, J.H., Kotze, J.M., 1993. Chemical control of mango blossom diseases and the effect on fruit set and yield. Plant Disease 77 (6), 558-562.

Lopes, P.M.O., Silva, B.B. da, Azevedo, P.V. de, Silva, V.P.R da, Teixeira, A.H. de C., Soares, J.M., Sobrinho, J.E. 2001. Balanço de energia num pomar de mangueiras irrigado. Revista Brasileira de Agrometeorologia 9, 1-8.

Lund, M.R., Soegaard, H., 2003. Modelling of evaporation in a sparse millet using a two source model including sensible heat advection within the canopy. Journal of Hydrology 280, 124-144.

Macdonald, R.B., Hall, F.G., 1980. Global crop forecasting. Science 208 (4445), 670–679.

Majumdar, T.J., Brattacharyya, R., Chattejee, S., 2007. On the utilization of ENVISAT AATSR data for geological/hydrological applications. Acta Astronautica 60, 899-905.

Manjunath, K.R., Potdar, M.B., 2002. Large area operational wheat yield model development and validation based on spectral and meteorological data. International Journal of Remote Sensing 23, 3023–3038.

Makkink, G.F., 1957. Testing the Penman formula by means of lysimeters, Journal of the Institution of Water Engineers 11, 277-288.

Maselli, F., Rembold, F., 2001. Analysis of GAC NDVI data for cropland identification and yield forecasting in Mediterranean African countries. Photogrammetric Engineering & Remote Sensing 67, 593–602.

Matsuoka, Y., Morita, T., Kainuma, M., 2001. Integrated assessment model of climate change: the AIM approach. Paper Presented at 14th Toyota Conference, Terrapub, Shizuoka, Japan.

McVicar, T.R., Zhang, G., Bradford, A.S., Wang, H., Dawes, W.R., Zhang, L. and Lingtao, L. 2000. Monitoring Regional

Agricultural Water Use Efficiency for Hebei Province on the North China Plain. Australian. Journal of Agricultural Research 53, 55-76.

Meijninger, W.M.L**.**, De Bruin, H.A.R., 2000. The Sensible Heat Fluxes over Irrigated Areas in Western Turkey Determined with a Large Aperture Scintillometer, Journal of Hydrology 229, 42-49.

Meijninger, W.M.L., Hartogensis, O.K., Kohsiek, W., Hoedjes, J.C.B., Zuurbier, R.M. and De Bruin, H.A.R., 2002, 'Determination of Area-Averaged Sensible Heat Fluxes with a Large Aperture Scintillometer over a Heterogeneous Surface – Flevoland Field Experiment', Boundary-Layer Meteorology 105, 37-62.

Menenti, M., Bastiaanssen, W. G. M., Van Eick, D., 1989. Determination of hemispheric reflectance with thematic mapper data. Remote Sensing of Environment 28, 327- 337.

Menenti, M., Choudhury, B.J., 1993. Parameterization of land surface evaporation by means of location dependent potential evaporation and surface temperature range, in (eds.) Bolle, Feddes and Kalma, Exchange processes at the land surface for a range of space and time scales, IAHS Publ. No. 212, 561-568.

Menenti, M., Azzali, S. and D'Urso, G. 1996. Remote sensing, GIS and hydrological modeling for irrigation management. p. 453-472. In: L.S. Pereira, R.A. Feddes, J.R. Gilley and B. Lesaffre (eds.), Sustainability of Irrigated Agriculture. Kluwer Academic Publishers.

Michell. S.W., Csillag, F., Tague, C., 2005. Impacts of spatial partitioning in hydrological models: Predicting grasslands productivity with RHESSys. Transations in GIS 9(3), 423-444.

Molden, D., 1997. Accounting for Water Use and Productivity. SWIM Paper 1, International Water Management Institute, Colombo, Sri Lanka.

Molden, D.J., Satkhivadivel, R., 1999. Water accounting to assess use and productivity of water, International Journal of Water Resources Development 15 (1/2), 55-72

Molden, D.J., R. Sakthivadivel and Z. Habib, 2000. Basin-level use and productivity of water: examples from South Asia, Research Report 49, International Water Management Institute, Colombo, Sri Lanka: 24 pp.

Molden, D., Bin, D., Loeve, R., Barker, R., Tuong, T. P., 2007a. Agricultural water productivity and savings: policy lessons from two diverse sites in China. Water Policy 9, 29-44.

Molden, D., Frenken, K., Barker, R., de Fraiture, C., Bancy, M., Svendsen, M., Sadoff, C., Finlayson, C.M., 2007b. Trends in water and agricultural development. In: Chapter 2 in Water for Food, Water for Life: A Comprehensive Assessment of Water Management in Agriculture, International Water Management Institute, London, Earthscan, Colombo.

Molden, D., Oweis, T., Steduto, P., Kijne, J.W., Hanjra, M.A., Bindraban, P.S., 2007c. Pathways for increasing agricultural water productivity. In: Chapter 7 in Water for Food, Water for Life: A Comprehensive Assessment of Water Management in Agriculture, International Water Management Institute, London, Earthscan, Colombo.

Molle, F., Sutthi, C., Keawkulaya, J., Korpraditskul, R., 1999. Water management in raised bed systems: a case study from the Chao Phraya delta, Thailand, Agricultural Water Management 39, 1-17.

Moller, M., Alchanatis, V. Cohen, Y., Meron, M., Tsipris, J., Naor, A., Ostrovsky, V., Sprintsin, M. and Cohen, S. 2007. Use of thermal and visible imagery for estimating crop water status of irrigated grapevine. Journal of Experimental Botany 58, 827-838.

Monteith, J.L., 1965. Evaporation and the environment. The state and movement of water in living organisms. Symposium of the Society of Experimental Biologists, XIX, 205-224.

Monteith, J.L., 1972. Solar radiation and productivity in tropical ecosystems. Journal of Applied Ecology 9, 747-766.

Monteith, J.L., 1973. Principles of environmental physics; Elsevier, New York, 241 pp.

Monteith, J.L., 1977. Climate and efficiency of crop production in Britain. <u>Philosophical Transactions of the Royal Society Series B</u> 281, 277–294.

Monteith J.L., Scott, R.K., 1982. Weather and yield variation of crops. In: Food, Nutrition and Climate (Blaxter K; Fowden L, eds), pp 127–149. Applied Science, Englewood Cliffs, NJ.

Monteith, J.L., Unsworth, M.H., 1990. Principles of environmental physics (2nd edition. Arnold, London, 291 pp.

Moore, C.J. 1986. Frequency response corrections for eddy correlation systems. Boundary Layer Meteorology 37, 17-35.

Moran, M.S., Maas, S.J., Pinter, P.J., 1995. Combining remote sensing and modelling for estimating surface evaporation and biomass production. Remote Sensing Review 12, 335–353.

Mostert, P.G., Wantenaar, L., 1994. Water needs and irrigation of mature mango trees. Yearbook South-African-Mango Growers Association 14, 21-23.

Moulin, S., Bondeau, A., Delecolle, R., 1998. Combining agricultural crop models and satellite observations: from field to regional scales. International Journal of Remote Sensing 19 (6), 1021–1036.

Muchow, R.C., 1985. An analysis of the effect of water-deficits on grain legumes grown in a semi-arid tropical environment in terms of radiation interception and its efficiency of use. Field Crops Research 11, 309–323.

Muchow, R.C., 1990. Effect of high temperature on grain growth in maize. Field Crops Research, 23, 145-158.

Muchow, R.C., Robertson, M.J., Pengelly, B.C., 1993. Radiation use efficiency of soybean, mungbean, and cowpea under different environmental conditions. Field Crops Research 32, 1-16.

Muchow, R.C., Sinclair, T.R., 1994. Nitrogen response of leaf photosynthesis and canopy radiation use efficiency in field-grown maize and sorghum. Crop Science 34, 721–727.

Nadler, A., Raveh, E., Yermiyahu, U., Green, S., 2006. Stress induced water content variations in mango stem by time domain reflectometry, Soil Science Society of America Journal 70, 510-520.

Naiman, R.J., Bunn, S.E., Nilsson, C., Petts, G.E., Pinay, G., Thompson, L.C., 2002. Legitimizing fluvial ecosystems as users of water, Environmental Management 30, 468-480.

Nagler, P.L., Scott, R.L., Westenburg, C., Cleverly, J.R., Glenn, E.P., Huete, A.R., 2005a. Evapotranspiration on western U. S. rivers estimated using the Enhanced Vegetation Index from MODIS and data from eddy covariance and Bowen ratio flux towers. Remote Sensing of Environment 97, 337 - 351.

Nagler, P.L., Jetton, A., Fleming, J., Didan, K., Glenn, E., Erker, J., Morino, K., Milliken, J., Gloss, S., 2007. Evapotranspiration in a cottonwood (*Populus fremontii*) restoration plantation estimated by sap flow and remote sensing methods. Agricultural and Forest Meteorology 144, 95- 110.

Naor, A. 2006. Irrigation scheduling and evaluation of tree water status in deciduous orchards. Horticultural Reviews 32:111-166.

Noordman, E. J. M., Moura, M. S. B., Teixeira, A. H. de C., Santos, M. A., Santos, M. G. L., Lopes, H. L. 2003. Crop classification for the Nilo Coelho scheme by using Landsat TM images, Anais XI SBSR, Belo Horizonte, Brasil, 05-10 Abril, INPE: 205-210.

Novello, V., Schubert, A., Antonietto, M., Boschi, A. 1992. Water relations of grapevine cv. Cortese with different training systems. Vitis. 31, 65-75.

Nunez-Elisea, R, Davenport, T.L., 1995. Effect of leaf age, duration of coal temperature treatment, and photoperiod on bud dormancy release in floral initiation of mango. Scientia Horticulturae 62, 63-73.

Oguntoyinbo, J.S., 1970. Reflection coefficient of natural vegetation, crops and urban surfaces in Nigeria. Quarterly Journal of the Royal Meteorological Society 96, 430-441.

Olejnik, J., Eulenstein, F. Kedziora, A., Werner, A., 2001. Evaluation of a water balance model using data for bare soil and crop surfaces in Middle Europe. Agricultural and Forest Meteorology 106, 105-116.

Oliver, H.R., Sene, K.J., 1992. Energy and water balances of developing vines. Agricultural and Forest Meteorology 61, 167-185.

Ortega-Farias, S., Carrasco, M., Olioso, A., Acevedo, C., Poblete, C., 2007. Latent heat flux over Cabernet Sauvignon vineyard using the Shuttleworth and Wallace model, Irrigation Science 25, 161-170.

Osborne, T.M., Lawrence, D.M., Challinor, A.J., Slingo, J.M., Wheeler, T.R., 2007. Development and assessment of a coupled crop-climate model. Global Change Biology 13, 169–183.

Oweis, T., Hachum, A., 2003. Improving water productivity in the dry areas of west Asia and North Africa. In: Kijne, J.W., Barker, R. and Molden, D., Eds, Water Productivity in Agriculture: Limits and Opportunities for Improvement. Comprehensive Assessment of Water Management in Agriculture Series 1, CABI/IWMI, Wallingford/Colombo, pp. 179–198.

Oweis, T., Hachum, A., 2006. Water harvesting and supplemental irrigation for improved water productivity of dry farming systems in West Asia and North Africa. Agricultural Water Management 80, 57-73.

Paço, T.A., Ferreira, M.I, Conceição, N., 2006. Peach orchard evapotranspiration in a sandy soil: Comparison between eddy

covariance measurements and estimates by the FAO 56 approach. Agricultural Water Management 85 (3), 305-313.

Paw U, K.T., Baldocchi, D.D., Meyers, T.P., Wilson, K.B., 2000. Corrections of eddy covariance measurements incorporating both advective effects and density fluxes, Boundary Layer Meteorology 97, 487-511.

Peacock, W. L., Rolston, D. E., Aljibury, F. K., Rauschkolb, R. S., 1977. Evaluating drip, flood, and sprinkler irrigation of wine grapes. American Journal of Enology and Viticulture 28, 193-195.

Pelgrum, H., Bastiaanssen, W.G.M., 1996. An inter comparison of techniques to determine the area-averaged latent heat flux from individual in situ observations: a remote sensing approach using the European Field Experiment in a Desertification-Threatened Area delta. Water Resources Research 9, 2775-2786.

Pellenq, J. Boulet, G., 2004. A methodology to test the pertinence of remote-sensing data assimilation into vegetation models for water and energy exchange at the land surface. Agronomie 24, 197-204.

Penman, H.L., 1948. Natural evaporation from open water, bare soil and grass. Proceedings of the Royal Society of London Ser. A., 193, 120-145.

Pinker, R.T., Thompson, O.E., Eck, T.F., 1980. The albedo of a tropical evergreen forest. Quarterly Journal of the Royal Meteorological Society 106, 551–558.

Pirmoradian, N., Sepaskhah, A.R., 2005. A very simple model for yield prediction of rice under different water and nitrogen applications. Biosystems Engineering 93(1), 25–34

Prasad, A.K., Chai, L., Singh, R.P., Kafatos, M., 2006. Crop yield estimation model for Iowa using remote sensing and surface parameters. International Journal of Applied Earth Observation Geoinformatics 8 (1), 26–33.

Prince, S.D., 1990. High temporal frequency remote sensing of primary production using NOAA/AVHRR. In: Steven, M.D., Clark, J.A.

(Eds.), Applications of Remote Sensing in Agriculture, 4. Butterworths, UK, pp. 169–183.

Prueger, J.H., Kustas, W.P., Hipps, L.E., Hatfield, J.L., 2004. Aerodynamic parameters and sensible heat flux estimates for a semi-arid ecosystem. Journal of Arid Environments 57, 87-100.

Rana, G. Katerji, N., Michele I.M., Hammami, A. 2004. Microclimate and plant water relationship of the "overhead" table grape vineyard managed with three different covering techniques. Scientia Horticulturae 102, 105-120.

Rana, G., Katerji, N., Lorenza, F. de., 2005. Measuring and modelling of evapotranspiration of irrigated citrus orchard under Mediterranean conditions. Agricultural and Forest Meteorology 128, 199-209.

Rasmussen, M.S., 1992. Assessment of millet yields and production in northern Burkina Faso using integrated NDVI from the AVHRR. International Journal of Remote Sensing 13, 3431–3442.

Renaut, D., Hemakumara, M., Molden, D., 2001. Importance of water consumption by perennial vegetation in irrigated areas of the humid tropics: Evidence from Sri Lanka. Agricultural Water Management 46 (3), 215-230.

Riou, C., Pieri, P., Valancogne, C., 1987. Variation de la vitesse du vent a línterieur et au-dessus dúne vigne. Agricultural and Forest Meteorology 39, 143-154.

Rockstrom, J., Barron, J. and Fox, P. 2003. Water Productivity in Rainfed Agriculture: Challenges and Opportunities for Smallholder Farmers in Drought- prone Tropical Agroecosystems. In: Water Productivity in Agriculture: Limits and Opportunities for Improvement, eds. Kijne, J.W., Barker, R., and Molden, D. Wallingford (UK): CABI Publishing, pp.145-162.

Rockstrom, J., Barron, J., 2007. Water productivity in rainfed systems: overview of challenges and analysis of opportunities in water scarcity prone savannahs. Irrigation Science 25 (3), 299-311.

223

Roerink, G.J., Bastiaanssen, W.G.M., Chambouleyron, J., Menenti, M., 1997. Relating crop water consumption to irrigation water supply by remote sensing. Water Resource Management 11, 445-465.

Roerink, G.J., Su, Z., Menenti, M., 2000. S-SEBI: A simple remote sensing algorithm to estimate the surface energy balance. Physics and Chemistry of the Earth 25, 147-157.

Russell, G., Jarvis, P.G., Monteith, J.L., 1989. Absorption of radiation by canopies and stand growth. In: Russell, G., Marshall, B., Jarvis, P.G. (Eds.), Plant Canopies: Their Growth, Form and Function. Cambridge University Press, Cambridge, pp. 21–40.

Saarikko, R.A., 2000. Applying a site based crop model to estimate regional yields under current and changed climates. Ecological Modelling 131, 191–206.

Sakthivadivel, R., de Fraiture, C., Molden, D.J., Perry, C., Kloezen, W., 1999. Indicators of land and water productivity in irrigated agriculture, International Journal of Water Resource Development 15, 161-180.

Sammis, T.W., Mexal, J.G., Miller D., 2004. Evapotranspiration of flood-irrigated pecans. Agricultural Water Management 69, 179-190.

Schaffer, B; Andersen, P.C., Crane, J.H., 1994. Mango. In: Schaffer, B.; Andersen, P.C. (eds) Handbook of Environmental Physiology of Fruit Crops 2, Sub-tropical ad Tropical Crops. CRC Press, Boca Raton.

Schlesinger, W.H., 1997. Biogeochemistry: An Analysis of Global Change. Academic Press, San Diego, 443 pp.

Schmugge, T., Hook, S.l., CoII, C., 1998. Recovering surface temperature and emissivity from thermal infrared multispectral scanner data. Remote Sensing of Environment 65, 121-131.

Scott, C.A., W.G.M. Bastiaanssen, M.D. Ahmad, 2003. Mapping root zone soil moisture using remotely sensed optical imagery, ASCE Journal of Irrigation and Drainage Engineer 129, 326-335.

Seckler, D., Amarasinghe, U., Molden, D.J., de Silva, R., Barker, R., 1998. World water demand and supply, 1990 to 2025: Scenarios and Issues, Research Report 19 (Colombo, Sri Lanka, International Water Management).

Sene, K.J., 1994. Parameterizations for energy transfers from a sparse vine crop. Agricultural and Forest Meteorology 71, 1-18.

Sene, K.J., 1994. Parameterizations for energy transfers from a sparse vine crop. Agricultural Forest Meteorology 71, 1-18.

Sharma, P.K., Chaurasia, R., Mahey, R.K., 2000. Wheat production forecasts using remote sensing and other techniques-experience of Punjab State. Indian Journal of Agricultural Econonomics 55 (2), 68–80.

Sheehy, J.E., Peng, S., Doberman, A., Mitchell, P.L., 2004. Fantastic yields in the system of rice intensification: fact or fallacy? Field Crops Research 88, 1-8.

Shuttleworth, W.J., 1988. Evaporation from Amazonian rain forest. Proceedings of the Royal Society of London. Series B, Biological Sciences 233, 321–346.

Shuttleworth, 1991. Evaporation models in hydrology. In: Schmugge, T. J. and André, J. (editors), Land Surface Evaporation. Springer, New York, pp. 93-120.

Simmons, L.J. Wang, J., Sammis, T.W., Miller, D.R., 2007. An evaluation of two inexpensive energy-balance techniques for measuring water use in flood-irrigated pecans (*Carya illioinensis*). Agricultural Water Management 88, 181-191.

Sinclair, T.R., Muchow, R.C., 1999. Radiation use efficiency. Advances in Agronomy 65, 215–265.

Singh, L.B., 1977. Mango. In: Alvim, P.T.; Koz T.T. Ecophysiology of Tropical Crops, P.T. Alvim e T.T. Kozlowski. (Eds.), Academic Press, New York, 479 p.

Singh, P., Sri Rama, Y.V., 1989. Influence of water deficit on transpiration and radiation use efficiency of chickpea (*Cicer arietinum* L.). Agricultural and Forest Meteorology 48, 317–330.

Sivakumar, M.V.K., Virmani, S.M., 1984. Crop productivity in relation to interception of photosynthetically active radiation. Agricultural and Forest Meteorology 31, 131–141.

Smakthin, V., Revenga, C., Doll, P. 2004. Taking into account environmental water requirements in global-scale water resources assessments. Colombo, Sri Lanka: IWMI., 24p. (Comprehensive Assessment of Water Management in Agriculture Research Report 2)

Smart, R.E., 1985. Principle of grapevine canopy management microclimate with implications for yield and quality. A review. American Journal of Enology and Viticulture 336 (3), 230-239.

Smith, R.G.C., Barrs, H.D., Meyer, W.S., 1989. Evaporation from irrigated wheat estimated using radiative surface temperature: an operational approach. Agricultural and Forest Meteorology 48, 331-344.

Snyder, R.L., B.J. Lanini, D.A. Shaw and W.O. Pruitt, 1989. Using reference Evapotranspiration (ET$_0$) and crop coefficients to estimate crop evapotranspiration (ET$_c$) for trees and vines, Leaflet no. 21428, cooperative extension, University of California, Berkeley, California

Sobrino, J.A., Gómez, M., Jiménez-Muñoz, J.C., Olioso, A., 2007. Application of a simple algorithm to estimate daily evapotranspiration from NOAA-AVHRR images for the Iberian Peninsula. Remote Sensing of Environment 110 (2), 139-148.

Spaeth, S.C., Sinclair, T.R., Ohunuma, T.K., Onno, S., 1987. Temperature, radiation and duration dependence of light soybean

yields: measurements and simulation. Field Crops Research 16, 297-307

Spano, D., Snyder, R.L., Duce, P., Paw U, K. T., 2000. Estimating sensible and latent heat flux densities from grapevine canopies using surface renewal. Agricultural and Forest Meteorology 104, 171-183.

Srinivas, K. Shikhamany, S.D., Reddy, N.N., 1999. Yield and water-use of 'Änab-e Shahi' grape (*Vitis vinifera*) vines under drip and basin irrigation. Indian Journal of Agricultural Science, 69, 21-23.

Steduto, P., Albrizio, R., 2005. Resource-use efficiency of field-grown sunflower, sorghum, wheat and chickpea. II. Water use efficiency and comparison with radiation use efficiency. Agricultural and Forest Meteorology 130, 269-281.

Stehfest, E., Heistermann, M., Priess, J., Ojima, D., Alcamo, J., 2007. Simulation of global crop production with the ecosystem model DayCent. Ecological Modelling 209, 103-219.

Stewart, J.B. 1989. On the use of the Penman-Monteith equation for determining areal evapotranspiration. 3-2. In: Black, T. A., Spittlehouse, D. L., Novak, M. D., and Price, D. T. (ed)., Estimation of Areal Evapotranspiration, IAHS, Pub. No. 177.

Stull, R.B. An Introduction to Boundary Layer Meteorology, 1988. Ed. Kluer Academic Plublishers, Boston.

Su, Z., 2002. The Surface Energy Balance System (SEBS) for estimation of turbulent heat fluxes. Hydrology and Earth System Sciences 6, 85-99.

Su, H., McCabe, M.F., Wood, E.F., Su, Z., Prueguer, J.H., 2005. Modeling evapotranspiration during SMACEX02: Comparing two approaches for local and regional scale prediction. Journal of Hydrometeorology 6(6), 910-922.

Swinbank, W.C., 1963. Longwave radiation from clear skies. Quarterly Journal of the Royal Meteorological Society 89, 339-348.

Tanner, C. B., Sinclair, T. R., 1983. Efficient water use in crop production: Research or Re-search? In: Taylor, H. M., Jordan, W. A. and Sinclair, T. R., eds., Limitations to efficient water use in crop production. Madison, Wisc.: American Society of Agronomy.

Tanner, B.D. Swiatek, E., Greene, J.P., 1993. Density fluctuations and use of the krypton hygrometer in surface flux measurements. In: Proceedings of the National Irrigation Drainage Engineering, Park City, UT, 21-23 July 1993. ASCE, New York, NY.

Tasumi, M., Allen, R.G., 2007. Satellite-based ET mapping to assess variation in ET with timing of crop development. Agricultural Water Management 88, 54 - 62.

Teixeira, A.H. de C., Lima Filho, J.M.P., 1997. Relações entre o índice de área foliar e radiação solar na cultura da videira. Revista Brasileira de Agrometeorologia 5, 143-146.

Teixeira A.H. de C., 2001. Informações agrometeorológicas do Pólo Petrolina-PE / Juazeiro-BA. Petrolina: Embrapa Semi-Árido, 46p. (Documentos, 168)

Teixeira, A.H. de C., W.G.M. Bastiaanssen, L.H. Bassoi, 2007. Crop water parameters of irrigated wine and table grapes to support water productivity analysis in Sao Francisco River basin, Brazil. Agricultural Water Management 94, 31-42.

Teixeira, A.H. de C., W.G.M., Bastiaanssen, Moura, M. S. B., Soares, J. M., Ahmad, M–ud–D, Bos, M. G., 2008a. Energy and Water Balance Measurements for Water Productivity Analysis in Irrigated Mango Trees, Northeast Brazil. Agricultural and Forest Meteorology 148, 1524-1537

Teixeira, A.H. de C. Bastiaanssen, W.G.M., Ahmad, M.D., Moura, M.S.B., Bos, M.G., 2008b. Analysis of energy fluxes and vegetation-atmosphere parameters in irrigated and natural

ecosystems of semi-arid Brazil, Journal of Hydrology. 10.1016/j.jhydrol.2008.08.011

Ten Berge, H.F.M., 1990. Heat and water transfer in bare topsoil and the lower atmosphere. Simulation Monographs 33. Pudoc, Wageningen, 207 pp.

Tesfaye, K., Walker , S., Tsubo, M., 2006. Radiation interception and radiation use efficiency of three grain legumes under water deficit conditions in a semi-arid environment. European Journal of Agronomy 25, 60-70.

Testi, L., Villalobos, F.J., Orgaz, F., 2004. Evapotranspiration of a young olive orchard in southern Spain. Agricultural and Forest Meteorology 121, 1-18.

Testi, L., Orgaz F., Villalobos F.J. 2006. Variations in bulk canopy conductance of an irrigated olive (*Olea europaea L.*) orchard. Environmental and Experimental Botany 55, 15-28.

Thiruvengadachari, S., Sakthivadivel, R., 1997. Satellite Remote Sensing Techniques to Aid Irrigation System Performance Assessment: a Case Study in India. Research Report 9, International Water Management Institute, Colombo, Sri Lanka, 23 pp.

Thom, A. S., 1972. Momentum, mass and heat exchange of vegetation. Quarterly Journal of the Royal Meteorological Society 98, 124-134.

Trambouze, W., Bertuzzi, P., Voltz, M., 1998. Comparison of methods for estimating actual evapotranspiration in a row-cropped vineyard. Agricultural and Forest Meteorology 81, 193-208.

Troufleau, D., Lhomme, J.-P., Monteny, B., Vidal, A., 1997. Sensible heat flux and radiometric surface temperature over sparse sahelian vegetation: is the kB^{-1} a relevant parameter? Journal of Hydrology 189, 815–838.

Tubiello, F.N., Ewert, F., 2002. Simulating the effects of elevated CO_2 on crops: Approaches and applications for climate change. European Journal of Agronomy 18, 57-74.

Twine, T.E, Kustas, W.P., Norman, J.M., Cook, D.R., Houser, P.R., Meyers, T.P, Prueger, J.H., Starks, P.J., Wesely, M.L., 2000. Correcting eddy-covariance flux estimates over grassland. Agricultural and Forest Meteorology 103, 279-300.

Unland, H.E.; Houser, P.R.; Shuttleworth, W.J.; Yand, Z., 1996. Surface flux measurement and modelling at a semi-arid Sonoran Desert site. Agricultural and Forest Meteorology 82, 119-153.

van Bavel, C.H.M., 1996. Evaporation and energy balance of alfafa. Part 1, Annual Report., USAERDA, Research Report No. 381, U.S. Water Conservation Laboratory, Phoenix, AZ.

van der Griend, A.A., Owe, M., 1993. Determination of microwave vegetation optical depth and single scattering albedo from large scale moisture and Nimbus/SMMR satellite observations. International Journal of Remote Sensing 14(10), 1975-1996.

van den Hurk, B. J. J. M.; Verhoef, A., vand den Berg, A. R., de Bruin, H. A. R., 1996. An intercomparison of three vegetation/soil models for a sparce vineyard canoelpy. Quarterly Journal of the Royal Meteorological Society 121, 1967-1889.

van Dijk, A.I.J.M.; Bruijnzeel, L.A.; Schellekens, J., 2004. Micrometeorology and water use of mixed crops in upland West Java, Indonesia. Agricultural and Forest Meteorology 124, 31-49.

van Dijk, A., Moene, A.F., de Bruin, R., 2004. The principles of surface flux physics: theory, practice and description of the Ecpack library, Internal Report, Meteorology and Air Quality Group, Wageningen University, Wageningen, The Netherlands: 99 pp.

van Niel, T.G., McVicar, T.R., 2004. Current and potential uses of optical remote sensing in rice-based irrigation systems: a review. Australian Journal of Agricultural Research 55, 155-185.

Verhoef, A., McNaughton, K.G., Jacobs A.F.G., 1997. A parameterization of momentum roughness length and displacement height for a wide range of canopy densities. Hydrology and Earth System Sciences 2(1), 81-91.

Vilalolobos F.J., Testi, L., Rizzalli, R., Orgaz, F., 2004. Evapotranspiration and crop coefficients of irrigated garlic (*Allium sativum L.*) in a semi-arid climate. Agricultural Water Management 64, 233-249.

Vörösmarty, C.J., Sahagian, D., 2000. Anthropogenic disturbance of the terrestrial water cycle. BioScience 50, 753-65.

Walker, R., Gibberd, M., Stevens, R., Pech, J., 2004. Application of carbon isotopic discrimination technology to understand and managing wine grape water use efficiency. Final report to Grape and Wine Research and Development Corporation. Project Number CRV99/10.

Wang, K., Li, Z., Cribb, M., 2007. Estimation of evaporative fraction from a combination of day and night land surface temperatures and NDVI: A new method to determine the Priestly-Taylor parameter. Remote Sensing Environment 102, 293-305.

Watiki, J.M., Fukai, S., Banda, J.A., Keating, B.A., 1993. Radiation interception and growth of maize/cowpea intercrop as affected by maize plant density and cowpea cultivar. Field Crops Research 35, 123–133.

Webb , E.K., Pearmen, G.L., Leuning, R., 1980. Correction of flux measurements for density effects due to heat and water vapour transfer. Quarterly Journal of the Royal Meteorological Society 106, 85-100.

Williams, L.E., Phene, C.J., Grimes, D.W., Trout, T.J., 2003. Water use of mature Thompson Seedless grapevines in California. Irrigation Science 22, 11-18.

Williams, L.E., Ayars, J.E., 2005. Grapevine water use and the crop coefficient are linear functions of the shaded area measured

beneath the canopy. Agricultural and Forest Meteorology 132, 201-211.

Wilson, K., Goldstein, A., Falge, E., Aubinet, M., Baldocchi, D., Berbigier, P., Bernhofer, C., Ceulemans, R., Dolman, H., Field, C., Grelle, A., Ibrom, A., Law, B.E., Kowalski, A., Meyers, T., Moncrieff, J., Monson, R., Oechel, W., Tenhunen , J., Valentini , R., Verma, S., 2002. Energy balance closure at Fluxnet sites, Agricultural and Forest Meteorology 113, 223-243.

Winkel, T., Rambal, S., 1990. Stomatal conductance of some grapevines growing in the field under a Mediterranean environment. Agricultural and Forest Meteorology 51, 107-121.

Wylie, B., Johnson, D., Laca, E., Saliendra, N., Gilmanov, T., Reed, B., Tieszen, L., Bruce B. Worstell, B., 2003. Calibration of remotely sensed, coarse resolution NDVI to CO2 fluxes in a sage-brush-steppe ecosystem. Remote Sensing of Environment 85, 243-255.

Yunusa, I. A. M., Walker, R. R, Blackmore, D. H., 1997a. Characterization of water use by Sultana grapevines (Vitis vinifera L.) on their own roots or on Ramsey rootstock drip-irrigated with water of different salinities. Irrigation Science 17, 77-86.

Yunusa, I.A.M., Walker, R.R, Guy, J.R., 1997b. Partitioning of seasonal evapotranspiration from a commercial furrow-irrigated Sultana vineyard. Irrigation Science 18, 45-54.

Yunusa, I.A.M., Walker, R.R., Lu, P. 2004. Evapotranspiration components from energy balance, sapflow and microlysimetry techniques for an irrigated vineyard in inland Australia. Agricultural and Forest Meteorology 127, 93-107.

Zhang, H., 2003. Improving water productivity through deficit irrigation: Examples from Syria, the North China Plain and Oregon, USA. In: Kijne, J.W., Barker, R., Molden, D., eds., Water Productivity in Agriculture: Limits and opportunities for improvement. Wallingford, UK, and Colombo: CABI Publishing and International Water Management Institute.

Zwart, S.J., Bastiaanssen, W.G.M., 2004. Review of measured crop water productivity values for irrigated wheat, rice, cotton and maize. Agricultural Water Management 69, 115-153.

Zwart, S., Bastiaanssen, W. G. M., 2007. SEBAL for detecting spatial variation of water productivity and scope for improvement in eight irrigated wheat systems. Agricultural Water Management 89, 287- 296.

Curriculum Vitae

Personal data

Name: Antônio Heriberto de Castro Teixeira
Date of Birth: 30 May 1960
Place of Birth: Fortaleza/CE - Brazil

Office address:
Embrapa Semi-Árido, BR 428, Km 152, Zona Rural, 56300-970
Petrolina, PE - Brazil - CP: 23. Tel: 55(87) 38621711, Fax: 8621744, E-mail: heribert@cpatsa.embrapa.br

Education

1990 – 1993
Master in Meteorology [C. Grande].
Federal University of Paraíba, UFPB, Paraíba, Brazil.
Title: Agro climatic Potential of Pernambuco State for acerola (Malpiguia glabra L.) crop, 1993.

1982 - 1988
Graduation in Agronomy
Federal University Rural of Pernambuco, UFRPE, Pernambuco, Brazil.

Research experience

Empresa Brasileira de Pesquisa Agropecuária – EMBRAPA
- Embrapa Semi-Árido : Researcher: 1994 - current
* Petrolina-PE, Brazil

ACTIVITIES:
December, 1994 – Current: Development and Research in Agro-meteorology

Publications during the Ph.D. study

Teixeira, A.H. de C., W.G.M. Bastiaanssen, L.H. Bassoi, 2007. Crop water parameters of irrigated wine and table grapes to support water productivity analysis in Sao Francisco River basin, Brazil. Agricultural Water Management 94, 31-42

Teixeira, A.H. de C., W.G.M., Bastiaanssen, Moura, M. S. B., Soares, J. M., Ahmad, M–ud–D, Bos, M. G., 2008a. Energy and Water Balance Measurements for Water Productivity Analysis in Irrigated Mango Trees, Northeast Brazil. Agricultural and Forest Meteorology 148, 1524-1537.

Teixeira, A. H. de C., Bastiaanssen, W.G.M., Ahmad, M. D., Moura, M. S. B., Bos, M. G., 2008b. Analysis of energy fluxes and vegetation-atmosphere parameters in irrigated and natural ecosystems of semi-arid Brazil, Journal of Hydrology. 10.1016/j.jhydrol.2008.08.011.

Teixeira, A. H. de C., Bastiaanssen, W.G.M., Ahmad, M. D., Bos, M.G., 2008c. Reviewing SEBAL Input Parameters for Assessing Evapotranspiration and Water Productivity for the Low-Middle São Francisco River basin, Brazil Part A: Calibration and Validation, Agricultural and Forest Meteorology, in press.

Teixeira, A. H. de C., Bastiaanssen, W.G.M., Ahmad, M. D., Bos, M.G., 2008c. Reviewing SEBAL Input Parameters for Assessing Evapotranspiration and Water Productivity for the Low-Middle São Francisco River Basin, Brazil. Part B: Applications, Agricultural and Forest Meteorology, in press.

Bastiaanssen, W.G.M., Pelgrum, H., Soppe, R.W.O., Allen, R.G. , Thoreson, B.P., **Teixeira, A.H. de C.**, 2008. Thermal infrared technology for local and regional scale irrigation analysis in horticultural systems. ISHS Acta Hort. 792, Proc. V[th] IS on Irrigation of Horticultural Crops.

Netherlands Research School for the
Socio-Economic and Natural Sciences of the Environment

CERTIFICATE

The Netherlands Research School for the
Socio-Economic and Natural Sciences of the Environment
(SENSE), declares that

Antônio Heriberto de Castro Teixeira

Born on: 30 May 1960 at: Fortaleza-CE, Brazil

has successfully fulfilled all requirements of the
Educational Programme of SENSE.

Place: Wageningen Date: 21 October 2008

the Chairman of the
SENSE board

Prof. dr. R. Leemans

the SENSE Director
of Education

Dr. A. van Dommelen

237

The SENSE Research School declares that Mr. Antônio Heriberto de Castro Teixeira has successfully fulfilled all requirements of the Educational PhD Programme of SENSE with a work load of 42 ECTS, including the following activities:

SENSE PhD courses:

°   Environmental Research in Context
°   Research Context Activity: " Writing the first chapter of my thesis including multidisciplinary considerations "
°   Basic Statistics

Other Phd and MSc courses:

°   English Academic Writing
°   English PhD Scientific Writing
°   English PhD Presentation Skills
°   Advanced Use of Remote Sensing in Water Resource Management, Irrigation and Drainage

Research and Management Skills:

°   Organising a scientific workshop about Water Productivity 15 December 2005, at Petrolina-PE, 2005, Brazil

Oral Presentations:

°   "Applications of Energy Balance", 15 December 2005, Petrolina-PE, Brazil
°   "Water Productivity of irrigated vineyards in the semi-arid region of Brazil", 5 July 2007, Aracaju-SE, Brazil
°   "Irrigation Performance Assessment in Mango Crop in the Semi-Arid Region of Northeast Brazil", 5 July 2007, Aracaju-SE, Brazil
°   "Energy Balance in Vineyards Under Different Cultural Management", 13 March 2008, Lima, Peru

Mr. J. Feenstra
SENSE Coordinator PhD Education and Research

This research reported in this thesis is a result of the collaboration between the Wageningen University and the International Institute for Geo-Information Science and Earth Observation-ITC.